doi : 10.17596/0002905

R/V MIRAI Cruise Report
MR14-04

WHP P10N, P01 Revisit in 2014
(North Pacific)

July 9, 2014 – August 29, 2014

Japan Agency for Marine-Earth Science and Technology
(JAMSTEC)

Leg 1 (Yokosuka – Kushiro)

Leg 2 (Kushiro – Dutch Harbor)

Contents

1 Cruise Narrative

September 28, 2014

Hiroshi Uchida (JAMSTEC)

1.1 Highlight

WOCE Section Designation: P10N, P01

Cruise code: MR14-04

Expedition Designation: Leg 1: 49NZ20140709
Leg 2: 49NZ20140717

Chief Scientist and Affiliation:

Hiroshi Uchida
huchida@jamstec.go.jp
Research and Development Center for Global Change (RCGC)
Japan Agency for Marine-Earth Science and Technology (JAMSTEC)
2-15 Natsushima, Yokosuka, Kanagawa, Japan 237-0061
Tel: +81-46-867-9474, Fax: +81-46-867-9835

Ship: R/V Mirai

Ports of Call: Leg 1: Yokosuka, Japan – Kushiro, Japan
Leg 2: Kushiro, Japan – Dutch Harbor, USA

Cruise Dates: Leg 1: July 9, 2014 – July 15, 2014
Leg 2: July 17, 2014 – August 29, 2014

Number of Stations: 121 stations for CTD/Carousel Water Sbampler (Leg 1: 5, Leg 2: 116)
30 stations for XCTD
19 stations for radiosonde and 4 stations for HYVIS
2 stations for ORI net and 10 stations for NORPAC net

Geographic Boundaries (for hydrographic stations):

30ºN – 50ºN
143ºE – 125ºW

Floats and Drifters Deployed:

6 Argo floats
(2 S2A floats with RINKO oxygen sensor and 4 NAVIS floats)

Mooring Deployed or Recovered Mooring:

None

Title of the cruise:

Heat and material transport and their changes in the ocean general circulation

Titles of the proposals and their representatives:

Heat and material transport and their changes in the ocean general circulation

Akihiko Murata (Japan Agency for Marine-Earth Science and Technology)

Collaborative study on the zonal distribution of dissolved organic carbon in the far North Pacific

Takeshi Yoshimura (Central Research Institute of Electric Power Industry)

1.2 Cruise Summary

It is well known that the oceans play a central role in determining global climate. However heat and material transports in the ocean and their temporal changes have not yet been sufficiently quantified. Therefore, global climate change is not understood satisfactorily. The main purposes of this research are to evaluate heat and material transports such as anthropogenic CO_2, nutrients, etc. in the Pacific Ocean and to detect their long-term changes and basin-scale biogeochemical changes since the 1990s.

This cruise is a reoccupation of the hydrographic sections called WHP-P10N along 149ºE and WHP-P01 along 47ºN of the North Pacific (Fig. 1.1.1). The WHP-P10N section was previously observed by the Japan Agency for Marine-Earth Science and Technology (JAMSTEC) in 2005 (Kawano and Uchida, 2007), in 2011 (Uchida et al., 2014), and in 2014 by the Japan Meteorological Agency. The WHP-P01 section was previously observed in 1985 by the Scripps Institution of Oceanography (USA), in 1999 by the Japan Fisheries Agency / the JAMSTEC / the Institute of Ocean Sciences (Canada) (Uchida et al., 2002), and in 2007 by the JAMSTEC (Kawano et al., 2009). This study was conducted under the Global Ocean Ship-based Hydrographic Investigations Program (abbreviated as GO-SHIP, http://www.go-ship.org/). Data obtained from those cruises are available from the CLIVAR & Carbon Hydrographic Data Office (CCHDO) web site (http://cchdo.ucsd.edu).

In leg 1 of this cruise, we conducted CTD and discrete water sampling at selected 5 stations and zooplankton sampling by using ORI net at two stations along the WHP-P10N section mainly for estimation of dispersion of radioactive substances released into the sea by the Fukushima Dai-ichi nuclear power plant accident in March 2011. To understand the oceanographic condition along the WHP-P10N section in detail, we deployed XCTDs between the CTD stations. In addition, we launched radiosondes and HYdrometer VIdeo Sondes (HYVIS) to understand the atmospheric condition along the cruise track. Especially in the section across the Kuroshio Extension, we densely launched radiosondes simultaneously with the XCTDs (Fig. 1.1.2). At station 1, an ARGO float was deployed to take a photograph and recovered after that.

In leg 2 of this cruise, we conducted full-depth CTD, lowered acoustic Doppler current profiler (LADCP), Micro-Rider measurements, and discrete water sampling for physical, chemical and biogeochemical properties of seawater from a maximum of 36 layers along the WHP-P01 section and at the ocean station PAPA (Figs. 1.1.3 and 1.1.4). We deployed two ARGO floats with RINKO oxygen sensor in an anticyclonic eddy off Hokkaido and four ARGO floats in the area where the number of ARGO floats is small to maintain the global array. Furthermore, we sampled marine plankton by using NORPAC net to examine changes in calcification responses of planktonic organisms and pH in the subarctic North Pacific.

Also, we sampled seawater to examine horizontal and vertical distribution of microbial population (picoeukaryotes, bacteria, archaea, and viruses) in gene level to explain relationship between the microbial population and ocean circulations (seawater properties). In addition, we observed physical, chemical, and biogeochemical properties of seawater and atmosphere, and geophysical parameters (sea bottom topography, gravity acceleration, etc.) continuously along the cruise track in order to accumulate basic scientific data in global scale, especially for unobserved regions.

References

Kawano, T., and H. Uchida (Eds.) (2007): WHP P10 Revisit Data Book, JAMSTEC, 139 pp.
Kawano, T., H. Uchida, and T. Doi (Eds.) (2009): WHP P01, P14 Revisit Data Book, JAMSTEC, 212 pp.
Uchida, H., A. Murata, and T. Doi (Eds.) (2014): WHP P10 Revisit in 2011 Data Book, JAMSTEC, 179 pp.
Uchida, H., M. Fukasawa, and H. J. Freeland (Eds.) (2002): WHP P01 Revisit Data Book, JAMSTEC, 73 pp.

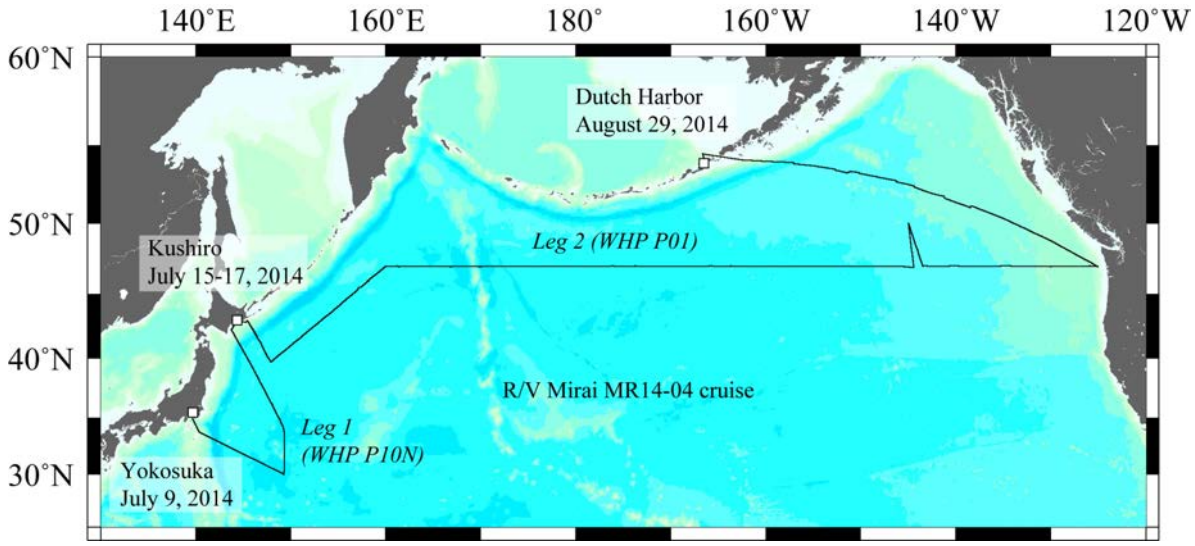

Fig. 1.1.1. Cruise track of the R/V Mirai cruise MR14-04.

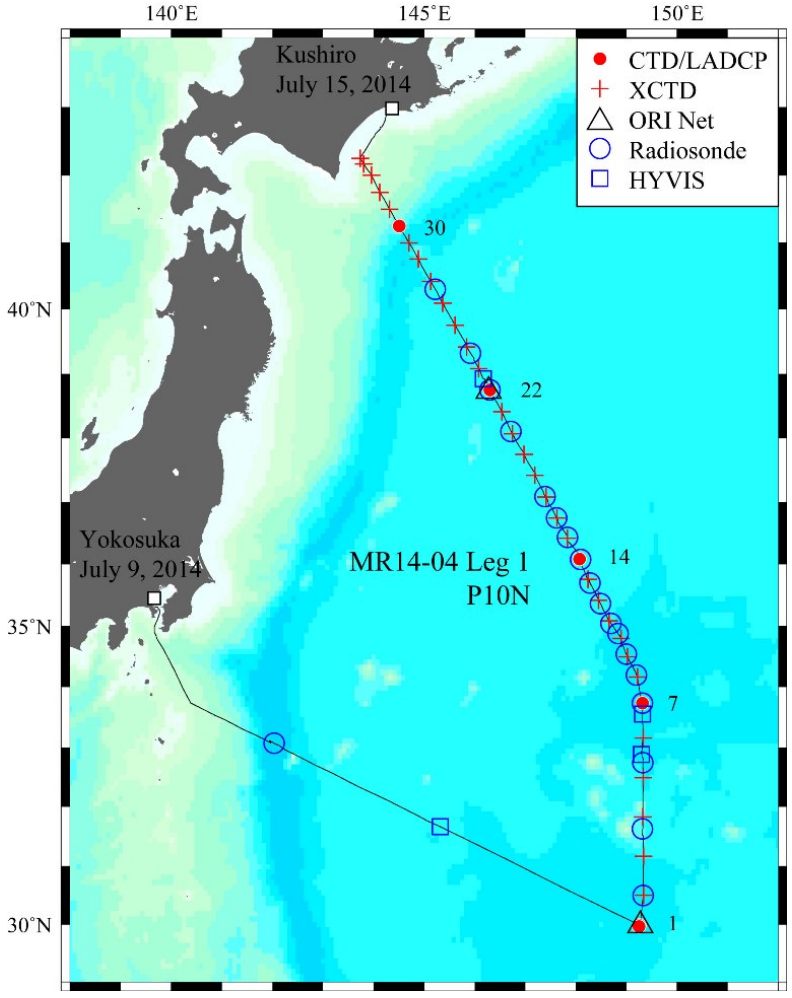

Fig. 1.1.2. Station locations for MR14-04 leg 1.

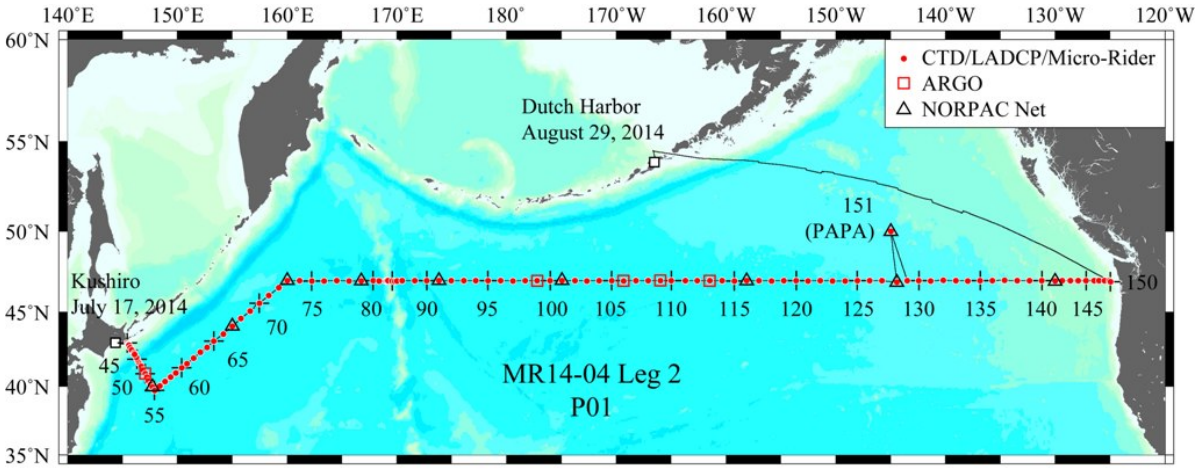

Fig. 1.1.3. Station locations for MR14-04 leg 2.

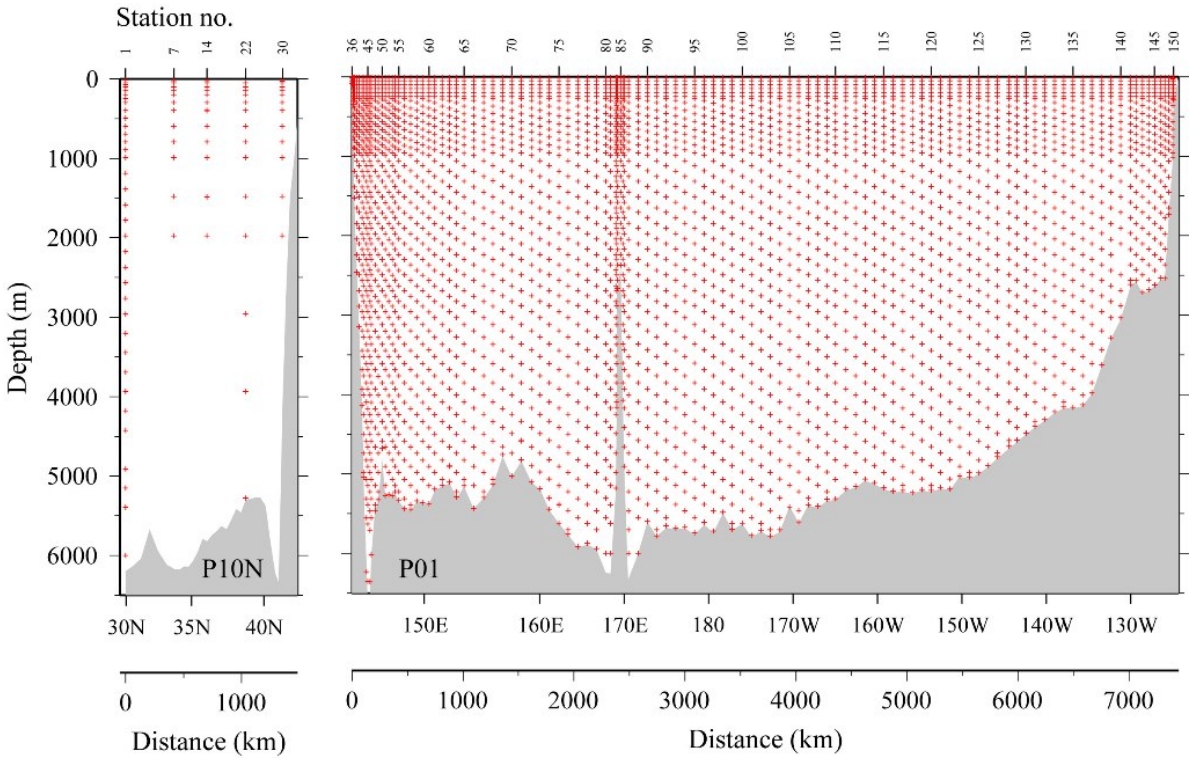

Fig. 1.1.4. Bottle depth diagram.

1.3 List of Principal Investigator and Person in Charge on the Ship

The principal investigator (PI) and the person in charge responsible for major parameters measured on the cruise are listed in Table 1.3.1.

Table 1.3.1. List of principal investigator and person in charge on the ship.

Item	Principal Investigator	Person in Charge on the Ship
Underway		
Navigation	Hiroshi Uchida (JAMSTEC) *huchida@jamstec.go.jp*	Ryo Oyama (GODI) (leg 1) Wataru Tokunaga (GODI) (leg 2)
Bathymetry	Takeshi Matsumoto (Univ. of Ryukyus) *tak@sci.u-ryukyu.ac.jp*	Ryo Oyama (GODI) (leg 1) Wataru Tokunaga (GODI) (leg 2)
Meteorology	Masaki Katsumata (JAMSTEC) *katsu@jamstec.go.jp*	Ryo Oyama (GODI) (leg 1) Wataru Tokunaga (GODI) (leg 2)
TSG	Hiroshi Uchida (JAMSTEC) *huchida@jamtec.go.jp*	Keitaro Matsumoto (MWJ)
pCO_2	Akihiko Murata (JAMSTEC) *murataa@jamstec.go.jp*	Atsushi Ono (MWJ)
ADCP	Shinya Kouketsu (JAMSTEC) *skouketsu@jamstec.go.jp*	Ryo Oyama (GODI) (leg 1) Wataru Tokunaga (GODI) (lge 2)
XCTD	Hiroshi Uchida (JAMSTEC) *huchida@jamstec.go.jp*	Ryo Oyama (GODI) (leg 1) Wataru Tokunaga (GODI) (leg 2)
FlowCAM	Hiroshi Uchida (JAMSTEC) *huchida@jamstec.go.jp*	Hiroshi Uchida (JAMSTEC)
Ceilometer	Masaki Katsumata (JAMSTEC) *katsu@jamstec.go.jp*	Ryo Oyama (GODI) (leg 1) Wataru Tokunaga (GODI) (leg 2)
Raindrop	Masaki Katsumata (JAMSTEC) *katsu@jamstec.go.jp*	Masaki Katsumata (JAMSTEC)
Doppler Radar	Masaki Katsumata (JAMSTEC) *katsu@jamstec.go.jp*	Ryo Oyama (GODI) (leg 1) Wataru Tokunaga (GODI) (leg 2)
Radiosonde	Masaki Katsumata (JAMSTEC) *katsu@jamstec.go.jp*	Ryo Oyama (GODI)
HYVIS	Masaki Katsumata (JAMSTEC) *katsu@jamstec.go.jp*	Ryo Oyama (GODI)
Gravity	Takeshi Matsumoto (Univ. of Ryukyus) *tak@sci.u-ryukyu.ac.jp*	Ryo Oyama (GODI) (leg 1) Wataru Tokunaga (GODI) (leg 2)
Magnetic Field	Takeshi Matsumoto (Univ. of Ryukyus) *tak@sci.u-ryukyu.ac.jp*	Ryo Oyama (GODI) (leg 1) Wataru Tokunaga (GODI) (leg 2)
Satellite Image	Masaki Katsumata (JAMSTEC) *katsu@jamstec.go.jp*	Ryo Oyama (GODI) (leg 1) Wataru Tokunaga (GODI) (leg 2)
Sky Radiometer	Kazuma Aoki (Univ. of Toyama) *kazuma@sci.u-toyama.ac.jp*	none
MAX-DOAS	Hisahiro Takashima (JAMSTEC) *hisahiro@jamstec.go.jp*	none

Ozone and CO	Yugo Kanaya (JAMSTEC) *yugo@jamstec.go.jp*	none
Black Carbon	Takuma Miyakawa (JAMSTEC) *miyakawat@jamstec.go.jp*	none
Fluorescent Aerosol		
	Fumikazu Taketani (JAMSTEC) *taketani@jamstec.go.jp*	none
Aerosol Particle Size		
	Fumikazu Taketani (JAMSTEC) *taketani@jamstec.go.jp*	none

Hydrography

CTD/O_2	Hiroshi Uchida (JAMSTEC) *huchida@jamstec.go.jp*	Shinsuke Toyoda (MWJ)
Salinity	Hiroshi Uchida (JAMSTEC) *huchida@jamstec.go.jp*	Tatsuya Tanaka (MWJ)
Density	Hiroshi Uchida (JAMSTEC) *huchida@jamstec.go.jp*	Hiroshi Uchida (JAMSTEC)
Oxygen	Yuichiro Kumamoto (JAMSTEC) *kumamoto@jamstec.go.jp*	Keitaro Matsumoto (MWJ)
Nutrients	Michio Aoyama (Fukushima Univ.) *r706@ipc.fukushima-u.ac.jp*	Yasuhiro Arii (MWJ)
CFCs/SF_6	Ken'ichi Sasaki (JAMSTEC) *ksasaki@jamstec.go.jp*	Ken'ichi Sasaki (JAMSTEC) (leg 1) Hironori Sato (MWJ) (leg 2)
DIC	Akihiko Murata (JAMSTEC) *murataa@jamstec.go.jp*	Atsushi Ono (MWJ)
Alkalinity	Akihiko Murata (JAMSTEC) *murataa@jamstec.go.jp*	Tomonori Watai (MWJ)
Alkalinity duplicate by potentiometry		
	Yoshihiro Shinoda (JAMSTEC) *yshinoda@jamstec.go.jp*	Yoshihiro Shinoda (JAMSTEC)
pH	Akihiko Murata (JAMSTEC) *murataa@jamstec.go.jp*	Tomonori Watai (MWJ)
Chlorophyll *a*	Kosei Sasaoka (JAMSTEC) *sasaoka@jamstec.go.jp*	Keitaro Matsumoto (MWJ)
CDOM/Absorption Coefficients		
	Kosei Sasaoka (JAMSTEC) *sasaoka@jamstec.go.jp*	Kosei Sasaoka (JAMSTEC)
Calcium	Yoshihiro Shinoda (JAMSTEC) *Yshinoda@jamstec.go.jp*	Yoshihiro Shinoda (JAMSTEC)
DOC	Dennis A. Hansell (RSMAS) *dhansell@rsmas.miami.edu* Takeshi Yoshimura (CRIEPI) *ytakeshi@criepi.denken.or.jp*	Yuichiro Kumamoto (JAMSTEC)

DOC duplicate at station 73 (K2)		
	Masahide Wakita (JAMSTEC) *mwakita@jamstec.go.jp*	Hiroshi Uchida (JAMSTEC)
$\Delta^{14}C/\delta^{13}C$	Yuichiro Kumamoto (JAMSTEC) *kumamoto@jamstec.go.jp*	Yuichiro Kumamoto (JAMSTEC)
$^{134}Cs/^{137}Cs$	Yuichiro Kumamoto (JAMSTEC) *kumamoto@jamstec.go.jp*	Yuichiro Kumamoto (JAMSTEC)
Iodine-129	Yuichiro Kumamoto (JAMSTEC) *kumamoto@jamstec.go.jp*	Yuichiro Kumamoto (JAMSTEC)
$\delta^{18}O/\delta D$	Hiroshi Uchida (JAMSTEC) *huchida@jamstec.go.jp*	Hiroshi Uchida (JAMSTEC)
PFASs	Nobuyoshi Yamashita (AIST) *nob.yamashita@aist.go.jp*	Nobuyoshi Yamashita (AIST) (leg 1) Sachi Taniyasu (AIST) (leg 2)
N_2O/CH_4	Osamu Yoshida (RGU) *yoshida@rakuno.ac.jp*	Osamu Yoshida (RGU) (leg 1) Takuya Takahashi (RGU) (leg 2)
Cell abundance	Takuro Nunoura (JAMSTEC) *takuron@jamstec.go.jp*	Taichi Yokokawa (Ehime Univ.) (leg 1) Takuro Nunoura (JAMSTEC) (leg 2)
Microbial diversity	Takuro Nunoura (JAMSTEC) *takuron@jamstec.go.jp*	Takuro Nunoura (JAMSTEC)
Microbial carbon uptake		
	Takuro Nunoura (JAMSTEC) *takuron@jamstec.go.jp*	Taichi Yokokawa (Ehime Univ.) (leg 1) Takuro Nunoura (JAMSTEC) (leg 2)
Nitrification	Akiko Makabe (TUAT) *a-makabe@cc.tuat.ac.jp*	Akiko Makabe (TUAT)
Nitrogen fixation	Masanori Kaneko (JAMSTEC) *m_kaneko@jamstec.go.jp*	Masanori Kaneko (JAMSTEC) (leg 1) Shuichiro Matushima (TITECH) (leg 2)
Methanogen biomarker		
	Masanori Kaneko (JAMSTEC) *m_kaneko@jamstec.go.jp*	Masanori Kaneko (JAMSTEC) (leg 1) Takuya Takahashi (RGU) (leg 2)
$\delta^{13}C/CH_4$	Masanori Kaneko (JAMSTEC) *m_kaneko@jamstec.go.jp*	Masanori Kaneko (JAMSTEC) (leg 1) Takuya Takahashi (RGU) (leg 2)
$\delta^{15}N\ \delta^{18}O/NO_3^-$	Chisato Yoshikawa (JAMSTEC) *yoshikawac@jamstec.go.jp*	Chisato Yoshikawa (JAMSTEC) (leg 1) Akiko Makabe (TUAT) (leg 2)
$\delta^{15}N$/chlorophyll	Chisato Yoshikawa (JAMSTEC) *yoshikawac@jamstec.go.jp*	Chisato Yoshikawa (JAMSTEC) (leg 1) Takuya Takahashi (TUAT) (leg 2)
$\delta^{15}N\ \delta^{18}O/N_2O$, NO_2		
	Sakae Toyoda (TITECH) *toyoda.s.aa@m.titech.ac.jp*	Shuichiro Matsushima (TITECH) (leg 2)
$\delta^{15}N/NH_4^+$, DON, urea		
	Akiko Makabe (TUAT) *a-makabe@cc.tuat.ac.jp*	Akiko Makabe (TUAT)
LADCP	Shinya Kouketsu (JAMSTEC) *skouketsu@jamstec.go.jp*	Hiroshi Uchida (JAMSTEC) (leg 1) Shinya Kouketsu (JAMSTEC) (leg 2)
Micro-Rider	Ichiro Yasuda (AORI) *ichiro@aori.u-tokyo.ac.jp*	Shinya Kouketsu (JAMSTEC)

Biology

ORI net	Minoru Kitamura (JAMSTEC) *kitamura@jamstec.go.jp*	Minoru Kitamura (JAMSTEC)
NORPAC net	Katsunori Kimoto (JAMSTEC) *kimopy@jamstec.go.jp*	Shinya Iwasaki (AORI)
Phytoplankton Incubation	Koji Sugie (JAMSTEC) *sugie@jamstec.go.jp*	Koji Sugie (JAMSTEC)

Floats

ARGO float	Toshio Suga (JAMSTEC) *sugat@jamstec.go.jp*	Hiroshi Matsunaga (MWJ)

JAMSTEC	Japan Agency for Marine-Earth Science and Technology
GODI	Global Ocean Development Inc.
MWJ	Marine Works Japan, Ltd.
RSMAS	Rosenstiel School of Marine and Atmospheric Science, University of Miami
CRIEPI	Central Research Institute of Electric Power Industry
AIST	National Institute of Advanced Industrial Science and Technology
RGU	Rakuno Gakuen University
TUAT	Tokyo University of Agriculture and Technology
TITECH	Tokyo Institute of Technology
AORI	Atmosphere and Ocean Research Institute, The Univ. of Tokyo

1.4 List of Cruise Participants

Table 1.4.1. List of cruise participants for leg 1.

Name	Responsibility	Affiliation
Hiroshi Uchida	Density/FlowCAM/LADCP/$\delta^{18}O$	RCGC/JAMSTEC
Yuichiro Kumamoto	DO/Radionuclides/Water sampling	RCGC/JAMSTEC
Yoshihiro Shinoda	Water sampling	RCGC/JAMSTEC
Minoru Kitamura	ORI net	RCGC/JAMSTEC
Masaki Katsumata	HYVIS/Radiosonde/Doppler rader/Raindrop	RCGC/JAMSTEC
Biao Geng	HYVIS/Radiosonde/Doppler rader	RCGC/JAMSTEC
Shuichi Mori	HYVIS/Radiosonde/Doppler rader	DCOP/JAMSTEC
Ryuichi Shirooka	HYVIS/Radiosonde/Doppler rader	DCOP/JAMSTEC
Ken'ichi Sasaki	CFCs/SF_6	MIO/JAMSTEC
Takuro Nunoura	Microbiology	RCMB/JAMSTEC
Miho Hirai	Microbiology	RCMB/JAMSTEC
Chisato Yoshikawa	Chlorophyll/NO_3 isotope geochemistry	BGC/JAMSTEC
Masanori Kaneko	CH_4 geochemistry/Nitrogen fixation	BGC/JAMSTEC
Akiko Makabe	Nitrification/Nitrogen geochemistry	TUAT
Taichi Yokokawa	Microbiology	Ehime Univ.
Nobuyoshi Yamashita	PFASs	AIST
Osamu Yoshida	N_2O/CH_4	RGU
Kanta Chida	N_2O/CH_4	RGU
Takuya Takahashi	N_2O/CH_4	RGU
Tomoyuki Shirakawa	TV camera	JBC
Fumihiko Saito	TV camera	JBC
Ryo Oyama	Chief technologist /meteorology/ geophysics/ADCP/XCTD	GODI
Souichiro Sueyoshi	Meteorology/geophysics/ADCP/XCTD	GODI
Katsuhisa Maeno	Meteorology/geophysics/ADCP/XCTD	GODI
Koichi Inagaki	Meteorology/geophysics/ADCP/XCTD	GODI
Yutaro Murakami	Meteorology/geophysics/ADCP/XCTD	GODI
Shinsuke Toyoda	Chief technologist/CTD/water sampling	MWJ
Hiroshi Matsunaga	CTD/ARGO	MWJ
Kenichi Katayama	CTD	MWJ
Rei Ito	CTD	MWJ
Akira Watanabe	CTD	MWJ
Tatsuya Tanaka	Salinity	MWJ
Sonoka Wakatsuki	Salinity	MWJ
Keitaro Matsumoto	DO/Chlorophyll-a/TSG	MWJ
Misato Kuwahara	DO/Chlorophyll-a/TSG	MWJ
Haruka Tamada	DO/Chlorophyll-a/TSG	MWJ
Yasuhiro Arii	Nutrients	MWJ
Mironu Kamata	Nutrients	MWJ

Tomomi Sone	Nutrients	MWJ
Katsunori Sagishima	$CFCs/SF_6$	MWJ
Hironori Sato	$CFCs/SF_6$	MWJ
Hideki Yamamoto	$CFCs/SF_6$	MWJ
Atsushi Ono	DIC	MWJ
Yoshiko Ishikawa	DIC	MWJ
Tomonori Watai	pH/Alkalinity	MWJ
Emi Deguchi	pH/Alkalinity	MWJ

JAMSTEC	Japan Agency for Marine-Earth Science and Technology
RCGC	Research and Development Center for Global Change
DCOP	Department of Coupled Ocean-Atmosphere-Land Processes Research
MIO	Mutsu Institute of Oceanography
RCMB	Research and Development Center for Marine Biosciences
BGC	Department of Biogeochemistry
TUAT	Tokyo University of Agriculture and Technology
AIST	National Institute of Advanced Industrial Science and Technology
RGU	Rakuno Gakuen University
JBC	Japan Broadcasting Corporation
GODI	Global Ocean Development Inc.
MWJ	Marine Works Japan, Ltd.

Table 1.4.2. List of cruise participants for leg 2.

Name	Responsibility	Affiliation
Hiroshi Uchida	Density/FlowCAM/LADCP/Micro-Rider/$\delta^{18}O$	RCGC/JAMSTEC
Yuichiro Kumamoto	DO/Radionuclides/Water sampling	RCGC/JAMSTEC
Yoshihiro Shinoda	Calcium/Water sampling	RCGC/JAMSTEC
Shinya Koketsu	LADCP/Micro-Rider/$\delta^{18}O$	RCGC/JAMSTEC
Kosei Sasaoka	CDOM/Absorption coefficient	RCGC/JAMSTEC
Koji Sugie	Phytoplankton incubation/NORPAC net	RCGC/JAMSTEC
Shinya Iwasaki	NORPAC net/Phytoplankton incubation	AORI/Univ. of Tokyo
Takuro Nunoura	Microbiology	RCMB/JAMSTEC
Akiko Makabe	Nitrification/Nitrogen geochemistry	TUAT
Shuichiro Matsushima	Nitrogen fixation/Nitrogen geochemistry/CH_4	TITECH
Seiya Takahashi	Microbiology	Tsukuba Univ.
Sachi Taniyasu	PFASs	AIST
Kanta Chida	N_2O/CH_4	RGU
Takuya Takahashi	N_2O/CH_4	RGU
Wataru Tokunaga	Chief technologist /meteorology/ geophysics/ADCP/XCTD	GODI

Kazuho Yoshida	Meteorology/geophysics/ADCP/XCTD	GODI
Yutaro Murakami	Meteorology/geophysics/ADCP/XCTD	GODI
Tetsuya Kai	Meteorology/geophysics/ADCP/XCTD	GODI
Shinsuke Toyoda	Chief technologist/CTD/water sampling	MWJ
Hiroshi Matsunaga	CTD/ARGO	MWJ
Tomoyuki Takamori	CTD	MWJ
Rei Ito	CTD	MWJ
Akira Watanabe	CTD	MWJ
Tatsuya Tanaka	Salinity	MWJ
Sonoka Wakatsuki	Salinity	MWJ
Keitaro Matsumoto	DO/Chlorophyll-a/TSG	MWJ
Katsunori Sagishima	DO/Chlorophyll-a/TSG	MWJ
Haruka Tamada	DO/Chlorophyll-a/TSG	MWJ
Yasuhiro Arii	Nutrients	MWJ
Kenichiro Sato	Nutrients	MWJ
Elena Hayashi	Nutrients	MWJ
Hironori Sato	CFCs/SF_6	MWJ
Hideki Yamamoto	CFCs/SF_6	MWJ
Shoko Tatamisashi	CFCs/SF_6	MWJ
Kanako Yoshida	CFCs/SF_6	MWJ
Atsushi Ono	DIC	MWJ
Yoshiko Ishikawa	DIC	MWJ
Tomonori Watai	pH/Alkalinity	MWJ
Emi Deguchi	pH/Alkalinity	MWJ
Rina Tajima	Water sampling	MWJ
Toshiki Nosho	Water sampling	MWJ
Miho Arai	Water sampling	MWJ
Kohei Kumagai	Water sampling	MWJ
Yuki Kawabuchi	Water sampling	MWJ
Yuki Komuro	Water sampling	MWJ

JAMSTEC	Japan Agency for Marine-Earth Science and Technology
RCGC	Research and Development Center for Global Change
AORI	Atmosphere and Ocean Research Institute, The Univ. of Tokyo
RCMB	Research and Development Center for Marine Biosciences
TUAT	Tokyo University of Agriculture and Technology
TITECH	Tokyo Institute of Technology
AIST	National Institute of Advanced Industrial Science and Technology
RGU	Rakuno Gakuen University
GODI	Global Ocean Development Inc.
MWJ	Marine Works Japan, Ltd.

1.5 List of Titles of Proposals and Their Representatives

Title of the cruise

Heat and material transport and their changes in the ocean general circulation
Akihiko Murata (Japan Agency for Marine-Earth Science and Technology)

Collaborative study on the zonal distribution of dissolved organic carbon in the far North Pacific
Takeshi Yoshimura (Central Research Institute of Electric Power Industry)

Investigation for the relationship among primary production, ocean circulation and deep-sea microbial ecosystems
Takuro Nunoura (Japan Agency for Marine-Earth Science and Technology)

Investigation for the trench biosphere in the Chishima Trench and biogeography of deep-sea microbes in the north Pacific
Takuro Nunoura (Japan Agency for Marine-Earth Science and Technology)

Applied research of MIRAI brand-new shipboard weather radar: Validation and utilization of dual-polarization information for global deployment
Masaki Katsumata (Japan Agency for Marine-Earth Science and Technology)

Global distribution of drop size distribution of precipitating particles over pure-oceanic background
Masaki Katsumata (Japan Agency for Marine-Earth Science and Technology)

Changes in calcification responses of marine planktonic organisms and pH in the subarctic North Pacific
Katsunori Kimoto (Japan Agency for Marine-Earth Science and Technology)

Aerosol optical characteristics measured by Ship-borne Sky radiometer
Kazuma Aoki (University of Toyama)

Activity concentrations of Fukushima-derived radiocesium in oceanic zooplankton
Minoru Kitamura (Japan Agency for Marine-Earth Science and Technology)

Standardisation of marine geophysical data and its application to geodynamics studies
Takeshi Matsumoto (University of the Ryukyus)

The study of the ocean circulation and the transport of heat and fresh water in the Pacific Ocean using by Argo floats
Toshio Suga (Japan Agency for Marine-Earth Science and Technology)

Advanced continuous measurements of aerosols in the marine atmosphere: Elucidation of the roles in the Earth system
Yugo Kanaya (Japan Agency for Marine-Earth Science and Technology)

Estimation of hazardous chemicals discharge form the melting ice in the Arctic Ocean
Nobuyoshi Yamashita (National Institute of Advanced Industrial Science and Technology)

Biogeochemical cycles of biogenic greenhouse gases in the North Pacific
Osamu Yoshida (Rakuno Gakuen University)

2 Underway Measurements

2.1 Navigation

September 17, 2014

(1) Personnel

Hiroshi Uchida	JAMSTEC: Principal investigator	
Ryo Oyama	Global Ocean Development Inc., (GODI)	- leg 1 -
Souichiro Sueyoshi	GODI	- leg 1 -
Katsuhisa Maeno	GODI	- leg 1 -
Koichi Inagaki	GODI	- leg 1 -
Wataru Tokunaga	GODI	- leg 2 -
Kazuho Yoshida	GODI	- leg 2 -
Tetsuya Kai	GODI	- leg 2 -
Yutaro Murakami	GODI	- leg 1, leg 2 -
Masanori Murakami	MIRAI crew	- leg 1, leg 2 -

(2) System description

Ship's position and velocity were provided by Navigation System on R/V MIRAI. This system integrates GPS position, Doppler sonar log speed, Gyro compass heading and other basic data for navigation, and calculated speed and course over ground on workstation. This system also distributed ship's standard time synchronized to GPS time server via Network Time Protocol. These data were logged on the network server as "SOJ" data every 5 seconds.

Sensors for navigation data are listed below;

i) GPS system:

R/V MIRAI has four GPS systems, all GPS positions were offset to radar-mast position, datum point. Anytime changeable manually switched as to GPS receiving state.

a) MultiFix6 (software version 1.01), Differential GPS system.
Receiver: Trimble SPS751, with GPS antenna located on navigation deck, starboard.
Decoder: FUGURO STARFIX 4100LRS

b) MultiFix6 (software version 1.01), Differential GPS system.
Receiver: Trimble SPS751, with two GPS antenna located on compass deck, port side.
Decoder: FUGURO STARFIX 4100LRS

c) Standalone GPS system.
Receiver: Trimble 4000DS, GPS antenna located on navigation deck, port side.

d) Standalone GPS system.
Receiver: FURUNO GP-36, GPS antenna located on navigation deck, starboard.

ii) Doppler sonar log:

FURUNO DS-30, which use three acoustic beam for current measurement under the hull.

iii) Gyro compass:

TOKYO KEIKI TG-6000, sperry type mechanical gyrocompass.

iv) GPS time server:

SEIKO TS-2540 Time Server, synchronizing to GPS satellites every 1 second.

(3) Data period (Times in UTC)

Leg 1: 22:10, 08 Jul. 2014 to 04:00, 15 Jul. 2014

Leg 2: 02:00, 17 Jul. 2014 to 18:00, 29 Aug. 2014

(4) Remarks (Times in UTC)

i) The following periods, navigation data (position, speed and course over ground) was often invalid due to position fix error for loss of GPS satellites.

Leg 1: 14 Jul. to 15 Jul., 2014

Leg 2: 17 Jul. to 16 Aug., 2014

ii) The following periods, navigation data was invalid due to the system error.

Leg 2: 12:37 to 12:45 23 Aug., 2014

iii) Some data records were lacked due to the system error or GPS trouble. See data "readme.txt" which contains the time of data lost.

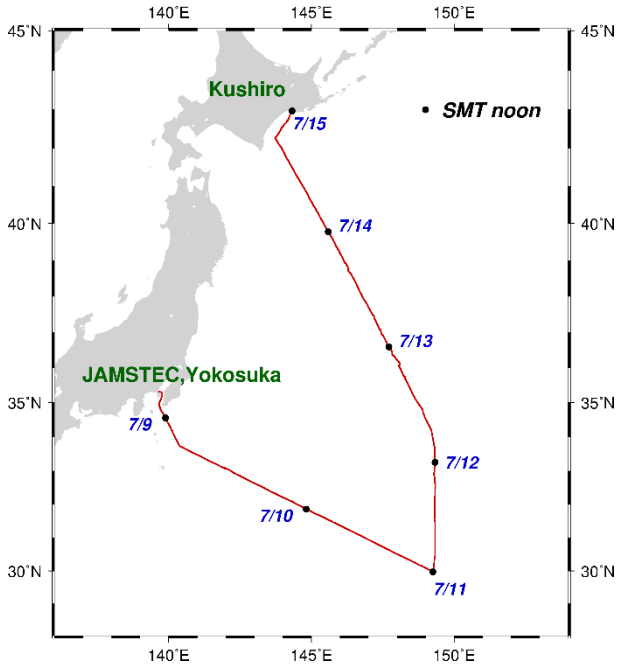

Fig.2.1.1. Cruise track of MR14-04 Leg 1.

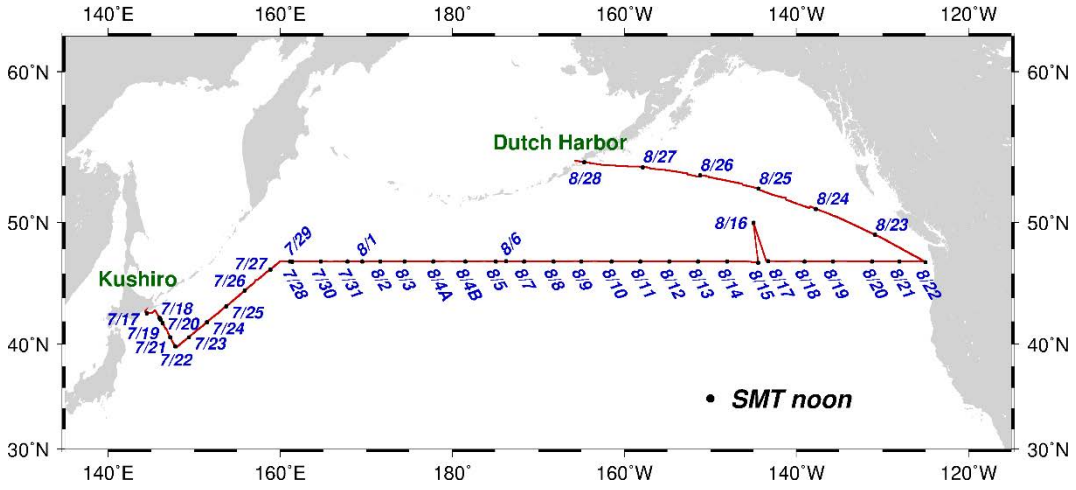

Fig.2.1.2. Cruise track of MR14-04 Leg 2.

2.2 Swath Bathymetry

September 17, 2014

(1) Personnel

Takeshi Matsumoto	Univ. of Ryukyus: Principal investigator	(Not-onboard)
Ryo Oyama	Global Ocean Development Inc., (GODI)	- leg 1 -
Souichiro Sueyoshi	GODI	- leg 1 -
Katsuhisa Maeno	GODI	- leg 1 -
Koichi Inagaki	GODI	- leg 1 -
Wataru Tokunaga	GODI	- leg 2 -
Kazuho Yoshida	GODI	- leg 2 -
Tetsuya Kai	GODI	- leg 2 -
Yutaro Murakami	GODI	- leg 1, leg 2 -
Masanori Murakami	MIRAI crew	- leg 1, leg 2 -

(2) Introduction

R/V MIRAI is equipped with a Multi narrow Beam Echo Sounding system (MBES), SEABEAM 3012 (L3 Communications, ELAC Nautik). The objective of MBES is collecting continuous bathymetric data along ship's track to make a contribution to geological and geophysical investigations and global datasets.

(3) Data Acquisition

The "SEABEAM 3012" on R/V MIRAI was used for bathymetry mapping during the MR14-04 cruise.

To get accurate sound velocity of water column for ray-path correction of acoustic multibeam, we used Surface Sound Velocimeter (SSV) data to get the sea surface sound velocity (at 6.62m), and the deeper depth sound velocity profiles were calculated by temperature and salinity profiles from CTD and XCTD data by the equation in Del Grosso (1974) during this cruise.

Table 2.2.1 shows system configuration and performance of SEABEAM 3012.

Table 2.2.1. SEABEMA 3012 system configuration and performance.

Frequency:	12 kHz
Transmit beam width:	2.0 degree
Transmit power:	4 kW
Transmit pulse length:	2 to 20 msec.
Receive beam width:	1.6 degree
Depth range:	50 to 11,000 m
Number of beams:	301 beams (Spacing mode: Equi-angle)
Beam spacing:	1.5 % of water depth (Spacing mode: Equi-distance)
Swath width:	60 to 150 degrees
Depth accuracy:	< 1 % of water depth (average across the swath)

(4) Data processing

i) Sound velocity correction

Each bathymetry data were corrected with sound velocity profiles calculated from the nearest CTD or XCTD data in the distance. The equation of Del Grosso (1974) was used for calculating sound velocity. The data correction were carried out using the HIPS software version 8.1.7 (CARIS, Canada)

ii) Editing and Gridding

Editing for the bathymetry data were carried out using the HIPS. Firstly, the bathymetry data during ship's turning was basically deleted, and spike noise of each swath data was removed. Then the bathymetry data were checked by "BASE surface (resolution: 100 m averaged grid)".

Finally, all accepted data were exported as XYZ ASCII data (longitude [degree], latitude [degree], depth [m]), and converted to 150 m grid data using "nearneighbor" utility of GMT (Generic Mapping Tool) software.

Table 2.2.2. Parameters for gridding on "nearneighbor" in GMT.

Gridding mesh size:	150 m
Search radius size (-S):	150 m
Number of sectors (-N):	1

(5) Data Archives

Bathymetric data obtained during this cruise will be submitted to the Data Management Group (DMG) of JAMSTEC, and will be archived there.

(6) Remarks (Times in UTC)

i) The following periods, the observation were carried out.

Leg 1: 02:52 09 Jul. to 23:22 14 Jul., 2014

Leg 2: 06:19 17 Jul. to 12:29 28 Aug., 2014

ii) The following periods, navigation data (position, speed and course over ground) was often invalid due to position fix error for loss of GPS satellites. If bathymetric data were included error position and heading information, we interpolated from the just before and behind correct data using the HIPS.

Leg 1: 14 Jul. to 15 Jul., 2014

Leg 2: 17 Jul. to 16 Aug., 2014

iii) The following periods, navigation data was invalid due to the server error.

Leg 2: 12:37 to 12:45 23 Aug., 2014

iv) The following periods, data acquisition was suspended due to the system error and maintenance.

01:55 30 Jul. to 01:59 30 Jul., 2014

06:43 30 Jul. to 07:40 30 Jul., 2014

2.3 Surface Meteorological Observations

September 17, 2014

(1) Personnel

Masaki Katsumata	(JAMSTEC): Principal Investigator	
Ryo Oyama	(Global Ocean Development Inc., GODI)	-leg1-
Souichiro Sueyoshi	(GODI)	-leg1-
Katsuhisa Maeno	(GODI)	-leg1-
Koichi Inagaki	(GODI)	-leg1-
Wataru Tokunaga	(GODI)	-leg2-
Kazuho Yoshida	(GODI)	-leg2-
Tetsuya Kai	(GODI)	-leg2-
Yutaro Murakami	(GODI)	-leg1, leg2-
Masanori Murakami	(MIRAI Crew)	-leg1, leg2-

(2) Objectives

Surface meteorological parameters are observed as a basic dataset of the meteorology. These parameters provide the temporal variation of the meteorological condition surrounding the ship.

(3) Methods

Surface meteorological parameters were observed during the MR14-04 cruise from 8th July 2014 to 29th August 2014, except for the USA territorial watars . In this cruise, we used two systems for the observation.

i. MIRAI Surface Meteorological observation (SMet) system

Instruments of SMet system are listed in Table 2.3.1 and measured parameters are listed in Table 2.3.2. Data were collected and processed by KOAC-7800 weather data processor made by Koshin-Denki, Japan. The data set consists of 6-second averaged data.

ii. Shipboard Oceanographic and Atmospheric Radiation (SOAR) measurement system

SOAR system designed by BNL (Brookhaven National Laboratory, USA) consists of major five parts.

a) Portable Radiation Package (PRP) designed by BNL – short and long wave downward radiation.
b) Analog meteorological data sampling with CR1000 logger manufactured by Campbell Inc. Canada – wind, pressure, and rainfall (by a capacitive rain gauge) measurement.
c) Digital meteorological data sampling from individual sensors – air temperature, relative humidity and rainfall (by ORG (optical rain gauge)) measurement.
d) Photosynthetically Available Radiation (PAR) sensor manufactured by Biospherical Instruments Inc. (USA) - PAR measurement.
e) Scientific Computer System (SCS) developed by NOAA (National Oceanic and Atmospheric Administration, USA) – centralized data acquisition and logging of all data sets.

SCS recorded PRP data every 6 seconds, CR1000 data every 10 seconds, air temperature and relative humidity data every 2 seconds and ORG data every 5 seconds. SCS composed Event data (JamMet) from these data and ship's navigation data. Instruments and their locations are listed in Table 2.3.3 and measured parameters are listed in Table 2.3.4.

For the quality control as post processing, we checked the following sensors, before and after the cruise.

i. Young rain gauge (SMet and SOAR)
Inspect of the linearity of output value from the rain gauge sensor to change input value by adding fixed quantity of test water.

ii. Barometer (SMet and SOAR)
Comparison with the portable barometer value, PTB220, VAISALA

iii. Thermometer (air temperature and relative humidity) (SMet and SOAR)
Comparison with the portable thermometer value, HMP41/45, VAISALA

(4) Preliminary results

Fig. 2.3-1 shows the time series of the following parameters;
Wind (SOAR)
Air temperature (SMet)
Relative humidity (SMet)
Precipitation (SOAR, rain gauge)
Short/long wave radiation (SOAR)
Pressure (SMet)
Sea surface temperature (SMet)
Significant wave height (SMet)

(5) Data archives

These meteorological data will be submitted to the Data Management Group (DMG) of JAMSTEC just after the cruise.

(6) Remarks (Times in UTC)

i) Data acquisition was suspended in the territorial waters of USA.

ii) The following periods, sea surface temperature of SMet data was available.
Leg 1: 01:39, 09 Jul. 2014 - 23:31, 14 Jul. 2014
Leg 2: 02:04, 17 Jul. 2014 - 12:30, 28 Aug. 2014

iii) The following periods, navigation data (position, speed and course over ground) of SMet and JamMet were often invalid due to position fix error for loss of detected GPS satellites.
Leg 1: 14 Jul. to 15 Jul. 2014
Leg 2: 17 Jul. to 16 Aug. 2014

iv) The following period, navigation data of SMet was invalid due to network server trouble.
Leg 2: 12:37, 23 Aug. 2014 - 12:44, 23 Aug. 2014

v) The following period, ship gyro and LOG of JamMet were invalid due to communication error to network server.
Leg 1: 07:57:06, 18:38:32; 11 Jul. 2014
Leg 2: 11:28:40, 08 Aug. 2014
19:21:00, 21 Aug. 2014

vi) The following time, increasing of SMet capacitive rain gauge data were invalid due to test transmitting for VHF radio.
Leg 2: 14:23, 23:14; 19 Jul. 2014

05:18, 25 Jul. 2014
06:17, 26 Jul. 2014
06:06, 18:32; 27 Jul. 2014
18:13, 28 Jul. 2014
06:04, 17:19; 30 Jul. 2014

vii) The following period, PRP data was invalid due to PC trouble.
Leg 1: 01:08, 09 Jul. 2014 - 01:25, 09 Jul. 2014
14:48, 09 Jul. 2014 - 14:54, 09 Jul. 2014

viii) The following period, logging interval of PRP was longer than normal.
Leg 1: 08:50, 09 Jul. 2014 - 14:54, 09 Jul. 2014

ix) The following period, ORG data was invalid due to senser error.
Leg 2: 19:37:51 to 19:40:33, 27 Aug. 2014,

Table 2.3.1. Instruments and installation locations of MIRAI Surface Meteorological observation system.

Sensors	Type	Manufacturer	Location (altitude from surface)
Anemometer	KE-500	Koshin Denki, Japan	foremast (24 m)
Tair/RH	HMP155	Vaisala, Finland	
with 43408 Gill aspirated radiation shield		R.M. Young, USA	compass deck (21 m) starboard side and port side
Thermometer: SST	RFN2-0	Koshin Denki, Japan	4th deck (-1m, inlet -5m)
Barometer	Model-370	Setra System, USA	captain deck (13 m) weather observation room
Capacitive rain gauge	50202	R. M. Young, USA	compass deck (19 m)
Optical rain gauge	ORG-815DS	Osi, USA	compass deck (19 m)
Radiometer (short wave)	MS-802	Eko Seiki, Japan	radar mast (28 m)
Radiometer (long wave)	MS-202	Eko Seiki, Japan	radar mast (28 m)
Wave height meter	WM-2	Tsurumi-seiki, Japan	bow (10 m)

Table 2.3.2. Parameters of MIRAI Surface Meteorological observation system.

Parameter	Units	Remarks
1 Latitude	degree	
2 Longitude	degree	
3 Ship's speed	knot	Mirai log, DS-30 Furuno
4 Ship's heading	degree	Mirai gyro,TG-6000,TOKYO-KEIKI
5 Relative wind speed	m/s	6sec./10min. averaged
6 Relative wind direction	degree	6sec./10min. averaged
7 True wind speed	m/s	6sec./10min. averaged
8 True wind direction	degree	6sec./10min. averaged
9 Barometric pressure	hPa	adjusted to sea surface level 6sec. averaged
10 Air temperature (starboard side)	degC	6sec. averaged
11 Air temperature (port side)	degC	6sec. averaged
12 Dewpoint temperature (starboard side)	degC	6sec. averaged
13 Dewpoint temperature (port side)	degC	6sec. averaged
14 Relative humidity (starboard side)	%	6sec. averaged
15 Relative humidity (port side)	%	6sec. averaged
16 Sea surface temperature	degC	6sec. averaged
17 Rain rate (optical rain gauge)	mm/hr	hourly accumulation
18 Rain rate (capacitive rain gauge)	mm/hr	hourly accumulation
19 Down welling shortwave radiation	W/m^2	6sec. averaged
20 Down welling infra-red radiation	W/m^2	6sec. averaged
21 Significant wave height (bow)	m	hourly
22 Significant wave height (aft)	m	hourly
23 Significant wave period (bow)	second	hourly
24 Significant wave period (aft)	second	hourly

Table 2.3.3. Instruments and installation locations of SOAR system.

Sensors (Meteorological)	Type	Manufacturer	Location (altitude from surface)
Anemometer	05106	R.M. Young, USA	foremast (25 m)
Barometer	PTB210	Vaisala, Finland	
with 61002 Gill pressure port		R.M. Young, USA	foremast (23 m)
Capacitive rain gauge	50202	R.M. Young, USA	foremast (24 m)
Tair/RH	HMP155	Vaisala, Finland	
with 43408 Gill aspirated radiation shield		R.M. Young, USA	foremast (23 m)
Optical rain gauge	ORG-815DR	Osi, USA	foremast (24 m)

Sensors (PRP)	Type	Manufacturer	Location (altitude from surface)
Radiometer (short wave)	PSP	Epply Labs, USA	foremast (25 m)
Radiometer (long wave)	PIR	Epply Labs, USA	foremast (25 m)
Fast rotating shadowband radiometer		Yankee, USA	foremast (25 m)

Sensor (PAR)	Type	Manufacturer	Location (altitude from surface)
PAR sensor	PUV-510B	Biospherical Instruments Inc., USA	Navigation deck (18m)

Table 2.3.4. Parameters of SOAR system (JamMet).

Parameter	Units	Remarks
1 Latitude	degree	
2 Longitude	degree	
3 SOG	knot	
4 COG	degree	
5 Relative wind speed	m/s	
6 Relative wind direction	degree	
7 Barometric pressure	hPa	
8 Air temperature	degC	
9 Relative humidity	%	
10 Rain rate (optical rain gauge)	mm/hr	
11 Precipitation (capacitive rain gauge)	mm	reset at 50 mm
12 Down welling shortwave radiation	W/m^2	
13 Down welling infra-red radiation	W/m^2	
14 Defuse irradiance	W/m^2	
15 PAR	$\mu E/cm^2/sec$	

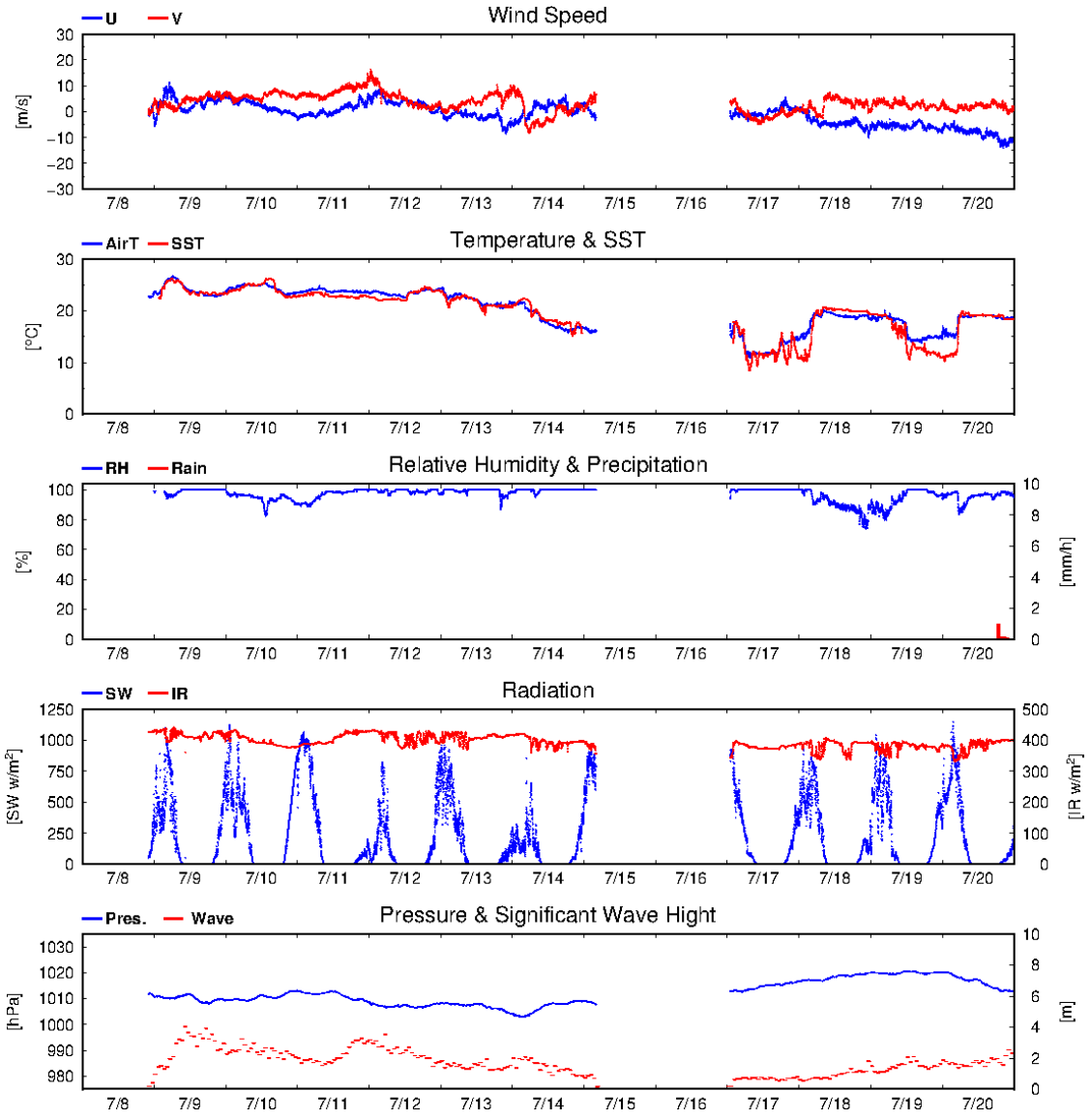

Fig. 2.3.1. Time series of surface meteorological parameters during the MR14-04 cruise.

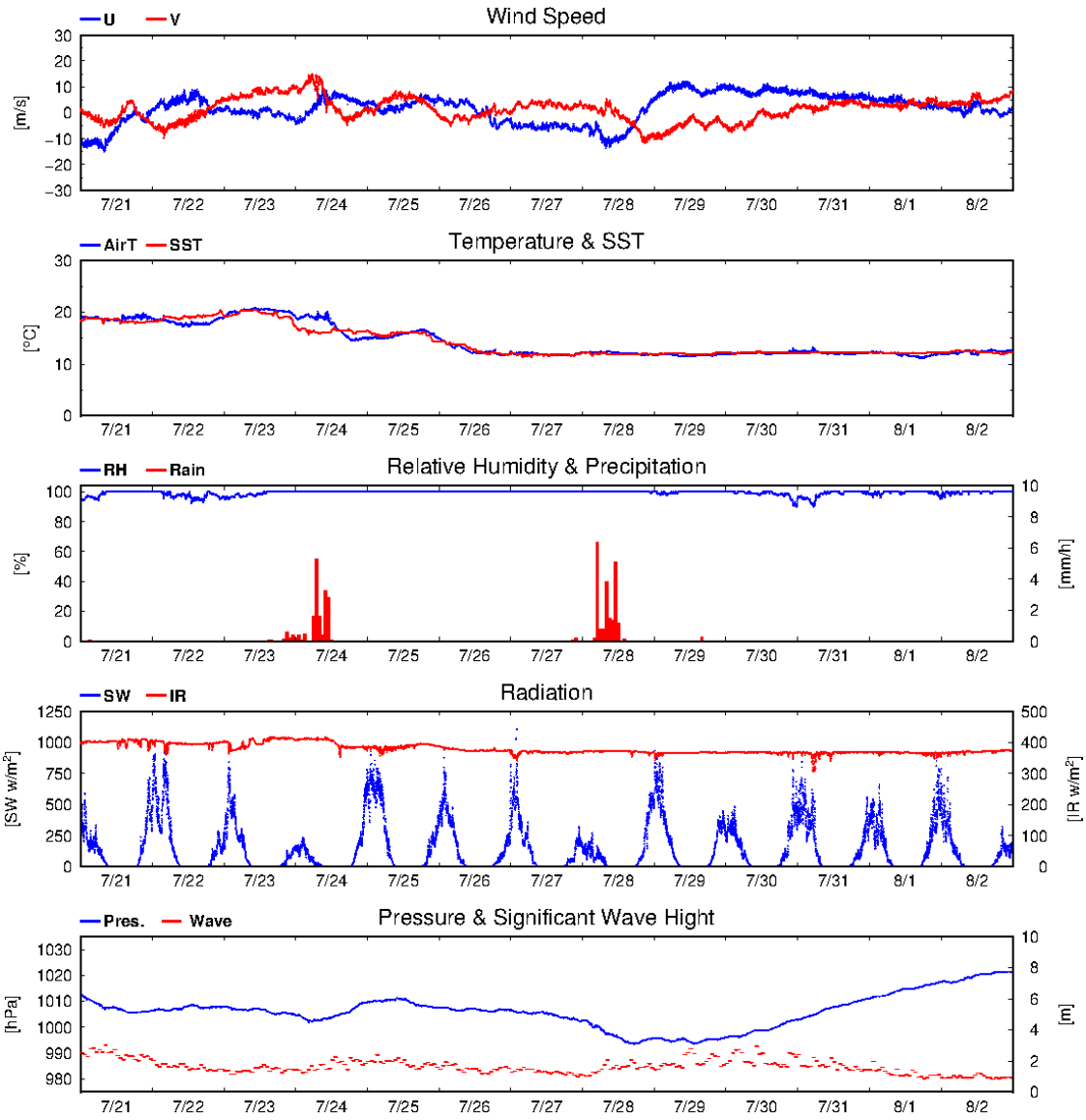

Fig. 2.3.1. (Continued)

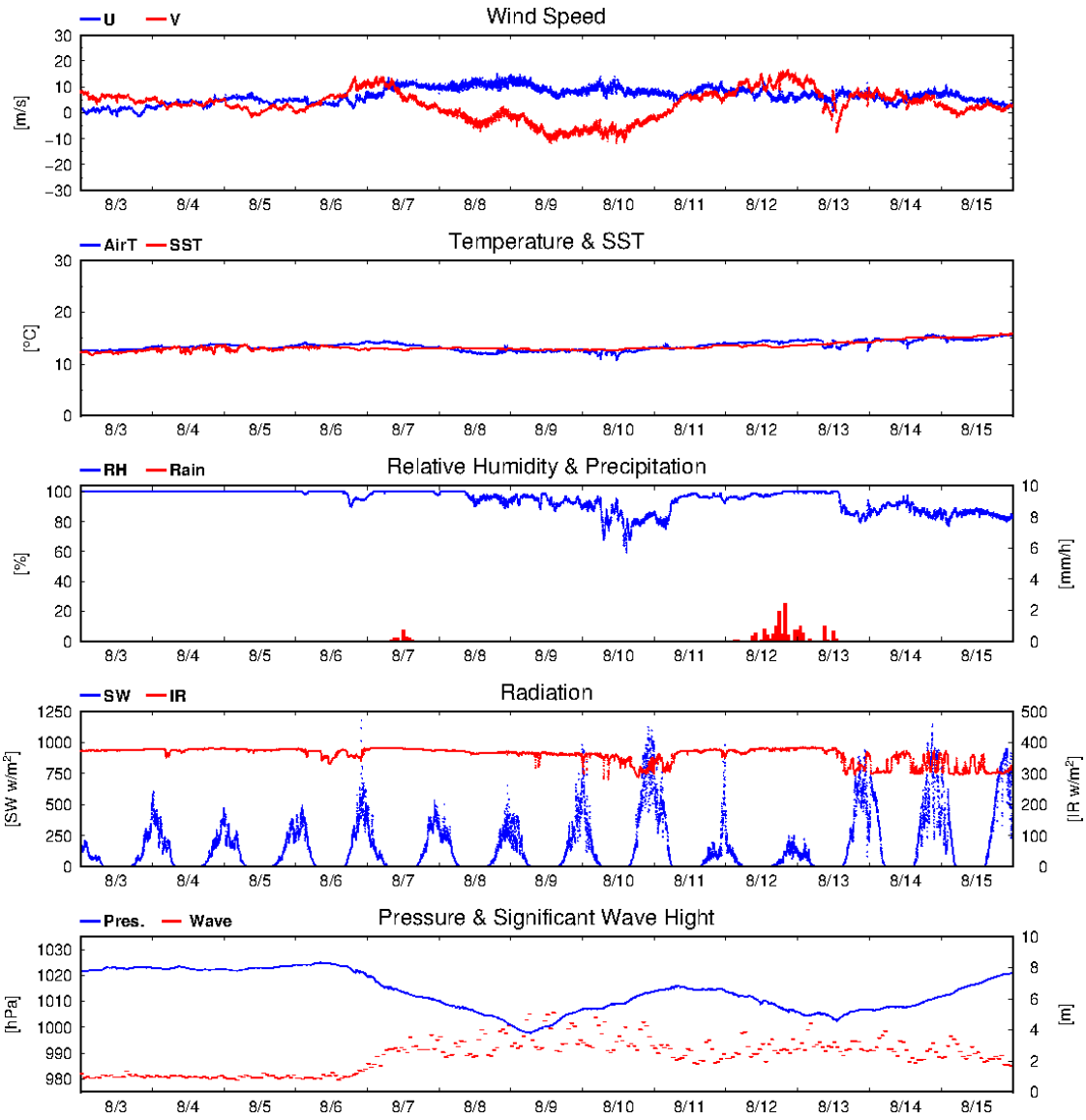

Fig. 2.3.1. (Continued)

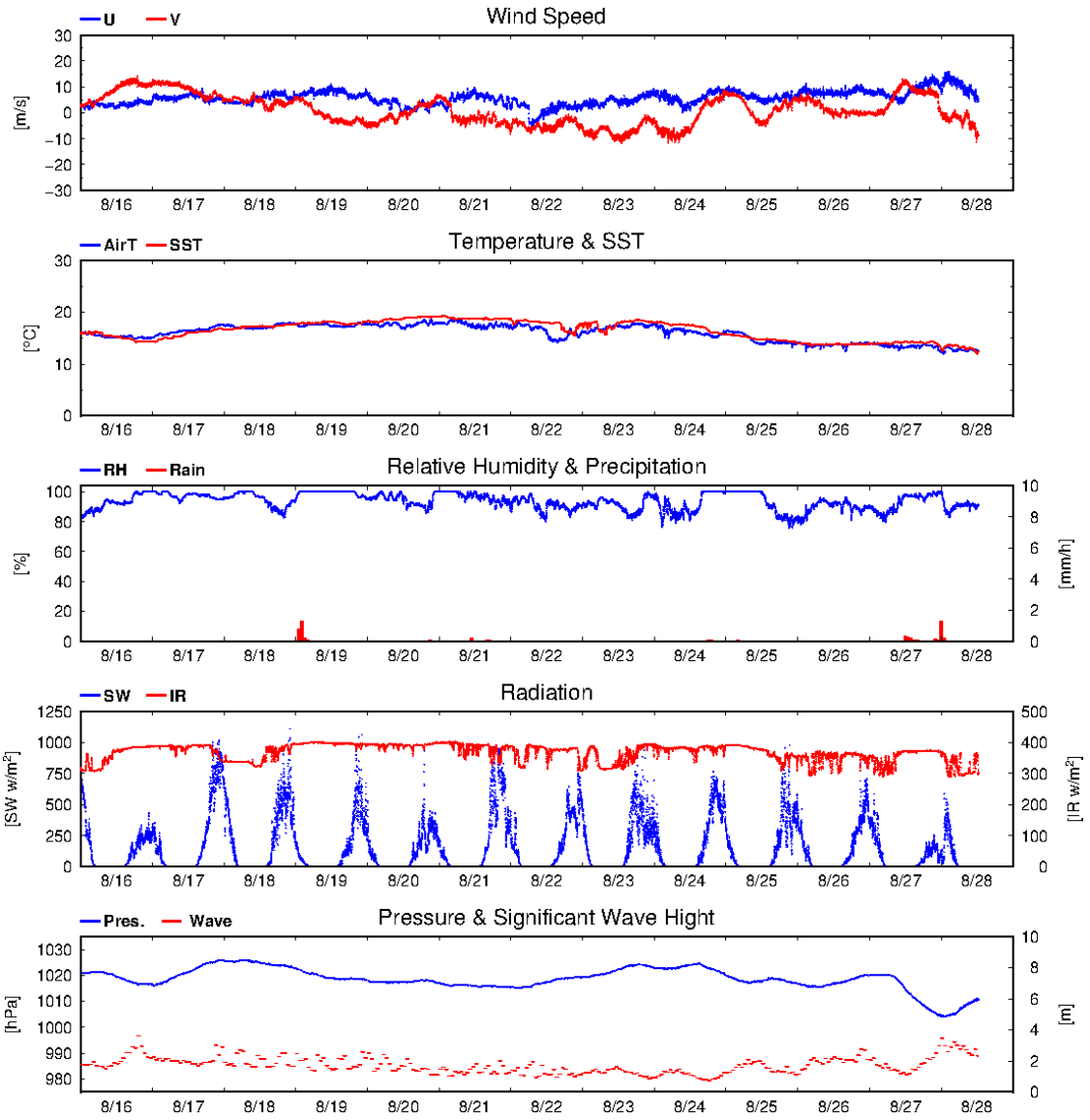

Fig. 2.3.1. (Continued)

2.4 Thermo-Salinograph and Related Measurements

September 25, 2014

(1) Personnel

Hiroshi Uchida (JAMSTEC)
Keitaro Matsumoto (MWJ)
Katsunori Sagishima (MWJ)
Haruka Tamada (MWJ)

(2) Objectives

The objective is to collect sea surface salinity, temperature, dissolved oxygen, fluorescence, and nitrate data continuously along the cruise track.

(3) Materials and methods

The Continuous Sea Surface Water Monitoring System (Marine Works Japan Co, Ltd.) has six sensors and automatically measures salinity, temperature, dissolved oxygen, and fluorescence in sea surface water every one minute. This system is located in the sea surface monitoring laboratory and connected to shipboard LAN system. Measured data along with time and location of the ship were displayed on a monitor and stored in a desktop computer. The sea surface water was continuously pumped up to the laboratory from about 5 m water depth and flowed into the system through a vinyl-chloride pipe. The flow rate of the surface seawater was controlled to be about 1.2 L/min. Periods of measurement, maintenance and problems are listed in Table 2.4.1.

A chemical-free nitrate sensor was also used with the Continuous Sea Surface Water Monitoring System in leg 2. The nitrate sensor was attached using a flow cell next to the thermo-salinograph.

Software and sensors used in this system are listed below.

i. Software

Seamoni-kun Ver.1.50

ii. Sensors

Temperature and conductivity sensor

Model:	SBE-45, SEA-BIRD ELECTRONICS, INC.
Serial number:	4552788-0319

Bottom of ship thermometer

Model:	SBE 38, SEA-BIRD ELECTRONICS, INC.
Serial number:	3852788-0457

Dissolved oxygen sensor

Model:	OPTODE 3835, Aanderaa Data Instruments, AS.
Serial number:	1519

Medel:	RINKO-II, JFE Advantech Co. Ltd.
Serial number:	0013

Fluorometer

Model: C3, TURNER DESIGNS

Serial number: 2300123

Nitrate sensor

Model: Deep SUNA, Satlantic, LP. (used only for leg 2)

Serial number: 0385

Table 2.4.1. Events of the Continuous Sea Surface Water Monitoring System operation.

System Date [UTC]	System Time [UTC]	Event
2014/07/09	02:32	Logging for leg 1 start
2014/07/14	23:30	Logging for leg 1 end
2014/07/17	02:50	Logging for leg 2 start
2014/07/28	23:52	Logging stop for filter cleaning
2014/07/29	00:48	Logging restart
2014/08/12	01:42	Logging stop for filter cleaning
2014/08/12	03:20	Logging restart
2014/08/22	02:27	Logging stop for filter cleaning
2014/08/22	03:27	Logging restart
2014/08/25	16:55	Logging stop for filter cleaning
2014/08/25	17:00	Logging restart
2014/08/28	12:29	Logging for leg 2 end

(4) Data Processing and Quality Control

The navigation data (latitude and longitude) for leg 2 was often invalid due to position fix error for loss of GPS satellites. The invalid navigation data were replaced by using the dataset "interpoGGA". The "interpoGGA" was made using all available navigation data and was interpolated on a time interval of 1 second and low-pass filtered with a window of 20 seconds.

Data from the Continuous Sea Surface Water Monitoring System were obtained at 1 minute intervals. Data from the nitrate sensor were obtained at 1 minute intervals until 2014/07/18 03:50. However, the nitrate sensor frequently continued to show invalid data (-1.0) and needed to restart the system. Therefore, the time interval was changed to 2 minutes since then.

These data were processed as follows. Spikes in the temperature and salinity data were removed using a median filter with a window of 3 scans (3 minutes) when difference between the original data and the median filtered data was larger than 0.1 ºC for temperature and 0.5 for salinity. Data gaps were linearly interpolated when the gap was ≤ 7 minutes. Fluorometer data were low-pass filtered using a median filter with a window of 3 scans (3 minutes) to remove spikes. Raw data from the RINKO oxygen sensor, fluorometer and nitrate data were low-pass filtered using a Hamming filter with a window of 15 scans (15 minutes).

Salinity (S [PSU]), dissolved oxygen (O [μmol/kg]), fluorescence (Fl [RFU]), and nitrate (NRA [μmol/kg]) data were corrected using the water sampled data. Details of the measurement methods are described in Sections 3.2, 3.4, 3.5, and 3.8 for salinity, dissolved oxygen, nitrate and chlorophyll-a, respectively. Corrected salinity (S_{cor}), dissolved oxygen (O_{cor}), estimated chlorophyll *a* (Chl-a), and nitrate (NRA_{cor}) were calculated from following equations

S_{cor} [PSU] = $c_0 + c_1 S + c_2 t$

O_{cor} [μmol/kg] = $c_0 + c_1 O + c_2 T + c_3 t$

Chl-a [μg/L] = $c_0 + c_1$ Fl

NRA_{cor} [μmol/kg] = NRA + $c_0 + c_1 t$

where S is practical salinity, t is days from a reference time (2014/07/09 02:32 [UTC]), T is temperature in ºC. The best fit sets of calibration coefficients (c_0~c_3) were determined by a least square technique to minimize the deviation from the water sampled data. The calibration coefficients were listed in Table 2.4.2. Comparisons between the Continuous Sea Surface Water Monitoring System data and water sampled data are shown in from Figs. 2.4.1 to 2.4.4.

For fluorometer data, water sampled data obtained at night [PAR (Photosynthetically Available Radiation) < 50 μE/(m^2 sec), see Section 2.3] were used for the calibration, since sensitivity of the fluorometer to chlorophyll *a* is different at nighttime and daytime (Section 2.4 in Uchida et al., 2015). Sensitivity of the fluorometer to chlorophyll *a* may be also different between high and low temperature. Therefore, slope (c_1) of the calibration coefficients was changed for temperature range (Table 2.4.3). For temperature between 20.5 ºC and 19.5 ºC, chlorophyll *a* was estimated from weighted mean of the two equations as

Chl-a = Chl-a_1 f_2 + Chl-a_2 f_1

f_1 = 1 – (TSG temperature + 19.5 ºC)

f_2 = 1 – f_1

where Chl-a1 is chlorophyll *a* calculated by using the set of coefficients A, and Chl-a_2 is chlorophyll *a* calculated by using the set of coefficients B (Table 2.4.2).

Noise of the nitrate data tended to become large over time (Fig. 2.4.4). Dismounting of the flow cell improved the data quality probably because the optical windows were wiped and cleaned by the O rings of the flow cell. Data affected by the large noise were flagged as questionable data (Fig. 2.4.4).

(5) Reference

Uchida, H., A. Murata, and T. Doi (2015): WHP P14S, S04I Revisit in 2012/2013 Data Book (in prep.).

Table 2.4.2. Calibration coefficients for the salinity, dissolved oxygen, chlorophyll *a*, and nitrate.

	c0	c1	c2	c3
Salinity				
	-8.026137e-02	1.002264	4.381446e-04	
Dissolved oxygen				
	5.929262	0.9575661	0.1590061	-5.164405e-02
Chlorophyll a				
	4.845356e-02	0.1030891 (A: for TSG temperature ≥ 20.5 ºC)		
	4.845356e-02	5.411620e-02 (B: for TSG temperature < 19.5 ºC)		
Nitrate				
	-23.140	2.7154355 (t ≤ 14.76)		
	14.304	0.2678845 (14.76 < t ≤ 34.0)		
	-29.419	1.044715855 (34.0 < t ≤ 44.0)		
	-46.856	1.044715855 (44.0 < t)		

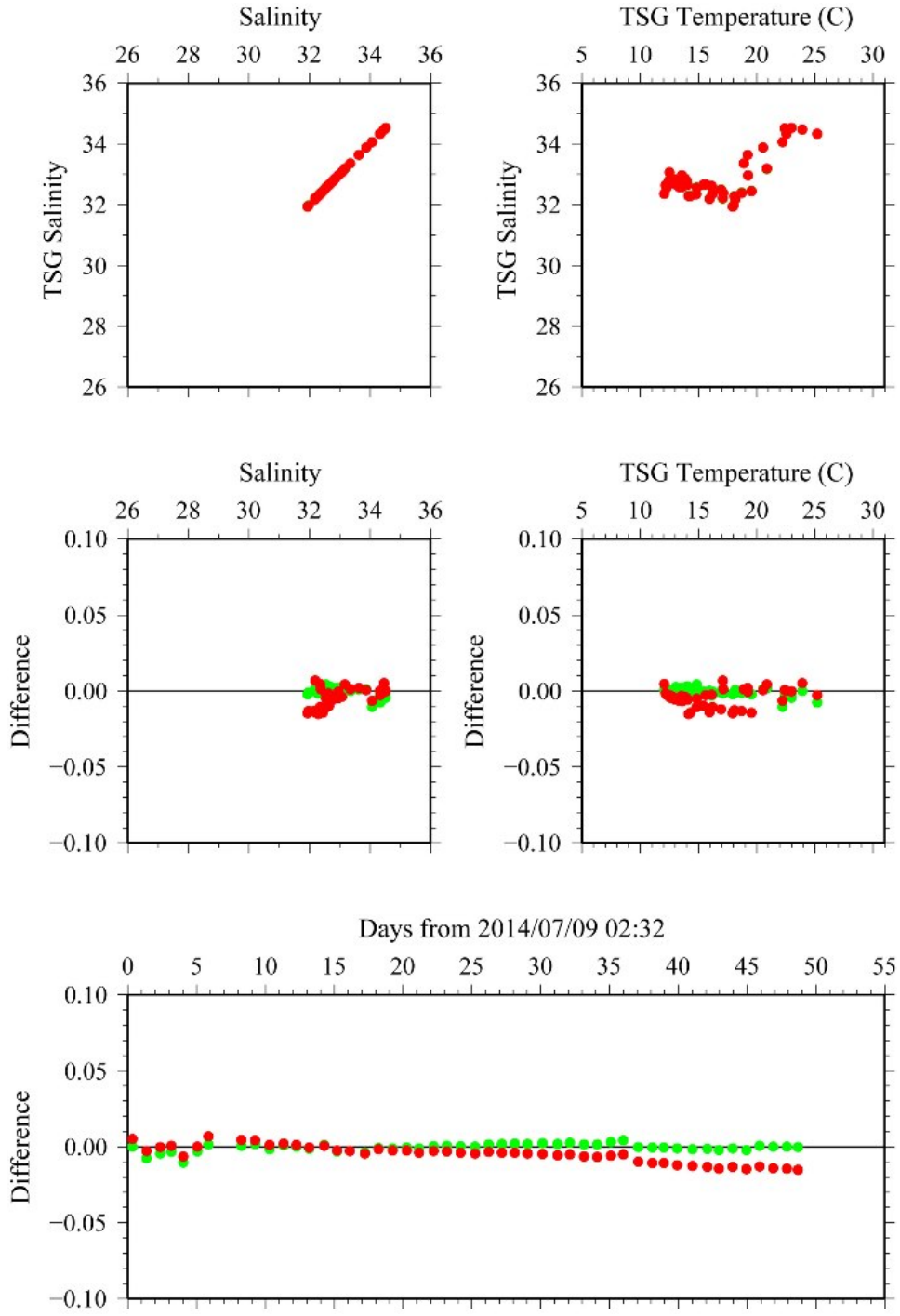

Figure 2.4.1. Comparison between TSG salinity (red: before correction, green: after correction) and sampled salinity.

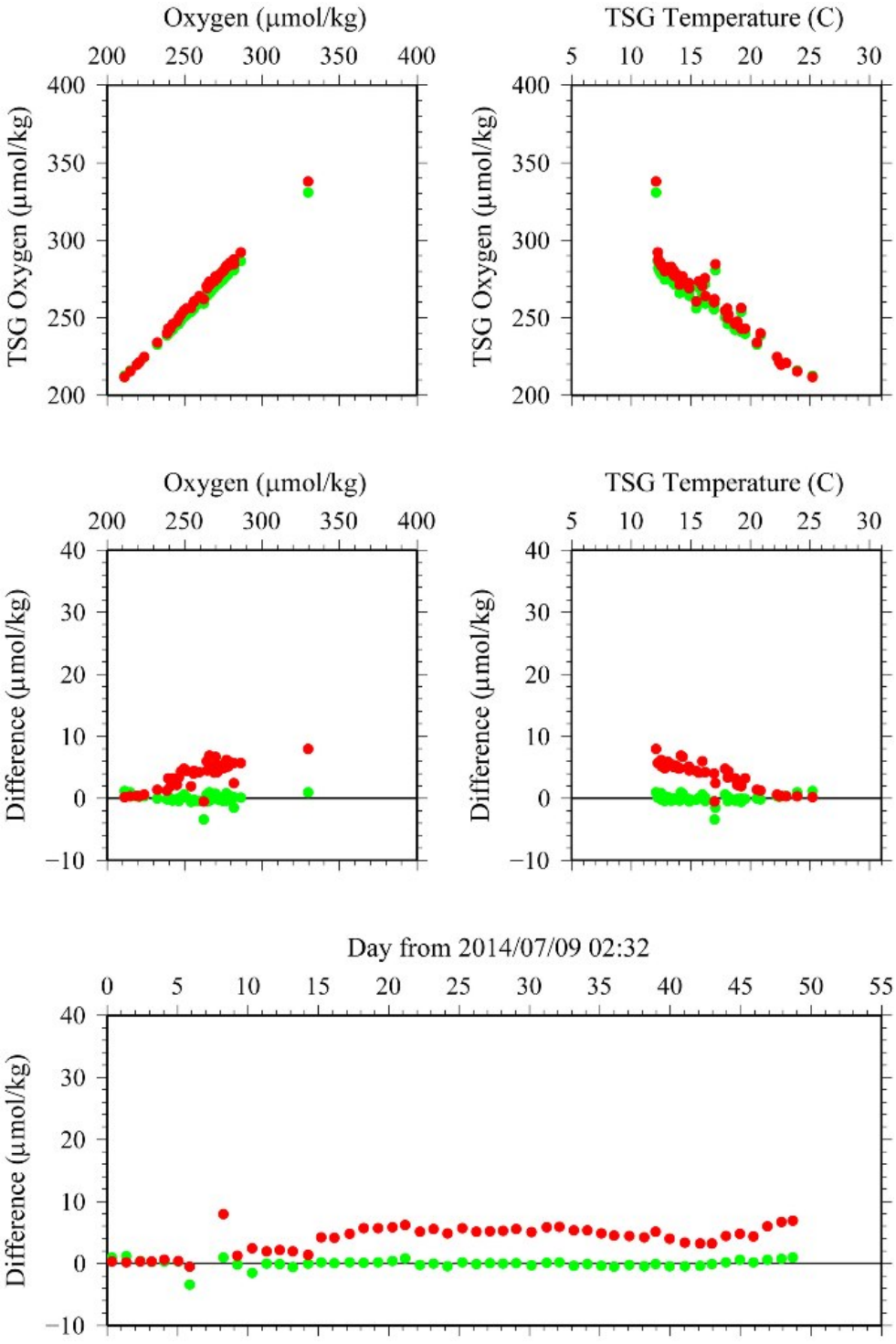

Figure 2.4.2. Comparison between TSG oxygen (red: before correction, green: after correction) and sampled oxygen.

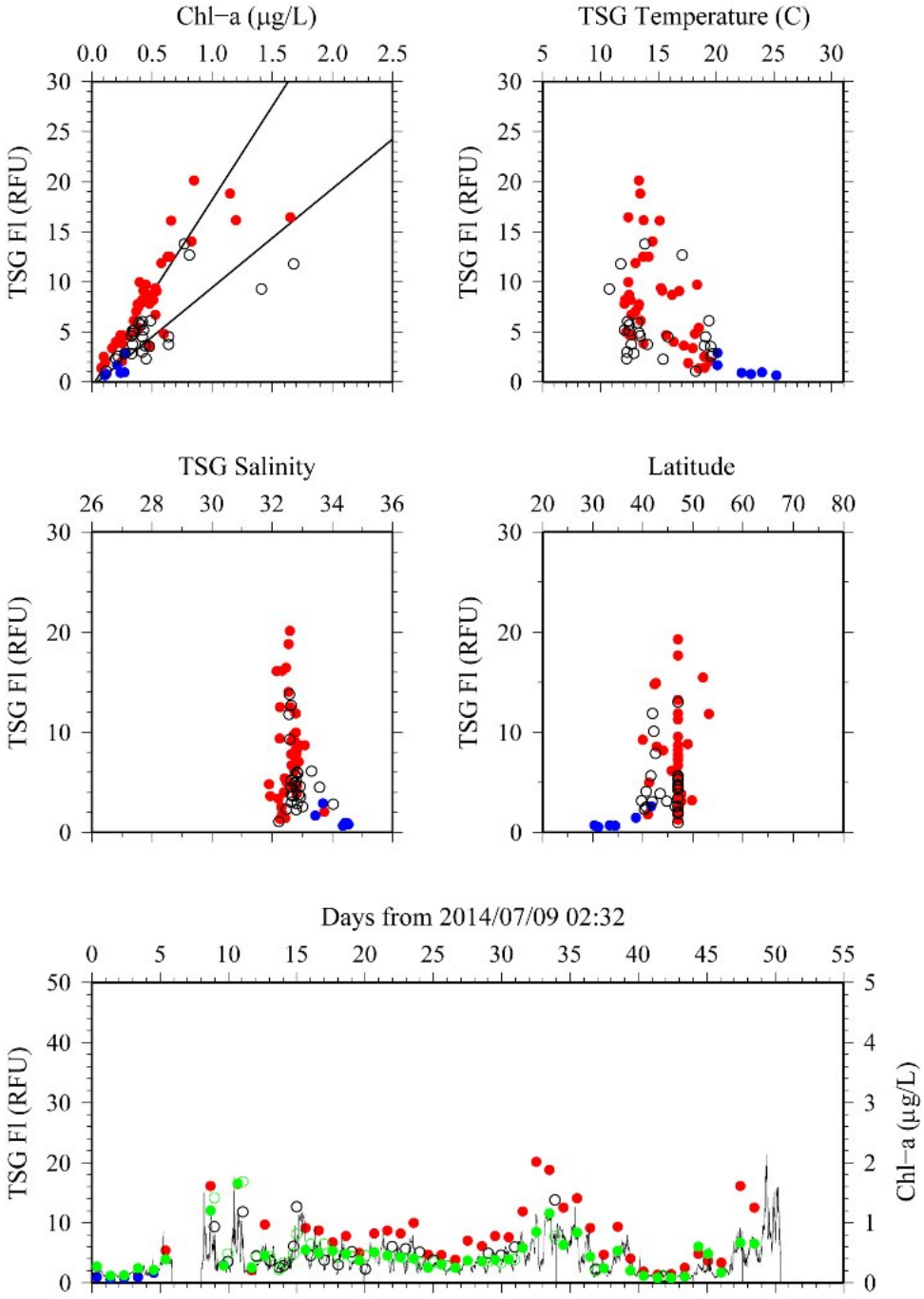

Figure 2.4.3. Comparison between TSG fluorescence and sampled chlorophyll *a*. Open circles indicate the daytime data. Blue dots indicate data obtained at temperature higher than or equal to 20 ºC and red dots indicate data obtained at temperature lower than 20 ºC. For bottom panel, blue or red dots indicate fluorescence and green dots indicate water sampled chlorophyll *a*. Line indicates chlorophyll *a* estimated from fluoremeter.

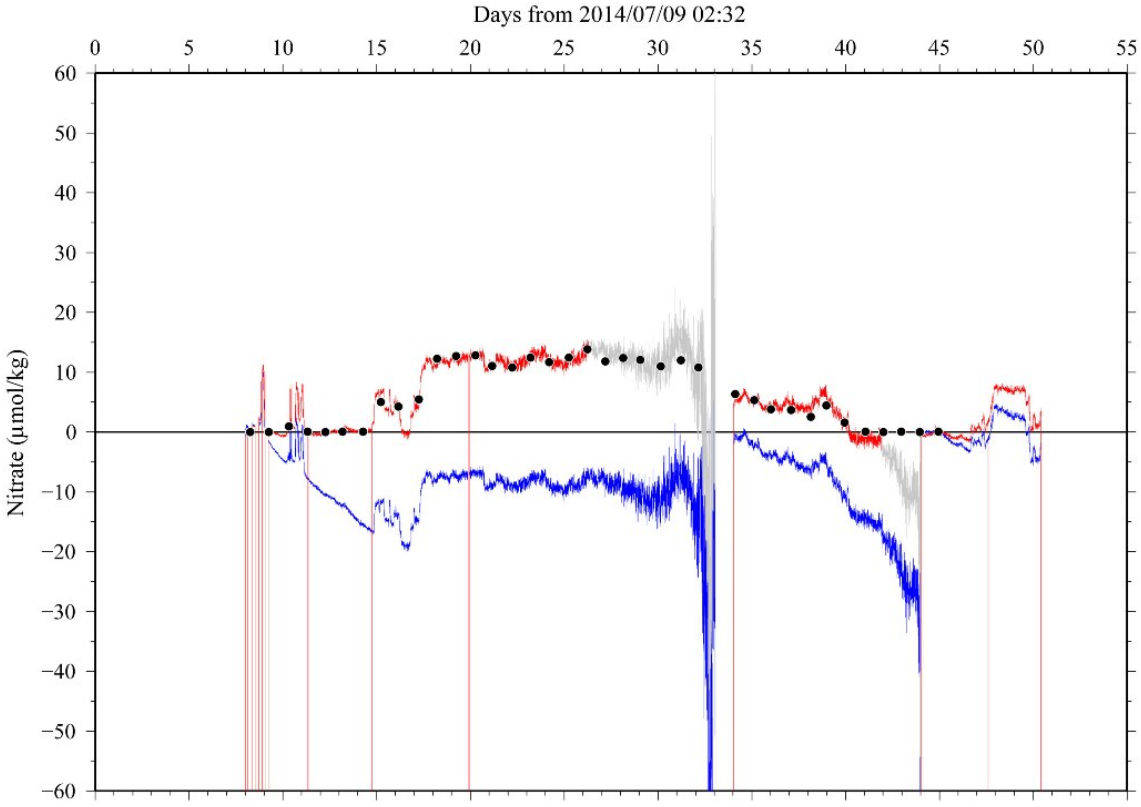

Figure 2.4.4. Comparison between TSG nitrate (blue line: before correction, red and gray lines: after correction) and sampled nitrate (dots). Gray lines indicate questionable data obtained during following periods: $26.3 < t \leq 34.0$ and $41.9 < t \leq 44.0$.

2.5 pCO_2

September 18, 2014

(1) Personnel

Akihiko Murata (JAMSTEC)
Atsushi Ono (MWJ)
Yoshiko Ishikawa (MWJ)

(2) Objective

Concentrations of CO_2 in the atmosphere are now increasing at a rate of about 2.0 ppmv y^{-1} owing to human activities such as burning of fossil fuels, deforestation, and cement production. It is an urgent task to estimate as accurately as possible the absorption capacity of the oceans against the increased atmospheric CO_2, and to clarify the mechanism of the CO_2 absorption, because the magnitude of the anticipated global warming depends on the levels of CO_2 in the atmosphere, and because the ocean currently absorbs 1/3 of the 6 Gt of carbon emitted into the atmosphere each year by human activities.

In this cruise, we were aimed at quantifying how much anthropogenic CO_2 absorbed in the surface ocean in the North Pacific. For the purpose, we measured pCO_2 (partial pressure of CO_2) in the atmosphere and surface seawater.

(3) Apparatus

Concentrations of CO_2 in the atmosphere and the sea surface were measured continuously during the cruise using an automated system with a non-dispersive infrared (NDIR) analyzer (Li-COR LI-7000). The automated system (Nippon ANS) was operated by about one and a half hour cycle. In one cycle, standard gasses, marine air and an air in a headspace of an equilibrator were analyzed subsequently. The nominal concentrations of the standard gas were 250, 300, 399 and 450 ppmv. The standard gases will be calibrated after the cruise.

The marine air taken from the bow was introduced into the NDIR by passing through a mass flow controller, which controlled the air flow rate at about 0.6 – 0.8 L/min, a cooling unit, a perma-pure dryer (GL Sciences Inc.) and a desiccant holder containing $Mg(ClO_4)_2$.

A fixed volume of the marine air taken from the bow was equilibrated with a stream of seawater that flowed at a rate of 4.0 – 5.0 L/min in the equilibrator. The air in the equilibrator was circulated with a pump at 0.7-0.8L/min in a closed loop passing through two cooling units, a perma-pure dryer (GL Science Inc.) and a desiccant holder containing $Mg(ClO_4)_2$.

(4) Results

Concentrations of CO_2 (xCO_2) of marine air and surface seawater are shown in Fig. 2.5.1, together with SST.

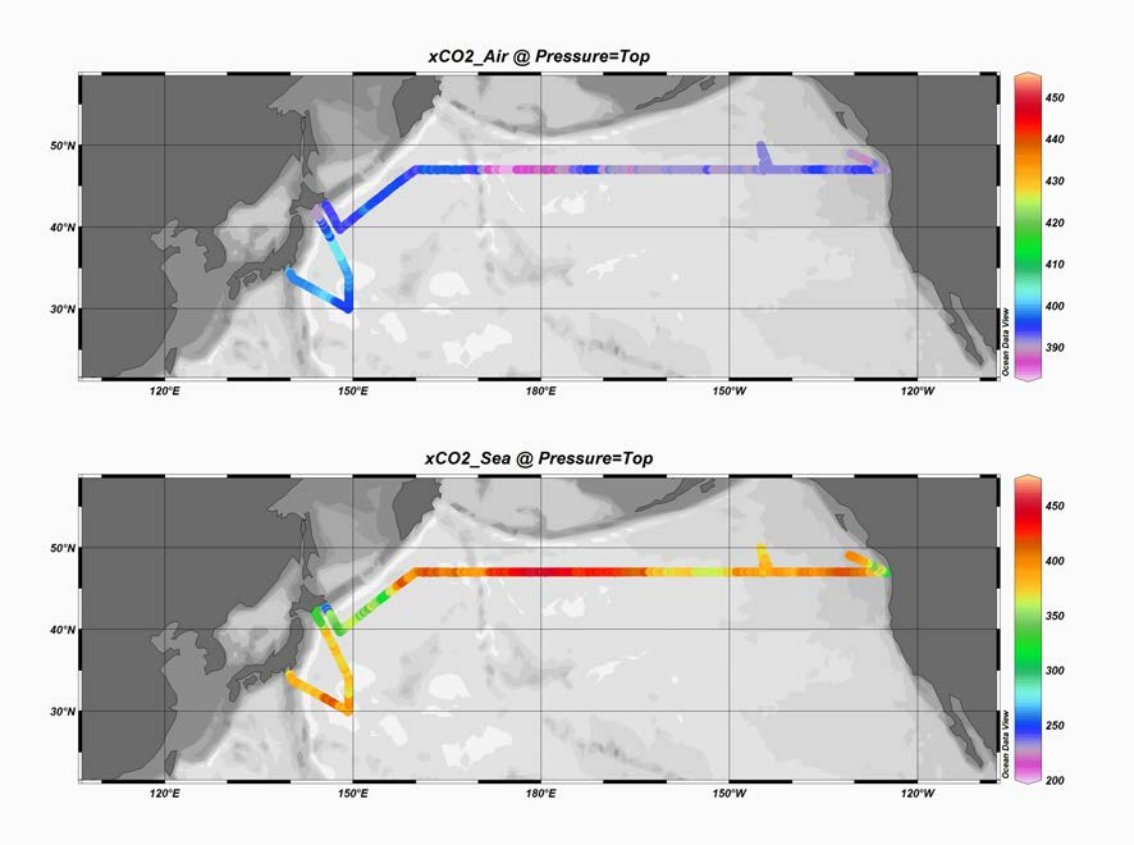

Fig. 2.5.1. Preliminary results of concentrations of CO_2 (xCO_2) in atmosphere (upper panel) and surface seawater (lower panel) observed during MR14-04.

2.6 Shipboard ADCP

September 16, 2014

(1) Personnel

Shinya Kouketsu	(JAMSTEC)	: Principal Investigator
Ryo Oyama	(Global Ocean Development Inc., GODI)	-leg1-
Souichiro Sueyoshi	(GODI)	-leg1-
Katsuhisa Maeno	(GODI)	-leg1-
Koichi Inagaki	(GODI)	-leg1-
Wataru Tokunaga	(GODI)	-leg2-
Kazuho Yoshida	(GODI)	-leg2-
Tetsuya Kai	(GODI)	-leg2-
Yutaro Murakami	(GODI)	-leg1, leg2-
Masanori Murakami	(MIRAI Crew)	-leg1, leg2-

(2) Objective

To obtain continuous measurement of the current profile along the ship's track.

(3) Methods

Upper ocean current measurements were made in the MR14-04 Leg1 and Leg2 cruises, using the hull-mounted Acoustic Doppler Current Profiler (ADCP) system. For most of its operation the instrument was configured for water-tracking mode. Bottom-tracking mode, interleaved bottom-ping with water-ping, was made to get the calibration data for evaluating transducer misalignment angle in the shallow water. The system consists of following components;

1) R/V MIRAI has installed vessel-mount ADCP (acoustic frequency 76.8 kHz "Ocean Surveyor", Teledyne RD Instruments). It has a phased-array transducer with single ceramic assembly and creates 4 acoustic beams electronically. We mounted the transducer head rotated to a ship-relative angle of 45 degrees azimuth from the keel.
2) For heading source, we use ship's gyro compass (TOKYO KEIKI, Japan), continuously providing heading to the ADCP system directory. Also we have Inertial Navigation System (PHINS, IXBLUE) which provide high-precision heading and attitude information are stored in ".N2R" data files.
3) DGPS system (Trimble SPS751 & StarFixXP) and GPS systems (Trimble 4000DS and FURUNO GP-36) providing position fixes. We selected the best system according to their positioning condition.
4) We used VmDas version 1.46.5 (TRDI) for data acquisition.
5) To synchronize time stamp of pinging with GPS time, the clock of the logging computer is adjusted to GPS time every 5 minutes.
6) The sound speed at the transducer does affect the vertical bin mapping and vertical velocity measurement, is calculated from temperature, salinity (constant value; 35.0 psu) and depth (6.5 m; transducer depth) by equation in Medwin (1975).

Data was configured for 8-m intervals starting 23-m below the surface. Every ping was recorded as raw ensemble data (.ENR). Also, 60 seconds and 300 seconds averaged data were recorded as short term average (.STA) and long term average (.LTA) data, respectively. Major parameters for the measurement (Direct Command) are shown in Table 2.6.1. After the cruises, we plan to carry out the alignment correction and

provide the processed data.

(4) Preliminary results

Fig.2.6.1 and 2.6.2 shows surface current profile along the ship's track, averaged four depth cells from 12th to 15th, about 110m to 135 m with 60 minutes average.

(5) Data archive

These data obtained in this cruise will be submitted to the Data Management Group (DMG) of JAMSTEC, and will be opened to the public via JAMSTEC home page.

(6) Remarks (Times in UTC)

i) Data acquisition was suspended in the territorial waters of USA.

ii) During the Leg1 cruise, background signal under sail was large due to biofouling on the ship bottom window.

iii) The following periods, data acquisition was suspended for system condition check.

Leg1: 23:29UTC 09 Jul. 2014 - 00:15UTC 10 Jul. 2014
05:55UTC 10 Jul. 2014 - 06:48UTC 10 Jul. 2014
03:42UTC 11 Jul. 2014 - 04:11UTC 11 Jul. 2014
11:13UTC 12 Jul. 2014 - 11:20UTC 12 Jul. 2014
00:42UTC 14 Jul. 2014 - 01:07UTC 14 Jul. 2014

iv) The following periods, navigation data was often invalid due to GPS position fix error.

Leg1: 14 Jul. to 15 Jul. 2014
Leg2: 17 Jul. to 16 Aug. 2014

Table 2.6.1. Major parameters

Bottom-Track Commands	
BP = 001	Pings per Ensemble (almost less than 1300m depth) Leg1: 22:32UTC 08 Jul. 2014 – 03:08UTC 09 Jul. 2014 16:44UTC 14 Jul. 2014 – 03:45UTC 14 Jul. 2014 Leg2: 00:07UTC 17 Jul. 2014 – 14:21UTC 17 Jul. 2014 14:49UTC 22 Aug. 2014 – 23:59UTC 22 Aug. 2014 11:57UTC 28 Aug. 2014 – 12:30UTC 28 Aug. 2014
Environmental Sensor Commands	
EA = +04500	Heading Alignment (1/100 deg)
EB = +00000	Heading Bias (1/100 deg)
ED = 00065	Transducer Depth (0 - 65535 dm)
EF = +001	Pitch/Roll Divisor/Multiplier (pos/neg) [1/99 - 99]
EH = 00000	Heading (1/100 deg)
ES = 35	Salinity (0-40 pp thousand)
EX = 00000	Coord Transform (Xform:Type; Tilts; 3Bm; Map)
EZ = 10200010	Sensor Source (C; D; H; P; R; S; T; U) C (1): Sound velocity calculates using ED, ES, ET (temp.) D (0): Manual ED H (2): External synchro P (0), R (0): Manual EP, ER (0 degree) S (0): Manual ES T (1): Internal transducer sensor U (0): Manual EU
Timing Commands	
TE = 00:00:02.00	Time per Ensemble (hrs:min:sec.sec/100)
TP = 00:02.00	Time per Ping (min:sec.sec/100)
Water-Track Commands	
WA = 255	False Target Threshold (Max) (0-255 count)
WB = 1	Mode 1 Bandwidth Control (0=Wid, 1=Med, 2=Nar)
WC = 120	Low Correlation Threshold (0-255)
WD = 111 100 000	Data Out (V; C; A; PG; St; Vsum; Vsum^2;#G;P0)
WE = 1000	Error Velocity Threshold (0-5000 mm/s)
WF = 0800	Blank After Transmit (cm)
WG = 001	Percent Good Minimum (0-100%)
WI = 0	Clip Data Past Bottom (0 = OFF, 1 = ON)
WJ = 1	Rcvr Gain Select (0 = Low, 1 = High)
WM = 1	Profiling Mode (1-8)
WN = 100	Number of depth cells (1-128)
WP = 00001	Pings per Ensemble (0-16384)
WS= 0800	Depth Cell Size (cm)
WT = 000	Transmit Length (cm) [0 = Bin Length]
WV = 0390	Mode 1 Ambiguity Velocity (cm/s radial)

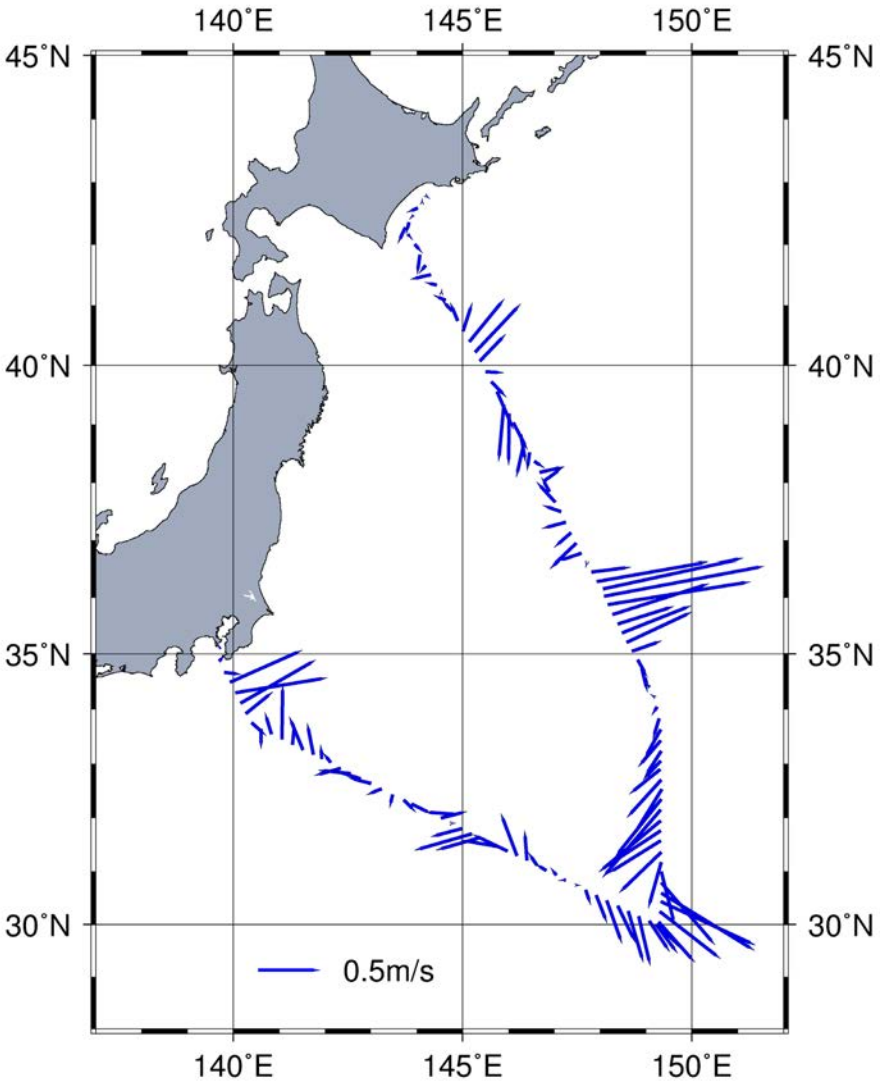

Fig 2.6.1. Current profile along the ship's track, about 110m to 136m depth, averaged every 60 minutes (Leg1).

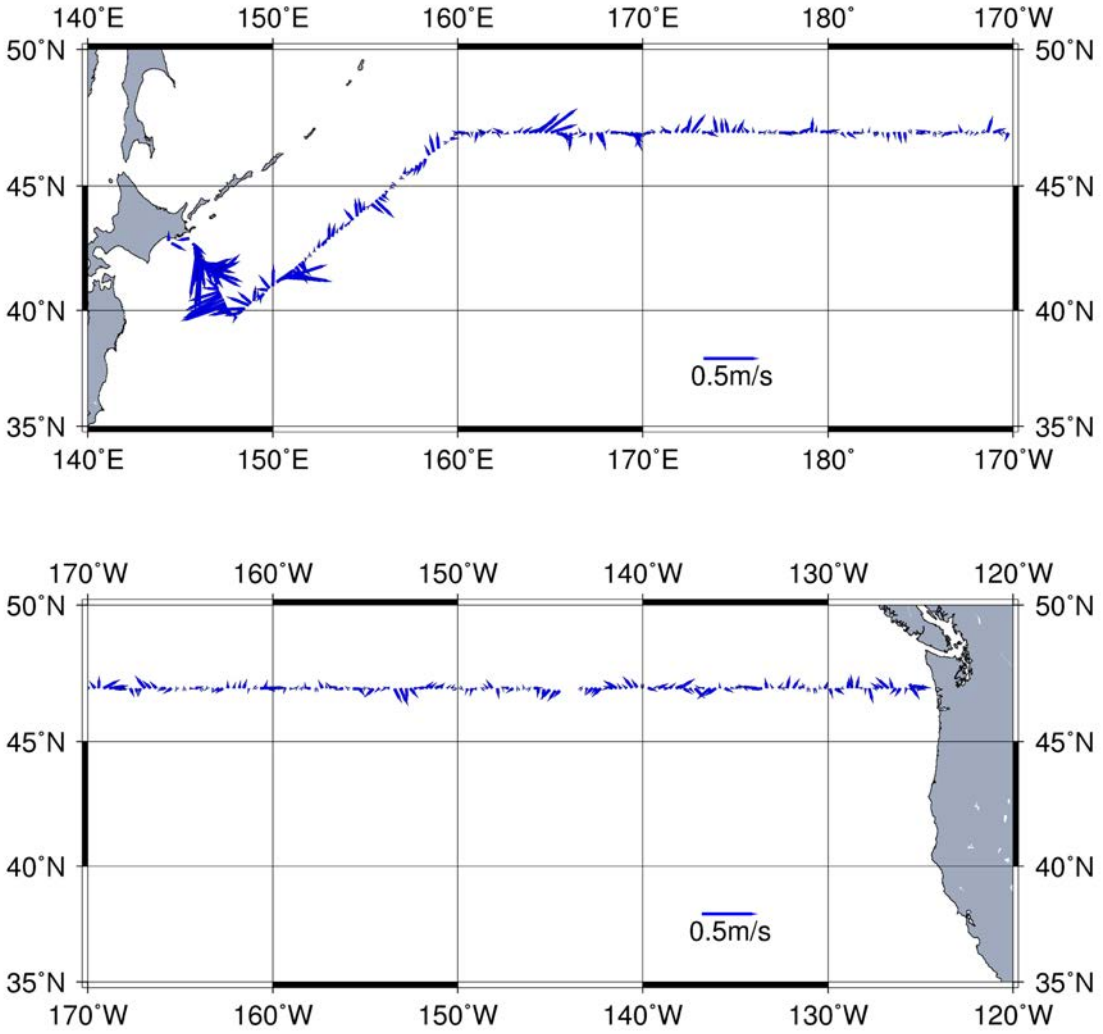

Fig 2.6.2. Current profile along the ship's track, about 110m to 135m, averaged every 60 minutes (Leg2).

2.7 XCTD

September 16, 2014

(1) Personnel

Hiroshi Uchida (JAMSTEC)
Ryo Oyama (GODI) (Leg 1)
Soichiro Sueyoshi (GODI) (Leg 1)
Katsuhisa Maeno (GODI) (Leg 1)
Koichi Inagaki (GODI) (Leg 1)
Yutaro Murakami (GODI) (Legs 1 and 2)
Wataru Tokunaga (GODI) (Leg 2)
Kazuho Yoshida (GODI) (Leg 2)
Tetsuya Kai (GODI) (Leg 2)

(2) Objectives

In this cruise, XCTD (eXpendable Conductivity, Temperature and Depth profiler) measurements were carried out to substitute for CTD measurements and to evaluate the fall rate equation and temperature by comparing with CTD (Conductivity, Temperature and Depth profiler) measurements.

(3) Instrument and Method

The XCTD used was XCTD-4 (Tsurumi-Seiki Co., Ltd., Yokohama, Kanagawa, Japan) with an MK-150N deck unit (Tsurumi-Seiki Co., Ltd.). The manufacturer's specifications are listed in Table 2.7.1. In this cruise, the XCTD probes were deployed by using 8-loading automatic launcher or hand launcher (Tsurumi-Seiki Co., Ltd.). For comparison with CTD, XCTD was deployed at about 10 minutes after the beginning of the down cast of the CTD (P10N_1, P10N_7, P10N_14, P10N_30, P01_77, P01_78, P01_80 and P01_81).

The fall-rate equation provided by the manufacturer was initially used to infer depth Z (m), $Z = at - bt^2$, where t is the elapsed time in seconds from probe entry into the water, and a (terminal velocity) and b (acceleration) are the empirical coefficients (Table 2.7.2).

(4) Data Processing and Quality Control

The XCTD data were processed and quality controlled based on a method by Uchida et al. (2011). Differences between XCTD and CTD depths were shown in Fig. 2.7.1. The terminal velocity error was estimated for the XCTD-4 (Table 2.7.2). The XCTD data were corrected for the depth error by using the estimated terminal velocities. Differences of temperature on pressure surfaces were examined by using side-by-side XCTD and CTD data (Fig. 2.7.2). The XCTD data used were corrected for the depth error. Average thermal bias below 900 dbar was 0.011 °C. Mean of the thermal biases of XCTD data estimated from five cruises was 0.014 ± 0.004 °C (Table 2.7.3). The XCTD data were corrected for the mean thermal bias (0.014 °C). Differences of salinity on pressure surfaces were examined by using side-by-side XCTD and CTD data (Fig. 2.7.3). The XCTD data used were corrected for the depth error and thermal bias. Average salinity bias was 0.013 ± 0.007 (Table 2.7.4). The XCTD data were corrected for the salinity bias. Temperature-salinity plot using the quality controlled XCTD data is shown in Fig. 2.7.4.

(5) References

Kizu, S., H. Onishi, T. Suga, K. Hanawa, T. Watanabe, and H. Iwamiya (2008): Evaluation of the fall rates of

the present and developmental XCTDs. *Deep-Sea Res I*, **55**, 571–586.
Uchida, H., K. Shimada, and T. Kawano (2011): A method for data processing to obtain high-quality XCTD data. *J. Atmos. Oceanic Technol.*, **28**, 816–826.
Uchida, H., A. Murata, and T. Doi (eds.) (2014): WHP P10 Revisit in 2011 Data Book, 179 pp., JAMSTEC.
Uchida, H., A. Murata, and T. Doi (eds.) (2015): WHP P14S, S04I Revisit in 2012/2013 Data Book (in prep.)

Table 2.7.1. Manufacturer's specifications of XCTD-4.

Parameter	Range	Accuracy
Conductivity	0 ~ 60 mS cm^{-1}	±0.03 mS cm^{-1}
Temperature	–2 ~ 35 °C	±0.02 °C
Depth	0 ~ 1850 m	5 m or 2%, whichever is greater *

* Depth error is shown in Kizu et al (2008).

Table 2.7.2. Manufacturer's coefficients for the fall-rate equation.

Model	*a* (terminal velocity, m/s)	*b* (acceleration, m/s^2)	*e* (terminal velocity error, m/s)
XCTD-4	3.68081	0.00047	–0.0075

Table 2.7.3. Thermal biases of the XCTD temperature data.

Cruise	Average thermal bias (°C)	Depth range	Source
MR09-01	0.016	>= 1100 dbar	Uchida et al. (2011)
KH-02-3	0.019	>= 1100 dbar	Uchida et al. (2011)
MR11-08	0.014	>= 1100 dbar	Uchida et al. (2014)
MR12-05	0.009	>= 400 dbar	Uchida et al. (2015)
MR14-04	0.011	>= 900 dbar	This report
Mean	0.014 ± 0.004		

Table 2.7.4. Salinity bias of the XCTD data.

Cruise	Average salinity bias (°C)	Data
MR14-04	0.013 ± 0.007	Stations 1, 7, 14, 30, 77, 78, 80, 81

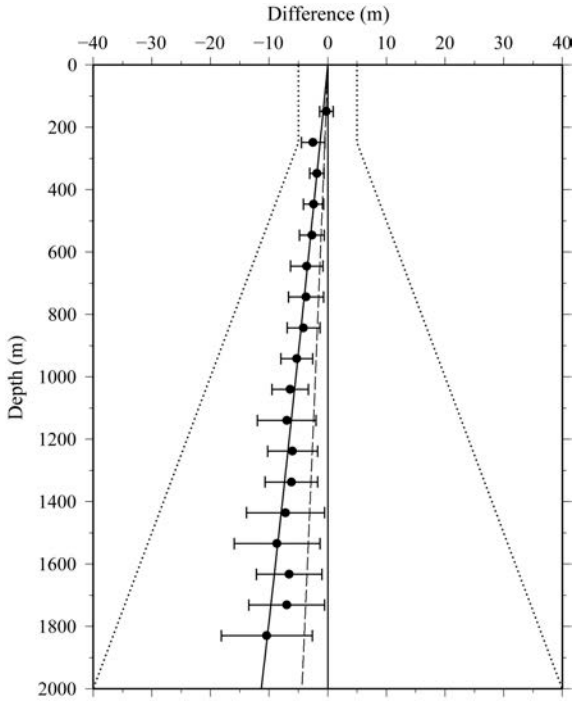

Figure 2.7.1. Differences between XCTD and CTD depths for XCTD-4. Differences were estimated with the same method as Uchida et al. (2011). Standard deviation of the estimates (horizontal bars) and the manufacturer's specification for XCTD depth error (dotted lines) are shown. The regressions for the data (solid line) and for the data obtained in the cruise MR12-05 (broken line) are also shown.

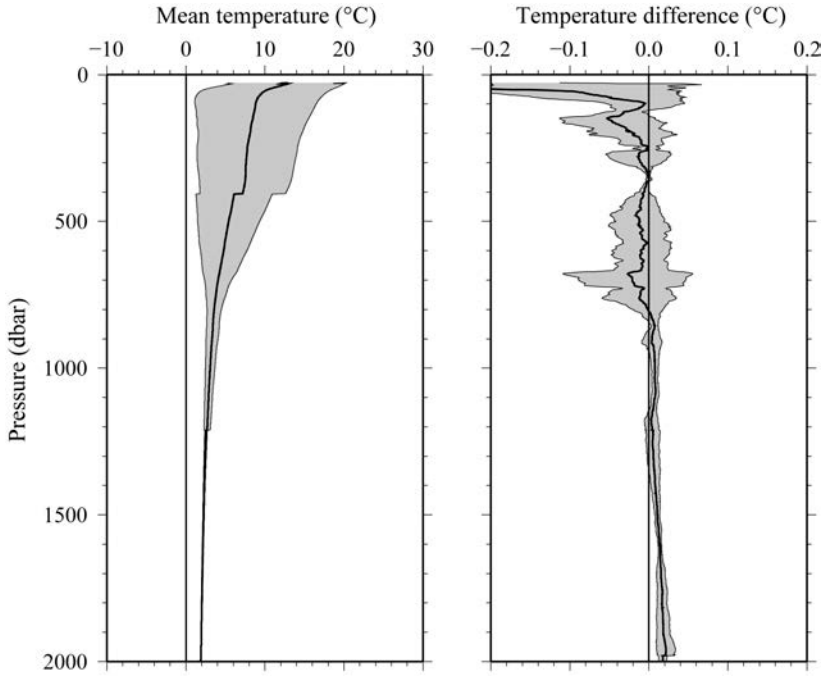

Figure 2.7.2. Comparison between XCTD and CTD temperature profiles. (a) Mean temperature of CTD profiles with standard deviation (shade) and (b) mean temperature difference with standard deviation (shade) between the XCTD and CTD. Mean profiles were low-pass filtered by a running mean with a window of 51 dbar.

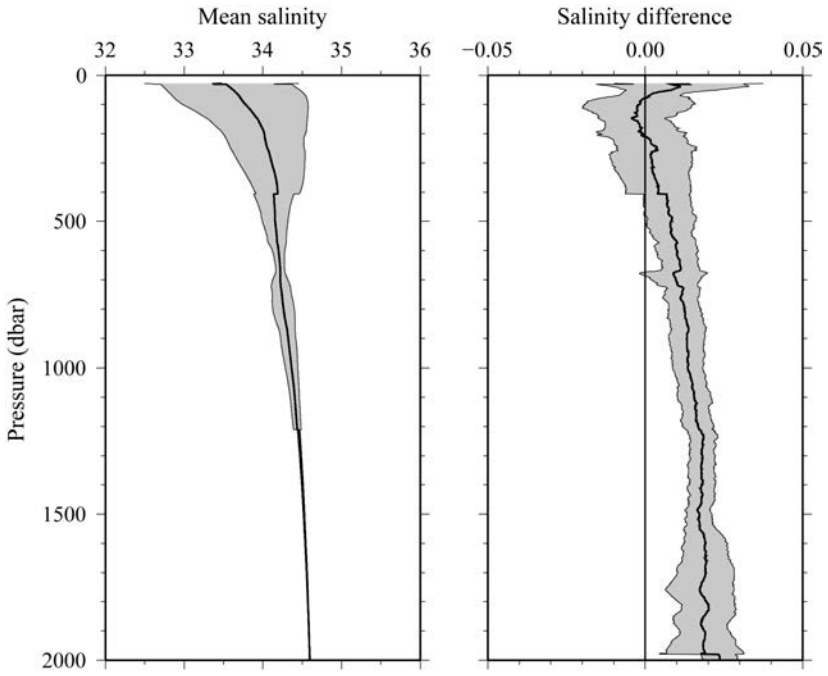

Figure 2.7.3. Comparison between XCTD and CTD salinity profiles. (a) Mean salinity of CTD profiles with standard deviation (shade) and (b) mean salinity difference with standard deviation (shade) between the XCTD and CTD. Mean profiles were low-pass filtered by a running mean with a window of 51 dbar.

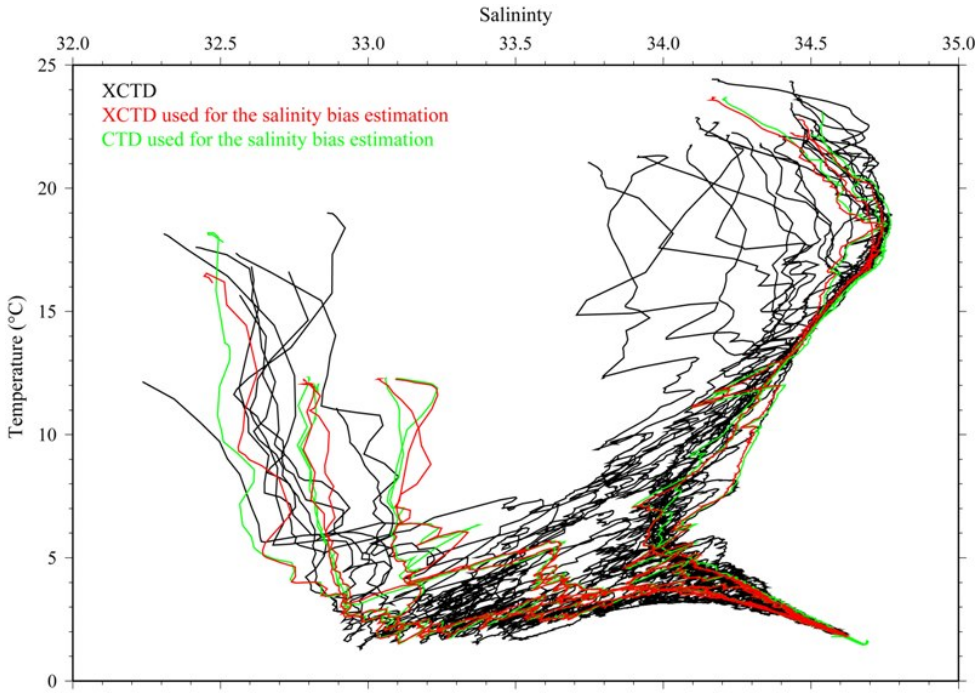

Figure 2.7.3. Comparison of temperature-salinity profiles of CTD (green lines) data used for the XCTD salinity bias estimation and salinity bias-corrected XCTD (red and black lines) data.

2.8 Imaging Flow Cytometory

September 25, 2014

(1) Personnel

Hiroshi Uchida (JAMSTEC)
Tetsuichi Fujiki (JAMSTEC) (not on board)
Kosei Sasaoka (JAMSTEC)
Keitaro Matsumoto (MWJ)

(2) Objectives

The objective is to examine the abundance and size structure of the plankton community and their geographical distribution.

(3) Materials and methods

The Flow Cytometer And Microscope (FlowCAM, Fluid Imaging Technologies, Scarborough, Maine, USA) collects an image and provides an in-depth characterization of whole data populations, sub-populations, and even individual particles. The FlowCAM imaging particle analysis system contains three core technologies: optics, electronics and fluidics. The fluidics system uses an ultra-high precision computer controlled syringe pump to pull the fluid sample through a flow cell perpendicular to the optical path. The optical system is similar to a microscope, and is used to capture real-time images of the particles in the fluid as they pass through the flow cell. Additional optical electronics can also capture two channels of fluorescence information per particle.

The FlowCAM used in this cruise was VS series (portable model, serial number: 649). The camera magnification was 40 (particle size range of 30 – 300 μm). The water sample to be analyzed was taken from sea surface water pumped from about 5 m water depth (see Section 2.4) or bucket sampling from sea surface (0 m). The water samples were pre-filtered through a mesh of 200 μm and filled in one to four sample bottles (1 L). Then the water samples were concentrated by reverse filtration with a mesh of 20 μm. The fluorescence-triggered and side-scatter-triggered modes, which takes images only when a particle matching a triggering criterion is the presence of fluorescent particles or the scatter of light due to any kind of particles, were used.

The samples analyzed were listed in Table 2.8.1 and an example of obtained images was shown in Fig. 2.8.1.

Table 2.8.1. List of samples and their concentration rate (R) and analysis volume.

Date	Time	Latitude	Longitude	Note
2014/ 7/ 9	11:07 UTC	33º 23.04’ N	141º 14.01’ E	R=111 (5ml)x2
2014/ 7/ 10	11:07 UTC	31º 8.07’ N	146º 34.83’ E	R=95 (5ml)x2
2014/ 7/ 11	11:21 UTC	30º 22.91’ N	149º 19.14’ E	R=87 (5ml)x3
2014/ 7/ 12	11:35 UTC	34º 29.42’ N	149º 1.57’ E	R=95 (5ml)
2014/ 7/ 13	15:09 UTC	38º 40.44’ N	146º 20.14’ E	R=78 (5ml)
2014/ 7/ 14	Station 036 bucket sampling			R=127 (5ml)
2014/ 7/ 14	12:36 UTC	41º 14.9’ N	144º 30.49’ E	R=63 (5ml)
2014/ 7/ 17	19:01 UTC	42º 38.39’ N	145º 42.08’ E	R=39 (5ml) R=83 (5ml)

2014/	7/	18	18:04	UTC	41º	42.68’	N	146º	25.23’	E	R=73 (5ml)
2014/	7/	19	18:43	UTC	42º	19.77’	N	146º	0.57’	E	R=68 (5ml)
2014/	7/	20	19:40	UTC	40º	59.78’	N	146º	58.11’	E	R=82 (5ml)
2014/	7/	21	18:46	UTC	39º	59.62’	N	147º	40.28’	E	R=1 (5ml) R=1 (10ml)
2014/	7/	22	19:40	UTC	40º	19.37’	N	148º	52.23’	E	R=54 (10ml) R=39 (10ml)
2014/	7/	23	3:34	UTC	40º	37.33’	N	149º	24.33’	E	R=58 (10ml)
2014/	7/	23	21:09	UTC	41º	33.41’	N	150º	53.72’	E	R=1 (10ml)x3 R=2 (10ml) R=10 (10ml)
2014/	7/	24	2:46	UTC	41º	56.29’	N	151º	28.72’	E	R=2 (10ml)x3 R=4 (10ml)
2014/	7/	24	18:09	UTC	42º	46.67’	N	152º	51.62’	E	R=2 (10ml)x3 R=4 (10ml)
2014/	7/	25	3:18	UTC	43º	29.55’	N	154º	3.25’	E	R=10 (10ml)
2014/	7/	25	17:19	UTC	44º	5.06’	N	155º	1.29’	E	R=10 (10ml)
2014/	7/	26	2:58	UTC	44º	46.12’	N	156º	6.67’	E	R=10 (10ml)
2014/	7/	26	17:59	UTC	45º	45.81’	N	157º	48.68’	E	R=20 (10ml) R=100 (10ml)
2014/	7/	27	3:08	UTC	46º	28.4’	N	159º	4.46’	E	R=100 (10ml)
2014/	7/	27	16:58	UTC	47º	2.16’	N	160º	0.66’	E	R=100 (10ml)
2014/	7/	28	3:25	UTC	46º	58.04’	N	161º	27.14’	E	R=50 (10ml) R=100 (10ml)
2014/	7/	28	16:59	UTC	47º	0.21’	N	161º	11.35’	E	R=100 (10ml)
2014/	7/	29	3:23	UTC	46º	59.81’	N	161º	34.47’	E	R=200 (10ml)
2014/	7/	29	18:49	UTC	46º	59.59’	N	163º	48.08’	E	R=200 (10ml)
2014/	7/	30	17:37	UTC	46º	58.38’	N	166º	44.85’	E	R=200 (10ml)
2014/	7/	31	2:23	UTC	46º	59.75’	N	167º	49.93’	E	R=200 (10ml)
2014/	7/	31	16:33	UTC	46º	59.89’	N	169º	4.23’	E	R=200 (10ml)
2014/	8/	1	2:13	UTC	46º	59.04’	N	169º	34.46’	E	R=200 (10ml)
2014/	8/	1	15:52	UTC	46º	59.75’	N	170º	28.42’	E	R=200 (10ml)
2014/	8/	2	2:39	UTC	46º	59.82’	N	171º	37.2’	E	R=200 (10ml)
2014/	8/	2	17:08	UTC	47º	0.36’	N	173º	50.17’	E	R=200 (10ml)
2014/	8/	3	2:03	UTC	47º	0.43’	N	174º	46.81’	E	R=200 (10ml)
2014/	8/	3	16:43	UTC	47º	0.04’	N	176º	47.67’	E	R=200 (10ml)
2014/	8/	4	2:23	UTC	46º	59.85’	N	178º	17.87’	E	R=200 (5ml)
2014/	8/	4	16:39	UTC	46º	59.8’	N	179º	28.27’	W	R=200 (10ml)
2014/	8/	5	14:55	UTC	47º	0.73’	N	176º	18.11’	W	R=200 (10ml)
2014/	8/	6	16:01	UTC	46º	59.77’	N	173º	44.14’	W	R=200 (10ml)
2014/	8/	7	2:52	UTC	46º	59.27’	N	173º	45.3’	W	R=200 (10ml)
2014/	8/	7	15:11	UTC	46º	59.69’	N	173º	6.03’	W	R=200 (10ml)
2014/	8/	8	1:26	UTC	47º	0.51’	N	171º	33.53’	W	R=200 (10ml)
2014/	8/	8	14:57	UTC	46º	59.9’	N	169º	28.27’	W	R=200 (10ml)
2014/	8/	9	1:31	UTC	46º	59.59’	N	168º	12.43’	W	R=200 (10ml)

2014/	8/	9	15:29	UTC	47º	0.59’	N	165º	58.99’	W	R=200 (10ml)
2014/	8/	10	15:05	UTC	47º	0.23’	N	162º	37.2’	W	R=200 (10ml)
2014/	8/	11	14:08	UTC	46º	59.22’	N	159º	15.29’	W	R=200 (10ml)
2014/	8/	12	0:22	UTC	46º	59.7’	N	158º	8.06’	W	R=200 (10ml)
2014/	8/	12	14:41	UTC	46º	59.88’	N	156º	0.35’	W	R=200 (10ml)
2014/	8/	13	14:40	UTC	46º	59.25’	N	152º	31.73’	W	R=200 (10ml)
2014/	8/	14	13:42	UTC	46º	59.43’	N	149º	8.63’	W	R=200 (10ml)
2014/	8/	14	23:23	UTC	47º	0.47’	N	148º	2.29’	W	R=200 (10ml)
2014/	8/	15	13:51	UTC	46º	59.63’	N	145º	48.41’	W	R=200 (10ml)
2014/	8/	16	14:08	UTC	48º	57.88’	N	144º	48.62’	W	R=200 (10ml)
2014/	8/	16	Station 151 bucket sampling								R=200 (10ml)
2014/	8/	17	12:56	UTC	47º	43.81’	N	143º	51.14’	W	R=200 (10ml)
2014/	8/	18	11:50	UTC	47º	0.72’	N	140º	43.57’	W	R=200 (5ml)
2014/	8/	19	12:12	UTC	46º	59.53’	N	136º	51.2’	W	R=200 (10ml)
2014/	8/	19	22:21	UTC	47º	0.56’	N	135º	22.98’	W	R=200 (10ml)
2014/	8/	20	12:07	UTC	46º	59.73’	N	132º	55.61’	W	R=200 (10ml)
2014/	8/	21	12:12	UTC	46º	59.77’	N	129º	22.94’	W	R=200 (10ml)
2014/	8/	22	11:56	UTC	47º	0.21’	N	126º	0.22’	W	R=200 (5ml)
2014/	8/	22	Station 149 bucket sampling								R=100 (10ml)
2014/	8/	24	4:25	UTC	49º	47.36’	N	133º	12.26’	W	R=100 (10ml) R=100 (10ml)
2014/	8/	25	13:26	UTC	51º	59.81’	N	142º	34.26’	W	R=200 (10ml)
2014/	8/	26	14:19	UTC	53º	13.33’	N	149º	42.55’	W	R=200 (10ml)
2014/	8/	28	12:27	UTC	54º	5.95’	N	162º	18.75’	W	R=100 (10ml)

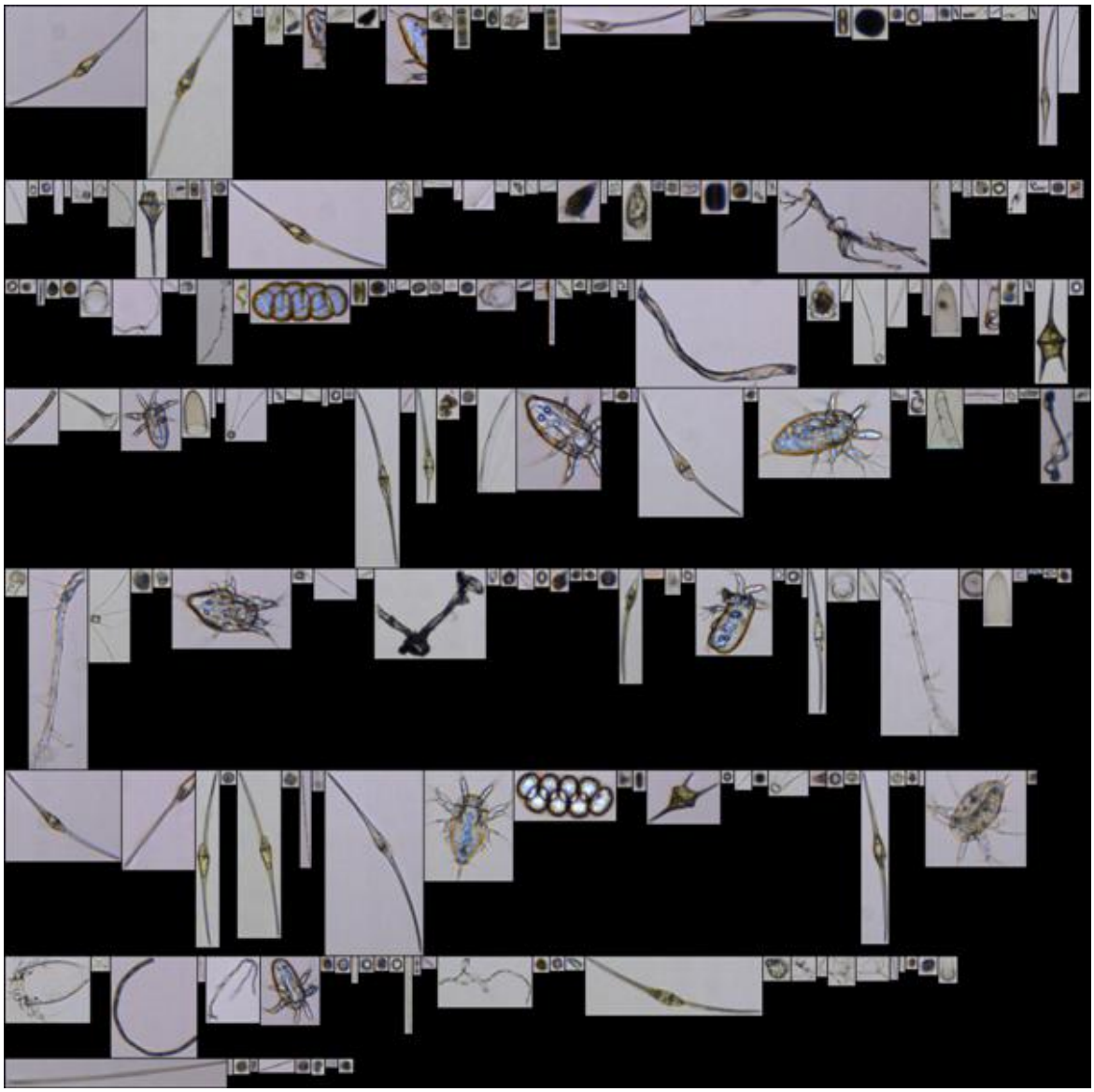

Fig. 2.8.1. An example of obtained images of particles.

2.9 Ceilometer Observation

September 17, 2014

(1) Personnel

Masaki Katsumata	(JAMSTEC): Principal Investigator	
Ryo Oyama	(Global Ocean Development Inc., GODI)	-leg1-
Souichiro Sueyoshi	(GODI)	-leg1-
Katsuhisa Maeno	(GODI)	-leg1-
Koichi Inagaki	(GODI)	-leg1-
Wataru Tokunaga	(GODI)	-leg2-
Kazuho Yoshida	(GODI)	-leg2-
Tetsuya Kai	(GODI)	-leg2-
Yutaro Murakami	(GODI)	-leg1, leg2-
Masanori Murakami	(MIRAI Crew)	-leg1, leg2-

(2) Objectives

The information of cloud base height and the liquid water amount around cloud base is important to understand the process on formation of the cloud. As one of the methods to measure them, the ceilometer observation was carried out.

(3) Parameters

1. Cloud base height [m].
2. Backscatter profile, sensitivity and range normalized at 10 m resolution.
3. Estimated cloud amount [oktas] and height [m]; Sky Condition Algorithm.

(4) Methods

We measured cloud base height and backscatter profile using ceilometer (CL51, VAISALA, Finland). Major parameters for the measurement configuration are shown in Table 2.9.1;

(5) Preliminary results

Fig.2.9.1 shows the time series of 1st, 2nd and 3rd lowest cloud base height during the cruise.

(6) Data archives

The raw data obtained during this cruise will be submitted to the Data Management Group (DMG) of JAMSTEC.

(7) Remarks (Times in UTC)

i) Data acquisition was suspended in the territorial waters of USA.

ii) The following time, the window was cleaned.

23:20UTC 16 Jul. 2014

20:40UTC 17 Aug. 2014

Table 2.9.1. Major parameters.

Laser source:	Indium Gallium Arsenide (InGaAs) Diode
Transmitting center wavelength:	910±10 nm at 25 degC
Transmitting average power:	19.5 mW
Repetition rate:	6.5 kHz
Detector:	Silicon avalanche photodiode (APD)
	Responsibility at 905 nm: 65 A/W
Cloud detection range	0 ~ 13 km
Measurement range:	0 ~ 15 km
Resolution:	10 meter in full range
Sampling rate:	36 sec
Sky Condition:	Cloudiness in octas (0 ~ 9)
	(0:Sky Clear, 1:Few, 3:Scattered, 5-7:Broken,
	8:Overcast, 9:Vertical Visibility)

On the archive dataset, cloud base height and backscatter profile are recorded with the resolution of 10 m (33 ft).

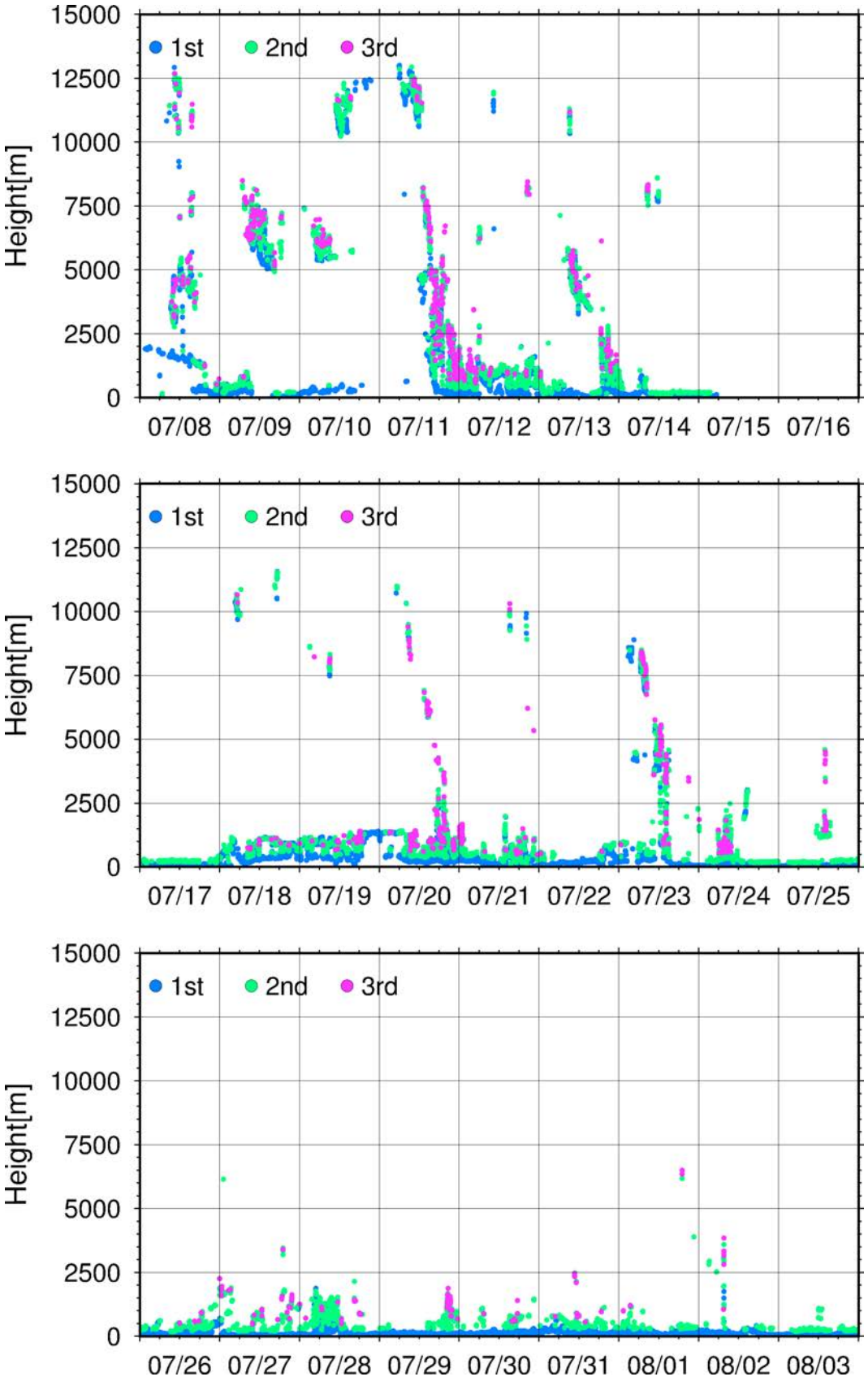

Fig. 2.9.1. 1st, 2nd and 3rd lowest cloud base height during the MR14-04 cruise.

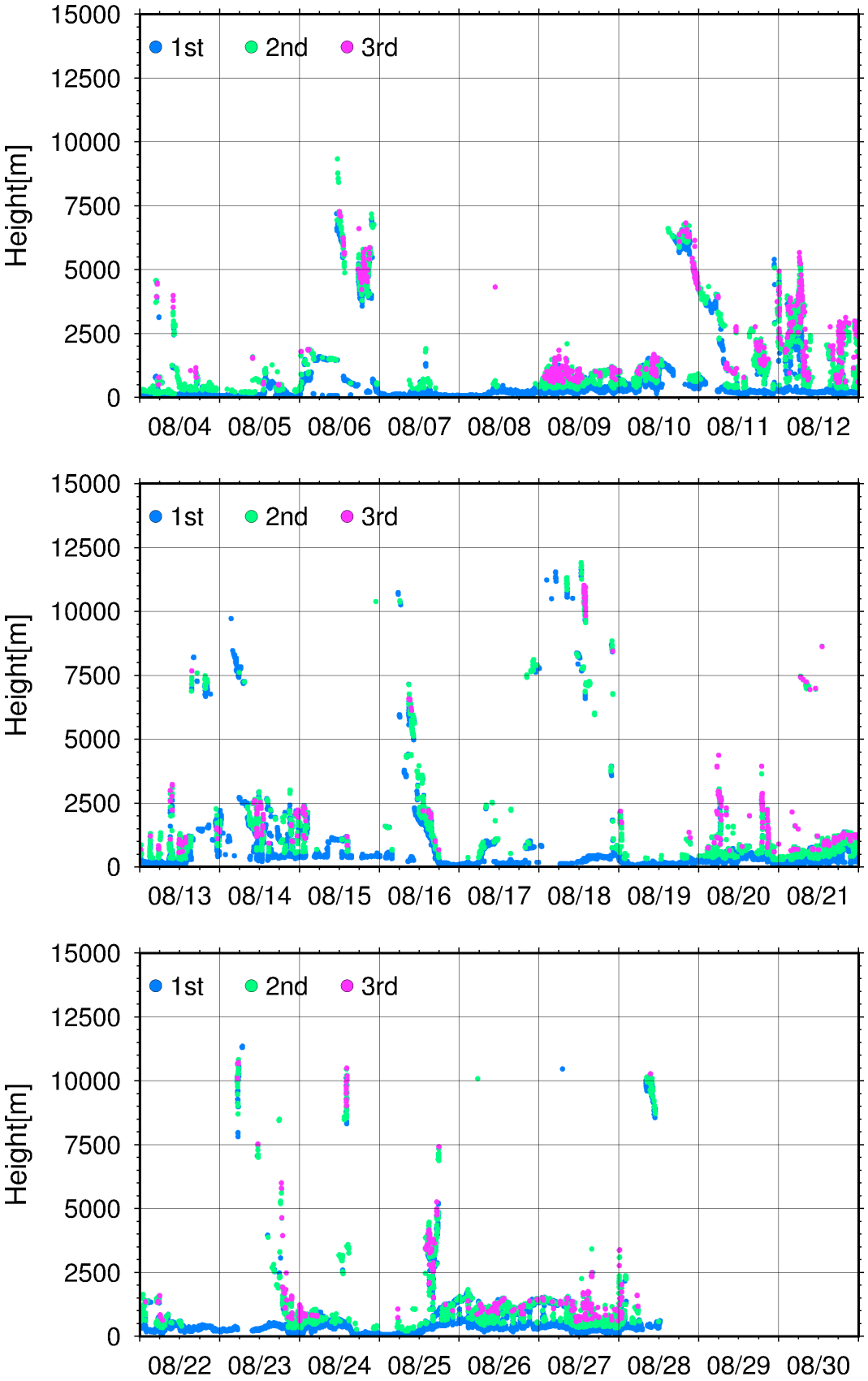

Fig. 2.9.1. (Continue)

2.10 Raindrop Observations

September 13, 2014

(1) Personnel

Masaki KATSUMATA (JAMSTEC) - Principal Investigator

(2) Objectives

The disdrometer can continuously obtain size distribution of raindrops. The objective of this observation is (a) to reveal microphysical characteristics of the rainfall, depends on the type, temporal stage, etc. of the precipitating clouds, (b) to retrieve the coefficient to convert radar reflectivity to the rainfall amount, and (c) to validate the algorithms and the product of the satellite-borne precipitation radars; TRMM/PR and GPM/DPR.

(3) Methods

Four different types of disdrometers are utilized to obtain better reasonable and accurate value on the moving vessel. Three of the disdrometers and one optical rain gauge are installed in one place, the starboard side on the roof of the anti-rolling system of R/V Mirai, as in Fig. 2.10.1. One of the disdrometers named "micro rain radar" is installed at the starboard side of the anti-rolling systems (see Fig. 2.10.2).

The details of the sensors are described below. All the sensors archive data every one minute.

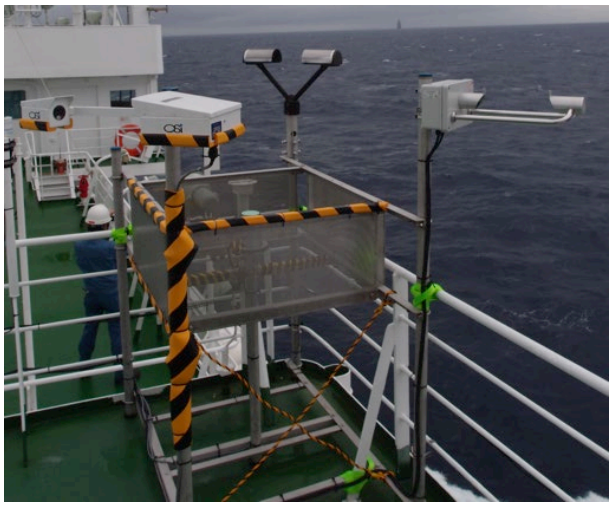

Fig. 2.10.1: The three disdrometers (Parsivel, LPM and Joss-Waldvogel disdrometer) and an optical rain gauge, installed on the roof of the anti-rolling tank.

Fig. 2.10.2: The micro rain radar, installed on the starboard side of the anti-rolling tank.

(3-1) Joss-Waldvogel type disdrometer

The "Joss-Waldvogel-type" disdrometer system (RD-80, Disdromet Inc.) (hereafter JW) equipped a microphone on the top of the sensor unit. When a raindrop hit the microphone, the magnitude of induced sound is converted to the size of raindrops. The logging program "DISDRODATA" determines the size as one

of the 20 categories as in Table 2.10.1, and accumulates the number of raindrops at each category. The rainfall amount could be also retrieved from the obtained drop size distribution. The number of raindrops in each category, and converted rainfall amount, are recorded every one minute.

(3-2) Laser Precipitation Monitor (LPM) optical disdrometer

The "Laser Precipitation Monitor (LPM)" (Adolf Thies GmbH & Co) is an optical disdrometer. The instrument consists of the transmitter unit which emit the infrared laser, and the receiver unit which detects the intensity of the laser come thru the certain path length in the air. When a precipitating particle fall thru the laser, the received intensity of the laser is reduced. The receiver unit detect the magnitude and the duration of the reduction and then convert them onto particle size and fall speed. The sampling volume, i.e. the size of the laser beam "sheet", is 20 mm (W) x 228 mm (D) x 0.75 mm (H).

The number of particles are categorized by the detected size and fall speed and counted every minutes. The categories are shown in Table 2.10.2.

(3-3) "Parsivel" optical disdrometer

The "Parsivel" (Adolf Thies GmbH & Co) is another optical disdrometer. The principle is same as the LPM. The sampling volume, i.e. the size of the laser beam "sheet", is 30 mm (W) x 180 mm (D). The categories are shown in Table 2.10.3.

(3-4) Optical rain gauge

The optical rain gauge, which detect scintillation of the laser by falling raindrops, is installed beside the above three disdrometers to measure the exact rainfall. The ORG-815DR (Optical Scientific Inc.) is utilized with the controlling and recording software (manufactured by Sankosha Co.).

(3-5) Micro rain radar

The MRR-2 (METEK GmbH) was utilized. The specifications are in Table 2.10.4. The antenna unit was installed at the starboard side of the anti-rolling systems (see Fig. 2.10.2), and wired to the junction box and laptop PC inside the vessel.

The data was averaged and stored every one minute. The vertical profile of each parameter was obtained every 200 meters in range distance (i.e. height) up to 6200 meters, i.e. well beyond the melting layer. The drop size distribution is recorded, as well as radar reflectivity, path-integrated attenuation, rain rate, liquid water content and fall velocity.

(4) Preliminary Results

The data were obtained continuously thru the cruise except in the territorial water and in the EEZ without permissions. The further analyses will be done after the cruise.

(5) Data Archive

All data obtained during this cruise will be submitted to the JAMSTEC Data Integration and Analysis Group (DMG).

(6) Acknowledgment

The optical rain gauge is kindly provided by National Institute for Information and Communication Technology (NICT). The operations are supported by Japan Aerospace Exploration Agency (JAXA) Precipitation Measurement Mission (PMM).

Table 2.10.1: Category number and corresponding size of the raindrop for JW disdrometer.

Category	Corresponding size range [mm]		
1	0.313	-	0.405
2	0.405	-	0.505
3	0.505	-	0.696
4	0.696	-	0.715
5	0.715	-	0.827
6	0.827	-	0.999
7	0.999	-	1.232
8	1.232	-	1.429
9	1.429	-	1.582
10	1.582	-	1.748
11	1.748	-	2.077
12	2.077	-	2.441
13	2.441	-	2.727
14	2.727	-	3.011
15	3.011	-	3.385
16	3.385	-	3.704
17	3.704	-	4.127
18	4.127	-	4.573
19	4.573	-	5.145
20	5.145	or larger	

Table 2.10.2: Categories of the size and the fall speed for LPM.

Particle Size		
Class	Diameter [mm]	Class width [mm]
1	≥ 0.125	0.125
2	≥ 0.250	0.125
3	≥ 0.375	0.125
4	≥ 0.500	0.250
5	≥ 0.750	0.250
6	≥ 1.000	0.250
7	≥ 1.250	0.250
8	≥ 1.500	0.250
9	≥ 1.750	0.250
10	≥ 2.000	0.500
11	≥ 2.500	0.500
12	≥ 3.000	0.500
13	≥ 3.500	0.500
14	≥ 4.000	0.500
15	≥ 4.500	0.500
16	≥ 5.000	0.500
17	≥ 5.500	0.500
18	≥ 6.000	0.500
19	≥ 6.500	0.500
20	≥ 7.000	0.500
21	≥ 7.500	0.500
22	≥ 8.000	unlimited

Fall Speed		
Class	Speed [m/s]	Class width [m/s]
1	≥ 0.000	0.200
2	≥ 0.200	0.200
3	≥ 0.400	0.200
4	≥ 0.600	0.200
5	≥ 0.800	0.200
6	≥ 1.000	0.400
7	≥ 1.400	0.400
8	≥ 1.800	0.400
9	≥ 2.200	0.400
10	≥ 2.600	0.400
11	≥ 3.000	0.800
12	≥ 3.400	0.800
13	≥ 4.200	0.800
14	≥ 5.000	0.800
15	≥ 5.800	0.800
16	≥ 6.600	0.800
17	≥ 7.400	0.800
18	≥ 8.200	0.800
19	≥ 9.000	1.000
20	≥ 10.000	10.000

Table 2.10.3: Categories of the size and the fall speed for Parsivel.

Particle Size		
Class	Average Diameter [mm]	Class spread [mm]
1	0.062	0.125
2	0.187	0.125
3	0.312	0.125
4	0.437	0.125
5	0.562	0.125
6	0.687	0.125
7	0.812	0.125
8	0.937	0.125
9	1.062	0.125
10	1.187	0.125
11	1.375	0.250
12	1.625	0.250
13	1.875	0.250
14	2.125	0.250
15	2.375	0.250
16	2.750	0.500
17	3.250	0.500
18	3.750	0.500
19	4.250	0.500
20	4.750	0.500
21	5.500	1.000
22	6.500	1.000
23	7.500	1.000
24	8.500	1.000
25	9.500	1.000
26	11.000	2.000
27	13.000	2.000
28	15.000	2.000
29	17.000	2.000
30	19.000	2.000
31	21.500	3.000
32	24.500	3.000

Fall Speed		
Class	Average Speed [m/s]	Class Spread [m/s]
1	0.050	0.100
2	0.150	0.100
3	0.250	0.100
4	0.350	0.100
5	0.450	0.100
6	0.550	0.100
7	0.650	0.100
8	0.750	0.100
9	0.850	0.100
10	0.950	0.100
11	1.100	0.200
12	1.300	0.200
13	1.500	0.200
14	1.700	0.200
15	1.900	0.200
16	2.200	0.400
17	2.600	0.400
18	3.000	0.400
19	3.400	0.400
20	3.800	0.400
21	4.400	0.800
22	5.200	0.800
23	6.000	0.800
24	6.800	0.800
25	7.600	0.800
26	8.800	1.600
27	10.400	1.600
28	12.000	1.600
29	13.600	1.600
30	15.200	1.600
31	17.600	3.200
32	20.800	3.200

Table 2.10.4: Specifications of the MRR-2.

Transmitter power	50 mW
Operating mode	FM-CW
Frequency	24.230 GHz (modulation 1.5 to 15 MHz)
3dB beam width	1.5 degrees
Spurious emission	< -80 dBm / MHz
Antenna Diameter	600 mm
Gain	40.1 dBi

2.11 C-band Weather Radar

September 13, 2014

(1) Personnel

Masaki KATSUMATA*	(JAMSTEC)	- Principal Investigator
Ryuichi SHIROOKA*	(JAMSTEC)	
Biao GENG*	(JAMSTEC)	
Shuichi MORI*	(JAMSTEC)	
Ryo OYAMA*	(GODI)	- Operation Leader (Leg-1)
Wataru TOKUNAGA**	(GODI)	- Operation Leader (Leg-2)
Kouichi INAGAKI*	(GODI)	
Katsuhisa MAENO*	(GODI)	
Souichiro SUEYOSHI*	(GODI)	
Yutaro MURAKAMI***	(GODI)	
Kazuho YOSHIDA**	(GODI)	
Tetsuya KAI**	(GODI)	
Masanori MURAKAMI***	(MIRAI Crew)	

(*:on board Leg-1; **:on board Leg-2; ***:onboard Leg-1 and 2)

(2) Objective

The objective of the C-band weather radar observation in this cruise is to test the performance of the radar and to develop the better strategy of the radar observation to capture the spatial and temporal variations of precipitating systems.

(3) Method

The C-band weather radar on board of Mirai is used. The specification of the radar is as follows:

Frequency:	5370 MHz (C-band)
Polarimetry:	Horizontal and vertical (simultaneously transmitted and received)
Pulse Configuration:	Using pulse-compression
Beam Width:	1.0 degrees
Output Power:	6 kW (H) + 6 kW (V)
Inertial Navigation Unit:	PHINS (Ixsea S.A.S., France)

Parameters of the radar are checked and calibrated at the beginning and the end of the cruise. Meanwhile, daily checking is performed for (1) frequency, (2) mean output power, (3) pulse width, and (4) PRF (pulse repetition frequency).

During the cruise, the radar was operated typically by repeating a volume scan with 17 PPIs (Plan Position Indicators) every 6-minute. A dual PRF mode with the maximum range of, typically 100 km, is used for the volume scan. Meanwhile, a surveillance PPI scan is performed every 30 minutes in a single PRF mode with the maximum range of 300 km. Furthermore, RHI (Range Height Indicator) scans are also operated whenever detailed vertical structures are necessary in certain azimuth directions. The detailed setting was changed frequently to test the performance and to seek the best combination of the parameters.

The radar was operated from Jul. 9 to Jul. 14 during Leg-1, and Jul. 20 to Aug. 28 during Leg-2.

(4) Preliminary results

Figure 2.11.1 shows samples of the obtained data. At the time, the frontal system was passing over the vessel. The left panel shows the precipitating band with the width of 100km or more. The left panel, a vertical cross section of the band, indicates the echo top height reaches 12km or more, and the difference below and above 5-km height corresponding to the height with 0 degree-C in temperature.

The further detailed analyses will be studied after the cruise.

(5) Data archive

All data of the Doppler radar observation during this cruise will be submitted to the JAMSTEC Data Integration and Analysis Group (DMG).

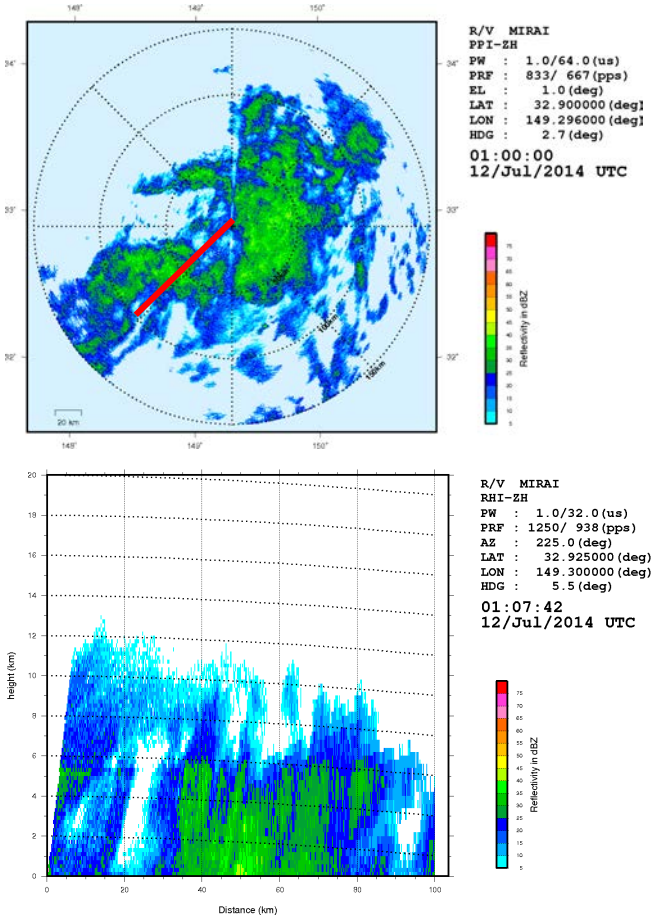

Fig. 2.11.1: A sample of obtained data, at 01UTC, Jul. 12. (left) PPI image of radar reflectivity at elevation angle of 0.5 degrees. (right) RHI image of radar reflectivity at azimuth angle of 225 degrees (red line at left panel).

2.12 Radiosonde

September 13, 2014

(1) Personnel

Masaki KATSUMATA	(JAMSTEC)	- Principal Investigator
Ryuichi SHIROOKA	(JAMSTEC)	
Biao GENG	(JAMSTEC)	
Shuichi MORI	(JAMSTEC)	
Ryo OYAMA	(GODI)	- Operation Leader
Kouichi INAGAKI	(GODI)	
Katsuhisa MAENO	(GODI)	
Souichiro SUEYOSHI	(GODI)	
Yutaro MURAKAMI	(GODI)	
Masanori MURAKAMI	(MIRAI Crew)	

(2) Objectives

To obtain atmospheric profile of temperature, humidity, and wind speed/direction, and their temporal variations

(3) Methods

Atmospheric sounding by radiosonde by using system by Vaisala Oyj was carried out. The GPS radiosonde sensor (RS92-SGPD) was launched with the balloons (Totex TA-200/350). The on-board system to calibrate, to launch, to log the data and to process the data, consists of processor (Vaisala, SPS-311), processing and recording software (DigiCORA III, ver.3.64), GPS antenna (GA20), UHF antenna (RB21), ground check kit (GC25), and balloon launcher (ASAP). In the ”ground-check” process, the pressure sensor (Vaisala PTB-330) was also utilized as the standard. In case the relative wind to the ship (launcher) is not appropriate for the launch, the handy launch was selected.

(4) Preliminary Results

The radiosondes were launched eventually when the precipitating systems were in vicinity of the vessel, during Leg-1. The radiosondes from 12Z on Jul.12 to 06Z on Jul.13 were launched simultaneously to the XCTD observations to capture the high-resolution meridional structure of air-sea interaction. In total, 19 soundings were carried out, as listed in Table 2.12.1.

The further analyses will be done after the cruise.

(5) Data archive

Data were sent to the world meteorological community via Global Telecommunication System (GTS) through the Japan Meteorological Agency, immediately after each observation. Raw data is recorded in Vaisala original binary format during both ascent and descent. The ASCII data is also available. These raw datasets will be submitted to JAMSTEC Data Integration and Analyses Group.

Table 2.12.1: Radiosonde launch log, with surface values and maximum height.

ID	Nominal Time	Launched Location		Surface Values						Max height	Cloud	
		Lat	Lon	P	T	RH	WD	Wsp	SST		Amount	Type
	YYYYMMDDH	degN	degE	hPa	deg.C	%	deg.	m/s	deg.C	m		
RS001	2014070915	33.098	141.913	1006.9	23.3	100	220	4.8	23.217	22977	9	As,St
RS002	2014071112	30.339	149.313	1010.0	23.5	99	174	7.0	22.863	22202	8	St,As,Cu
RS003	2014071118	31.442	149.333	1007.4	23.6	98	200	12.0	22.758	20696	10	St,Sc
RS004	2014071200	32.574	149.343	1006.1	23.6	98	194	14.1	22.880	22702	10	St
RS005	2014071206	33.688	149.325	1004.3	23.3	98	219	7.6	23.311	22229	10	St
RS006	2014071210	34.095	149.231	1004.8	22.9	99	204	6.8	22.383	18758	10	As,St
RS007	2014071212	34.408	149.077	1005.0	22.7	100	225	7.4	22.161	16844	5	-
RS008	2014071214	34.719	148.918	1004.7	23.3	99	245	3.6	23.421	18181	7	-
RS009	2014071215	35.006	148.727	1004.1	23.4	98	252	4.5	23.764	21905	8	St,Cu
RS010	2014071217	35.325	148.510	1004.0	23.8	99	239	5.3	23.939	20751	10	-
RS011	2014071219	35.654	148.310	1004.9	24.1	97	257	2.9	24.627	24783	10	St
RS012	2014071223	36.080	148.084	1005.6	24.0	99	189	2.2	24.009	24269	10	St,Ac
RS013	2014071302	36.344	147.874	1005.7	23.1	100	87	2.2	23.159	17707	10	St
RS014	2014071304	36.636	147.682	1005.2	22.7	100	139	2.4	22.159	22123	10	St
RS015	2014071306	37.024	147.440	1005.4	23.1	98	38	0.4	22.656	26256	10	St,Ac
RS016	2014071312	37.996	146.792	1005.5	22.2	100	177	3.2	22.152	23457	10	Cu,St
RS017	2014071318	38.750	146.302	1003.8	21.1	100	165	6.6	21.203	23567	10	St
RS018	2014071400	39.158	146.029	1001.4	21.5	99	153	11.5	20.836	25628	10	St
RS019	2014071406	40.157	145.317	1001.2	20.1	100	9	8.0	22.076	24445	10	St

2.13 HYVIS

September 13, 2014

(1) Personnel

Masaki Katsumata (JAMSTEC): Principal Investigator
Shuichi Mori (JAMSTEC)
Ryuichi Shirooka (JAMSTEC)
Biao Geng (JAMSTEC)
Soichiro Sueyoshi (GODI)
Katsuhisa Maeno (GODI)
Ryo Oyama (GODI)
Koichi Inagaki (GODI)
Yutaro Murakami (GODI)

(2) Objective

We conducted HYdrometer VIdeo Sonde (HYVIS) observations for validation of the newly installed C-band dual polarimetric radar system (see Section 2.11). The HYVIS obtains sequential images of raindrops, snow crystals, and other ice particles in and out of clouds up to approximately 20 km high from the sea surface as well as profiles of pressure, temperature, relative humidity, wind direction, and wind speed. The profiles of hydrometer images and atmospheric conditions are utilized as *in situ* data to validate dual polarimetric parameters and hydrometer identification (or classification) function observed with the C-band dual polarimetric radar.

(3) Method

Four (4) HYVISs were launched during 10 and 14 July 2014 only when we identified rainclouds covered over the *R/V Mirai* by the C-band dual polarimetric radar. HYVIS observation system consists of a Meisei HYVIS receiver/antenna controller, a 1680 MHz Yagi antenna for video image signals, HYVIS transmitters (Meisei WUA-11), and 1,200 g balloons (Totex TA-1200). Each The HYVIS transmitter was launched with a GPS rawinsondes transmitter (Meisei RS-06G) by the same balloon. The GPS rawinsondes signals were received by a receiver/signal processor (Meisei RD-08AC) with MGPS_R software through a 400 MHz omnidirectional whip antenna. The 1680 MHz Yagi antenna was automatically controlled to direct the HYVIS transmitter based on geolocation and height of the RS-06G transmitter detected by the RD-08AC receiver.

The HYVIS transmitter has two charge-coupled device (CCD) video cameras: one is a close-up camera and the other is a microscopic one. The former (latter) has a size of 7.00 mm x 5.25 mm (1.200 mm x 0.90 mm). The video images are sent every 10 sec by a sequence of 7 sec microscopic image, 1 sec blank, and 3 sec close-up one. The minimum detectable particle size is approximately 10 micro m by the microscopic camera.

(4) Preliminary results

Summary of HYVIS launch log with surface observations and maximum sounding height is listed in Table 2.13.1. Although the primary objective of HYVIS observation is validation of the C-band dual polarimetric radar, we made importance on both preparation and launching procedures of HYVIS observation as well because this is the very first challenge to use it on the vessel. Specific notes for each HYVIS observation are described as follows:

No.01
Water cloud droplets images were obtained approximately 5-7 km high in altocumulus (or altostratus) with temperature of around -5 deg. C. Because SOJ data was not introduce into the RD-08AC receiver to chase RS-06G transmitter automatically (i.e., we controlled the Yagi antenna manually), video image quality was quite low.

No.02
Video image signal was terminated just after we launched it under the moderate rain with wind speed of 15.4 m/s. Dry cell batteries might be dropped out from a battery case inside the HYVIS transmitter because of shock during the launching.

No.03
No rain and water cloud droplets image was obtained in the lower to middle troposphere because cloud layers were thin and scattered. Quite little number of ice cloud particles images was recorded in cirrus (or cirrostratus) at approximately 8-12 km high.

No.04
Much number of rain (drizzle) droplet images was obtained after launching to approximately 2.5 km high in shallow and dense stratus or stratocumulus cloud. I addition, bullet- and/or plate-type snow crystal images were recorded at 8.2 km and 9.2 km in altocumulus or altostratus cloud. Figures 2.13.1 and 2.13.2 show sounding profiles of temperature, relative humidity, zonal and meridional wind velocities, and corresponding HYVIS microscopic images, respectively.

Further analyses of HYVIS images, e.g., hydrometer classification, drop size distribution, and number density, are expected as a next step for the validation of dual polarimetric parameters obtained by the Mirai new radar system.

(5) Data archive

Raw HYVIS and sounding data are stored in digital video image (MPEG) and ASCII (CSV) formats, respectively, that are available through JAMSTEC Data Management Office (DMO).

Table 2.13.1 HYVIS launch log with surface observation and maximum sounding height.

No.	Date(YYYY/MMDD) Time (HH:MM) UTC	Lat(degN) Lon(degE)	Psfc (hPa)	Tsfc (degC)	RHsfc (%)	WD (deg) WS (m/s)	SST (degC)	Max Alt (m)
01	2014/0710 05:13	31.666 145.319	1009.2	24.8	95	224 5.5	24.5	31,730
02	2014/0712 00:51	32.880 149.300	1007.2	23.3	100	196 14.8	22.7	25,975
03	2014/0712 04:26	33.550 149.322	1006.6	23.6	96	228 11.6	22.2	30,256
04	20140723 21:40	38.928 146.174	1004.6	21.1	94	125 10.1	21.3	18,876

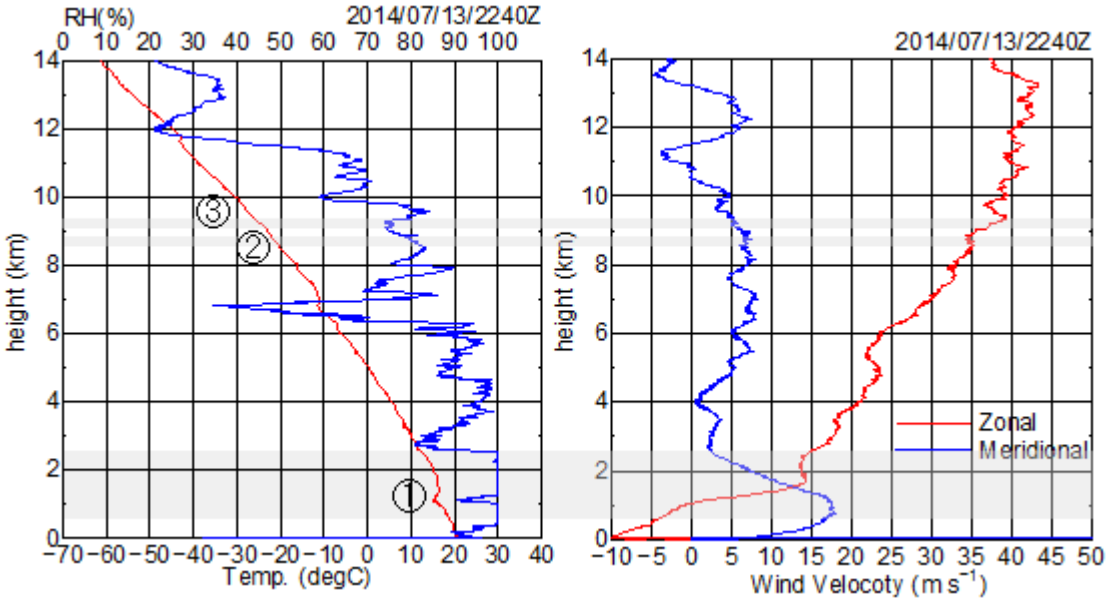

Fig. 2.13.1 Sounding profiles of temperature, relative humidity (left panel), zonal and meridional wind velocities (right panel) observed by the Meisei RS-06G transmitter launched at 2240Z on 13 July 2014. Three grey shaded rectangles (1, 2, and 3) indicate heights where droplets and snow crystals images were obtained by the No.4 HYVIS sounding.

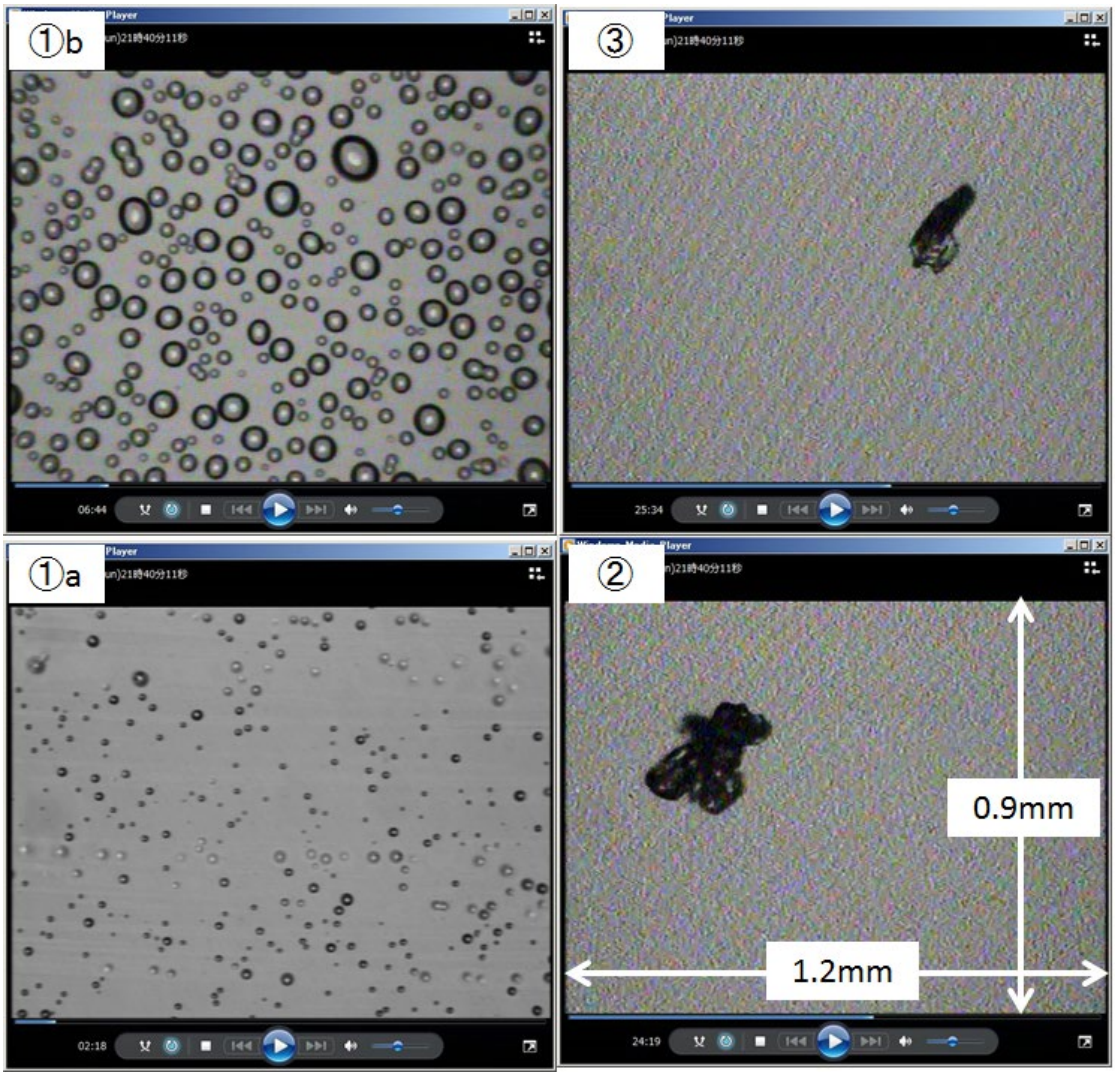

Fig. 2.13.2 Snapshot microscopic images obtained by No.4 HYVIS sounding launched at 2240Z on 13 July 2013. Images 1a, 1b, 2, and 3 were recorded at heights of approximately 600 m, 2000 m, 8700 m, and 9200 m, respectively, and correspond to those sings as shown in Fig. 2.13.1. Size of droplet diameter in images 1a and 1b range from tens to hundreds micro meters. Snow crystals in images 2 and 3 are can be classified as bullet- or plate type, however, further detailed analyses are required.

2.14 Sea Surface Gravity

September 17, 2014

(1) Personnel

Takeshi Matsumoto	Univ. of the Ryukyus: Principal investigator	(Not on-board)
Ryo Oyama	Global Ocean Development Inc., (GODI)	- leg1 -
Souichiro Sueyoshi	GODI	- leg1 -
Katsuhisa Maeno	GODI	- leg1 -
Koichi Inagaki	GODI	- leg1 -
Wataru Tokunaga	GODI	- leg2 -
Kazuho Yoshida	GODI	- leg2 -
Tetsuya Kai	GODI	- leg2 -
Yutaro Murakami	GODI	- leg1, leg2 -
Masanori Murakami	MIRAI crew	- leg1, leg2 -

(2) Introduction

The local gravity is an important parameter in geophysics and geodesy. We collected gravity data at the sea surface.

(3) Parameters

Relative Gravity [CU: Counter Unit]

[mGal] = (coef1: 0.9946) * [CU]

(4) Data Acquisition

We measured relative gravity using LaCoste and Romberg air-sea gravity meter S-116 (Micro-G LaCoste, LLC) during the MR14-04 cruise.

To convert the relative gravity to absolute one, we measured gravity, using portable gravity meter (CG-5, Scintrex), at Yokohama, Yokosuka and Kushiro as the reference points.

(5) Preliminary Results

Absolute gravity table is shown in Table 2.14.1.

Table 2.14.1. Absolute gravity table of the MR14-04 cruise.

No.	Date M/D	UTC hh:mm	Port	Absolute Gravity [mGal]	Sea level [cm]	Draft [cm]	Gravity at Senor*1 [mGal]	L&R*2 [mGal]
#01	04/Jul	04:30	Yokohama	979741.75	281	655	979742.89	12034.09
#02	07/Jul	07:41	Yokosuka	979757.91	276	650	979759.03	12051.11
#03	16/Jul	22:02	Kushiro	980600.69	132	655	980601.31	12892.39
#04	30/Aug	20:40	Dutch Harbor	-	385	633	-	-

*1: Gravity at Sensor= Absolute Gravity + Sea Level*0.3086/100 + (Draft-530)/100*0.2222

*2: Micro-g LaCoste air-sea gravity meter S-116

(6) Data Archive

Surface gravity data obtained during this cruise will be submitted to the Data Management Group (DMG) in JAMSTEC, and will be archived there.

(7) Remarks (Times in UTC)

i) The following periods, navigation data (position, speed and course over ground) was often invalid due to position fix error for loss of GPS satellites.

Leg 1: 14 Jul. to 15 Jul., 2014

Leg 2: 17 Jul. to 16 Aug., 2014

ii) The following periods, navigation data was invalid due to the server error.

Leg 2: 12:37 to 15:45 23 Aug., 2014

2.15 Sea Surface Magnetic Field

September 17, 2014

(1) Personnel

Takeshi Matsumoto	Univ. of the Ryukyus: Principal investigator	(Not on-board)
Ryo Oyama	Global Ocean Development Inc., (GODI)	- leg1 -
Souichiro Sueyoshi	GODI	- leg1 -
Katsuhisa Maeno	GODI	- leg1 -
Koichi Inagaki	GODI	- leg1 -
Wataru Tokunaga	GODI	- leg2 -
Kazuho Yoshida	GODI	- leg2 -
Tetsuya Kai	GODI	- leg2 -
Yutaro Murakami	GODI	- leg1, leg2 -
Masanori Murakami	MIRAI crew	- leg1, leg2 -

(2) Introduction

Measurement of magnetic force on the sea is required for the geophysical investigations of marine magnetic anomaly caused by magnetization in upper crustal structure. We measured geomagnetic field using a three-component magnetometer during the MR14-04 cruise.

(3) Principle of ship-board geomagnetic vector measurement

The relation between a magnetic-field vector observed on-board, Hob, (in the ship's fixed coordinate system) and the geomagnetic field vector, F, (in the Earth's fixed coordinate system) is expressed as:

$$Hob = \tilde{\mathbf{A}}\,\tilde{\mathbf{R}}\,\tilde{\mathbf{P}}\,\tilde{\mathbf{Y}}\,F + Hp \quad (a)$$

where $\tilde{\mathbf{R}}$, $\tilde{\mathbf{P}}$ and $\tilde{\mathbf{Y}}$ are the matrices of rotation due to roll, pitch and heading of a ship, respectively. $\tilde{\mathbf{A}}$ is a 3 x 3 matrix which represents magnetic susceptibility of the ship, and Hp is a magnetic field vector produced by a permanent magnetic moment of the ship's body. Rearrangement of Eq. (a) makes

$$\tilde{\mathbf{R}}\,Hob + Hbp = \tilde{\mathbf{R}}\,\tilde{\mathbf{P}}\,\tilde{\mathbf{Y}}\,F \quad (b)$$

where $\tilde{\mathbf{R}} = \tilde{\mathbf{A}}$-1, and $Hbp = -\tilde{\mathbf{R}}\,Hp$. The magnetic field, F, can be obtained by measuring $\tilde{\mathbf{R}}$, $\tilde{\mathbf{P}}$, $\tilde{\mathbf{Y}}$ and Hob, if $\tilde{\mathbf{R}}$ and Hbp are known. Twelve constants in $\tilde{\mathbf{R}}$ and Hbp can be determined by measuring variation of Hob with $\tilde{\mathbf{R}}$, $\tilde{\mathbf{P}}$ and $\tilde{\mathbf{Y}}$ at a place where the geomagnetic field, F, is known.

(4) Instruments on R/V MIRAI

A shipboard three-component magnetometer system (Tierra Tecnica SFG1214) is equipped on-board R/V MIRAI. Three-axes flux-gate sensors with ring-cored coils are fixed on the fore mast. Outputs from the sensors are digitized by a 20-bit A/D converter (1 nT/LSB), and sampled at 8 times per second. Ship's heading, pitch, and roll are measured by the Inertial Navigation System (INS) for controlling attitude of a Doppler radar. Ship's position and speed data are taken from LAN every second.

(5) Data Archive

Sea surface magnetic data obtained during this cruise will be submitted to the Data Management Group (DMG) in JAMSTEC, and will be archived there.

(6) Remarks (Times in UTC)

i) The following periods, navigation data (position, speed and course over ground) was often invalid

due to position fix error for loss of GPS satellites.

Leg 1: 14 Jul. to 15 Jul., 2014

Leg 2: 17 Jul. to 16 Aug., 2014

ii) The following periods, navigation data was invalid due to the server error.

Leg 2: 12:37 to 12:45 23 Aug., 2014

iii) The following periods, we made a "figure-eight" turn (a pair of clockwise and anti-clockwise rotation) for calibration of the ship's magnetic effect.

Leg 1: 19:51 to 20:15 14 Jul. 2014, around 42-17N, 143-44E

Leg 2: 05:55 to 06:20 18 Jul. 2014, around 41-52N, 149-19E
06:22 to 06:49 28 Jul. 2014, around 46-58N, 161-26E
08:09 to 08:38 06 Aug. 2014, around 47-00N, 174-56W
02:36 to 03:10 16 Aug. 2014, around 46-15N, 144-26W
07:49 to 08:15 21 Aug. 2014, around 46-58N, 130-02W
22:59 to 23:24 24 Aug. 2014, around 51-04N, 138-33W

2.16 Satellite Image Acquisition

September 17, 2014

(1) Personnel

Masaki Katsumata	(JAMSTEC): Principal Investigator	
Ryo Oyama	(Global Ocean Development Inc., GODI)	-leg1-
Souichiro Sueyoshi	(GODI)	-leg1-
Katsuhisa Maeno	(GODI)	-leg1-
Koichi Inagaki	(GODI)	-leg1-
Wataru Tokunaga	(GODI)	-leg2-
Kazuho Yoshida	(GODI)	-leg2-
Tetsuya Kai	(GODI)	-leg2-
Yutaro Murakami	(GODI)	-leg1, leg2-
Masanori Murakami	(MIRAI Crew)	-leg1, leg2-

(2) Objectives

The objectives are to collect cloud data in a high spatial resolution mode from the Advance Very High Resolution Radiometer (AVHRR) on the NOAA and MetOp polar orbiting satellites, and to verify the data from Doppler radar on board.

(3) Methods

We received the down link High Resolution Picture Transmission (HRPT) signal from satellites, which passed over the area around the R/V MIRAI. We processed the HRPT signal with the in-flight calibration and computed the brightness temperature. A cloud image map around the R/V MIRAI was made from the data for each pass of satellites.

We received and processed polar orbiting satellites data throughout MR14-04 cruise from 09 July to 29 Aug, 2014.

(4) Data archives

The raw data obtained during this cruise will be submitted to the Data Management Group (DMG) in JAMSTEC.

2.17 Aerosol optical characteristics measured by ship-borne sky radiometer

August 15, 2014

(1) Personnel

Kazuma Aoki (University of Toyama) Principal Investigator / not onboard
Tadahiro Hayasaka (Tohoku University) Co-worker / not onboard
Sky radiometer operation was supported by Global Ocean Development Inc.

(2) Objective

Objective of this observation is to study distribution and optical characteristics of marine aerosols by using a ship-borne sky radiometer (POM-01 MKII: PREDE Co. Ltd., Japan). Furthermore, collections of the data for calibration and validation to the remote sensing data were performed simultaneously.

(3) Parameters

- Aerosol optical thickness at five wavelengths (400, 500, 675, 870 and 1020 nm)
- Ångström exponent
- Single scattering albedo at five wavelengths
- Size distribution of volume (0.01 μm – 20 μm)
- # GPS provides the position with longitude and latitude and heading direction of the vessel, and azimuth and elevation angle of the sun. Horizon sensor provides rolling and pitching angles.

(4) Instruments and Methods

The sky radiometer measures the direct solar irradiance and the solar aureole radiance distribution with seven interference filters (0.34, 0.4, 0.5, 0.675, 0.87, 0.94, and 1.02 μm). Analysis of these data was performed by SKYRAD.pack version 4.2 developed by Nakajima *et al*. 1996.

(5) Data archives

Aerosol optical data are to be archived at University of Toyama (K.Aoki, SKYNET/SKY: http://skyrad.sci.u-toyama.ac.jp/) after the quality check and will be submitted to JAMSTEC.

2.18 Aerosols in the Marine Atmosphere

September 12, 2014

(1) Personnel

Yugo KANATA (JAMSTEC DEGCR, not on board)
Fumikazu TAKETANI (JAMSTEC DEGCR, not on board)
Takuma MIYAKAWA (JAMSTEC DEGCR, not on board)
Hisahiro TAKASHIMA (JAMSTEC DEGCR, not on board)
Yuichi KOMAZAKI (JAMSTEC DEGCR, not on board)
Maki NOGUCHI (JAMSTEC RCGC, not on board)
Operation was supported by Global Ocean Development Inc.

(2) Objective

- To investigate roles of aerosols in the marine atmosphere in relation to climate change
- To investigate processes of biogeochemical cycles between the atmosphere and the ocean

(3) Description of instruments deployed

(3-1) Aerosol observations: black carbon (BC), fluorescent properties, and size distribution

BC and fluorescent properties of aerosol particles were measured by an instrument based on laser-induced incandescence (SP2, Droplet Measurement Technologies) and by a single particle fluorescence sensor, WIBS4 (Waveband Integrated bioaerosol sensor, leg 2 only). The size distribution of particles was measured by the two instruments and also by a handheld optical particle counter (KR-12A, Rion). For KR-12A and SP2, ambient air was commonly sampled from the flying bridge by a 3-m-long conductive tube, and then introduced to each instrument.

The measurements of fluorescent properties by WIBS4 were made on the flying bridge. Two pulsed xenon lamps emitting UV light (280 nm and 370 nm) were used for excitation and fluorescence emitted from a single particle within 310−400 nm and 420−650 nm wavelength windows was recorded.

(3-2) MAX-DOAS

Multi-Axis Differential Optical Absorption Spectroscopy (MAX-DOAS), a passive remote sensing technique measuring spectra of scattered visible and ultraviolet (UV) solar radiation, was used for atmospheric aerosol and gas profile measurements. Our MAX-DOAS instrument consists of two main parts: an outdoor telescope unit and an indoor spectrometer (Acton SP-2358 with Princeton Instruments PIXIS-400B), connected to each other by a 14-m bundle optical fiber cable. The telescope unit was updated before the cruise; only one-axis scan for elevation angle was attained, while capability of azimuth scan was not employed. The line of sight was in the directions of the portside of the vessel and the scanned elevation angles were 1.5, 3, 5, 10, 20, 30, 90 degrees in the 30-min cycle. The roll motion of the ship was measured to autonomously compensate additional motion of the prism, employed for scanning the elevation angle.

For the selected spectra recorded with elevation angles with good accuracy, DOAS spectral fitting was performed to quantify the slant column density (SCD) of NO_2 (and other gases) and O_4 (O_2-O_2, collision complex of oxygen) for each elevation angle. Then, the O_4 SCDs were converted to the aerosol optical depth (AOD) and the vertical profile of aerosol extinction coefficient (AEC) using an optimal estimation inversion method with a radiative transfer model. Using derived aerosol information, retrievals of the tropospheric

vertical column/profile of NO_2 and other gases were made.

(3-3) CO and O_3

Ambient air was continuously sampled on the compass deck and drawn through ~20-m-long Teflon tubes connected to a gas filter correlation CO analyzer (Model 48C, Thermo Fisher Scientific) and a UV photometric ozone analyzer (Model 49C, Thermo Fisher Scientific), located in the Research Information Center. The data will be used for characterizing air mass origins.

(4) Preliminary results

N/A (All the data analysis is to be conducted.)

(5) Data archive

The data files will be submitted to JAMSTEC Data Integration and Analyses Group (DMG), after the full analysis is completed, which will be <2 years after the end of the cruise.

3 Hydrographic Measurements

3.1 $CTDO_2$ Measurements

September 26, 2014

(1) Personnel

Hiroshi Uchida (JAMSTEC)
Shinsuke Toyoda (MWJ)
Hiroshi Matsunaga (MWJ)
Rei Ito (MWJ)
Akira Watanabe (MWJ)
Kenichi Katayama (MWJ) (leg 1)
Tomoyuki Takamori (MWJ) (leg 2)
Michinari Sunamura (The University of Tokyo) (CDOM measurement)

(2) Winch arrangements

The CTD package was deployed by using 4.5 Ton Traction Winch System (Dynacon, Inc., Bryan, Texas, USA), which was renewed on the R/V Mirai in April 2014 (e.g. Fukasawa et al., 2004). Primary system components include a complete CTD Traction Winch System with up to 8500 m of 9.53 mm armored cable (Ocean Cable and Communications Co., Yokohama, Kanagawa, Japan).

(3) Overview of the equipment

The CTD system was SBE 911plus system (Sea-Bird Electronics, Inc., Bellevue, Washington, USA). The SBE 911plus system controls 36-position SBE 32 Carousel Water Sampler. The Carousel accepts 12-litre Niskin-X water sample bottles (General Oceanics, Inc., Miami, Florida, USA). The SBE 9plus was mounted horizontally in a 36-position carousel frame. SBE's temperature (SBE 3) and conductivity (SBE 4) sensor modules were used with the SBE 9plus underwater unit. The pressure sensor is mounted in the main housing of the underwater unit and is ported to outside through the oil-filled plastic capillary tube. A modular unit of underwater housing pump (SBE 5T) flushes water through sensor tubing at a constant rate independent of the CTD's motion, and pumping rate (3000 rpm) remain nearly constant over the entire input voltage range of 12-18 volts DC. Flow speed of pumped water in standard TC duct is about 2.4 m/s. Two sets of temperature and conductivity modules were used. An SBE's dissolved oxygen sensor (SBE 43) was placed between the primary conductivity sensor and the pump module. Auxiliary sensors, a Deep Ocean Standards Thermometer (SBE 35), an altimeter (PSA-916T; Teledyne Benthos, Inc., North Falmous, Massachusetts, USA), an oxygen optodes (RINKO-III; JFE Advantech Co., Ltd, Kobe Hyogo, Japan), a fluorometers (Seapoint sensors, Inc., Kingston, New Hampshire, USA), a transmissometer (C-Star Transmissometer; WET Labs, Inc., Philomath, Oregon, USA), a Photosynthetically Active Radiation (PAR) sensor (Satlantic, LP, Halifax, Nova Scotia, Canada), a colored dissolved organic matter (ECO FL CDOM, WET Labs, Inc., Philomath, Oregon, USA), and an UV nitrate sensor (Deep SUNA, Satlantic, LP, Halifax, Nova Scotia, Canada) were also used with the SBE 9plus underwater unit. To minimize rotation of the CTD package, a heavy stainless frame (total weight of the CTD package without sea water in the bottles is about 1000 kg) was used with an aluminum plate (54 × 90 cm).

An additional set of SBE 911plus CTD system with 12-position SBE 32 was also used for four shallow casts (stations 73_4, 73_5, 124_2, and 124_3) for water sampling for phytoplankton incubation in leg 2. The

SBE 9plus was mounted horizontally in a 12-position carousel frame. The 12-litre Niskin-X water sample bottles (General Oceanics, Inc.) were carefully cleaned and stored for the water sampling.

Summary of the system used in this cruise

36-position Carousel system

Deck unit:
SBE 11plus, S/N 11P54451-0872

Under water unit:
SBE 9plus, S/N 09P54451-117457 (pressure sensor S/N: 1027)

Temperature sensor:
SBE 3plus, S/N 4811 (primary)
SBE 3, S/N 1359 (secondary)

Conductivity sensor:
SBE 4, S/N 2435 (primary)
SBE 4, S/N 2854 (secondary)

Oxygen sensor:
SBE 43, S/N 0394 (stations from 001 to 057)
SBE 43, S/N 0330 (stations from 058 to 150)
JFE Advantech RINKO-III, S/N 0024 (foil batch no. 144002A)

Pump:
SBE 5T, S/N 4595 (primary)
SBE 5T, S/N 4598 (secondary)

Altimeter:
PSA-916T, S/N 1157

Deep Ocean Standards Thermometer:
SBE 35, S/N 0022

Fluorometer:
Seapoint Sensors, Inc., S/N 3618 (measurement range: 0-5 μg/L)

Transmissometer:
C-Star, S/N CST-1363DR

PAR:
Satlantic LP, S/N 0049

CDOM:
ECO FL CDOM, S/N 2014 (measurement range: 0-500 ppb)

Niterate:
Deep SUNA, S/N 0385 (used only for stations 001_2, 007_1, 014_1, and 030_1)

Carousel Water Sampler:
SBE 32, S/N 0278 (stations from 001_1 to 001_2)
SBE 32, S/N 0391 (stations from 007_1 to 150_1)

Water sample bottle:
12-litre Niskin-X model 1010X (no TEFLON coating)

12-position Carousel system (used for water sampling for phytoplankton incubation)

Deck unit:
SBE 11plus, S/N 11P54451-0872

Under water unit:

SBE 9plus, S/N 09P27443-79511 (pressure sensor S/N: 0677)

Temperature sensor:

SBE 3, S/N 1524

Conductivity sensor:

SBE 4, S/N 1088

Pump:

SBE 5T, S/N 3118

Carousel Water Sampler:

SBE 32, S/N 0278

Water sample bottle:

12-litre Niskin-X model 1010X (TEFLON coating)

(4) Pre-cruise calibration

i. Pressure

The Paroscientific series 4000 Digiquartz high pressure transducer (Model 415K: Paroscientific, Inc., Redmond, Washington, USA) uses a quartz crystal resonator whose frequency of oscillation varies with pressure induced stress with 0.01 per million of resolution over the absolute pressure range of 0 to 15000 psia (0 to 10332 dbar). Also, a quartz crystal temperature signal is used to compensate for a wide range of temperature changes at the time of an observation. The pressure sensor has a nominal accuracy of 0.015 % FS (1.5 dbar), typical stability of 0.0015 % FS/month (0.15 dbar/month), and resolution of 0.001 % FS (0.1 dbar). Since the pressure sensor measures the absolute value, it inherently includes atmospheric pressure (about 14.7 psi). SEASOFT subtracts 14.7 psi from computed pressure automatically.

Pre-cruise sensor calibrations for linearization were performed at SBE, Inc.

S/N 1027, 4 February 2011

S/N 0677, 5 March 2014

The time drift of the pressure sensor is adjusted by periodic recertification corrections against a dead-weight piston gauge (Model 480DA, S/N 23906; Piston unit, S/N 079K; Weight set, S/N 3070; Bundenberg Gauge Co. Ltd., Irlam, Manchester, UK). The corrections are performed at JAMSTEC, Yokosuka, Kanagawa, Japan by Marine Works Japan Ltd. (MWJ), Yokohama, Kanagawa, Japan, usually once in a year in order to monitor sensor time drift and linearity.

S/N 1027, 9 April 2014

slope = 0.99995022

offset = –0.74973

S/N 0677, 9 April 2014

slope = 0.99972807

offset = –0.10585

ii. Temperature (SBE 3)

The temperature sensing element is a glass-coated thermistor bead in a stainless steel tube, providing a pressure-free measurement at depths up to 10500 (6800) m by titanium (aluminum) housing. The SBE 3 thermometer has a nominal accuracy of 1 mK, typical stability of 0.2 mK/month, and resolution of 0.2 mK at 24 samples per second. The premium temperature sensor, SBE 3plus, is a more rigorously tested and calibrated version of standard temperature sensor (SBE 3).

Pre-cruise sensor calibrations were performed at SBE, Inc.

S/N 4811, 18 January 2014

S/N 1359, 1 May 2014

S/N 1524, 12 November 2013

Pressure sensitivities of SBE 3s were corrected according to a method by Uchida et al. (2007), for the following sensors.

S/N 4811, –2.7192e–7 [°C/dbar]

S/N 1359, –1.8386e–7 [°C/dbar]

iii. Conductivity (SBE 4)

The flow-through conductivity sensing element is a glass tube (cell) with three platinum electrodes to provide in-situ measurements at depths up to 10500 (6800) m by titanium (aluminum) housing. The SBE 4 has a nominal accuracy of 0.0003 S/m, typical stability of 0.0003 S/m/month, and resolution of 0.00004 S/m at 24 samples per second. The conductivity cells have been replaced to newer style cells for deep ocean measurements.

Pre-cruise sensor calibrations were performed at SBE, Inc.

S/N 2435, 1 May 2014

S/N 2854, 1 May 2014

S/N 1088, 17 July 2013

The value of conductivity at salinity of 35, temperature of 15 °C (IPTS-68) and pressure of 0 dbar is 4.2914 S/m.

iv. Oxygen (SBE 43)

The SBE 43 oxygen sensor uses a Clark polarographic element to provide in-situ measurements at depths up to 7000 m. The range for dissolved oxygen is 120 % of surface saturation in all natural waters, nominal accuracy is 2 % of saturation, and typical stability is 2 % per 1000 hours.

Pre-cruise sensor calibration was performed at SBE, Inc.

S/N 0394, 29 April 2014

S/N 0330, 29 April 2014

v. Deep Ocean Standards Thermometer

Deep Ocean Standards Thermometer (SBE 35) is an accurate, ocean-range temperature sensor that can be standardized against Triple Point of Water and Gallium Melt Point cells and is also capable of measuring temperature in the ocean to depths of 6800 m. The SBE 35 was used to calibrate the SBE 3 temperature sensors in situ (Uchida et al., 2007).

Pre-cruise sensor linearization was performed at SBE, Inc.

S/N 0022, 4 March 2009

Then the SBE 35 is certified by measurements in thermodynamic fixed-point cells of the TPW (0.01 °C) and GaMP (29.7646 °C). The slow time drift of the SBE 35 is adjusted by periodic recertification corrections. Pre-cruise sensor calibration was performed at SBE, Inc. From the end of 2011, the SBE has been applying a NIST correction to the fixed-point cells used for the calibration.

S/N 0022, 3 September 2013 (slope and offset correction)

Slope = 1.000006

Offset = 0.000187

The time required per sample = 1.1 × NCYCLES + 2.7 seconds. The 1.1 seconds is total time per an acquisition cycle. NCYCLES is the number of acquisition cycles per sample and was set to 4. The 2.7 seconds

is required for converting the measured values to temperature and storing average in EEPROM.

vi. Altimeter

Benthos PSA-916T Sonar Altimeter (Teledyne Benthos, Inc.) determines the distance of the target from the unit by generating a narrow beam acoustic pulse and measuring the travel time for the pulse to bounce back from the target surface. It is rated for operation in water depths up to 10000 m. The PSA-916T uses the nominal speed of sound of 1500 m/s.

vii. Oxygen optode (RINKO)

RINKO (JFE Alec Co., Ltd.) is based on the ability of selected substances to act as dynamic fluorescence quenchers. RINKO model III is designed to use with a CTD system which accept an auxiliary analog sensor, and is designed to operate down to 7000 m.

Data from the RINKO can be corrected for the time-dependent, pressure-induced effect by means of the same method as that developed for the SBE 43 (Edwards et al., 2010). The calibration coefficients, H1 (amplitude of hysteresis correction), H2 (curvature function for hysteresis), and H3 (time constant for hysteresis) were determined empirically as follows.

H1 = 0.007 (for S/N 0024)

H2 = 5000 dbar

H3 = 2000 seconds

Outputs from RINKO are the raw phase shift data. The RINKO can be calibrated by the modified Stern-Volmer equation slightly modified from a method by Uchida et al. (2010):

$$O_2\ (\mu mol/l) = [(V_0 / V)^E - 1] / K_{sv}$$

where V is voltage, V_0 is voltage in the absence of oxygen, K_{sv} is Stern-Volmer constant. The coefficient E corrects nonlinearity of the Stern-Volmer equation. The V_0 and the K_{sv} are assumed to be functions of temperature as follows.

$$K_{sv} = C_0 + C_1 \times T + C_2 \times T^2$$

$$V_0 = 1 + C_3 \times T$$

$$V = C_4 + C_5 \times V_b$$

where T is CTD temperature (°C) and V_b is raw output (volts). V_0 and V are normalized by the output in the absence of oxygen at 0°C. The oxygen concentration is calculated using accurate temperature data from the CTD temperature sensor instead of temperature data from the RINKO. The pressure-compensated oxygen concentration O_{2c} can be calculated as follows.

$$O_{2c} = O_2\ (1 + C_p p / 1000)$$

where p is CTD pressure (dbar) and C_p is the compensation coefficient. Since the sensing foil of the optode is permeable only to gas and not to water, the optode oxygen must be corrected for salinity. The salinity-compensated oxygen can be calculated by multiplying the factor of the effect of salt on the oxygen solubility. The coefficients of the equation by García and Gordon (1992) were modified based on the laboratory experiment (Uchida et al., in prep.) and used for the compensation (B0 = –6.33568e–3, B1 = –6.84389e–3, B2 = –1.18326e–2, B3 = –5.51960e–2, C0 = 3.40543e–6).

Pre-cruise sensor calibrations were performed at RCGC/JAMSTEC.

S/N 0024, 14 May 2014

viii. Fluorometer

The Seapoint Chlorophyll Fluorometer (Seapoint Sensors, Inc., Kingston, New Hampshire, USA) provides in-situ measurements of chlorophyll-a at depths up to 6000 m. The instrument uses modulated blue

LED lamps and a blue excitation filter to excite chlorophyll-a. The fluorescent light emitted by the chlorophyll-a passes through a red emission filter and is detected by a silicon photodiode. The low level signal is then processed using synchronous demodulation circuitry, which generates an output voltage proportional to chlorophyll-a concentration.

ix. Transmissometer

The C-Star Transmissometer (WET Labs, Inc., Philomath, Oregon, USA) measures light transmittance at a single wavelength (650 nm) over a know path (25 cm). In general, losses of light propagating through water can be attributed to two primary causes: scattering and absorption. By projecting a collimated beam of light through the water and placing a focused receiver at a known distance away, one can quantify these losses. The ratio of light gathered by the receiver to the amount originating at the source is known as the beam transmittance. Suspended particles, phytoplankton, bacteria and dissolved organic matter contribute to the losses sensed by the instrument. Thus, the instrument provides information both for an indication of the total concentrations of matter in the water as well as for a value of the water clarity.

Light transmission T_r (in %) and beam attenuation coefficient c_p are calculated from the sensor output (V in volt) as follows.

$$T_r = (c_0 + c_1 V) \times 100$$

$$c_p = -(1 / 0.25) \ln(T_r / 100)$$

The calibration coefficients were determined by using the data obtained in the R/V Mirai MR13-06 cruise.

x. PAR

Photosynthetically Active Radiation (PAR) sensors (Satlantic, LP, Halifax, Nova Scotia, Canada) provide highly accurate measurements of PAR (400 – 700 nm) for a wide range of aquatic and terrestrial applications. The ideal spectral response for a PAR sensor is one that gives equal emphasis to all photons between 400 – 700 nm. Satlantic PAR sensors use a high quality filtered silicon photodiode to provide a near equal spectral response across the entire wavelength range of the measurement.

Pre-cruise sensor calibration was performed at Satlantic, LP.

S/N 0049, 22 January 2009

xi. CDOM

The Environmental Characterization Optics (ECO) miniature fluorometer (WET Labs, Inc., Philomath, Oregon, USA) allows the user to measure relative Colored Dissolved Organic Matter (CDOM) concentrations by directly measuring the amount of fluorescence emission in a sample volume of water. The CDOM fluorometer uses an UV LED to provide the excitation source. An interference filter is used to reject the small amount of out-of-band light emitted by the LED. The light from the source enters the water volume at an angle of approximately 55-60degrees with respect to the end face of the unit. Fluoresced light is received by a detector positioned where the acceptance angle forms a 140-degree intersection with the source beam. An interference filter is used to discriminate against the scattered excitation light.

CDOM (Quinine Dihydrate Equivalent) concentration expressed in ppb can be derived using the equation as follows.

CDOM = Scale Factor * (Output – Dark Counts)

Pre-cruise sensor calibration was performed at WET Labs.

S/N 2014, 21 September 2010

Dark Counts: 0.027 V

Scale Factor: 101 ppb/V
Maximum Output: 4.94 V

xii. Deep SUNA

The SUNA (Submersible Ultraviolet Nitrate Analyzer) is a chemical-free nitrate sensor (Satlantic, LP, Halifax, Nova Scotia, Canada). It is based on the ISUS (In Situ Ultraviolet Spectroscopy) technology developed at Monterey Bay Aquarium Research Institute (MBARI). The Deep SUNA housing is made from anodized aluminum. The housing is designed to withstand depths of up to 2000 m. The SUNA measures the concentration of dissolved nitrate in water. The sensor illuminates the water sample with its deuterium UV light source, and measures the throughput using its photo-spectrometer. The difference between this measurement and a prior baseline reference measurement of pure water constitutes an absorption spectrum.

Absorbance characteristics of natural water components are provided in the sensor calibration file. The Beer-Lambert Law for multiple absorbers establishes the relationship between the total measured absorbance and the concentrations of individual components. Based on this relationship, the sensor obtains a best estimate for the nitrate concentration using multi-variable linear regression.

The Deep SUNA was used with the CTD system as an auxiliary analog sensor at shallow casts in leg 1 (stations 001_2, 007_1, 014_1, and 030_1), since it is designed to operate down to 2000 m and it was used with the Continuous Sea Surface Water Monitoring System (see Section 2.4) in leg 2.

(5) Data collection and processing

i. Data collection

CTD system was powered on at least 20 minutes in advance of the data acquisition to stabilize the pressure sensor and was powered off at least two minutes after the operation in order to acquire pressure data on the ship's deck.

The package was lowered into the water from the starboard side and held 10 m beneath the surface in order to activate the pump. After the pump was activated, the package was lifted to the surface and lowered at a rate of 1.0 m/s to 200 m (or 300 m when significant wave height was high) then the package was stopped to operate the heave compensator of the crane. The package was lowered again at a rate of 1.2 m/s to the bottom. For the up cast, the package was lifted at a rate of 1.1 m/s except for bottle firing stops. As a rule, the bottle was fired after waiting from the stop for 30 seconds (20 seconds from station 049_1 to save the observation time) and the package was stayed at least 5 seconds for measurement of the SBE 35 at each bottle firing stops. For depths where vertical gradient of water properties were expected to be large, the bottle was exceptionally fired after waiting from the stop for 60 seconds (50 seconds from station 049_1 to save the observation time) to enhance exchanging the water between inside and outside of the bottle. At 200 m (or 300 m) from the surface, the package was stopped to stop the heave compensator of the crane.

Water samples were collected using a 36-bottle (or 12-bottles) SBE 32 Carousel Water Sampler with 12-litre Niskin-X bottles. Before a cast taken water for CFCs, the bottle frame and Niskin-X bottles were wiped with acetone.

Data acquisition software

SEASAVE-Win32, version 7.23.2

ii. Data collection problems

(a) Miss trip, miss fire, and remarkable leak

Niskin bottles did not trip correctly at the following stations.

Miss trip	Miss fire	Remarkable leak
140_1, #16	001_1, #6	074_1 ~ 093_1, #3
	001_2, #24	

Since all of the latch assemblies for the SBE 32 (S/N 0924) was defective, the SBE 32 was replaced from S/N 0924 to S/N 0391 after the station 001_2. Also, the latch assembly for #16 of S/N 0391 was replaced after the station 140_1. The bottle sampled salinity data were relatively lower (about 0.001) than the CTD salinity data for the bottle #3 at stations from 074 to 093. The drain cock of the bottle #3 was replaced after the station 094_1.

(b) Failure of insulation of the CTD winch armored cable

Failure of insulation of the CTD winch armored cable occurred at 2608 dbar of up cast of the station 041_1. Therefore, the up cast was aborted and the armored cable was cut 1620 m after the cast.

(c) Detachment of some sensors at deep casts deeper than 6000 m

Fluorometer, transmissometer, CDOM, LADCP, and Micro Rider were detached at stations 047_1, 046_1, 045_1, and 044_1, because of the withstand depth of 6000 m for these sensors. At stations 001_1, 080_1, 081_1, 088_1, and 089_1, the CTD package was lowered depths up to 6000 m without detachment of these sensors, although water depths of these stations were deeper than 6000 m.

(d) Noise of SBE 43 (S/N 0394)

Relatively large noise was found in the SBE 43 data at about 4762~4789 dbar of down cast. Therefore, the SBE 43 was replaced from S/N 0394 to S/N 0330 after the station 056_1.

(e) Noise of primary temperature and salinity data

The primary temperature and/or salinity data were noisy for down cast of following stations: 074_1 and 145_1. Therefore, the secondary temperature and salinity data were used for these stations for vertical profile (wct file). The primary temperature and/or salinity data were noisy for up cast of following stations: 050_1, 144_1, and 145_1. Therefore, the secondary temperature and salinity data were used for these stations for bottle data (seafile).

(f) Noise of transmissometer

The transmissometer data were (partly) noisy for down cast at following stations: 022_1, 043_1, 057_1, 065_1, 077_1, 079_1, 080_1, 089_1, 091_2, 092_1, 095_1, 097_1, 126_1, 130_1, 141_1, 142_1, and 145_1. Therefore, the up cast data were used for vertical profile data (wct file) for these stations instead using the down cast data.

iii. Data processing

SEASOFT consists of modular menu driven routines for acquisition, display, processing, and archiving of oceanographic data acquired with SBE equipment. Raw data are acquired from instruments and are stored as unmodified data. The conversion module DATCNV uses instrument configuration and calibration coefficients to create a converted engineering unit data file that is operated on by all SEASOFT post processing modules. The following are the SEASOFT and original software data processing module sequence and specifications

used in the reduction of CTD data in this cruise.

Data processing software

SBEDataProcessing-Win32, version 7.23.2

DATCNV converted the raw data to engineering unit data. DATCNV also extracted bottle information where scans were marked with the bottle confirm bit during acquisition. The duration was set to 4.4 seconds, and the offset was set to 0.0 second. The hysteresis correction for the SBE 43 data (voltage) was applied for both profile and bottle information data.

TCORP (original module, version 1.1) corrected the pressure sensitivity of the SBE 3 for both profile and bottle information data.

RINKOCOR (original module, version 1.0) corrected the time-dependent, pressure-induced effect (hysteresis) of the RINKO for both profile data.

RINKOCORROS (original module, version 1.0) corrected the time-dependent, pressure-induced effect (hysteresis) of the RINKO for bottle information data by using the hysteresis-corrected profile data.

BOTTLESUM created a summary of the bottle data. The data were averaged over 4.4 seconds (or 1 second for the bottle fired without stop).

ALIGNCTD converted the time-sequence of sensor outputs into the pressure sequence to ensure that all calculations were made using measurements from the same parcel of water. For a SBE 9plus CTD with the ducted temperature and conductivity sensors and a 3000-rpm pump, the typical net advance of the conductivity relative to the temperature is 0.073 seconds. So, the SBE 11plus deck unit was set to advance the primary and the secondary conductivity for 1.73 scans (1.75/24 = 0.073 seconds). Oxygen data are also systematically delayed with respect to depth mainly because of the long time constant of the oxygen sensor and of an additional delay from the transit time of water in the pumped plumbing line. This delay was compensated by 6 seconds advancing the SBE 43 oxygen sensor output (voltage) relative to the temperature data. Delay of the RINKO data was also compensated by 1 second advancing sensor output (voltage) relative to the temperature data. Delay of the transmissometer data was also compensated by 2 seconds advancing sensor output (voltage) relative to the temperature data.

WILDEDIT marked extreme outliers in the data files. The first pass of WILDEDIT obtained an accurate estimate of the true standard deviation of the data. The data were read in blocks of 1000 scans. Data greater than 10 standard deviations were flagged. The second pass computed a standard deviation over the same 1000 scans excluding the flagged values. Values greater than 20 standard deviations were marked bad. This process was applied to pressure, temperature, conductivity, and SBE 43 output.

CELLTM used a recursive filter to remove conductivity cell thermal mass effects from the measured conductivity. Typical values used were thermal anomaly amplitude alpha = 0.03 and the time constant 1/beta = 7.0.

FILTER performed a low pass filter on pressure with a time constant of 0.15 seconds. In order to produce zero phase lag (no time shift) the filter runs forward first then backwards.

WFILTER performed as a median filter to remove spikes in fluorometer, transmissometer, and CDOM data. A median value was determined by 49 scans of the window.

SECTIONU (original module, version 1.1) selected a time span of data based on scan number in order to reduce a file size. The minimum number was set to be the start time when the CTD package was beneath the sea-surface after activation of the pump. The maximum number was set to be the end time when the depth of the package was 1 dbar below the surface. The minimum and maximum numbers were automatically calculated in the module.

LOOPEDIT marked scans where the CTD was moving less than the minimum velocity of 0.0 m/s (traveling backwards due to ship roll).

DESPIKE (original module, version 1.0) removed spikes of the data. A median and mean absolute deviation was calculated in 1-dbar pressure bins for both down- and up-cast, excluding the flagged values. Values greater than 4 mean absolute deviations from the median were marked bad for each bin. This process was performed 2 times for temperature, conductivity, SBE 43, and RINKO output.

DERIVE was used to compute oxygen (SBE 43).

BINAVG averaged the data into 1-dbar pressure bins. The center value of the first bin was set equal to the bin size. The bin minimum and maximum values are the center value plus and minus half the bin size. Scans with pressures greater than the minimum and less than or equal to the maximum were averaged. Scans were interpolated so that a data record exist every dbar.

BOTTOMCUT (original module, version 0.1) deleted the deepest pressure bin when the averaged scan number of the deepest bin was smaller than the average scan number of the bin just above.

DERIVE was re-used to compute salinity, potential temperature, and density (σ_θ).

SPLIT was used to split data into the down cast and the up cast.

Remaining spikes in the CTD data were manually eliminated from the 1-dbar-averaged data. The data gaps resulting from the elimination were linearly interpolated with a quality flag of 6.

(6) Post-cruise calibration

i. Pressure

The CTD pressure sensor offset in the period of the cruise was estimated from the pressure readings on the ship deck. For best results the Paroscientific sensor was powered on for at least 20 minutes before the operation. In order to get the calibration data for the pre- and post-cast pressure sensor drift, the CTD deck pressure was averaged over first and last one minute, respectively. Then the atmospheric pressure deviation from a standard atmospheric pressure (14.7 psi) was subtracted from the CTD deck pressure to check the pressure sensor time drift. The atmospheric pressure was measured at the captain deck (20 m high from the base line) and sub-sampled one-minute interval as a meteorological data. Time series of the CTD deck pressure is shown in Fig. 3.1.1. The CTD pressure sensor offset was estimated from the deck pressure. Mean of the pre- and the post-casts data over the whole period gave an estimation of the pressure sensor offset (–0.04 dbar) from the pre-cruise calibration. The post-cruise correction of the pressure data is not deemed necessary for the pressure sensor.

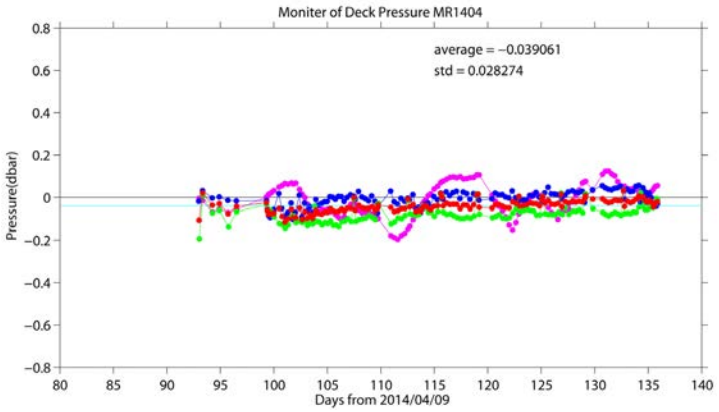

Fig. 3.1.1 Time series of the CTD deck pressure. Atmospheric pressure deviation (magenta dots) from a standard atmospheric pressure was subtracted from the CTD deck pressure. Blue and green dots indicate pre- and post-cast deck pressures, respectively. Red dots indicate averages of the pre- and the post-cast deck pressures.

ii. Temperature

The CTD temperature sensors (SBE 3) were calibrated with the SBE 35 under the assumption that discrepancies between SBE 3 and SBE 35 data were due to pressure sensitivity, the viscous heating effect, and time drift of the SBE 3, according to a method by Uchida et al. (2007).

Post-cruise sensor calibration for the SBE 35 will be performed at SBE, Inc in December 2014.

The CTD temperature was preliminary calibrated as

$$\text{Calibrated temperature} = T - (c_0 \times P + c_1 \times t + c_2)$$

where T is CTD temperature in °C, P is pressure in dbar, t is time in days from pre-cruise calibration date of the CTD temperature and c_0, c_1, and c_2 are calibration coefficients. The coefficients were determined using the data for the depths deeper than 1950 dbar.

The primary temperature data were basically used for the post-cruise calibration. The secondary temperature sensor was also calibrated and used instead of the primary temperature data when the data quality of the primary temperature data was bad. The calibration coefficients are listed in Table 3.1.1. The results of the post-cruise calibration for the CTD temperature are summarized in Table 3.1.2 and shown in Figs. 3.1.2 and 3.1.3.

Table 3.1.1 Calibration coefficients for the CTD temperature sensors.

Serial number	c_0 (°C/dbar)	c_1 (°C/day)	c_2 (°C)
4811	–1.29748e–8	4.02418e-6	–0.0003
1359	1.67653e–8	5.20248e-6	–0.0002

Table 3.1.2 Difference between the CTD temperature and the SBE 35 after the post-cruise calibration. Mean and standard deviation (Sdev) are calculated for the data below and above 950 dbar. Number of data used is also shown.

Serial number	Pressure ≥ 950 dbar			Pressure < 950 dbar		
	Number	Mean (mK)	Sdev (mK)	Number	Mean (mK)	Sdev (mK)
4811	1544	–0.0	0.2	2756	–0.1	11.7
1359	1546	0.0	0.2	2774	0.3	9.1

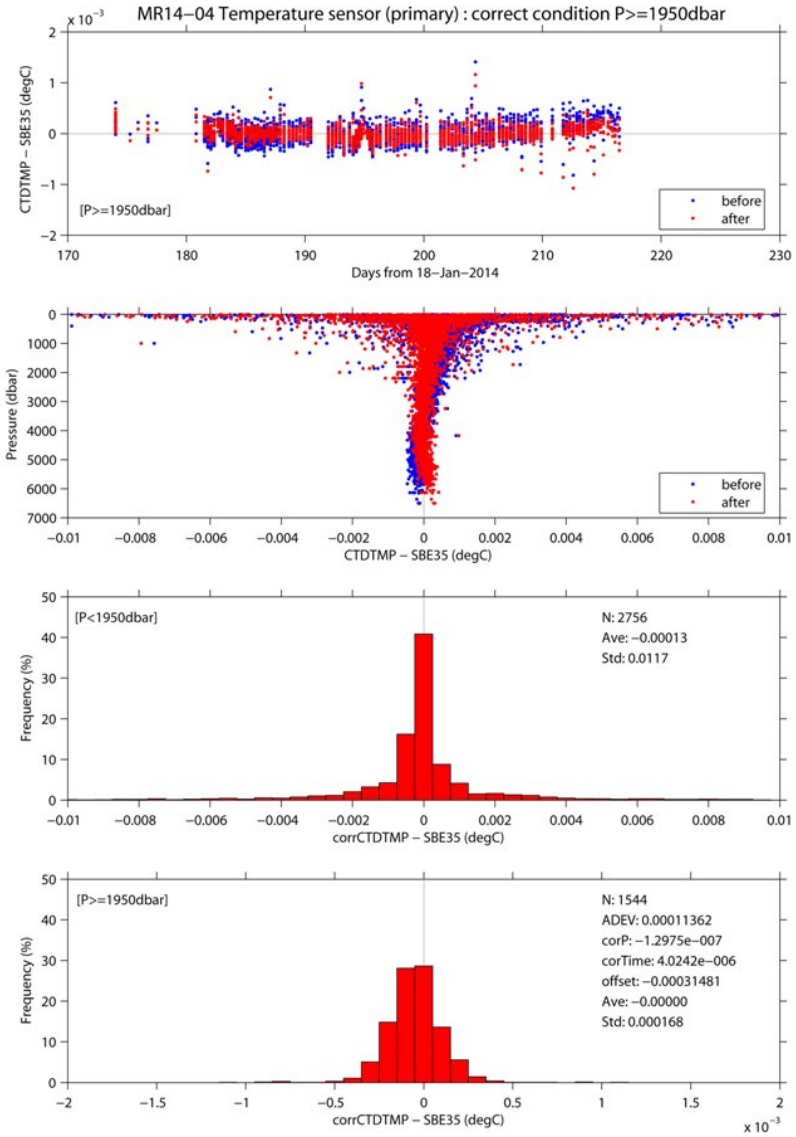

Fig. 3.1.2 Difference between the CTD temperature (primary) and the SBE 35. Blue and red dots indicate before and after the post-cruise calibration using the SBE 35 data, respectively. Lower two panels show histogram of the difference after the calibration.

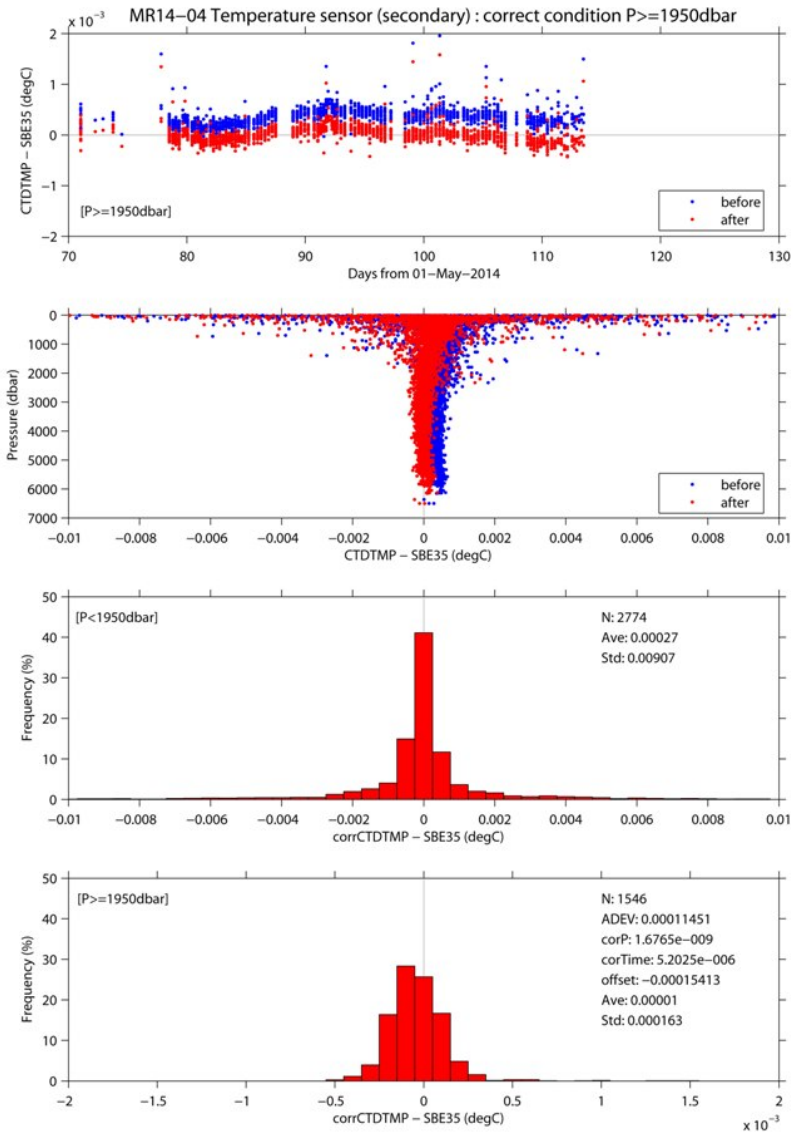

Fig. 3.1.3 Same as Fig. 3.1.2, but for secondary temperature sensor.

iii. Salinity

The discrepancy between the CTD conductivity and the conductivity calculated from the bottle salinity data with the CTD temperature and pressure data is considered to be a function of conductivity, pressure and time. The CTD conductivity was calibrated as

$$\text{Calibrated conductivity} = c_0 \times C + c_1 \times P + c_2 \times C \times P + c_3 \times t + c_4$$

where C is CTD conductivity in S/m, P is pressure in dbar, t is time in days from 11 July 2009, 00:58 (UTC) and c_0, c_1, c_2, c_3 and c_4 are calibration coefficients. The best fit sets of coefficients were determined by a least square technique to minimize the deviation from the conductivity calculated from the bottle salinity data.

The primary conductivity data created by the software module ROSSUM were basically used after the post-cruise calibration for the temperature data. The secondary conductivity sensor was also calibrated and used instead of the primary conductivity data when the data quality of the primary temperature or conductivity data was bad. The calibration coefficients are listed in Table 3.1.3. The results of the post-cruise calibration for the CTD salinity are summarized in Table 3.1.4 and shown in Figs. 3.1.4 and 3.1.5.

Table 3.1.3 Calibration coefficients for the CTD conductivity sensors.

Serial Number	c_0	c_1 [S/(m dbar)]	c_2 (1/dbar)	c_3 [S/(m day)]	c_4 (S/m)
2435	–7.51283e–5	2.42062e–7	–6.89235e–8	–5.29014e–7	1.93028e–4
2854	–2.18278e–4	–1.62860e–7	5.27345e–8	1.50084e–6	5.46236e–4

Table 3.1.4 Difference between the CTD salinity and the bottle salinity after the post-cruise calibration. Mean and standard deviation (Sdev) (in 10^{-3}) are calculated for the data below and above 1950 dbar. Number of data used is also shown.

Serial number	Pressure ≥ 1950 dbar			Pressure < 1950 dbar		
	Number	Mean	Sdev	Number	Mean	Sdev
2435	1574	0.0	0.4	2105	–0.9	7.3
2854	1580	0.0	0.5	2140	–0.9	7.5

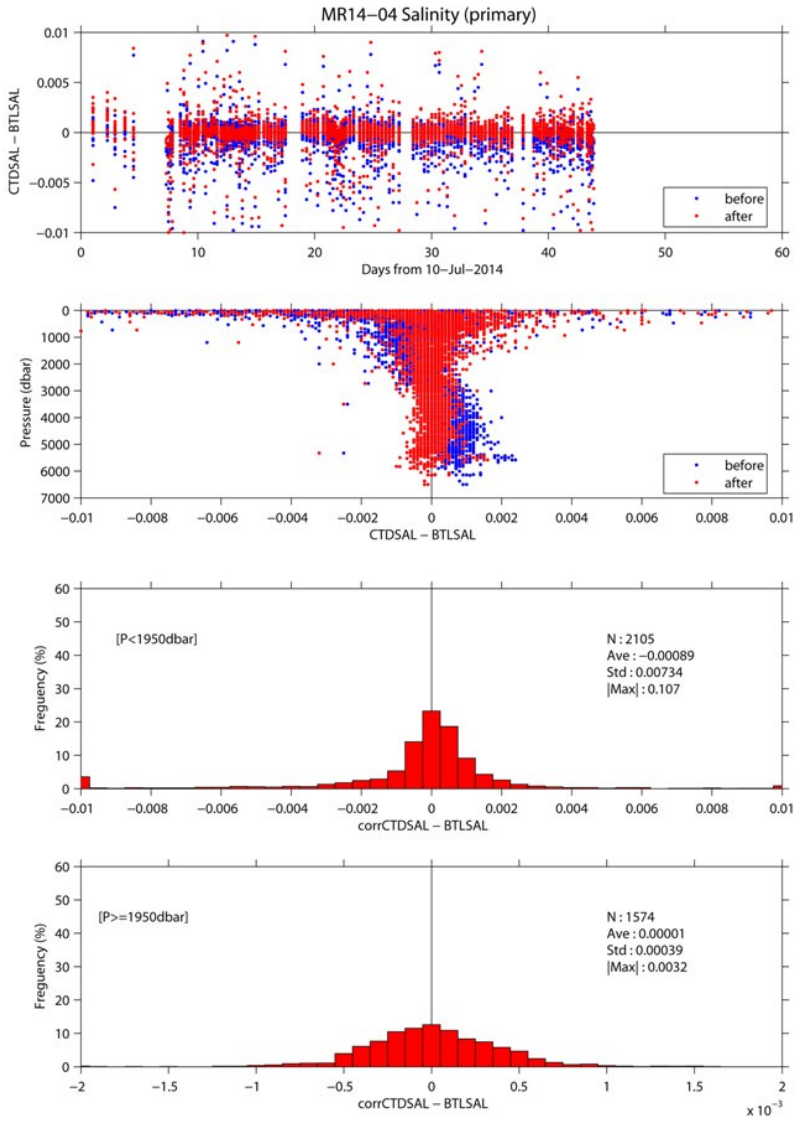

Fig. 3.1.4 Difference between the CTD salinity (primary) and the bottle salinity. Blue and red dots indicate before and after the post-cruise calibration, respectively. Lower two panels show histogram of the difference after the calibration.

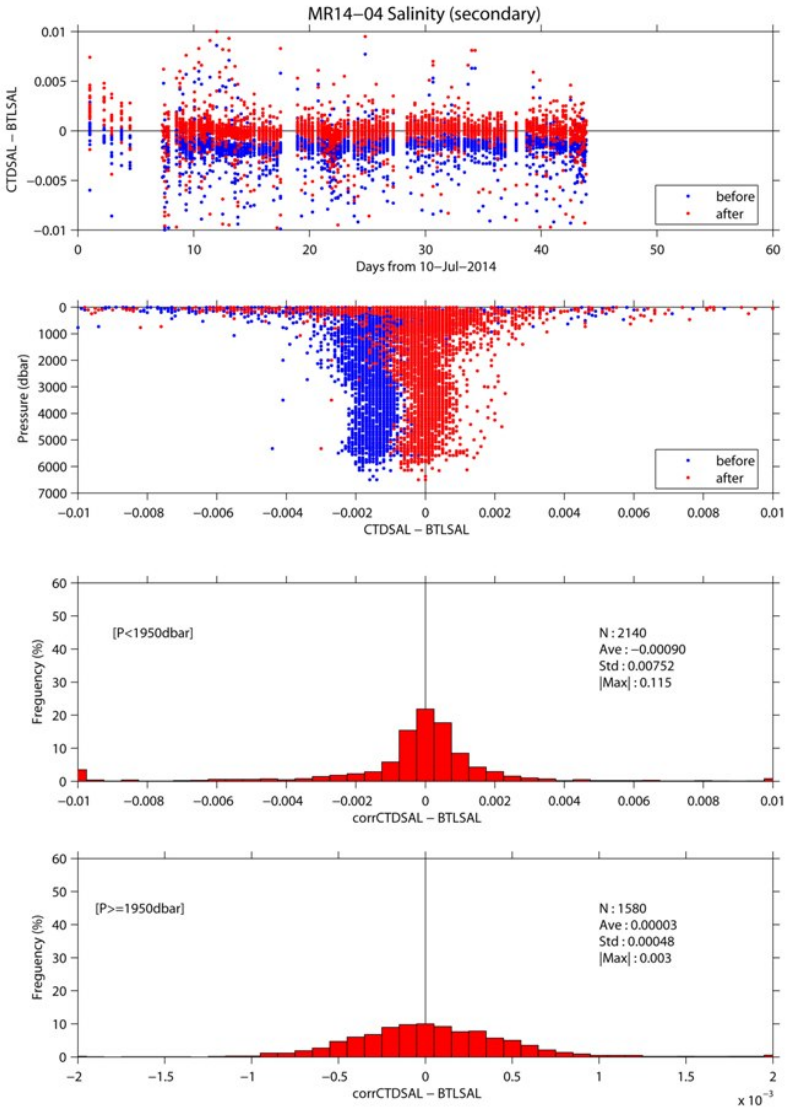

Fig. 3.1.5 Same as Fig. 3.1.4, but for secondary salinity.

iv. Oxygen

The RINKO oxygen optode (S/N 0024) was calibrated and used as the CTD oxygen data, since the RINKO has a fast time response. The pressure-hysteresis corrected RINKO data was calibrated by the modified Stern-Volmer equation, basically according to a method by Uchida et al. (2010) with slight modification:

$$[O_2]\ (\mu mol/l) = [(V_0 / V)^{1.1} - 1] / K_{sv}$$

and

$$K_{sv} = C_0 + C_1 \times T + C_2 \times T^2$$

$$V_0 = 1 + C_3 \times T$$

$$V = C_4 + C_5 \times V_b + C_6 \times t + C_7 \times t \times V_b$$

where V_b is the RINKO output (voltage), V_0 is voltage in the absence of oxygen, T is temperature in °C, and t is exciting time (days) integrated from the first CTD cast for each leg. Time drift of the RINKO output was corrected. The calibration coefficients were determined by minimizing the sum of absolute deviation with a weight from the bottle oxygen data. The revised quasi-Newton method (DMINF1) was used to determine the sets.

The post-cruise calibrated temperature and salinity data were used for the calibration. The calibration coefficients are listed in Table 3.1.5. The results of the post-cruise calibration for the RINKO oxygen are summarized in Table 3.1.6 and shown in Fig. 3.1.6.

Table 3.1.5 Calibration coefficients for the RINKO oxygen sensors.

Coefficient	S/N 0024
c_0	4.08789e–3
c_1	1.58333e–4
c_2	2.10854e–6
c_3	–1.14204e–3
c_4	–0.109961
c_5	0.356093
c_6	–2.55873e–4
c_7	3.13918e–4
C_p	0.014

Table 3.1.6 Difference between the RINKO oxygen and the bottle ooxygen after the post-cruise calibration. Mean and standard deviation (Sdev) are calculated for the data below and above 1950 dbar. Number of data used is also shown.

Serial number	Pressure ≥ 1950 dbar			Pressure < 1950 dbar		
	Number	Mean [μmol/kg]	Sdev	Number	Mean [μmol/kg]	Sdev
0024	1571	–0.03	0.30	2100	0.01	1.50

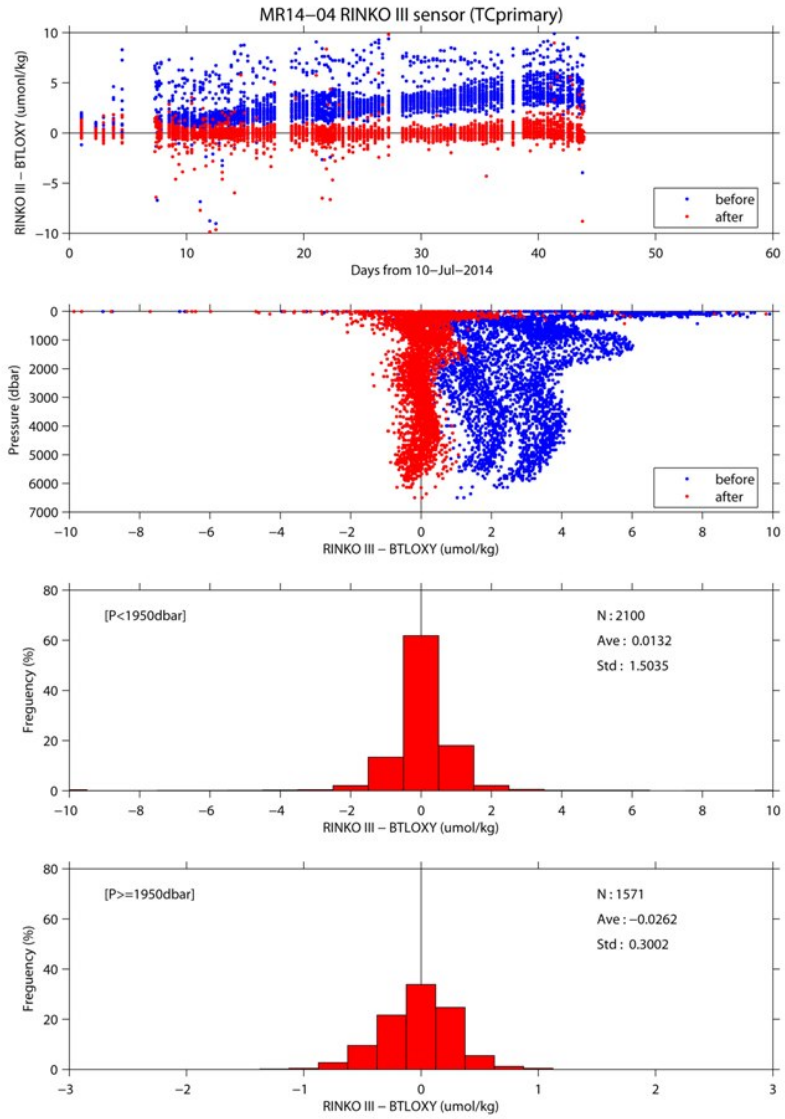

Fig. 3.1.6 Difference between the CTD oxygen and the bottle oxygen for leg 1. Blue and red dots indicate before and after the post-cruise calibration, respectively. Lower two panels show histogram of the difference after the calibration.

v. Fluorometer

The CTD fluorometer (FLUOR in µg/L) was calibrated by comparing with the bottle sampled chlorophyll-a as

$$FLUORc = c_0 + c_1 \times FLUOR$$

where c_0 and c_1 are calibration coefficients. The CTD fluorometer data is slightly noisy so that the up cast profile data which was averaged over one decibar agree with the bottle sampled data better than the discrete CTD fluorometer data obtained at bottle-firing stop. Therefore, the CTD fluorometer data at water sampling

depths extracted from the up cast profile data were compared with the bottle sampled chlorophyll-a data. The bottle sampled data obtained at dark condition [PAR (Photosynthetically Available Radiation) < 50 μE/(m^2 sec), see Section 2.3] were used for the calibration, since sensitivity of the fluorometer to chlorophyll *a* is different at nighttime and daytime (Section 2.4 in Uchida et al., 2015). Sensitivity of the fluorometer to chlorophyll *a* may be also different between high and low temperature (see Section 2.4). Therefore, the slope (c_1) of the calibration coefficients are determined for three groups of stations: stations south of 38.8°N in leg 1 (001, 007, 014, and 022), the closest station to the coast (036), and other stations (Fig. 3.1.7). For the last group of stations, sensitivity of the fluorometer to chlorophyll *a* change at about 0.3 μg/L of the fluorometer data, so that the slope (c_1) is changed for the fluorometer data larger than 0.3 μg/L. The calibration coefficients are listed in Table 3.1.7. The results of the post-cruise calibration for the fluorometer are summarized in Table 3.1.8 and shown in Fig. 3.1.8.

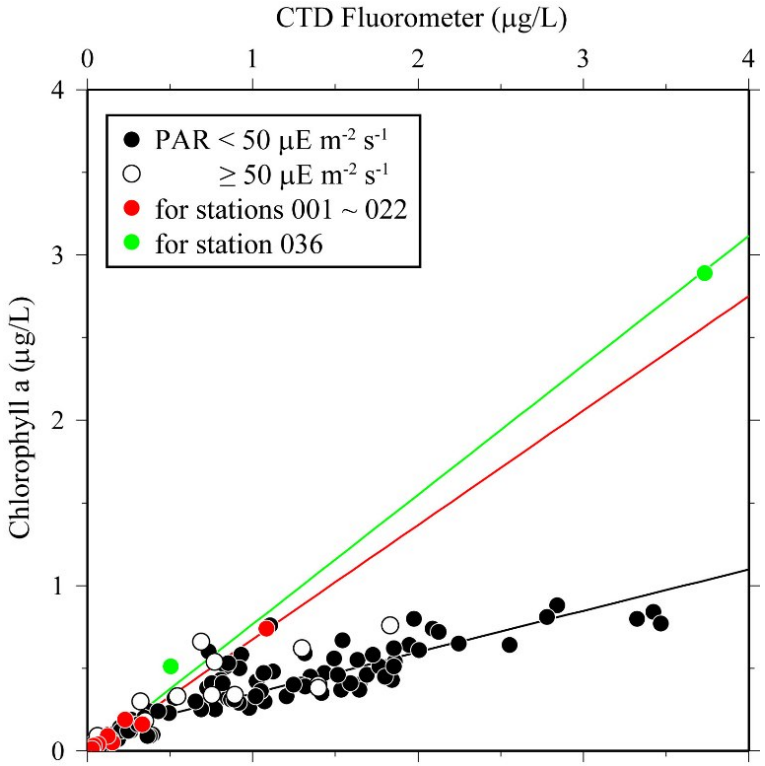

Fig. 3.1.7. Comparison of the CTD fluorometer and the bottle sampled chlorophyll-a. The regression lines are also shown.

Table 3.1.7. Calibration coefficients for the CTD fluorometer.

Stations	c_0	c_1	Note
001, 007, 014, 022	–1.64441e–2	0.691796	
036	–1.64441e–2	0.783024	
Other stations	–1.64441e–2	0.630088	Fluorometer data ≤ 0.3 μg/L
	9.75510e–2	0.250104	Fluorometer data > 0.3 μg/L

Table 3.1.8. Difference between the CTD fluorometer and the bottle chlorophyll-a after the post-cruise calibration. Mean, standard deviation (Sdev), and number of data used are shown. Data obtained at daytime are also used in this calculation.

Number	Mean	Sdev
221	–0.00 µg/L	0.08 µg/L

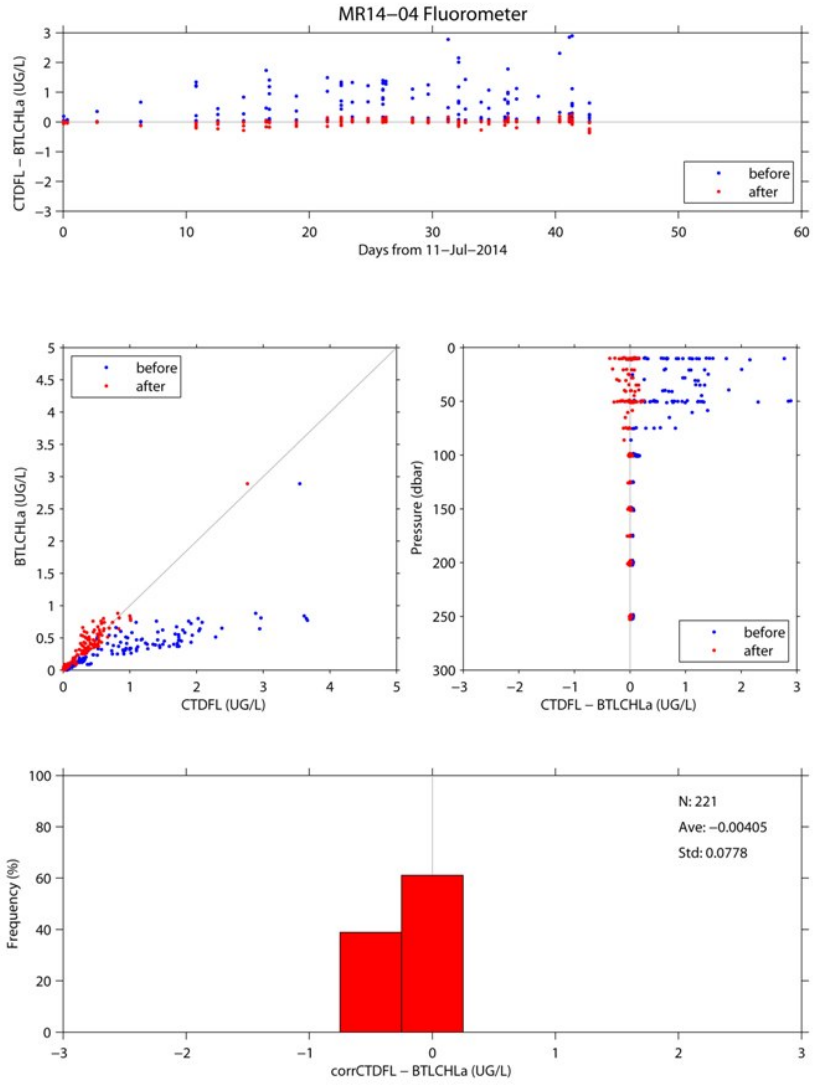

Fig. 3.1.8. Comparison of the CTD fluorometer and the bottle sampled chlorophyll-a. Blue and red dots indicate before and after the post-cruise calibration, respectively. Lower panel shows histogram of the difference after the calibration. Data obtained at daytime are also shown in this figure.

vi. Transmissometer

The transmissometer (T_r in %) is calibrated as

$$T_r = (V–V_d) / (V_r–V_d) \times 100$$

wehre V is the measured signal (voltage), V_d is the dark offset for the instrument, and V_r is the signal for clear water. V_d can be obtained by blocking the light path. V_d and V_{air}, which is the signal for air, were measured on deck before each cast after wiping the optical windows with ethanol. V_d was constant (0.0012) during the cruise. Vr is estimated from the measured maximum signal in the deep ocean at each cast. Since the transmissometer drifted in time (Fig. 3.1.9), Vr is expressed as

$$V_r = c_0 + c_1 \times t + c_2 \times t^2$$

where t is working time (in days) of the transmissometer, and c_0, c_1, and c_2 are calibration coefficients.

The calibration coefficients are listed in Table 3.1.9. For stations 066 and 097, V_r shifted though V_d was same as others. Therefore, V_r was individually estimated as to be 4.6166 and 4.6044 for stations 066 and 097, respectively. In addition, the transmissometer data for station 141_1 was also corrected with an offset of +0.0055 volts.

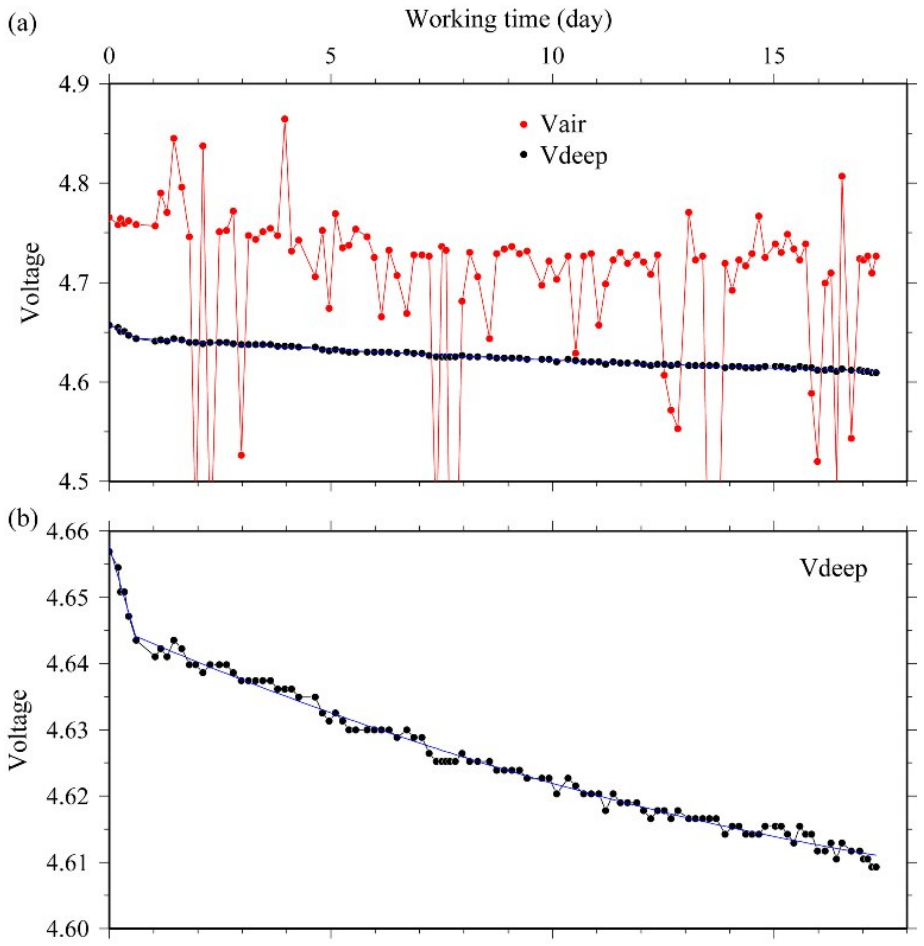

Fig. 3.1.9. Time series of an output signal (voltage) from transmissometer at on deck before CTD casts (Vair) and deep ocean (Vdeep). The solid line indicates the modeled signal in the deep clear ocean.

Table 3.1.9 Calibration coefficients for the CTD fluorometer.

Leg	c_0	c_1	c_2	V_d
1	4.65763	–2.28408e–2	–	0.0012
2	4.64582	–2.91438e–3	5.23667e–5	0.0012

vii. PAR

The PAR sensor was calibrated with an offset correction. The offset was estimated from the data measured in the deep ocean during the cruise. The corrected data (PARc) is calculated from the raw data (PAR) as follows:

PARc [$\mu E\ m^{-2}\ s^{-1}$] = PAR – 0.046.

vii. CDOM

The CDOM sensor wasn't calibrated, since the reference data (see Section 3.9) was not adequate for the in-situ calibration. The data were low-pass filtered by a running mean with a window of 15 seconds (about 13 m), since the data was noisy (Fig. 3.1.10). Moreover, the data were flagged as 4 (bad measurement) for depths deeper than about 4500 m due to large shift of the data (Fig. 3.1.10).

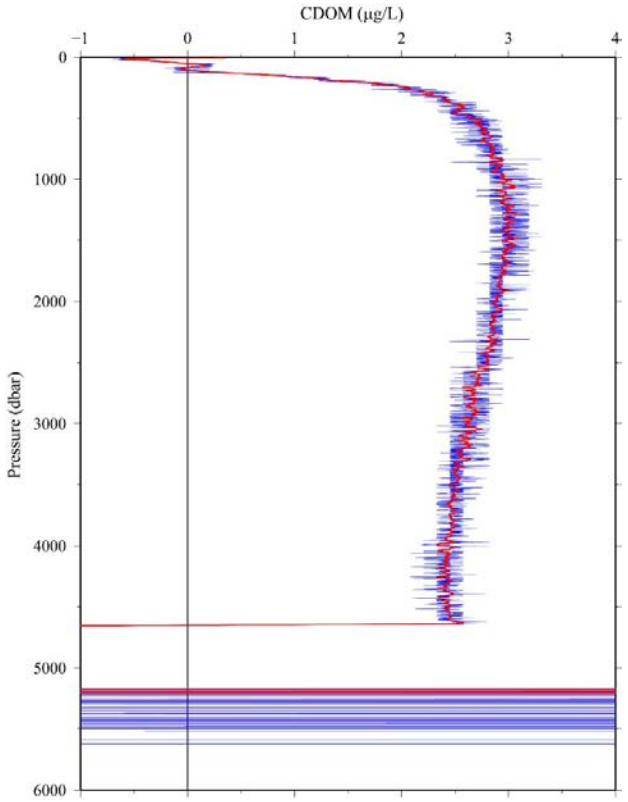

Fig. 3.1.10. An example of vertical profile of the CDOM sensor (station 100). Blue line shows original data and red line shows low-pass filtered data.

viii. Deep SUNA

The down and up cast profile from the Deep SUNA showed relatively large difference (Fig. 3.1.11). Maximum difference between the down and up cast data was about 0.084 volts and it corresponded to 4 μmol/kg of nitrate (Fig. 3.1.12). Since average of the down and up cast data at same pressure surface showed better linearity against the bottle sampled nitrate data (Fig. 3.1.12), nitrate from the Deep SUNA (NRA in μmol/kg) was estimated from the average data (NRAVave in volts) by comparing with the bottle sampled nitrate data as

$$NRA = c_0 + c_1 \times NRAVave$$

where c_0 and c_1 are calibration coefficients. The calibration coefficients are listed in Table 3.1.10. The average of the down and up cast data was used for the bottle sampled data (seafile) and profile data (wct file).

Table 3.1.10. Calibration coefficients for the Deep SUNA.

number of comparison	c_0	c_1	Sdev
43	–5.84651	22.7101	0.53 μmol/kg

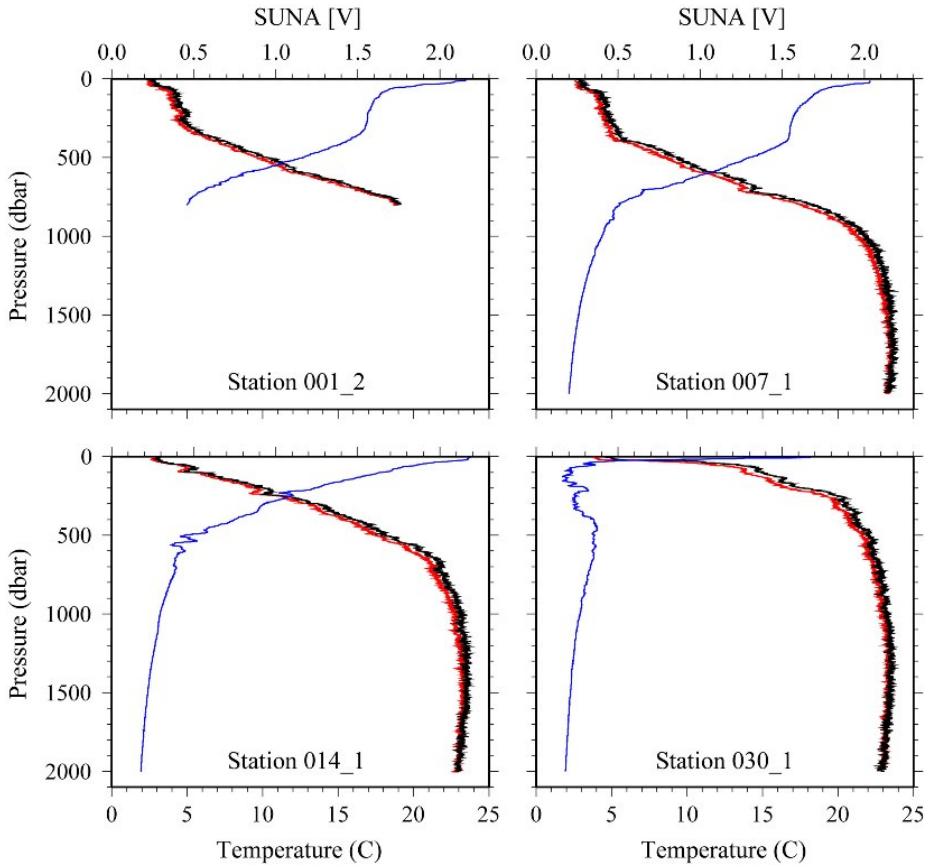

Fig. 3.1.11. Vertical profiles of raw data (voltage) of the Deep SUNA (red line: down cast, black line: up cast) and temperature (blue line).

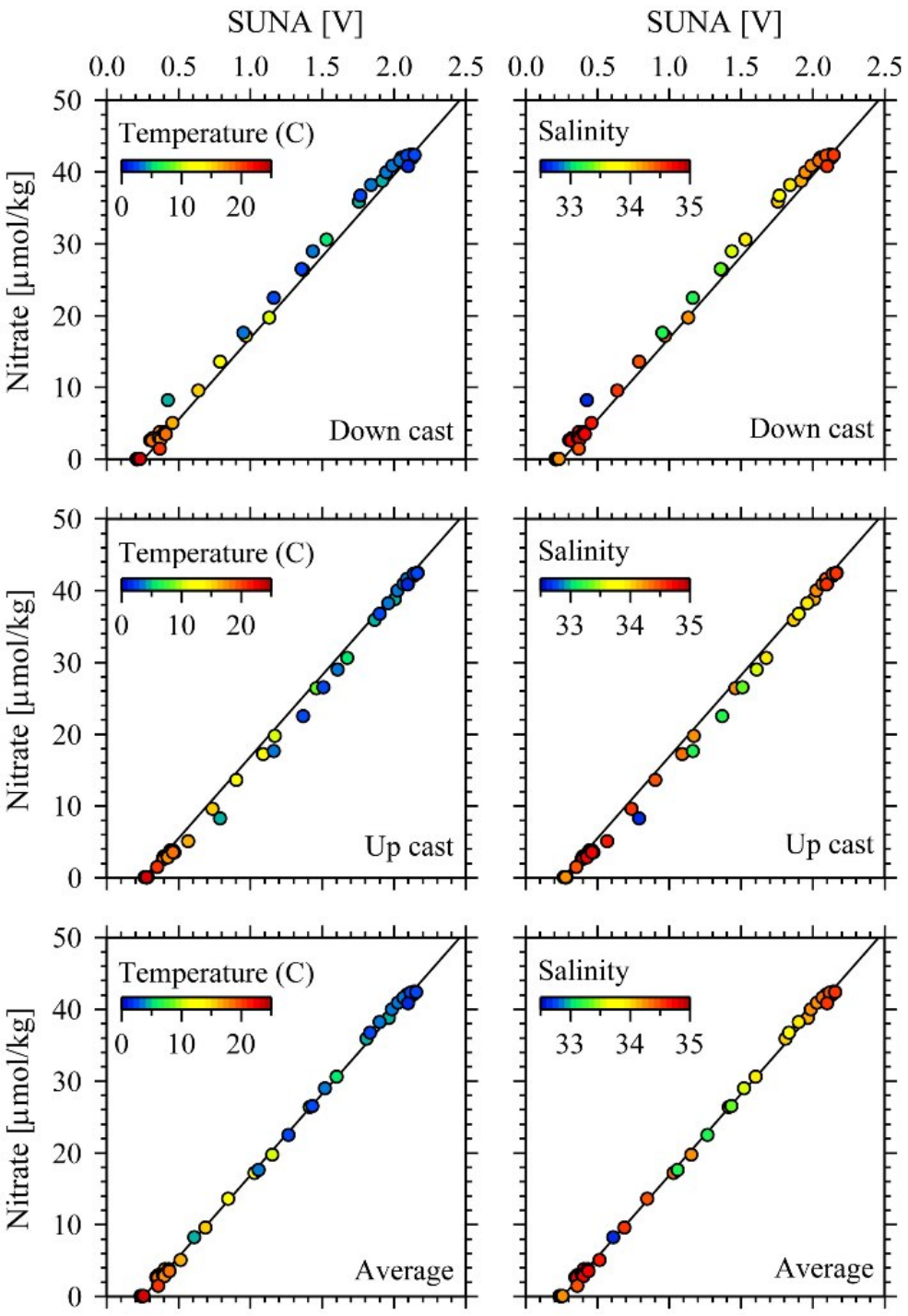

Fig. 3.1.12. Comparison of the Deep SUNA output (voltage) and the bottle sampled nitrate. Upper panels are for down cast, middle panels are for up cast, and lower panels are for average of the down and up cast for the Deep SUNA data. The regression lines for the average data are shown.

(7) References

Edwards, B., D. Murphy, C. Janzen and N. Larson (2010): Calibration, response, and hysteresis in deep-sea dissolved oxygen measurements, *J. Atmos. Oceanic Technol.*, 27, 920–931.

Fukasawa, M., T. Kawano and H. Uchida (2004): Blue Earth Global Expedition collects CTD data aboard Mirai, BEAGLE 2003 conducted using a Dynacon CTD traction winch and motion-compensated crane, *Sea Technology*, 45, 14–18.

García, H. E. and L. I. Gordon (1992): Oxygen solubility in seawater: Better fitting equations. *Limnol. Oceanogr.*, 37 (6), 1307–1312.

Uchida, H., G. C. Johnson, and K. E. McTaggart (2010): CTD oxygen sensor calibration procedures, The GO-SHIP Repeat Hydrography Manual: A collection of expert reports and guidelines, IOCCP Rep., No. 14, ICPO Pub. Ser. No. 134.

Uchida, H., A. Murata, and T. Doi (2015): WHP P14S, S04I Revisit Data Book (in prep.).

Uchida, H., K. Ohyama, S. Ozawa, and M. Fukasawa (2007): In situ calibration of the Sea-Bird 9plus CTD thermometer, *J. Atmos. Oceanic Technol.*, 24, 1961–1967.

3.2 Bottle Salinity

September 10, 2014

(1) Personnel

Hiroshi Uchida (JAMSTEC)
Tatsuya Tanaka (MWJ)
Sonoka Wakatsuki (MWJ)

(2) Objectives

Bottle salinities were measured to calibrate CTD salinity data.

(3) Instrument and Method

Salinity measurement was conducted basically based on a method by Kawano (2010).

i. Salinity Sample Collection

The bottles in which the salinity samples were collected and stored were 250 ml brown borosilicate glass bottles with screw caps (PTFE packing). Each bottle was rinsed three times with sample water and was filled to the shoulder of the bottle. The caps were also thoroughly rinsed. Salinity samples were stored more than 24 hours in the same laboratory as the salinity measurement was made.

ii. Instruments and Methods

Salinity of water samples was measured with a salinometer (Autosal model 8400B; Guildline Instruments Ltd., Ontario, Canada; S/N 62827), which was modified by adding an peristaltic-type intake pump (Ocean Scientific International Ltd., Hampshire, UK) and two platinum thermometers (Guildline Instruments Ltd., model 9450). One thermometer monitored an ambient temperature and the other monitored a salinometer's bath temperature. The resolution of the thermometers was 0.001 °C. The measurement system was almost same as Aoyama et al. (2002). The salinometer was operated in the air-conditioned laboratory of the ship at a bath temperature of 24 °C.

The ambient temperature varied from approximately 22.5 to 24.5 °C, while the bath temperature was stable and varied within ±0.002 °C. A measure of a double conductivity ratio of a sample was taken as a median of 31 readings. Data collection was started after 10 seconds and it took about 10 seconds to collect 31 readings by a personal computer. Data were sampled for the sixth and seventh filling of the cell. In case where the difference between the double conductivity ratio of this two fillings was smaller than 0.00002, the average value of the two double conductivity ratios was used to calculate the bottle salinity with the algorithm for practical salinity scale, 1978 (UNESCO, 1981). When the difference was grater than or equal to the 0.00003, we measured another additional filling of the cell. In case where the double conductivity ratio of the additional filling did not satisfy the criteria above, we measured other additional fillings of the cell within 10 fillings in total. In case where the number of fillings was 10 and those fillings did not satisfy the criteria above, the median of the double conductivity ratios of five fillings were used to calculate the bottle salinity.

The measurement was conducted about from 3 to 18 hours per day and the cell was cleaned with soap (50 times diluted solution of S-CLEAN WO-23 [Neutral], Sasaki Chemical Co. Ltd., Kyoto, Japan) after the measurement for each day. A total of 4584 water samples were measured during the cruise.

(4) Results

i. Standard Seawater

Standardization control was set to 512. The value of STANDBY was 5392 or 5393±0001 and that of ZERO was 0.00000 or -0.00001. We used IAPSO Standard Seawater batch P156 whose conductivity ratio is 0.99984 (double conductivity ratio is 1.99968) as the standard for salinity measurement. We measured 188 bottles of the Standard Seawater during the cruise. History of double conductivity ratio measurement of the Standard Seawater is shown in Fig. 3.2.1.

Time drift of the salinometer was corrected by using the Standard Seawater measurements. Linear time drift of the salinometer was estimated from the Standard Seawater measurement by using the least square method (thin black line in Fig. 3.2.1). No remarkable time drift was estimated from the Standard Seawater measurement. The average of double conductivity ratio was 1.99968 and the standard deviation was 0.00001, which is equivalent to 0.0003 in salinity.

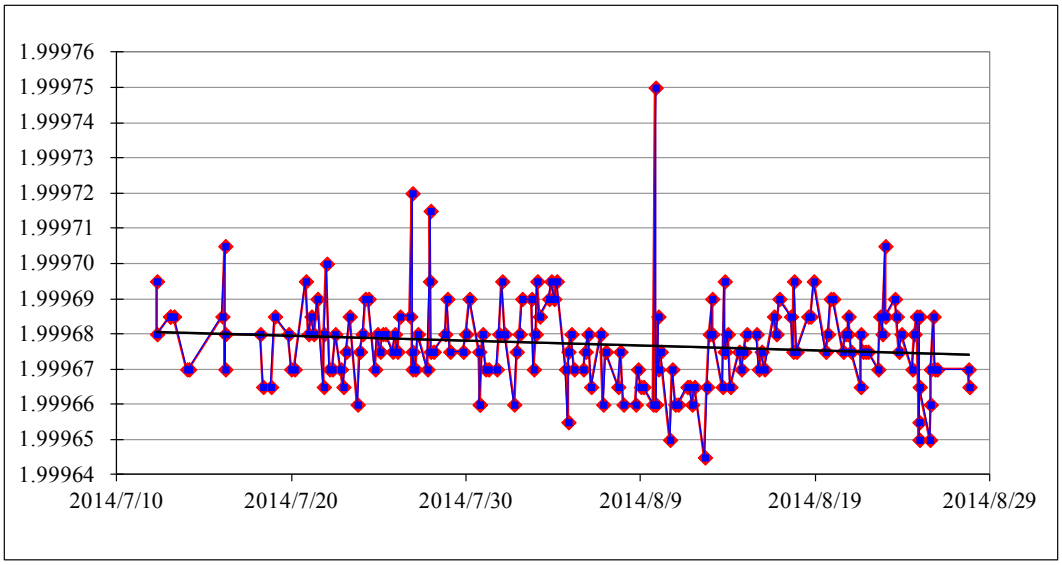

Fig. 3.2.1. History of double conductivity ratio measurement of the Standard Seawater (P156). Horizontal and vertical axes represents date and double conductivity ratio, respectively. Blue dots indicate raw data and red dots indicate corrected data.

ii. Sub-Standard Seawater

We also used sub-standard seawater which was deep-sea water filtered by pore size of 0.45 μm and stored in a 20 liter cubitainer made of polyethylene and stirred for at least 24 hours before measuring. It was measured every 6 samples in order to check the possible sudden drift of the salinometer. During the whole measurements, there was no detectable sudden drift of the salinometer.

iii. Replicate Samples

We took 675 pairs of replicate samples collected from the same Niskin bottle. Histogram of the absolute difference between replicate samples is shown in Fig. 3.2.2. The root-mean-square of the absolute deference was 0.0002.

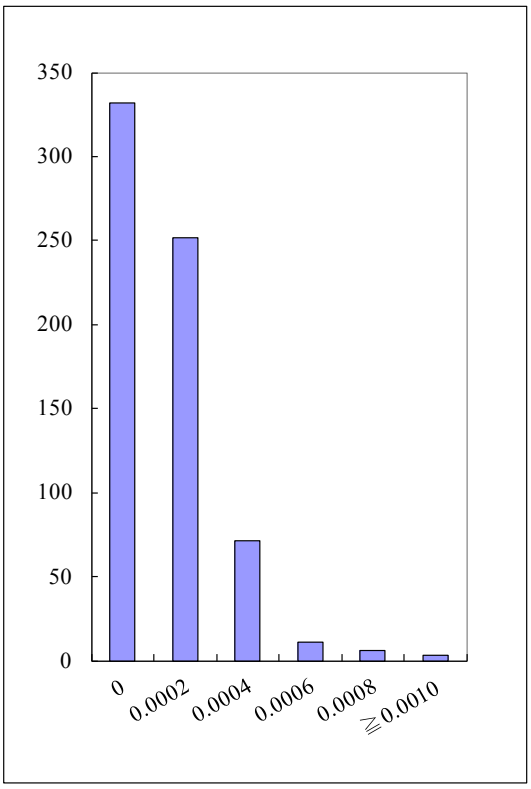

Fig. 3.2.2. Histogram of the absolute difference between replicate samples. Horizontal axis is absolute difference in salinity and vertical axis is frequency.

iv. Duplicate Samples

We took 37 pairs of duplicate samples collected from the different Niskin bottle at same depth. Histogram of the absolute difference between duplicate samples is shown in Fig. 3.2.3. The root-mean-square of the absolute deference was 0.0003.

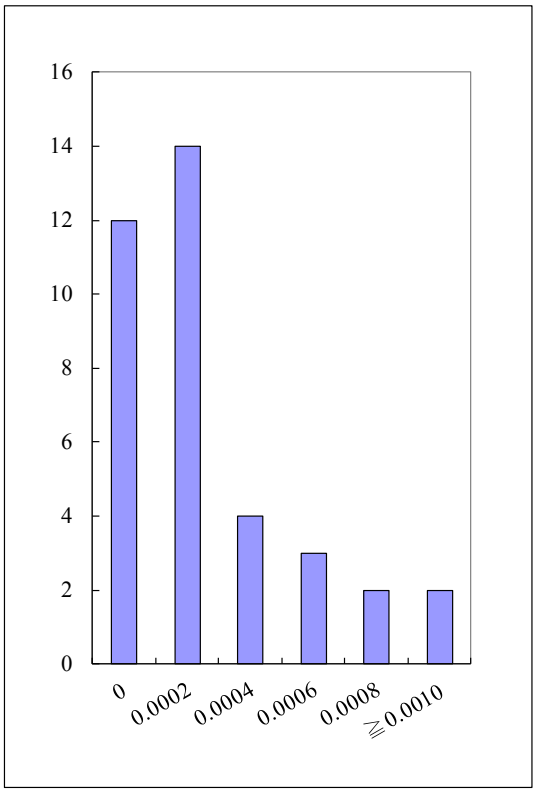

Fig. 3.2.3. Histogram of the absolute difference between duplicate samples. Horizontal axis is absolute difference in salinity and vertical axis is frequency.

(5) References

Aoyama, M., T. Joyce, T. Kawano and Y. Takatsuki (2002): Standard seawater comparison up to P129. Deep-Sea Research, I, Vol. 49, 1103-1114.

Kawano (2010): Salinity. The GO-SHIP Repeat Hydrography Manual: A collection of Expert Reports and Guidelines, IOCCP Report No. 14, ICPO Publication Series No. 134, Version 1.

UNESCO (1981): Tenth report of the Joint Panel on Oceanographic Tables and Standards. UNESCO Tech. Papers in Mar. Sci., 36, 25 pp.

3.3 Density

November 25, 2014

(1) Personnel

Hiroshi Uchida (JAMSTEC)

(2) Objectives

The objective of this study is to collect absolute salinity (also called "density salinity") data, and to evaluate an algorithm to estimate absolute salinity provided along with TEOS-10 (the International Thermodynamic Equation of Seawater 2010) (IOC et al., 2010).

(3) Materials and methods

Seawater densities were measured during the cruise with an oscillation-type density meter (DMA 5000M, serial no. 80570578, Anton-Paar GmbH, Graz, Austria) with a sample changer (Xsample 122, serial no. 80548492, Anton-Paar GmbH). The sample changer was used to load samples automatically from up to ninety-six 12-mL glass vials.

The water samples were collected in 100-mL aluminum bottles (Mini Bottle Can, Daiwa Can Company, Japan). The bottles were stored at room temperature (~23 ºC) upside down usually for 12 to 24 hours to make the temperature of the sample equal to the room temperature. The water sample was filled in a 12-mL glass vial and the glass vial was sealed with Parafilm M (Pechiney Plastic Packaging, Inc., Menasha, Wisconsin, USA) immediately after filling. Densities of the samples were measured at 20 ºC by the density meter two times for each bottle and averaged to estimate the density. When the difference between the two measurements was greater than 0.002, additional measurements were conducted until two samples satisfying the above criteria were obtained.

Time drift of the density meter was monitored by periodically measuring the density of ultra-pure water (Milli-Q water, Millipore, Billerica, Massachusetts, USA) prepared from Yokosuka (Japan) tap water in October 2012. The true density at 20 ºC of the Milli-Q water was estimated to be 998.2042 kg m^{-3} from the isotopic composition ($\delta D = -8.76$ ‰, $\delta^{18}O = -56.86$ ‰) and International Association for the Properties of Water and Steam (IAPWS)-95 standard. An offset correction was applied to the measured density by using the Milli-Q water measurements ($\rho_{Milli\text{-}Q}$) with a slight modification of the density dependency (Uchida et al., 2011). The offset (ρ_{offset}) of the measured density (ρ) was reevaluated in November 2014 as follows:

$$\rho_{offset} = (\rho_{Milli\text{-}Q} - 998.2042) - (\rho - 998.2042) \times 0.000411 \ [\mathrm{kg\ m^{-3}}].$$

The offset correction was verified by measuring Reference Material for Density in Seawater (prototype Dn-RM1 and Pre 18) developing with Marine Works Japan, Ltd., Kanagawa, Japan, and produced by Kanso Technos Co., Ltd., Osaka, Japan, along with the Milli-Q water.

Density salinity can be back calculated from measured density and temperature (20 ºC) with TEOS-10.

(4) Results

Results of density measurements of the Reference Material for Density in Seawater (Dn-RM1 and Pre 18) were shown in Table 3.3.1 and Table 3.3.2. Mean densities of the Dn-RM1 and Pre 18 were in good agreement with the measurements before the reevaluation of the offset of density measurements (Table 3.3.2).

A total of 16 pairs of replicate samples were measured. The root-mean square of the absolute difference of replicate samples was 0.0008 g/kg.

The measured density salinity anomalies (δS_A) are shown in Fig. 3.3.1. The measured δS_A well agree with calculated δS_A from Pawlowicz et al. (2011) which exploits the correlation between δS_A and nutrient concentrations and carbonate system parameters based on mathematical investigation using a model relating

composition, conductivity and density of arbitrary seawaters.

Table 3.3.1. Result of density measurements of the Reference Material for Density in Seawater (prototype Dn-RM1).

Date	Stations (sample no.)	Mean density of Dn-RM1 (kg/m^3)	Note
Leg 1			
2014/07/11	001	1024.2625	
2014/07/12	007,014	1024.2649	
2014/07/14	022,030	1024.2645	
Leg 2			
2014/07/18	036,037,038,040	1024.2641	
2014/07/19	045	1024.2627	
2014/07/20	043	1024.2622	
2014/07/21	051	1024.2643	
2014/07/25	060	1024.2617	
2014/07/27	067	1024.2632	
2014/07/29	073	1024.2621	
2014/08/01	079	1024.2619	
2014/08/03	089	1024.2615	
2014/08/05	095	1024.2613	
2014/08/07	101	1024.2621	
2014/08/11	110	1024.2625	
2014/08/14	120	1024.2618	
2014/08/16	128	1024.2631	
2014/08/17	151	1024.2620	
2014/08/20	136	1024.2623	
2014/08/22	140,143	1024.2639	Stn. 140 #16: Miss trip (flag 4)
2014/08/23	145,147	1024.2621	
2014/08/24	148,149,150	1024.2618	
	Average:	1024.2627 ± 0.0010	

Table 3.3.2. Comparison of density measurement of the Reference Material for Density in Seawater (prototype Dn-RM1 and Pre 18).

Date	Serial no.	Density [kg/m^3]	Note
Measurements on this cruise			
Pre 18			
2014/07/23	270	1024.2222	
2014/08/18	150	1024.2216	
2014/08/18	309	1024.2219	
2014/08/20	370	1024.2223	
2014/08/22	289	1024.2223	
	Average:	1024.2221 ± 0.0003	
Dn-RM1			
2014/07/11-2014/08/24		1024.2627 ± 0.0010	See Table 3.3.1
Recent measurements before this cruise			
Pre 18			
2014/03/27-2014/04/06		1024.2216 ± 0.0012	4 bottles
Dn-RM1			
2014/04/03-06		1024.2623 ± 0.0007	8 bottles

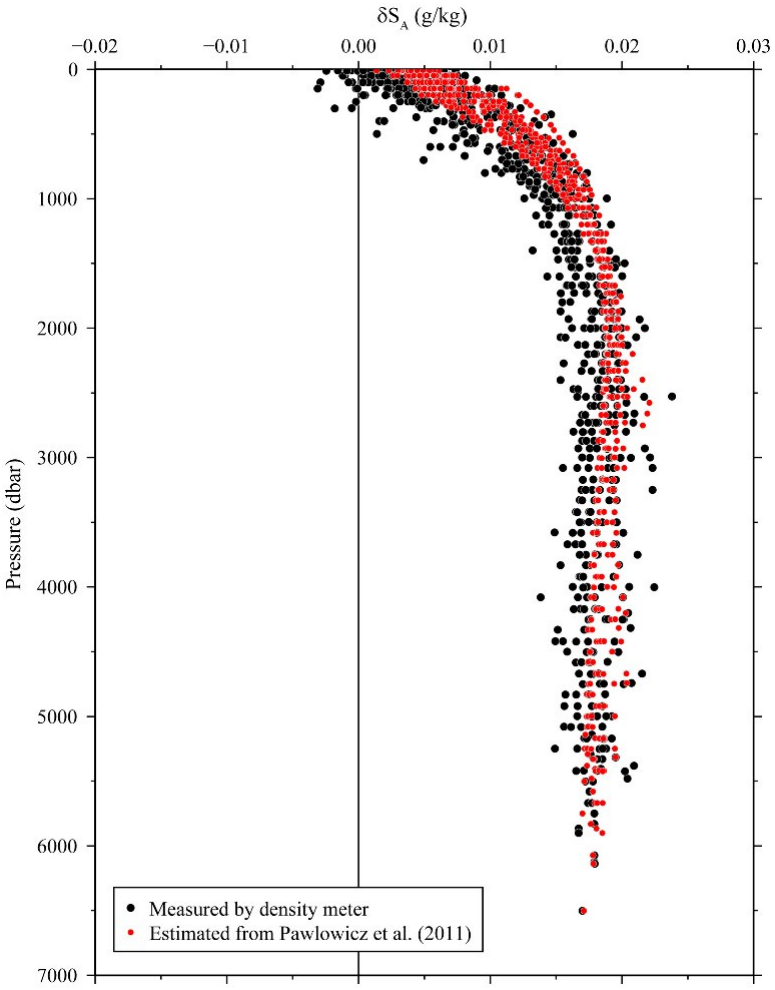

Figure 3.3.1. Vertical distribution of density salinity anomaly measured by the density meter. Absolute Salinity anomaly estimated from nutrients and carbonate parameters (Pawlowicz et al., 2011) are also shown for comparison.

(5) References

IOC, SCOR and IAPSO (2010): The international thermodynamic equation of seawater – 2010: Calculation and use of thermodynamic properties. Intergovernmental Oceanographic Commission, Manuals and Guides No. 56, United Nations Educational, Scientific and Cultural Organization (English), 196 pp.

Pawlowicz, R., D. G. Wright and F. J. Millero (2011): The effects of biogeochemical processes on ocean conductivity/salinity/density relationships and the characterization of real seawater. *Ocean Science*, 7, 363–387.

Uchida, H., T. Kawano, M. Aoyama and A. Murata (2011): Absolute salinity measurements of standard seawaters for conductivity and nutrients. *La mer*, 49, 237–244.

3.4 Oxygen

August 26, 2014

(1) Personnel

Yuichiro Kumamoto [1)], *Misato Kuwahara* [2)], *Keitaro Matsumoto* [2)], *Katsunori Sagishima* [2)], and *Haruka Tamada* [2)]

1) Japan Agency for Marine-Earth Science and Technology

2) Marine Works Japan Co. Ltd

(2) Objectives

Dissolved oxygen is one of good tracers for the ocean circulation. Climate models predict a decline in oceanic dissolved oxygen concentration and a consequent expansion of the oxygen minimum layers under global warming conditions, which results mainly from decreased interior advection and ongoing oxygen consumption by remineralization. The mechanism of the decrease, however, is still unknown. During MR14-04 cruise, we measured dissolved oxygen concentration from surface to bottom layers at all the hydrocast stations in the North Pacific Ocean. All the stations reoccupied the WOCE Hydrographic Program P10N (Leg-1) and P01 (Leg-2) stations in the 1990s. Our purpose is to evaluate temporal change in dissolved oxygen concentration in the North Pacific Ocean during the past decades.

(3) Reagents

Pickling Reagent I: Manganous chloride solution (3M)

Pickling Reagent II: Sodium hydroxide (8M) / sodium iodide solution (4M)

Sulfuric acid solution (5M)

Sodium thiosulfate (0.025M)

Potassium iodate (0.001667M): Wako Pure Chemical Industries, Ltd., volumetric standard, reference material for iodometry, Lot No.TLG0272, Purity: 99.97 ± 0.04 %

CSK standard of potassium iodate: Lot TLM1372, Wako Pure Chemical Industries Ltd., 0.0100N

(4) Instruments

Burette for sodium thiosulfate and potassium iodate;

APB-620 and APB-510 manufactured by Kyoto Electronic Co. Ltd. / 10 cm^3 of titration vessel

Detector;

Automatic photometric titrator, DOT-01X manufactured by Kimoto Electronic Co. Ltd.

(5) Seawater sampling

Following procedure is based on a determination method in the WHP Operations Manual (Dickson, 1996). Seawater samples were collected from 12-liters Niskin sampler bottles attached to the CTD-system. Seawater for bottle oxygen measurement was transferred from the Niskin sampler bottle to a volume calibrated glass flask (ca. 100 cm^3). Three times volume of the flask of seawater was overflowed. Sample temperature was measured using a thermometer (ARO-PR, JFE Advantech Co. Ltd.) that was calibrated with a standard thermometer (SBE 3plus, Sea-Bird Electronics, Inc.). Then two reagent solutions (Reagent I, II) of 0.5 cm^3 each were added immediately into the sample flask and the stopper was inserted carefully into the flask. The sample flask was then shaken vigorously to mix the contents and to disperse the precipitate finely throughout. After the precipitate has settled at least halfway down the flask, the flask was shaken again to disperse the precipitate. The sample flasks containing pickled samples were stored in a laboratory until they

were titrated.

(6) Sample measurement

At least two hours after the re-shaking, the pickled samples were measured on board. A magnetic stirrer bar and 1 cm^3 sulfuric acid solution were added into the sample flask and stirring began. Samples were titrated by sodium thiosulfate solution whose molarity was determined by potassium iodate solution. Temperature of sodium thiosulfate during titration was recorded by a thermometer. We measured dissolved oxygen concentration using two sets of the titration apparatus, named DOT-7 and DOT-8. Dissolved oxygen concentration ($\mu mol\ kg^{-1}$) was calculated by the sample temperature during the sampling, CTD salinity, flask volume, and titrated volume of the sodium thiosulfate solution.

(7) Standardization

Concentration of sodium thiosulfate titrant (ca. 0.025M) was determined by potassium iodate solution. Pure potassium iodate was dried in an oven at 130°C. 1.7835 g potassium iodate weighed out accurately was dissolved in deionized water and diluted to final volume of 5 dm^3 in a calibrated volumetric flask (0.001667M). 10 cm^3 of the standard potassium iodate solution was added to a flask using a volume-calibrated dispenser. Then 90 cm^3 of deionized water, 1 cm^3 of sulfuric acid solution, and 0.5 cm^3 of pickling reagent solution II and I were added into the flask in order. Amount of titrated volume of sodium thiosulfate (usually 5 times measurements average) gave the molarity of the sodium thiosulfate titrant. Table 3.4.1 shows result of the standardization during this cruise. Coefficient of variation (C.V.) for the standardizations was 0.02 ± 0.01 % (n = 36), c.a. 0.05 $\mu mol\ kg^{-1}$.

(8) Determination of the blank

The oxygen in the pickling reagents I (0.5 cm^3) and II (0.5 cm^3) was assumed to be 3.8×10^{-8} mol (Murray *et al.*, 1968). The blank from the presence of redox species apart from oxygen in the reagents (the pickling reagents I, II, and the sulfuric acid solution) was determined as follows. 1 and 2 cm^3 of the standard potassium iodate solution were added to two flasks respectively. Then 100 cm^3 of deionized water, 1 cm^3 of sulfuric acid solution, and 0.5 cm^3 of pickling reagent solution II and I each were added into the two flasks in order. The blank was determined by difference between the two times of the first (1 cm^3 of KIO_3) titrated volume of the sodium thiosulfate and the second (2 cm^3 of KIO_3) one. The results of 3 times blank determinations were averaged (Table 3.4.1). The averaged blank values for DOT-7 and DOT-8 were 0.000 ± 0.001 (standard deviation, S.D., n=18) and 0.000 ± 0.001 (S.D., n=18) cm^3, respectively.

Table 3.4.1 Results of the standardization (End point, E.P.) and the blank determinations (cm^3).

Date (UTC)	KIO_3 No.	$Na_2S_2O_3$ No.	DOT-7		DOT-8		Stations
			E.P.	blank	E.P.	blank	
2014/7/10	K1404B01	T1406A	3.957	-0.002	3.960	-0.002	001, 007, 014, 022, 030
2014/7/16	K1404B02	T1406C	3.956	0.000	3.961	-0.001	036, 037, 038, 039, 040, 047, 046, 045, 044, 041, 042, 043, 048, 049, 050, 051, 052, 053, 054
2014/7/22	K1404B03	T1406D	3.957	0.000	3.963	-0.001	055, 056, 057, 058, 059, 060, 061, 062, 063, 064, 065, 066, 067, 068
2014/7/26	K1404B04	T1406D	3.958	0.001	3.962	0.001	069, 070, 071, 072, 073, 074, 075, 076, 077, 078
2014/7/30	K1404B05	T1406E	3.958	0.001	3.958	0.000	079, 080, 081, 082, 083, 084, 085, 086, 087, 088, 089, 090, 091, 092, 093, 094, 095, 096, 097
2014/8/5	K1404B06	T1406E	3.956	0.000	3.962	-0.001	098, 099, 100, 101, 102, 103, 104
2014/8/8	K1404B07	T1406F	3.957	0.001	3.958	-0.001	105, 106, 107, 108, 109, 110, 111, 112, 113, 114, 115, 116, 117, 118
2014/8/13	K1404B09	T1406F	3.955	0.002	3.959	0.000	119, 120, 121, 122, 123, 124, 125, 126, 127, 128, 151
2014/8/17	K1404C01	T1406G	3.956	0.001	3.958	0.000	129, 130, 131, 132, 133, 134, 135, 136
2014/8/20	K1404C02	T1406G	3.955	0.000	3.958	0.000	137, 138, 139, 140, 141, 142, 143, 144, 145, 146, 147, 148, 149, 150

(9) Replicate sample measurement

From a routine CTD cast at all the stations, a pair of replicate samples was collected at four layers of 50, 400, 1800, and 3500 dbars. The total number of the replicate sample pairs in good measurement (flagged 2) was 447 (Fig. 3.4.1). The standard deviation of the replicate measurement was 0.12 μmol kg^{-1} calculated by a procedure (SOP23) in DOE (1994).

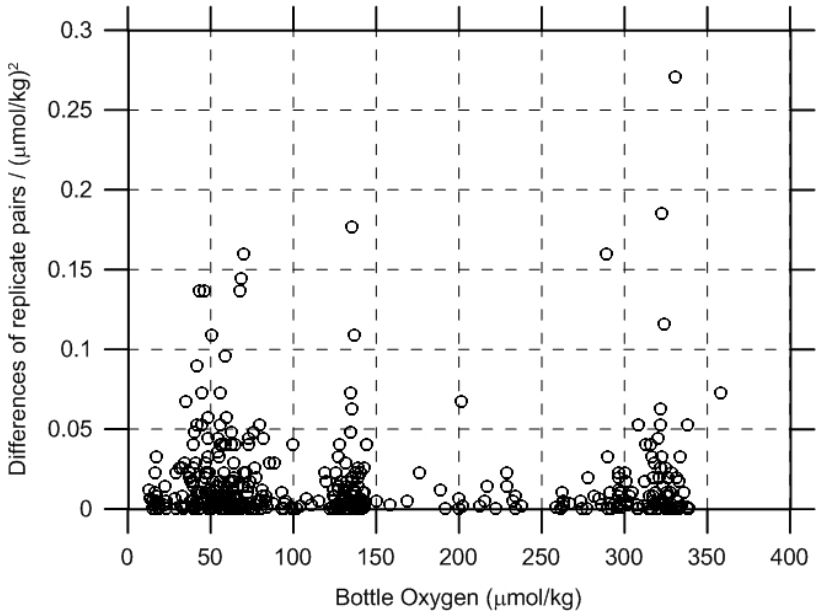

Figure 3.4.1 Oxygen difference between measurements of a replicate pair against oxygen concentration (Data from Stn. 139-1 #35: 0.79 and Stn. 146-1 #35: 4.00 $(\mu mol\ kg^{-1})^2$ are not shown in this figure).

(10) Duplicate sample measurement

During the Leg-2 duplicate sampling were taken for all the Niskin bottles (36 bottles, Table 3.4.2). The standard deviation of the duplicate measurements were calculated to be 0.09 μmol kg^{-1}, which were equivalent with that of the replicate measurements (0.12 μmol kg^{-1}, see section 9).

(11) CSK standard measurements

The CSK standard is a commercial potassium iodate solution (0.0100 N) for analysis of dissolved oxygen. We titrated the CSK standard solution (Lot TLM1372) against our KIO_3 standards as samples before and during the cruise (Table 3.4.3). A good agreement among them confirms that there was no systematic shift in our oxygen analyses between preparation of our KIO_3 standards onshore and the sample measurements on board.

(12) Quality control flag assignment

Quality flag values were assigned to oxygen measurements using the code defined in Table 0.2 of WHP Office Report WHPO 91-1 Rev.2 section 4.5.2 (Joyce *et al*., 1994). Measurement flags of 2 (good), 3 (questionable), 4 (bad), and 5 (missing) have been assigned (Table 3.4.4). For the choice between 2, 3, or 4, we basically followed a flagging procedure as listed below:

a. Bottle oxygen concentration at the sampling layer was plotted against sampling pressure. Any points not lying on a generally smooth trend were noted.
b. Difference between bottle oxygen and CTD oxygen was then plotted against sampling pressure. If a datum deviated from a group of plots, it was flagged 3.
c. Vertical sections against pressure and potential density were drawn. If a datum was anomalous on the section plots, datum flag was degraded from 2 to 3, or from 3 to 4.
d. If there was problem in the measurement, the datum was flagged 4.
e. If the bottle flag was 4 (did not trip correctly), a datum was flagged 4 (bad). In case of the bottle flag 3 (leaking) or 5 (unknown problem), a datum was flagged based on steps a, b, c, and d.

Table 3.4.2 Results of duplicate sample measurements.

	Leg	Stations	Duplicated Niskin #	Niskins	Duplicated Pres.(db)	Dissolved oxygen (umol/kg)	
1	2	042	2-9	X12J02, 03, 04, 05, 06, 07, 08 ,09	4000	150.62 150.56 150.68 150.49	150.54 150.63 150.53 150.44
2	2	048	1, (2)	X12J01	5575	160.04	159.98
3	2	049	(4), 10	X12J10	5330	159.42	159.25
4	2	051	(4), 11	X12J11	5250	159.90	160.04
5	2	052	(5), 12	X12J12	5080	159.06	159.29
6	2	053	(4), 13	X12113	5170	160.64	160.54
7	2	055	(4), 14	X12J14	5330	160.77	160.72
8	2	056	(3), 15	X12J15	5420	163.02	162.98
9	2	057	(3), 16	X12J16	5500	160.68	160.60
10	2	059	(4), 17	X12J17	5170	159.17	159.10
11	2	061	(5), 18	X12J18	5080	157.19	157.17
12	2	062	(4), 19	X12J19	5170	157.33	157.42
13	2	063	(5), 20	X12J20	5000	157.24	157.34
14	2	064	(4), 21	X12J21	5330	157.35	157.23
15	2	065	(4), 22	X12J22	5170	158.59	158.63
16	2	066	(4), 23	X12J23	5250	157.28	157.20
17	2	068	(4), 24	X12J24	5170	157.09	157.13
18	2	069	(6), 25	X12J25	4750	157.17	157.05
19	2	070	(6), 26	X12J26	4830	156.52	156.46
20	2	071	(6), 27	X12J27	4670	155.65	155.44
21	2	072	(5), 28	X12J28	5000	157.30	157.11
22	2	074	(3), 29	X12J29	5420	159.10	159.25
23	2	075	(3), 30	X12J30	5500	157.10	157.05
24	2	082	(5), 31	X12J31	5080	156.15	155.97
25	2	083	(8), 32	X12J32	4170	150.07	149.90
26	2	086	(9), 33	X12J33	3920	147.63	147.43
27	2	090	(3), 34	X12J34	5500	155.63	155.68
28	2	094	(3), 35	X12J35	5580	154.33	154.23
29	2	096	(3), 36	X12J36	5500	152.86	152.84
30	2	106	(2), 3	X12J03	5580	152.84	152.63
31	2	107	(2), 3	X12J03	5420	151.88	151.69

Table 3.4.3 Results of the CSK standard (Lot TLM1372) measurements.

Date (UTC)	KIO_3 ID No.	DOT-5		-		Remarks
		Conc. (N)	error (N)	-	-	
2014/05/13	K1404A01	0.010012	0.000005			Onshore lab.
2014/05/14	K1404C12	0.010013	0.000003			Onshore lab.
2014/05/15	K1404I12	0.010010	0.000002			Onshore lab.
		DOT-7		DOT-8		
		Conc. (N)	error (N)	Conc. (N)	error (N)	
2014/06/09	K1404A09	0.010009	0.000004	0.010005	0.000003	MR14-03
2014/07/10	K1404B01	0.010005	0.000003	0.010004	0.000005	MR14-04 Leg-1
2014/08/17	K1404C01	0.010007	0.000004	0.010006	0.000003	MR14-04 Leg-2

Table 3.4.4 Summary of assigned quality control flags.

Flag	Definition	Number*
2	Good	3714
3	Questionable	1
4	Bad	4
5	Not report (missing)	2
	Total	3721

*Replicate samples (n = 447) were not included.

References

Dickson, A. (1996) Determination of dissolved oxygen in sea water by Winkler titration, in WHPO Pub. 91-1 Rev. 1, November 1994, Woods Hole, Mass., USA.

DOE (1994) Handbook of methods for the analysis of the various parameters of the carbon dioxide system in sea water; version 2. A.G. Dickson and C. Goyet (eds), ORNL/CDIAC-74.

Joyce, T., and C. Corry, eds., C. Corry, A. Dessier, A. Dickson, T. Joyce, M. Kenny, R. Key, D. Legler, R. Millard, R. Onken, P. Saunders, M. Stalcup (1994) Requirements for WOCE Hydrographic Programme Data Reporting, WHPO Pub. 90-1 Rev. 2, May 1994 Woods Hole, Mass., USA.

Murray, C.N., J.P. Riley, and T.R.S. Wilson (1968) The solubility of oxygen in Winkler reagents used for determination of dissolved oxygen, Deep-Sea Res., 15, 237-238.

3.5 Nutrients

(1) Personnel

Michio AOYAMA (Fukushima University / JAMSTEC, Principal Investigator)

Leg 1

Yasuhiro ARII (Department of Marine Science, Marine Works Japan Ltd.)
Minoru KAMATA (Department of Marine Science, Marine Works Japan Ltd.)
Tomomi SONE (Department of Marine Science, Marine Works Japan Ltd.)

Leg 2

Yasuhiro ARII (Department of Marine Science, Marine Works Japan Ltd.)
Kenichiro SATO (Department of Marine Science, Marine Works Japan Ltd.)
Elena HAYASHI (Department of Marine Science, Marine Works Japan Ltd.)

(in preparation)

3.6 Chlorofluorocarbons and Sulfur hexafluoride

September 19, 2014

(1) Personnel

Ken'ichi Sasaki[1)]
Hironori Sato[2)]
Hideki Yamamoto[2)]
Shoko Tatamisashi[2)]
Kanako Yoshida[2)]
Katsunori Sagishima[2)]
[1)] Mutsu Institute for Oceanography, Japan Agency for Marine Earth Science and Technology
[2)] Marine Works Japan Ltd.

(2) Objectives

Chlorofluorocarbons (CFCs) and sulfur hexafluoride (SF_6) are man-made stable gases. These atmospheric gases can slightly dissolve in sea surface water by air-sea gas exchange and then are spread into the ocean interior. So dissolved these gases could be used as chemical tracers for the ocean circulation. We measured concentrations of three chemical species of CFCs, CFC-11 (CCl_3F), CFC-12 (CCl_2F_2), and CFC-113 ($C_2Cl_3F_3$), and SF_6 in seawater on board.

(3) Apparatus

We use three measurement systems. One of them is CFCs analyzing system. Other two are SF_6/CFCs simultaneous analyzing system. Both systems are basically purging and trapping gas chromatography.

Table 3.6.1. Instruments.

SF_6/CFCs simultaneous analyzing system	
Gas Chromatograph:	GC-14B (Shimadzu Ltd.)
Detector 1:	ECD-14 (Shimadzu Ltd.)
Detector 2:	ECD-14 (Shimadzu Ltd.)
Analytical Column:	
Pre-column:	Silica Plot capillary column [i.d.: 0.53 mm, length: 6 m, film thickness: 4 μm]
Main column 1:	Connected two columns (MS 5A packed column [1/16" OD, 20 cm length stainless steel tubing packed the section of 15 cm with 80/100 mesh Molecular Sieve 5A] followed by PoraBond Q [i.d.: 0.53 mm, length: 15 m])
Main culumn2:	Connected two capillary columns (Pola Bond-Q [i.d.: 0.53mm, length: 7 m, film thickness: 10μm] followed by Silica Plot [i. d.: 0.53mm, length: 13 m, film thickness: 6μm])
Purging & trapping:	Developed in JAMSTEC. Cold trap columns are 30 cm length stainless steel tubing packed the section of 5cm with 100/120 mesh Porapak T and followed by the section of 5cm of 100/120 mesh Carboxen 1000. Outer diameters of the main and focus trap columns are 1/8" and 1/16", respectively.

CFCs analyzing system

Gas Chromatograph:	GC-14B (Shimadzu Ltd.)
Detector:	ECD-14 (Shimadzu Ltd.)
Analytical Column:	
Pre-column:	Silica Plot capillary column [i.d.: 0.53mm, length: 6 m, film thickness: 6μm]
Main column:	Connected two capillary columns (Pola Bond-Q [i.d.: 0.53mm, length: 7 m, film thickness: 10μm] followed by Silica Plot [i. d.: 0.53mm, length: 13 m, film thickness: 6μm])
Purging & trapping:	Developed in JAMSTEC. Cold trap columns are 1/16" SUS tubing packed the section of 5cm with 100/120 mesh Porapak T.

(4) Procedures

(4.1) Sampling

Seawater sub-samples were collected from 12 litter Niskin bottles to 450 ml of glass bottles developed in JAMSTEC. The glass bottles were filled by nitrogen gas before sampling. Two times of the bottle volume of seawater sample were overflowed. The seawater samples were kept in water bathes controlled at 7ºC. The samples were taken to determination as soon as possible after sampling (usually within 12 hours).

In order to confirm CFC/SF_6 concentrations of standard gases and their stabilities and also to check saturation levels in sea surface water, mixing ratios in background air were periodically analyzed. Air samples were continuously led into laboratory by 10 mm OD Dekaron tubing. The end of the tubing was put on a head of the compass deck and another end was connected onto an air pump in the laboratory. The tubing was relayed by a T-type union which had a small stop cock. Air sample was collected from the flowing air into a 200ml glass cylinder attached on the cock.

(4.2) Analysis

SF_6/CFCs simultaneous analyzing system

Constant volume of sample water (200 ml) is taken into a sample loop. The sample is send into stripping chamber and dissolved SF_6 and CFCs are de-gassed by N2 gas purging for 8 minutes. The gas sample is dried by magnesium perchlorate desiccant and concentrated on a main trap column cooled down to -80 ºC. Stripping efficiencies are frequently confirmed by re-stripping of surface layer samples and more than 99 % of dissolved SF_6 and CFCs are extracted on the first purge. Following purging & trapping, the main trap column is isolated and electrically heated to 175 ºC. After 1 minute, the desorbed gases are sent onto focus trap cooled down to -80 ºC for 30 seconds. Gaseous sample on the focus trap are desorbed by same manner of the main trap, and lead into the pre-column. Sample gases are roughly separated on the pre-column. SF_6 and CFC-12 are sent onto main column 1 (MC 1) and CFC-11 and CFC-113 still remain on the pre-column. Main column connected on pre-column is switched to the main column 2 (MC 2). Another carrier gas line is connected to MC 1 and SF_6 and CFC-12 are further separated and detected by an electron capture detector, ECD 1. CFC-11 and CFC-113 lead to MC 2 are detected by ECD 2. When CFC-113 eluted from pre-column onto MC 2, the pre-column is switched onto another line and flushed by counter flow of pure nitrogen gas.

CFCs analyzing system

Constant volume of sample water (50 ml) is taken into a sample loop. The sample is send into stripping chamber and dissolved CFCs are de-gassed by N_2 gas purging for 8 minutes. The gas sample is dried by magnesium perchlorate desiccant and concentrated on a main trap column cooled down to -55 ºC. Stripping

efficiencies are frequently confirmed by re-stripping of surface layer samples and more than 99.5 % of dissolved CFCs are extracted on the first purge. Following purging & trapping, the trap column is isolated and electrically heated to 140 ºC. The desorbed gases are lead into the pre-column. Sample gases are roughly separated in the pre-column. When CFC-113 eluted from pre-column onto main column, the pre-column is switched onto another line and flushed by counter flow of pure nitrogen gas.

Nitrogen gases used in these system was filtered by gas purifier tube packed with Molecular Sieve 13X (MS-13X).

Table 3.6.2. Analytical conditions.

SF_6/CFCs simultaneous analyses

Temperature

Analytical Column:	95 ºC
Detector (ECD):	300 ºC
Trap column:	-80 ºC (at adsorbing) & 175 ºC (at desorbing)

Mass flow rate of nitrogen gas (99.99995%)

Carrier gas 1:	10 ml/min
Carrier gas 2:	10 ml/min
Detector make-up gas 1:	27 ml/min
Detector make-up gas 2:	27 ml/min
Back flush gas:	15 ml/min
Sample purge gas:	220 ml/min

CFCs analyses

Temperature

Analytical Column:	95 ºC
Detector (ECD):	240 ºC
Trap column:	-50 ºC (at adsorbing) & 140 ºC (at desorbing)

Mass flow rate of nitrogen gas (99.99995%)

Carrier gas:	13 ml/min
Detector make-up gas:	24 ml/min
Back flush gas:	20 ml/min
Sample purge gas:	130 ml/min

Standard gas (Japan Fine Products co. Ltd.)

Cylinder No.	Base gas	CFC-11	CFC-12	CFC113	SF_6	remarks
		ppt	ppt	ppt	ppt	
CPB17230	N_2	1304	671	99.7	10.0	for SF_6/CFC
CPB25837	N_2	1308	670	99.6	10.0	for SF_6/CFC
CPB27270	N_2	300	160	29.9	0.0	for CFC
CPB15651	N_2	299	159	30.2	0.0	Reference

(5) Performance

The analytical precisions are estimated from replicate sample analyses. The estimated preliminary precisions were ± 0.009 pmol/kg (n = 334), ± 0.005 pmol/kg (n = 334), ± 0.006 pmol/kg (n = 334), and ± 0.057 fmol/kg (n = 187) for CFC-11, CFC-12, CFC-113, and SF_6, respectively.

(6) Data archive

All data will be submitted to JAMSTEC Data Management office (DMO) and under its control.

3.7 Carbon Items

September 18, 2014

(1) Personnel

Akihiko Murata (JAMSTEC)
Yoshihiro Shinoda (JAMSTEC)
Tomonori Watai (MWJ)
Yoshiko Ishikawa (MWJ)
Atsushi Ono (MWJ)
Emi Deguchi (MWJ)

(2) Objectives

Concentrations of CO_2 in the atmosphere are now increasing at a rate of about 2.0 ppmv y^{-1} owing to human activities such as burning of fossil fuels, deforestation, and cement production. It is an urgent task to estimate as accurately as possible the absorption capacity of the oceans against the increased atmospheric CO_2, and to clarify the mechanism of the CO_2 absorption, because the magnitude of the anticipated global warming depends on the levels of CO_2 in the atmosphere, and because the ocean currently absorbs 1/3 of the 6 Gt of carbon emitted into the atmosphere each year by human activities.

The North Pacific is one of the regions where uncertainty of uptake of anthropogenic CO_2 is large. In this cruise, therefore, we were aimed at quantifying how much anthropogenic CO_2 was absorbed in the ocean interior of the North Pacific. For the purpose, we measured CO_2-system parameters such as dissolved inorganic carbon (C_T), total alkalinity (A_T) and pH along the extended WHP P10 and P01 lines at 149°E and 47°N, respectively, in the North Pacific.

(3) Apparatus

i. C_T

Measurement of C_T was made with two total CO_2 measuring systems (called as Systems C and D, respectively; Nippon ANS, Inc.), which were slightly different from each other. The systems comprised of a seawater dispensing system, a CO_2 extraction system and a coulometer. In this cruise, we used coulometers, Seacat2000 and Model23000 for Systems C and D, respectively, both of which were constructed by Nippon ANS. Each of the two systems had almost a same specification as follows:

The seawater dispensing system has an auto-sampler (6 ports), which dispenses seawater from a 300 ml borosilicate glass bottle into a pipette of about 15 ml volume by PC control. The pipette is kept at 20 °C by a water jacket, in which water from a water bath set at 20 °C is circulated. CO_2 dissolved in a seawater sample is extracted in a stripping chamber of the CO_2 extraction system by adding phosphoric acid (~ 10 % v/v) of about 2 ml. The stripping chamber is approx. 25 cm long and has a fine frit at the bottom. The acid is added to the stripping chamber from the bottom of the chamber by pressurizing an acid bottle for a given time to push out the right amount of acid. The pressurizing is made with nitrogen gas (99.9999 %). After the acid is transferred to the stripping chamber, a seawater sample kept in a pipette is introduced to the stripping chamber by the same method as in adding an acid. The seawater reacted with phosphoric acid is stripped of CO_2 by bubbling the nitrogen gas through a fine frit at the bottom of the stripping chamber. The CO_2 stripped in the chamber is carried by the nitrogen gas (flow rates is 140 ml min^{-1}) to the coulometer through a dehydrating module. The modules of Systems C and D consist of two electric dehumidifiers (kept at ~4 °C) and a chemical desiccant ($Mg(ClO_4)_2$).

The measurement sequence such as system blank (phosphoric acid blank), 1.865 % CO_2 gas in a nitrogen

base, sea water samples (6) is programmed to repeat. The measurement of 1.865 % CO_2 gas is made to monitor response of coulometer solutions purchased from UIC, Inc. or laboratory-made.

ii. A_T

In this cruise, we measured A_T using a new A_T measuring system based on spectrophotometry and constructed by Nippon ANS. In addition, we measured A_T based on potentiometry and constructed by Kimoto Electronic Co. Ltd. Both the methods are not yet fixed. Therefore we just show vertical distributions of A_T measured by spectrophotometry.

iii. pH

Measurement of pH was made by a pH measuring system (Nippon ANS, Inc.). For the detection of pH, spectrophotometry was adopted. The system comprises of a water dispensing unit and a spectrophotometer (Bio 50 Scan, Varian). For an indicator, *m*-cresol purple (2 mM) was used.

Seawater is transferred from borosilicate glass bottle (300 ml) to a sample cell in the spectrophotometer. The length and volume of the cell are 8 cm and 13 ml, respectively, and the sample cell is kept at 25.00 ± 0.05 ºC in a thermostated compartment. First, absorbance of seawater only is measured at three wavelengths (730, 578 and 434 nm). Then the indicator is injected and circulated for about 4 minutes to mix the indicator and seawater sufficiently. After the pump is stopped, the absorbance of seawater + indicator is measured at the same wavelengths. The pH is calculated based on the following equation (Clayton and Byrne, 1993):

$$\mathrm{pH} = \mathrm{pK}_2 + \log\left(\frac{\mathrm{A}_1/\mathrm{A}_2 - 0.00691}{2.2220 - 0.1331(\mathrm{A}_1/\mathrm{A}_2)}\right),$$

where A_1 and A_2 indicate absorbance at 578 and 434 nm, respectively, and pK_2 is calculated as a function of water temperature and salinity.

(4) Results

Cross sections of C_T, pH, and A_T along WOCE P01 line are illustrated in Figs. 3.7.1, 3.7.2 and 3.7.3, respectively.

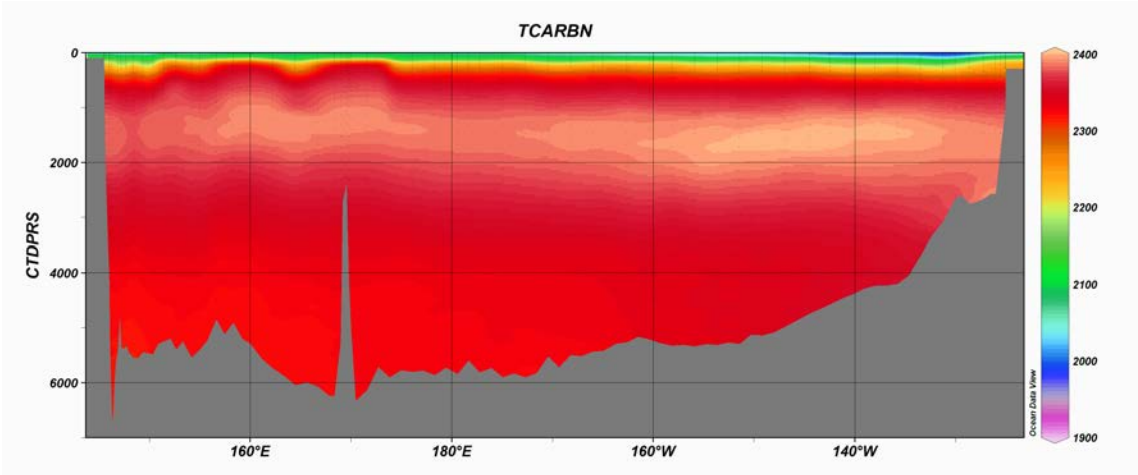

Fig. 3.7.1. Distributions of C_T along the P01 section.

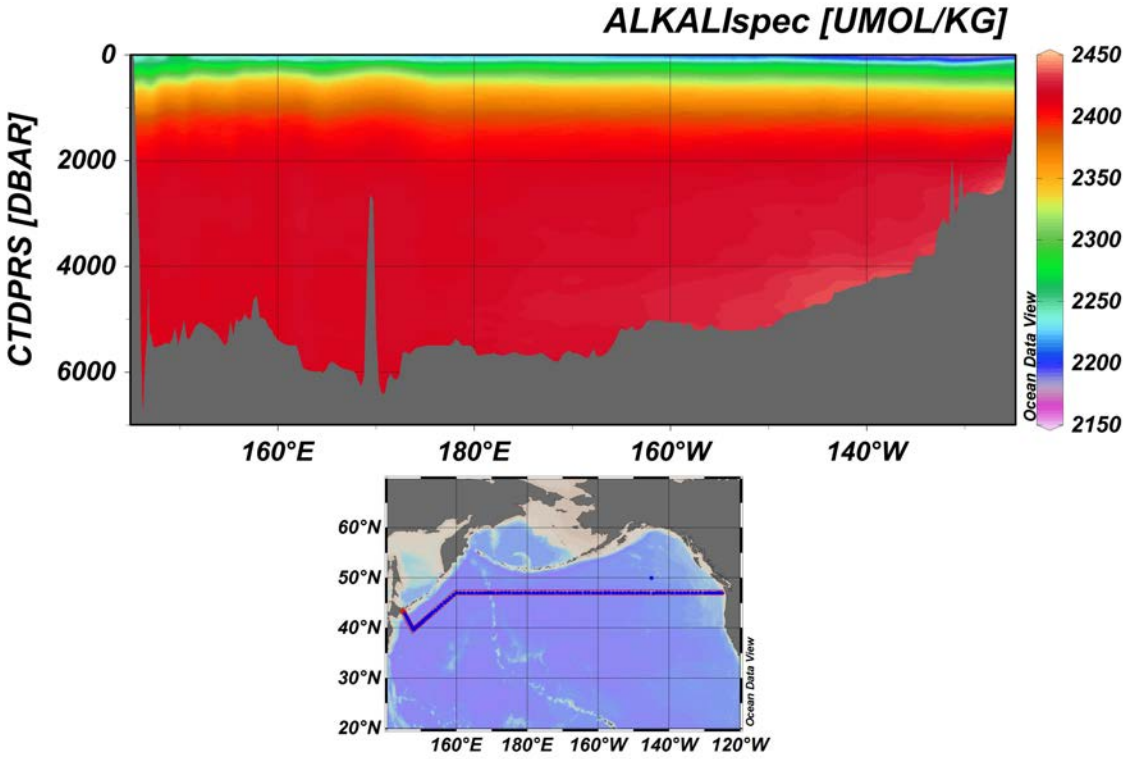

Fig. 3.7.2. Distributions of A_T along the P01 section.

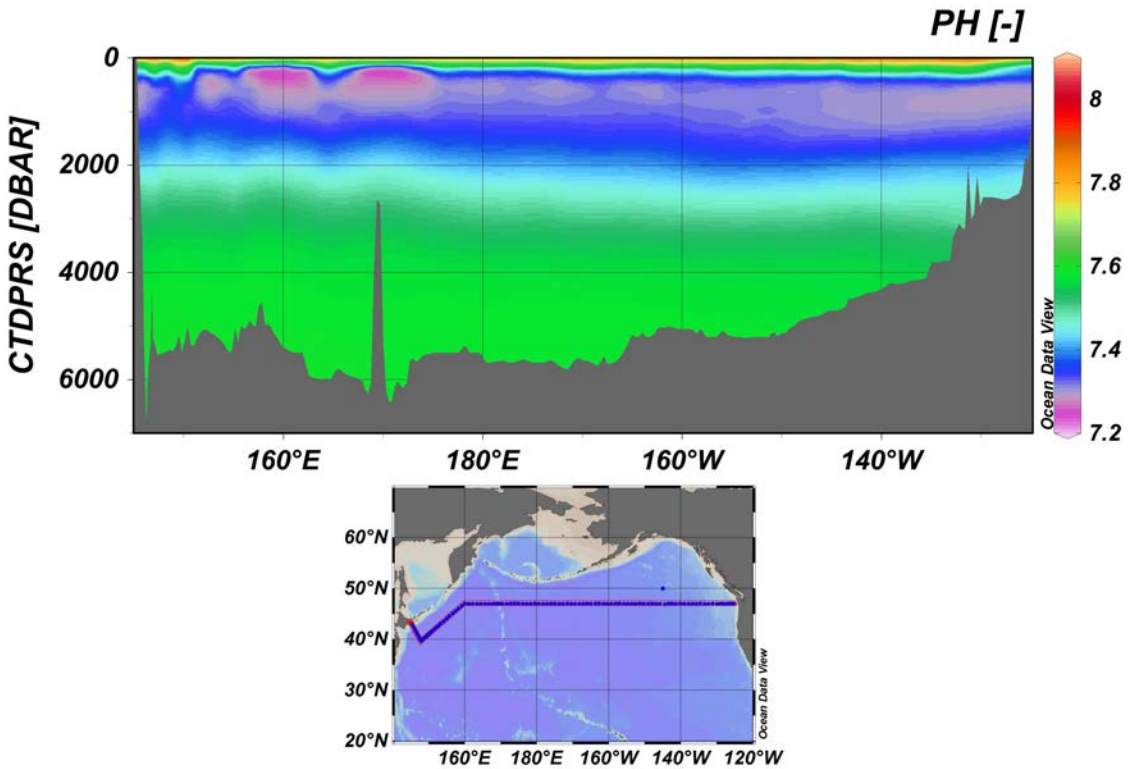

Fig. 3.7.3. Distributions of pH along the P01 section.

References

Clayton T.D. and R.H. Byrne (1993) Spectrophotometric seawater pH measurements: total hydrogen ion concentrtaion scale calibration of m-cresol purple and at-sea results. Deep-Sea Research 40, 2115-2129.

3.8 Chlorophyll *a*

September 12, 2014

(1) Personnel

Kosei Sasaoka (JAMSTEC) (Leg 2)
Hiroshi Uchida (JAMSTEC) (Legs 1, 2)
Kanta Chida (Rakuno Gakuen University) (Legs 1, 2)
Takuya Takahashi (Rakuno Gakuen University) (Legs 1, 2)
Keitaro Matsumoto (MWJ) (Legs 1, 2)
Katsunori Sagishima (MWJ) (Legs 1, 2)
Haruka Tamada (MWJ) (Legs 1, 2)
Misato Kuwahara (MWJ) (Legs 1)

(2) Objectives

Chlorophyll *a* is one of the most convenient indicators of phytoplankton stock, and has been used extensively for the estimation of phytoplankton abundance in various aquatic environments. In this study, we investigated horizontal and vertical distribution of phytoplankton along the P01 section in the North Pacific. The chlorophyll *a* data is also utilized for calibration of fluorometers, which were installed in the surface water monitoring and CTD profiler system.

(3) Instrument and Method

Seawater samples were collected in 250 ml brown Nalgene bottles without head-space (500 ml bottles for samples from the surface water monitoring system). The whole samples were gently filtrated by low vacuum pressure (<0.02 MPa) through Whatman GF/F filter (diameter 25 mm) in the dark room. Whole volume of each sampling bottle was precisely measured in advance. After filtration, phytoplankton pigments were immediately extracted in 7 ml of N,N-dimethylformamide (DMF), and samples were stored at –20°C under the dark condition to extract chlorophyll *a* more than 24 hours. Chlorophyll *a* concentrations were measured by the Turner fluorometer (10-AU-005, TURNER DESIGNS), which was previously calibrated against a pure chlorophyll *a* (Sigma-Aldrich Co., LLC) (Fig. 3.8.1). To estimate the chlorophyll *a* concentrations, we applied to the fluorometric "Non-acidification method" (Welschmeyer, 1994).

(4) Results

Cross section of chlorophyll *a* concentrations along the P01 line during the cruise is shown in Fig. 3.8.2. To estimate the measurement precision, 41-pairs of replicate samples were obtained from hydrographic casts. All pairs of the replicate samples were collected in 250 ml bottles. Standard deviation calculated from 41-pairs of the replicate samples was 0.008 μg/L, although absolute difference values between 36-pairs of the replicate samples were smaller than 0.01 μg/L.

(5) Reference

Welschmeyer, N. A. (1994): Fluorometric analysis of chlorophyll a in the presence of chlorophyll b and pheopigments. Limnor. Oceanogr., 39, 1985-1992.

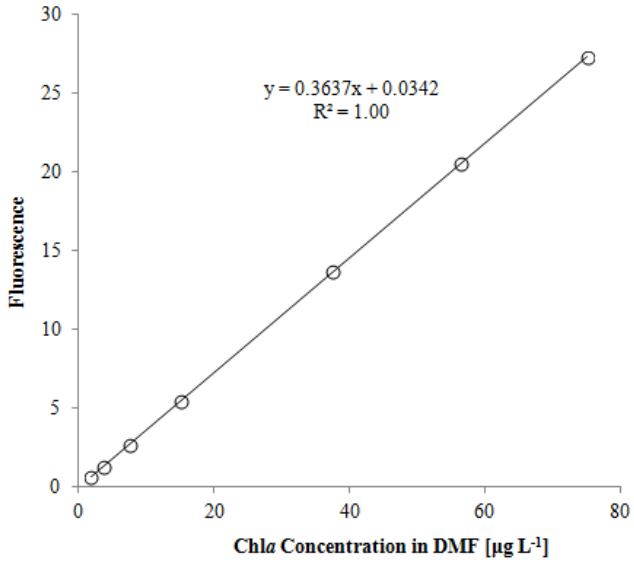

Figure 3.8.1. Relationships between pure chlorophyll *a* concentrations and fluorescence light intensity.

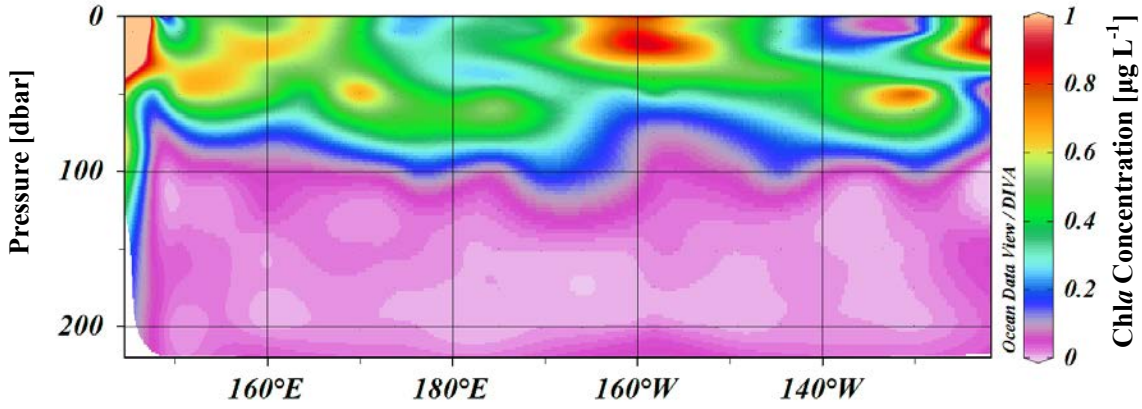

Figure 3.8.2. Cross section of chlorophyll *a* concentrations along the P01-line obtained from hydrographic casts.

3.9 Absorption Coefficients of Particulate Matter and Colored Dissolved Organic Matter (CDOM)

September 12, 2014

(1) Personnel

Kosei Sasaoka (JAMSTEC) (Leg 2)

(2) Objectives

Absorption coefficients of particulate matter (phytoplankton and non-phytoplankton particles, defined as 'detritus') and colored dissolved organic matter (CDOM) play an important role in determining the optical properties of seawater. In particular, light absorption by phytoplankton is a fundamental process of photosynthesis, and their chlorophyll *a* (Chl-*a*) specific coefficient, a^*_{ph}, can be essential factors for bio-optical models to estimate primary productivities. Absorption coefficients of CDOM are also important parameters to validate and develop the bio-optical algorithms for ocean color sensors, because the absorbance spectrum of CDOM overlaps that of Chl-*a*. The global colored detrital and dissolved materials (CDOM) distribution appears regulated by a coupling of biological, photochemical, and physical oceanographic processes all acting on a local scale, and greater than 50% of blue light absorption is controlled by CDOM (Siegel et al., 2002). Additionally, some investigators have reported that CDOM emerges as a unique tracer for diagnosing changes in biogeochemistry and the overturning circulation, similar to dissolved oxygen (e.g., Nelson et al., 2010). The objectives of this study are to understand the east-west variability of light absorption by phytoplankton and CDOM along the P01 section in the North Pacific.

(3) Methods

Seawater samples for absorption coefficient of total particulate matter ($a_p(\lambda)$) were performed using Niskin bottles and a bucket above 100m depth along the P01 section (Fig. 3-9-1, Table 3.9-1). Samples were collected in 3000ml dark bottles and filtered (500 – 3000 ml) through 25-mm What-man GF/F glass-fiber filters under a gentle vacuum (< 0.013 MPa) on board in the dark room. After filtration, the optical density of total particulate matter on filter ($OD_{fp}(\lambda)$) between 350 and 750 nm at a rate of 1.0 nm was immediately measured by an UV-VIS recording spectrophotometer (UV-2400, Shimadzu Co.), and absorption coefficient was determined from the OD according to the quantitative filter technique (QFT) (Mitchell, 1990). A blank filter with filtered seawater was used as reference. All spectra were normalized to 0.0 at 750nm to minimize difference between sample and reference filter. To determine the optical density of non-pigment detrital particles ($OD_{fd}(\lambda)$), the filters were then soaked in methanol for a few hours and rinsed with filtered seawater to extract and remove the pigments (Kishino et al., 1985), and its absorption coefficient was measured again by UV-2400. These measured optical densities on filters ($OD_{fp}(\lambda)$ and $OD_{fd}(\lambda)$) were converted to optical densities in suspensions ($OD_{sp}(\lambda)$ and $OD_{sd}(\lambda)$) using the pathlength amplification factor of Cleveland and Weidemann (1993) as follows:

$$OD_{sp}(\lambda) = 0.378\ OD_{fp}(\lambda) + 0.523\ OD_{fp}(\lambda)^2 \text{ and}$$
$$OD_{sd}(\lambda) = 0.378\ OD_{fd}(\lambda) + 0.523\ OD_{fd}(\lambda)^2.$$

The absorption coefficient of total particles ($a_p(\lambda)$ (m^{-1})) and non-pigment detrital particles ($a_d(\lambda)$ (m^{-1})) are computed from the corrected optical densities ($OD_s(\lambda)$):

$$a_p(\lambda) = 2.303 \times OD_{sp}(\lambda) / L \quad (L = V / S), \text{ and}$$

$$a_d(\lambda) = 2.303 \times OD_{sd}(\lambda) / L \quad (L = V / S),$$

Where S is the clearance area of the filter (m^2) and V is the volume filtered (m^3). Absorption coefficient of phytoplankton ($a_{ph}(\lambda)$) was obtained by subtracting $a_d(\lambda)$ from $a_p(\lambda)$ as follows:

$$a_{ph}(\lambda) = a_p(\lambda) - a_d(\lambda).$$

Finally, we calculated chl-*a* normalized specific absorption spectra (a^*_{ph}) to divide a_{ph} by chl-*a* concentrations obtained from same hydrographic casts.

Seawater samples for absorption coefficient of CDOM ($a_y(\lambda)$) were collected in 250ml bottles using Niskin bottles and a bucket from surface to bottom (Fig. 3.9.1, Table 3.9.1). CDOM samples were filtered using 0.2 μm Nuclepore polycarbonate filters on board. Optical densities of the CDOM ($OD_y(\lambda)$) in this filtered seawater were recorded against UV-2400 in the range from 300 to 800 nm using 10-cm pathlength glass cells. Milli-Q water was used as a base line. A blank (Milli-Q water versus Milli-Q water) was subtracted from each wavelength of the spectrum. The absorption coefficient of CDOM ($a_y(\lambda)$ (m^{-1})) was calculated from measured optical densities ($OD_y(\lambda)$) as follows:

$$a_y(\lambda) = 2.303 \times OD_y(\lambda) / L \quad (L \text{ is the cuvette path-length (m)}).$$

(4) Preliminary results

Some examples of chl-*a* normalized specific absorption spectra (a^*_{ph}) were shown in Fig.3.9.2. Cross section of CDOM (as absorption coefficient at 325 nm, unit = m^{-1}) along the P01 section were shown in Fig. 3.9.3.

(5) References

Cleveland, J.S. and Weidemann, A.D., 1993, Quantifying absorption by aquatic particles: a multiple scattering correction for glass fiber filters, Limnology and Oceanography, 38, 1321-1327.

Kishino, M., Takahashi, M., Okami, N. and Ichimura, S., 1985, Estimation of the spectral absorption coefficients of phytoplankton in the sea, Bulletin of Marine Science, 37, 634-642.

Mitchell, B.G., 1990, Algorithms for determining the absorption coefficient of aquatic particulates using the quantitative filter technique (QFT), Ocean Optics X, SPIE 1302, 137-148.

Nelson, N. B., D. A. Siegel, C. A. Carlson, and C. M. Swan, 2010, Tracing global biogeochemical cycles and meridional overturning circulation using chromophoric dissolved organic matter, Geophys. Res. Lett., 37, L03610, doi:10.1029/2009GL042325.

Siegel, D.A., Maritorena, S., Nelson, N.B., Hansell, D.A., Lorenzi-Kayser, M., 2002, Global distribution and dynamics of colored dissolved and detrital organic materials. J. Geophys. Res., 107, C12, 3228, doi:10.1029/2001JC000965.

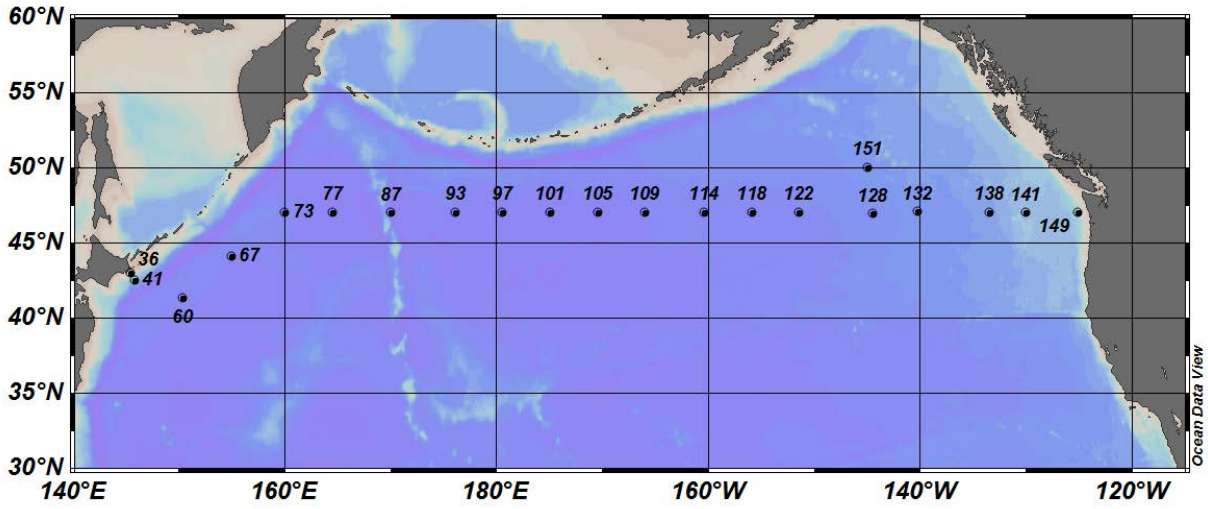

Fig. 3.9.1. Location of sampling stations for absorption coefficients of phytoplankton and CDOM along the P01 section during MR14-04.

Table 3.9.1. List of sampling stations for absorption coefficients of phytoplankton and CDOM during MR14-04.

Station	Date (UTC)	Time (UTC)	Latitude	Longitude	Sampling type	Cast No.	Sampling depth (db)	
							Particle absorbance	CDOM absorbance
36	07/17/2014	7:28	42.97 N	145.45 E	CTD + Bucket	1	0, 10, 50, 86	0, 10, 50, 86
41	07/19/2014	15:56	42.48 N	145.84 E	CTD + Bucket	2	none	Bottom-10, 2930, 1930, 970, 470, 200, 100, 50, 10, 0
60	07/23/2014	13:34	41.27 N	150.39 E	CTD + Bucket	1	0, 10, 50, 100	Bottom-10, 5000, 4000, 3000, 2000, 1000, 500, 200, 100, 50, 10, 0
67	07/25/2014	15:59	44.09 N	155.02 E	CTD + Bucket	2	0, 10, 50, 100	Bottom-10, 5080, 4080, 3080, 2070, 1070, 530, 200, 100, 50, 10, 0
73	07/27/2014	11:59	47.01 N	160.02 E	CTD + Bucket	1	0, 10, 50, 100	Bottom-10, 5000, 3000, 2000, 1000, 800, 500, 200, 100, 50, 10, 0
77	07/29/2014	22:47	47.00 N	164.51 E	CTD + Bucket	1	0, 10, 50, 100	Bottom-10, 4920, 2930, 1930, 970, 770, 470, 200, 100, 50, 10, 0
87	08/01/2014	11:06	46.98 N	170.00 E	CTD + Bucket	1	0, 10, 50, 100	Bottom-10, 3000, 2000, 1000, 800, 500, 200, 100, 50, 10, 0
93	08/03/2014	12:05	47.00 N	176.09 E	CTD + Bucket	1	0, 10, 50, 100	Bottom-10, 5000, 3000, 2000, 1000, 800, 500, 200, 100, 50, 10, 0
97	08/04/2014	18:25	46.99 N	179.43 W	CTD + Bucket	1	0, 10, 50	Bottom-10, 5080, 3080, 2070, 1070, 830, 530, 200, 100, 50, 10, 0
101	08/06/2014	5:30	47.00 N	174.95 W	CTD + Bucket	3	0, 10, 50, 100	Bottom-10, 4920, 2930, 1930, 970, 770, 470, 200, 100, 50, 10, 0
105	08/08/2014	9:33	47.00 N	170.42 W	CTD + Bucket	1	0, 10, 50	Bottom-10, 5000, 3000, 2000, 1000, 800, 500, 200, 100, 50, 10, 0
109	08/09/2014	15:55	47.01 N	165.98 W	CTD + Bucket	1	0, 10, 50, 100	Bottom-10, 5080, 3080, 2070, 1070, 830, 530, 200, 100, 50, 10, 0
114	08/11/2014	6:33	46.99 N	160.36 W	CTD + Bucket	1	0, 10, 50, 100	Bottom-10, 5000, 3000, 2000, 1000, 800, 500, 200, 100, 50, 10, 0
118	08/12/2014	16:39	46.99 N	155.85 W	CTD + Bucket	1	0, 10, 50, 100	Bottom-10, 5080, 3080, 2070, 1070, 830, 530, 200, 100, 50, 10, 0
122	08/13/2014	23:25	47.00 N	151.40 W	CTD + Bucket	2	0, 10, 50, 100	Bottom-10, 4920, 2930, 1930, 970, 770, 470, 200, 100, 50, 10, 0
128	08/15/2014	21:25	46.90 N	144.44 W	CTD + Bucket	1	0, 10, 50, 100	Bottom-10, 2930, 1930, 970, 770, 470, 280, 200, 100, 50, 10, 0
151	08/16/2014	20:20	50.00 N	144.99 W	CTD + Bucket	1	0, 10, 50, 100	Bottom-10, 3000, 2000, 1000, 800, 500, 300, 200, 100, 50, 10, 0
132	08/18/2014	14:48	47.03 N	140.23 W	CTD + Bucket	1	0, 10, 50, 100	Bottom-10, 3000, 2000, 1000, 800, 500, 300, 200, 100, 50, 10, 0
138	08/20/2014	8:35	46.99 N	133.47 W	CTD + Bucket	1	0, 10, 50, 100	Bottom-10, 3000, 2000, 1000, 800, 500, 300, 200, 100, 50, 10, 0
141	08/21/2014	3:25	46.98 N	130.03 W	CTD + Bucket	1	0, 10, 50, 100	Bottom-10, 2000, 1000, 800, 500, 300, 200, 100, 50, 10, 0
149	08/22/2014	18:29	47.00 N	125.06 W	CTD + Bucket	1	0, 10, 20, 30, 50, 100	Bottom-10, 970, 770, 470, 280, 200, 100, 50, 30, 20, 10, 0

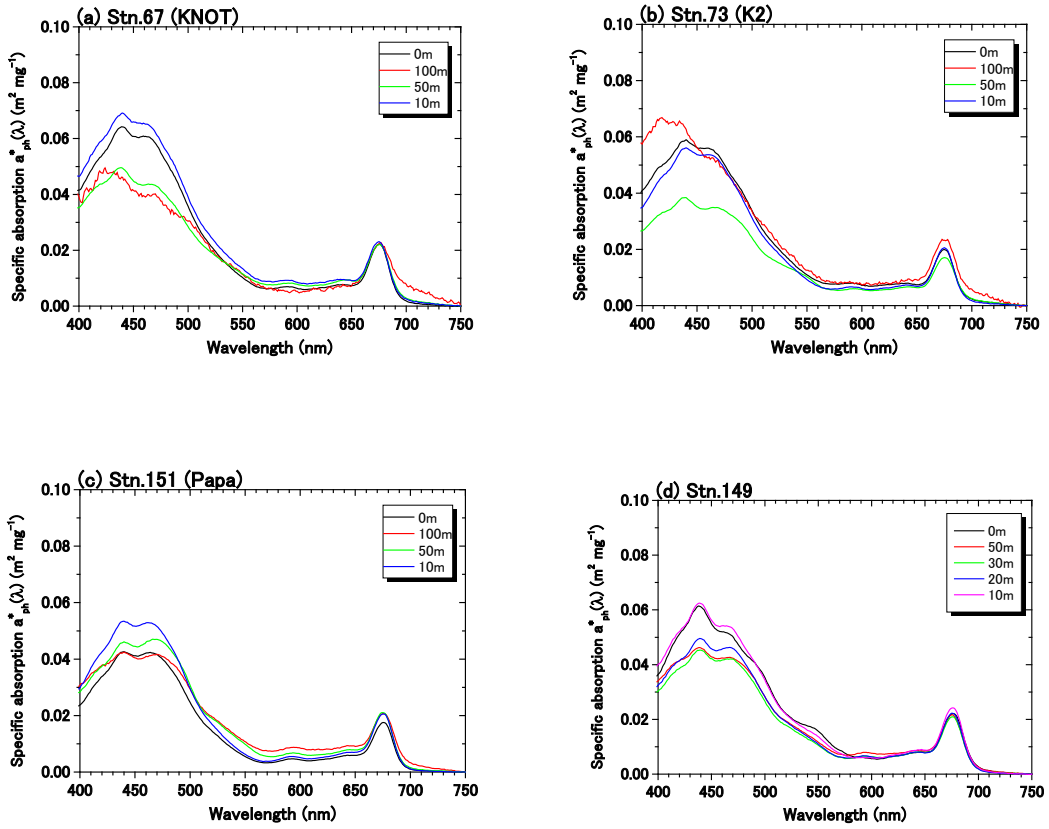

Fig.3.9.2. Examples of chlorophyll-specific phytoplankton absorption coefficient spectra ($a^*_{ph}(\lambda)$) at 400-750 nm, (a) Stn.KNOT, (b) Stn. K2, (c) Stn. Papa, (d) Stn. 149. All spectra were normalized to 0.0 at 750nm.

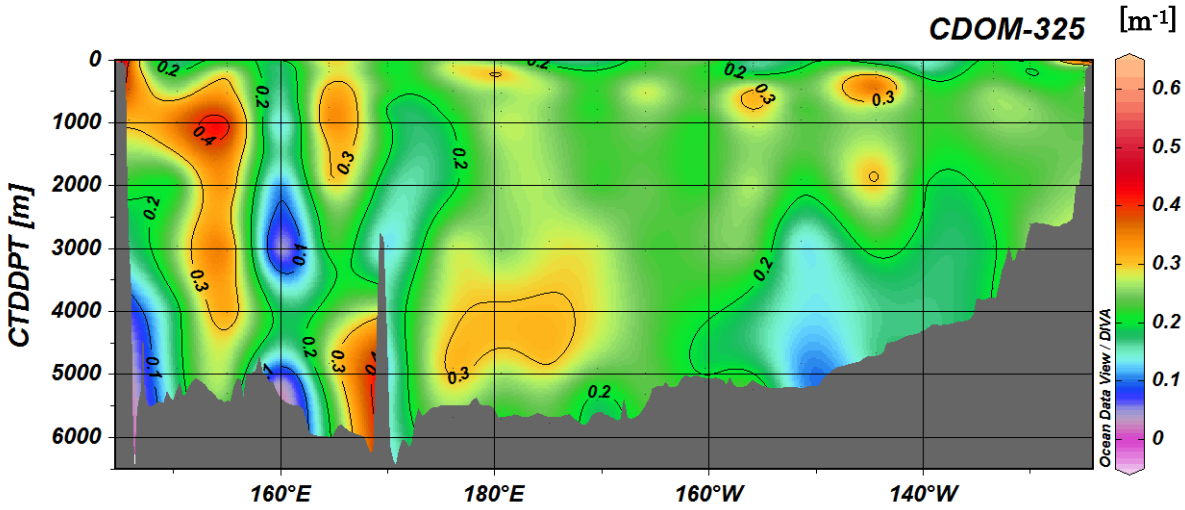

Fig.3.9.3. Contours showing distribution of CDOM (as absorption coefficient at 325 nm, unit = m^{-1}) along the P01 section during MR14-04.

3.10 Calcium

September 16, 2014

(1) Personnel

Yoshihiro Shinoda (JAMSTEC)

(2) Objectives

According to the recent IPCC report, concentrations of CO_2 in the atmosphere have increased by 40% since pre-industrial times, primarily from fossil fuel emissions and secondarily from net land use change emissions. The ocean has absorbed about 30% of the emitted anthropogenic carbon dioxide, causing ocean acidification. Ocean acidification is characterized by an increase of H^+ (i.e., a decrease of pH) and a concurrent decrease of carbonate ion concentration (CO_3^{2-}). The decrease of CO_3^{2-} is unfavorable to marine calcifying organisms, which utilize CO_3^{2-}, together with Ca^{2+}, to produce their calcium carbonate ($CaCO_3$) shells and skeletons. To evaluate dissolution and precipitation of calcium carbonate, we measured directly the concentration of calcium in the sea water in the subarctic region of the North Pacific.

(3) Reagents

NH_3/NH_4buffer:	0.4 mol/l NH_4Cl/ 0.4 mol/l NH_3 buffer
Zincon solution:	0.004 mol/l Zincon, 0.0925g Zincon was dissolved 0.8 ml 1M NaOH and was diluted to 50 ml
EGTA titrant:	0.02 mol/l EGTA, 3.80g EGTA was dissolved 30 ml 1M NaOH and was diluted to 500 ml
Zn/EGTA solution:	0.004 mol/l $ZnSO_4$/ 0.004 mol/l EGTA
STD solution:	40ml 1000mg/l Ca standard solution was diluted to 100ml

(4) Apparatus

Measurement of calcium was made by a modified Dissolved Oxygen Titrator DOT-01 (Kimoto Electronic Co. Ltd.). Bandpass filter was replaced to f_0=620nm. The system comprises of a light source, photodiode detectors, auto-burette and control unit.

Seawater of approx. 10ml is transferred from a sample bottle (60ml HDPE bottle) into 100 ml tall beaker by transfer pipet. A magnetic stirrer bar was added into beaker. 5ml NH_3/NH_4buffer, 1ml Zincon solution, 1ml Zn/EGTA solution and about 60ml H_2O were added into the beaker. The seawater samples were titrated by the EGTA titrant. The EGTA titrant was calibrated by measuring STD solution.

(5) Performances

The system worked well no troubles. The repeatability was estimated to 0.0089±0.0076 (n=20 pairs) mmol kg^{-1}.

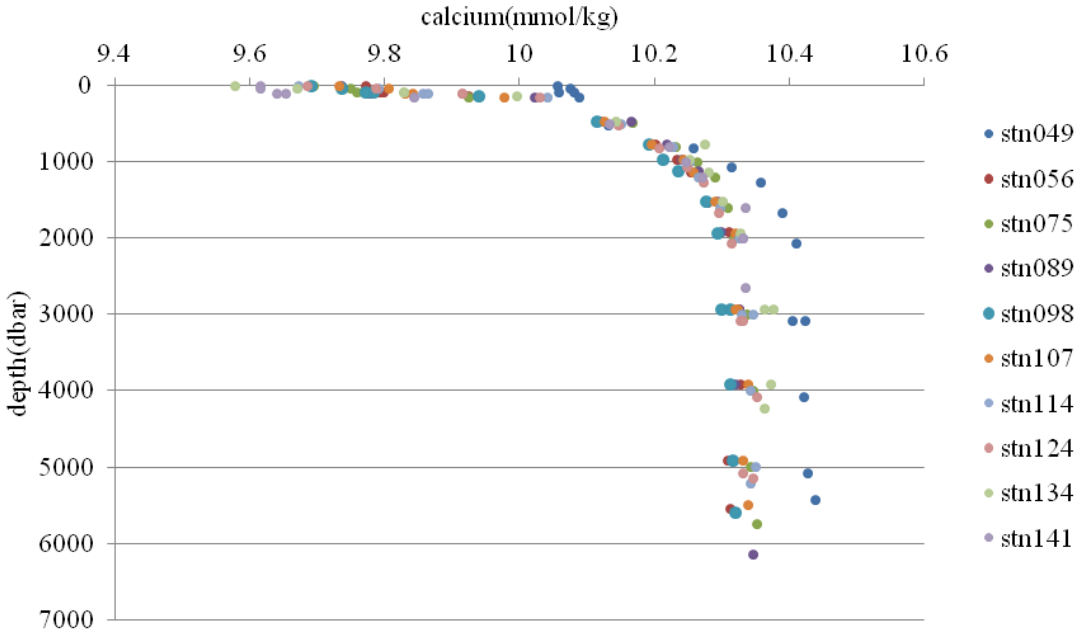

Fig. 3.10. Vertical profiles of calcium.

3.11 Dissolved Organic Carbon

3.11.1 Collaborative Study on the Zonal Distribution of Dissolved Organic Carbon in the Far North Pacific

August 13, 2014

(1) Personnel

Takeshi Yoshimura[1], Dennis A. Hansell[2], and Andrew Margolin[2]

[1] Central Research Institute of Electric Power Industry

[2] Rosenstiel School of Marine and Atmospheric Science, University of Miami

(2) Background and objectives

For several years, the Hansell Laboratory has pursued opportunities to determine the global ocean distribution of dissolved organic carbon (DOC), which plays a significant role in marine carbon cycle. In the Pacific, in collaboration with Prof. Craig Carlson at the Univ. of California Santa Barbara, we have measured DOC on several of the CLIVAR Repeat Hydrography lines, including P16 (north and south), P06, P02, and P18 (http://yyy.rsmas.miami.edu/groups/biogeochem/Data.html). On that map, the major gaps in coverage of the global ocean are readily apparent, including the NW and the NE Pacific Ocean. P10N and P01 is well located for filling these critical gaps as it covers the distal end of the global ocean thermohaline circulation cell. Ultimately our goal is to evaluate the cause of DOC concentration gradients in the deep Pacific, but those gradients must first be established by surveys such as P01. Gradients indicate sources and sinks for refractory DOC (RDOC) in the deep layers, processes that are not understood at the present. RDOC has been implicated by paleoceanographers as the source of carbon responsible for climate hyperthermals of the Paleocene/Eocene epochs (45–50M ybp), but we know too little about RDOC in the modern ocean to confirm or refute that role. To fill the gaps in global coverage of DOC, we collected seawater samples at the stations on P10N and P01 lines during the MR14-04 cruise.

(3) Samplings

Seawater samples were collected in P10N (Leg. 1) and P01 line (Leg. 2) at all of the stations and layers where inorganic carbon parameters were measured in the main subject of this cruise. Water was collected directly from the 12-L Niskin bottles attached to a CTD system into 60 mL polycarbonate bottles. The bottles were then stored frozen until analysis at our laboratory at the University of Miami. Total number of the samples collected was approximately 2100.

(4) Sample analyses and data managements

The frozen samples are returned to the laboratory and thawed for analysis by high temperature catalytic oxidation using a Shimadzu TOC analyzer. We require <1 year to complete the analyses. We typically submit all of our data to the CDIAC data center for carbon measurements (http://cdiac.ornl.gov/oceans/).

3.11.2 Dissolved Organic Carbon at station 73 (K2)

August 18, 2014

(1) Personnel

Masahide Wakita (JAMSTEC)
Hiroshi Uchida (JAMSTEC)

(2) Purpose of the study

Fluctuations in the concentration of dissolved organic carbon (DOC) in seawater have a potentially great impact on the carbon cycle in the marine system, because DOC is a major global carbon reservoir. A change by < 10% in the size of the oceanic DOC pool, estimated to be ~ 700 GtC, would be comparable to the annual primary productivity in the whole ocean. It is widely observed that in the ocean DOC accumulates in surface waters at levels above the more constant concentration in deep water, suggesting the presence of DOC associated with biological production in the surface ocean. To investigate the DOC associated with biological production in the surface ocean, we observed the DOC contents from 2010 to 2013 at station 73 (K2; 47°N, 160°E) in the western subarctic gyre of North Pacific Ocean (http://ebcrpa.jamstec.go.jp/k2s1/en/bottle.html). This study presents the distribution of DOC during summer.

(3) Sampling

Seawater samples were collected at stations 73 and brought the total to ~80. Seawater from each Niskin bottle was transferred into 60 ml High Density Polyethylene bottle (HDPE) rinsed with same water three times. Water taken from the surface to 250 m is filtered using precombusted (450°C) GF/F inline filters as they are being collected from the Niskin bottle. At depths > 250 m, the samples are collected without filtration. After collection, samples are frozen upright and preserved at ~ -20 °C cold until analysis in our land laboratory. Before use, all glassware was muffled at 550 °C for 5 hrs.

(4) Analysis

Prior to analysis, samples are returned to room temperature and acidified to pH < 2 with concentrated hydrochloric acid. DOC analysis was basically made with a high-temperature catalytic oxidation (HTCO) system improved a commercial unit, the Shimadzu TOC-L (Shimadzu Co.). In this system, the non-dispersive infrared was used for carbon dioxide produced from DOC during the HTCO process (temperature: 680 °C, catalyst: 0.5% Pt-Al_2O_3).

(5) Preliminary result

The distributions of DOC will be determined as soon as possible after this cruise.

(6) Data Archive

All data will be submitted to JAMSTEC Data Management Office (DMO) within 2 years.

3.12 Carbon Isotopes

August 24, 2014

(1) Personnel

Yuichiro Kumamoto

Japan Agency for Marine-Earth Science and Technology

(2) Objective

In order to investigate the water circulation and carbon cycle in the North Pacific Ocean, seawaters for measurements of carbon-14 (radiocarbon) and carbon-13 (stable carbon) of total dissolved inorganic carbon (TDIC) were collected by the hydrocasts from surface to near bottom.

(3) Sample collection

The sampling stations and number of samples are summarized in Table 3.12.1. All samples for carbon isotope ratios (total 292 samples) were collected at 12 stations in the Leg-2 using 12-liter Niskin-X bottles. The seawater sample was siphoned into a 250 cm^3 glass bottle with enough seawater to fill the glass bottle 2 times. Immediately after sampling, 10 cm^3 of seawater was removed from the bottle and poisoned by 0.1 cm^3 μl of saturated $HgCl_2$ solution. Then the bottle was sealed by a glass stopper with Apiezon grease M and stored in a cool and dark space on board.

(4) Sample preparation and measurements

In our laboratory, dissolved inorganic carbon in the seawater samples will be stripped cryogenically and split into three aliquots: radiocarbon measurement (about 200 μmol), carbon-13 measurement (about 100 μmol), and archive (about 200 μmol). The extracted CO_2 gas for radiocarbon will be then converted to graphite catalytically on iron powder with pure hydrogen gas. The carbon-13 of the extracted CO_2 gas will be measured using Finnigan MAT252 mass spectrometer. The carbon-14 in the graphite sample will be measured by Accelerator Mass Spectrometry (AMS).

Table 3.12.1 Sampling stations and number of samples for carbon isotope ratios.

Station	Lat. (N)	Long. (E)	Sampling Date (UTC)	Number of samples	Number of replicate samples	Max. Pressure (dbar)
054	39-56.83	147-42.79	2014/07/21	24	1	5328
067	44-05.04	154-59.23	2014/07/25	24	1	5405
073	47-00.73	160-01.15	2014/07/27	24	1	5291
079	46-58.31	166-44.83	2014/07/30	24	1	6074
091	47-00.35	173-53.00	2014/08/02	24	1	5910
101	47-00.14	185-02.76	2014/08/06	24	1	5901
110	46-59.63	195-00.73	2014/08/10	24	1	5425
116	47-00.01	201-51.79	2014/08/11	24	1	5326
122	47-00.21	208-35.71	2014/08/13	24	1	5296
128	46-53.98	215-33.73	2014/08/15	23	1	4742
136	46-59.80	224-15.85	2014/08/19	22	1	4202
141	46-58.69	229-58.21	2014/08/21	19	1	2653
			Total	280	12	

3.13 Radiocesium and Iodine-129

August 24, 2014

(1) Personnel

Yuichiro Kumamoto

Japan Agency for Marine-Earth Science and Technology

(2) Objective

In order to investigate the water circulation and ventilation process in the North Pacific, during the leg-1 and -2 of MR14-04 cruise seawater samples were collected for measurements of radiocesium (Cs-134 and Cs-137) and iodine-129, which were mainly released from the global fallout in the 1950s and 1960s and the Fukushima Daiichi nuclear power plant after its serious accident on the March 11 of 2011.

(3) Sample collection

The sampling stations and number of samples are summarized in Table 3.13.1. The total 319 and 155 of seawater samples for radioactive cesium and iodine-129 were collected at 20 stations, respectively. The seawaters were sampled vertically using 12-liter Niskin-X bottles. Surface seawater were collected using a bucket. For radiocesium surface seawater was also collected from continuously-pumped-up water from about 4-m depth. The seawater sample for radiocesium was collected into a 20-L plastic container and after two time washing. Immediately after sampling, the seawater collected in layers shallower than 100-m depth was filtrated using menbrane filter (Millipore HAWP14250, 142mm, 0.45μm). All the seawater samples were acidified by adding of 40-cm^3 of concentrated nitric acid (85%, Wako Pure Chemical Industries, Ltd.) on board. The seawater sample for iodine-129 was collected into a 1-L plastic bottle.

(4) Sample preparation and measurements

In our laboratory on shore, radiocesium in the seawater samples will be concentrated using ammonium phosphomolybdate (AMP) that forms insoluble compound with cesium. The radiocesium in AMP will be measured using Ge γ-ray spectrometer. Iodine-129 in the seawater sample will be concentrated and measured using accelerator mass spectrometer.

Table 3.13.1 Sampling stations and number of samples for radiocesium and iodine-129

Station	Lat. (N)	Long. (E)	Sampling Date (UTC)	No. of samples for radiocesium	No. of samples for I-129	Max. Pressure (dbar)
014 surface (pump)	36-04.19	148-04.19	2014/07/06	3	0	4
022 surface (pump)	38-45.04	146-18.39	2014/07/13	3	0	4
074 surface (pump)	46-58.06	161-27.24	2014/07/28	3	0	4
101 surface (pump)	47-00.26	174-57.30	2014/08/06	3	0	4
001	29-53.00	149-49.06	2014/07/11	17	9	800
007	33-52.00	149-49.00	2014/07/12	18	9	800
014	36-04.84	148-04.45	2014/07/13	18	9	800
022	38-45.08	146-18.45	2014/07/13	16	9	800
030	41-14.90	144-30.51	2014/07/14	18	9	800
067	44-05.04	154-59.23	2014/07/25	20	10	830
073	47-02.03	160-00.64	2014/7/27	20	10	830
079	46-59.17	166-44.30	2014/7/30	20	10	830
091	47-00.34	173-50.41	2014/08/02	20	10	830
101	46-59.87	185-02.97	2014/08/06	20	10	770
110	46-59.83	195-00.79	2014/08/09	20	10	770
116	46-59.62	201-52.06	2014/08/12	20	10	770
122	47-00.19	208-35.02	2014/08/13	20	10	770
128	46-54.40	215-33.94	2014/08/16	20	10	770
136	46-59.92	224-16.04	2014/08/19	20	10	830
141	46-58.49	229-58.49	2014/08/21	20	10	800
			Total	319	155	

3.14 Stable Isotopes of Water

September 12, 2014

(1) Personnel

Hiroshi Uchida (JAMSTEC)
Shinya Kouketsu (JAMSTEC)

(2) Objectives

The objective of this study is to collect stable isotopes of water to use as a tracer of ocean circulation.

(3) Materials and methods

The hydrogen (H) and oxygen (O) isotopic ratio of seawater are defined as follows:

$\delta D\ [‰] = 1000\ \{(D/H)_{sample}/(D/H)_{VSMOW} - 1\}$

$\delta^{18}O\ [‰] = 1000\ \{(^{18}O/^{16}O)_{sample}/(^{18}O/^{16}O)_{VSMOW} - 1\}$

where D is deuterium and VSMOW is Vienna Standard Mean Ocean Water. The isotopic ratios of VSMOW water are defined as follows:

$(D/H)_{VSMOW} = 155.76 \pm 0.1$ ppm

$(^{18}O/^{16}O)_{VSMOW} = 2005.20 \pm 0.43$ ppm.

The isotopic ratios will be measured in a laboratory in the Japan Agency for Marine-Earth Science and Technology, Yokosuka, Japan, after the cruise with a Cavity Ring-Down Spectroscopy (CRDS, L112-i, Picarro Inc., Santa Clare, CA, USA).

The water samples were collected in 10-mL borosilicate glass bottles (Butyl rubber stopper with aluminum cap, Maruemu Co., Osaka, Japan). The collected samples is storing at room temperature. A total of 2241 samples was collected including 128 pairs of replicate samples.

3.15 Perfluoroalkyl substances (PFASs)

September 2, 2014

(1) Personnel

Nobuyoshi YAMASHITA	National Institute of Advanced Industrial Science and Technology (AIST): PI
Sachi TANIYASU	AIST

(2) Objective

Environmentally persistent perfluoroalkyl substances (PFASs, shown in Figure 3.15.1) have appeared as a new class of global pollutants for the last thirteen years.

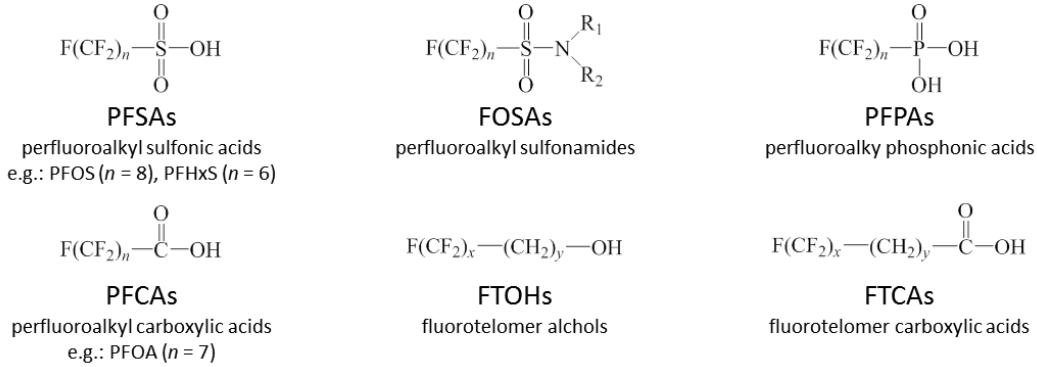

Figure 3.15.1 Perfluoroalkyl substances (PFASs)

These compounds have recently emerged as a priority environmental pollutant due to its widespread finding in biota including both Arctic and Antarctic species and its persistent and bioaccumulative nature, especially for PFOS (perfluorooctane sulfonate) and PFOA (perfluorooctane carboxylic acid). The physicochemical properties of PFASs, especially of PFSAs (perfluoro sulfonpnates) and PFCAs (perfluoro carboxylic acids) are unique in that they have high water solubility despite the low reactivity of carbon-fluorine bond, which also imparts high stability in the environment. However, little is known on the distribution of PFASs in the oceans around the world, so far. We have conducted several international joint cruises, including South China Sea and Sulu Seas (KH-02-4), the central to Western Pacific Ocean (KH03-1 and MR11-08), North Pacific Ocean (KH-12-04), Arctic Ocean (MR13-06), North and middle Atlantic Ocean, Southern Pacific and Antarctic Ocean (KH04-5, MR12-05), Labrador Sea and coastal seawater from Asian countries (Japan, China, Hong Kong, Korea) [1, 2, 3]. Vertical profiles of PFASs in the marine water column were associated with the global ocean circulation theory. We found that vertical profiles of PFASs in water columns from the Labrador Sea reflected the influx of the North Atlantic Current in surface waters, the Labrador Current in subsurface waters, and the Denmark Strait Overflow Water in deep layers below 2000 m. Striking differences in the vertical and spatial distribution of PFASs, depending on the oceans, suggest that these persistent organic acids can serve as useful chemical tracers to allow us to study oceanic transportation by major water currents. The results provide evidence that PFAS concentrations and profiles in the oceans adhere to a pattern consistent with the global ‘‘Broecker’s Conveyor Belt’’ theory of open ocean water circulation.

In MR14-04, we will survey PFASs in vertical seawater, air and precipitation to understand global distribution of PFASs in open ocean and atmosphere.

(3) Parameters

Perfluoroalkyl substances (PFASs)

(4) Instruments and Methods

Water samples were stored in clean polypropylene bottles and were kept frozen until analysis. Samples were thawed at room temperature, and a solid phase extraction method using Oasis®WAX-Sea cartridge (500 mg, 30 μm) (Waters Co.) for seawater samples which cartridge was developed specially for open seawater samples by AIST and Oasis®WAX cartridge (150 mg, 30 μm) (Waters Co.) [4,5] for air and precipitation samples. The HPLC tandem mass spectrometry (HPLC-MS/MS) was used for sample analysis [4,5]. Briefly, after preconditioning with ammonium hydroxide in methanol, methanol, and then Millipore water, the cartridges were loaded water samples at approximately 1 drop sec^{-1}. Seawater samples were adjusted pH3 by acetic acid and then spiked surrogate standard (1 ng of each compound) before sample loading. The cartridges were then washed with Milli-Q water and then 25 mM ammonium acetate buffer (pH 4) in Milli-Q water and dried. The elution was then divided into two fractions. The first fraction was carried out with methanol and the second with 0.1% ammoniumhydroxide in methanol. Both fractions were reduced to 1 mL under a nitrogen stream and analyzed separately. HPLC-MS/MS, composed of a HP1100 liquid chromatograph (Agilent Technologies, Palo Alto, CA) interfaced with a Micromass® (Beverly, MA) Quattro Ultima Pt mass spectrometer was operated in the electrospray negative ionization mode. A 10-μL aliquot of the sample extract was injected into a Betasil C18 column (2.1 mm i.d. × 50 mm length, 5 μm; Termo Hypersil-Keystone, Bellefonte, PA). The capillary is held at 1.2 kV. Cone-gas and desolvation-gas flows are kept at 60 and 650 L/h, respectively. Source and desolvation temperatures were kept at 120 and 420°C respectively. MS/MS parameters are optimized so as to transmit the [M-K]- or [M-H]- ions.

(5) Observation log

List of seawater samples (surface, subsurface and deep water) collected were presented in Table 3.15.1 and Table 3.15.2. Deep seawater samples were taken by Conductivity temperature depth profiler-Carousel multiple sampling system (CTD-CMS) attached X-Niskin samplers of 12 L, together with surface seawater samples taken by stainless bucket at all the water sampling stations. Subsurface waters were also collected from the out let tube of surface water analysis facility in MIRAI.

Table 3.15.1 Summary of surface and deep seawater sampling for PFASs analysis.

Stn	Cast	Date collected					Latitude			Longitude			Depth	Sampling Depth														
		YYYY	MM	DD	hh:mm		deg	min	N/S	deg	min	E/W	m	m														
1	1	2014	07	11	00:58	UTC	29	58.85	N	149	15.50	E	6198	0	11	50	99	149	200	299	397	595	990	1978	2763	3692	4907	5999
7	1	2014	07	12	06:18	UTC	33	43.96	N	149	19.31	E	6169	0	25	50	99	149	199	298	396	593	991	1978				
14	1	2014	07	12	22:03	UTC	36	04.84	N	148	04.45	E	5829	0	24	50	100	149	198	299	400	595	990	1978				
22	1	2014	07	13	18:15	UTC	38	45.08	N	146	18.45	E	5294	0	50	100	149	198	298	398	596	794	989	1976	2957	3934	5276	
30	1	2014	07	14	12:26	UTC	41	14.90	N	144	30.51	E	4061	0	26	50	99	149	199	297	397	594	989	1976				
36	1	2014	07	17	07:28	UTC	42	58.42	N	145	27.12	E	96	0	10	49	85											
49	1	2014	07	20	16:13	UTC	41	08.17	N	146	53.31	E	5336	0	10	50	99	149	199	328	425	624	1059	2044	3035	4010	4981	5320
60	1	2014	07	23	13:34	UTC	41	16.08	N	150	23.21	E	5382	0	10	50	99	149	198	298	398	596	991	1975	2959	3935	4903	5369
67	2	2014	07	25	15:59	UTC	44	05.15	N	155	00.92	E	5307	0	10	50	99	149	198	326	425	624	1059	2044	3032	4009	4980	5295
73	1	2014	07	27	11:59	UTC	47	00.56	N	160	01.31	E	5195	0	10	49	100	149	198	327	426	624	1057	2042	3032	4007	4977	5183
87	1	2014	08	01	11:06	UTC	46	58.86	N	169	59.75	E	4923	0	10	49	100	149	200	300	397	594	990	1974	2953	3930	4906	
98	1	2014	08	05	02:04	UTC	46	59.90	N	178	41.92	W	5494	0	10	49	99	149	199	278	367	565	960	1906	2885	3852	4824	5484
103	1	2014	08	07	18:05	UTC	46	59.35	N	172	17.74	W	5795	0	10	50	100	149	198	328	425	624	1059	2043	3032	4008	4979	5779
114	1	2014	08	11	06:33	UTC	46	59.66	N	160	38.38	W	5132	0	10	50	100	149	198	298	397	593	988	1977	2954	3930	4901	5110
124	1	2014	08	14	13:55	UTC	46	59.41	N	149	51.40	W	5060	0	10	50	100	150	198	326	427	625	1062	2044	3032	4007	4979	5038
132	1	2014	08	18	14:48	UTC	47	01.66	N	140	46.42	W	4333	0	10	50	100	149	200	297	396	596	988	1975	2955	3931	4317	
141	1	2014	08	21	03:25	UTC	46	58.69	N	130	58.21	W	2630	0	10	49	100	149	198	298	395	593	989	1973	2615			
145	1	2014	08	22	03:02	UTC	46	59.66	N	127	47.87	W	2635	0	10	49	99	149	198	327	425	625	1058	2043	2621			
150	1	2014	08	22	21:01	UTC	46	56.31	N	124	00.96	W	281	0	10	49	99	149	199	291								

Table 3.15.2 Summary of sub-surface seawater sampling for PFASs analysis.

On board ID	Stn	Cast	Date collected					Latitude			Longitude		
			YYYY	MM	DD	hh:mm		deg	min	N/S	deg	min	E/W
MR1404-WS01	1	1	2014	07	11	00:58	UTC	29	58.85	N	149	15.50	E
MR1404-WS02	7	1	2014	07	12	06:18	UTC	33	43.96	N	149	19.31	E
MR1404-WS03	14	1	2014	07	12	22:03	UTC	36	04.84	N	148	04.45	E
MR1404-WS04	22	1	2014	07	13	18:15	UTC	38	45.08	N	146	18.45	E
MR1404-WS05	30	1	2014	07	14	12:26	UTC	41	14.90	N	144	30.51	E
MR1404-WS06	-	-	2014	07	15	00:00	UTC	42	38.77	N	144	04.99	E
MR1404-WS07	36	1	2014	07	17	07:28	UTC	42	58.42	N	145	27.12	E
MR1404-WS08	49	1	2014	07	20	16:13	UTC	41	08.17	N	146	53.31	E
MR1404-WS09	-	-	2014	07	23	16:36	UTC	41	21.91	N	150	32.54	E
MR1404-WS10	67	2	2014	07	25	15:59	UTC	44	05.15	N	155	00.92	E
MR1404-WS11	73	1	2014	07	27	11:59	UTC	47	00.56	N	160	01.31	E
MR1404-WS12	87	1	2014	08	01	11:06	UTC	46	58.86	N	169	59.75	E
MR1404-WS13	98	1	2014	08	05	02:04	UTC	46	59.90	N	178	41.92	W
MR1404-WS14	103	1	2014	08	07	18:05	UTC	46	59.35	N	172	17.74	W
MR1404-WS15	114	1	2014	08	11	06:33	UTC	46	59.66	N	160	38.38	W
MR1404-WS16	124	1	2014	08	14	13:55	UTC	46	59.41	N	149	51.40	W
MR1404-WS17	-	-	2014	08	17	09:05	UTC	48	25.59	N	144	11.89	W
MR1404-WS18	132	1	2014	08	18	14:48	UTC	47	01.66	N	140	46.42	W
MR1404-WS19	141	1	2014	08	21	03:25	UTC	46	58.69	N	130	58.21	W
MR1404-WS20	145	1	2014	08	22	03:02	UTC	46	59.66	N	127	47.87	W
MR1404-WS21	150	1	2014	08	22	21:01	UTC	46	56.31	N	124	00.96	W
MR1404-WS22	-	-	2014	08	23	17:16	UTC	48	49.75	N	130	05.75	W
MR1404-WS23	-	-	2014	08	22	21:01	UTC	52	30.59	N	144	40.34	W
MR1404-WS24	-	-	2014	08	28	04:03	UTC	54	01.58	N	159	57.67	W

Atmospheric samples were taken with a comprehensive cryogenic moisture sampler (CMS; prototype type 5) which was developed by AIST and SIBATA Co (Figure 3.15.2). The air sampler was operated with a flow rate of 20 L/min. Gas and particle phase of PFASs in atmosphere were collected into bubbler solvent consisted of methanol in Milli-Q water by bubbling and then trapped into cold trap by cooling with -4 ˚C. Samples were collected during underway and CTD operation to avoid contamination from exhaust gas from ship. List of air samples were presented in Table 3.15.3.

Precipitation samples were also collected using polypropylene funnel (16.5 cm φ). List of precipitation samples were presented in Table 3.15.4.

All collected samples were stored at below -20°C until chemical analysis in AIST laboratory.

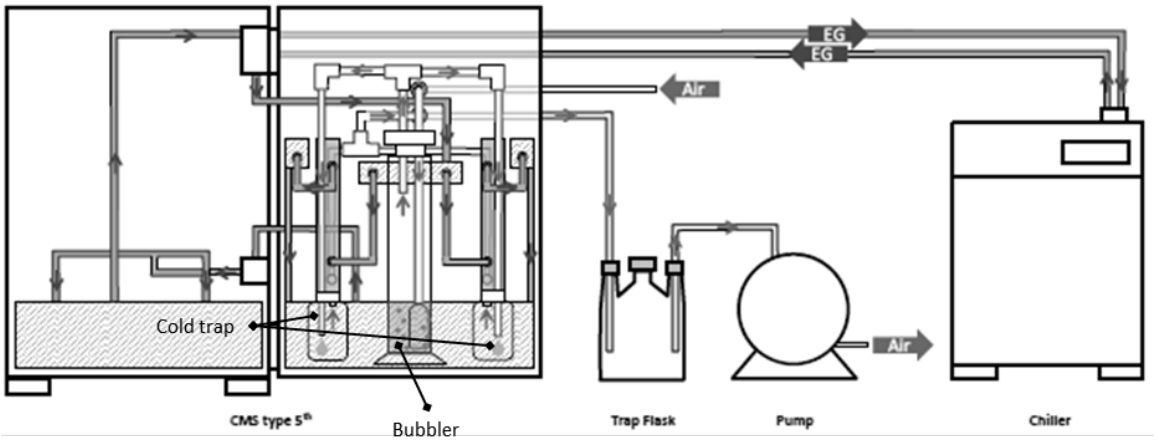

Figure 3.15.2 Schematic diagram of CMS type 5th system.

Table 3.15.3 Summary of air sampling by CMS for PFASs analysis.

On board ID		Date collected					Latitude			Longitude			Total Run Time	Total Vol.
		YYYY	MM	DD	hh:mm		deg	min	N/S	deg	min	E/W	(hrs)	(m^3)
MR1404-AR01	start	2014	07	08	23:17	UTC	33	38.27	N	140	37.08	E	37.70	45.251
	stop	2014	07	10	12:59	UTC	30	05.50	N	149	00.04	E		
MR1404-AR02	start	2014	07	11	09:44	UTC	30	04.97	N	149	16.94	E	30.00	36.026
	stop	2014	07	12	20:30	UTC	35	56.85	N	148	08.05	E		
MR1404-AR03	start	2014	07	13	01:00	UTC	36	18.77	N	147	54.66	E	34.78	34.838
	stop	2014	07	15	00:00	UTC	42	50.06	N	144	06.67	E		
MR1404-AR04	start	2014	07	17	01:24	UTC	42	57.96	N	144	20.73	E	13.60	16.386
	stop	2014	07	18	08:31	UTC	41	42.59	N	146	24.90	E		
MR1404-AR05	start	2014	07	20	04:21	UTC	42	00.97	N	146	05.51	E	13.60	18.574
	stop	2014	07	22	03:10	UTC	40	00.94	N	148	23.29	E		
MR1404-AR06	start	2014	07	25	07:43	UTC	43	34.78	N	154	12.96	E	31.89	48.218
	stop	2014	07	28	21:20	UTC	46	59.42	N	161	09.19	E		
MR1404-AR07	start	2014	07	29	13:26	UTC	46	59.68	N	163	22.87	E	67.87	81.591
	stop	2014	08	02	14:02	UTC	47	00.52	N	173	48.41	E		
MR1404-AR08	start	2014	08	02	15:00	UTC	47	00.34	N	173	49.61	E	86.35	103.647
	stop	2014	08	06	12:31	UTC	47	00.11	N	173	49.12	W		
MR1404-AR09	start	2014	08	06	13:24	UTC	47	00.22	N	173	44.73	W	52.80	63.458
	stop	2014	08	10	02:45	UTC	46	59.29	N	164	59.26	W		
MR1404-AR10	start	2014	08	10	07:10	UTC	47	00.63	N	163	43.26	W	83.23	103.665
	stop	2014	08	15	02:24	UTC	47	00.18	N	147	44.12	W		
MR1404-AR11	start	2014	08	15	00:00	UTC	46	54.87	N	144	25.87	W	25.48	30.590
	stop	2014	08	17	16:49	UTC	47	01.84	N	143	30.21	W		
MR1404-AR12	start	2014	08	17	17:17	UTC	47	00.80	N	143	29.73	W	61.65	41.156
	stop	2014	08	19	21:00	UTC	46	59.63	N	135	44.17	W		
MR1404-AR13	start	2014	08	20	00:54	UTC	47	01.24	N	134	37.09	W	46.30	55.676
	stop	2014	08	22	21:14	UTC	46	56.32	N	124	59.04	W		
MR1404-AR14	start	2014	08	22	22:34	UTC	47	02.82	N	125	17.38	W	40.90	49.096
	stop	2014	08	24	15:35	UTC	50	41.33	N	136	24.61	W		
MR1404-AR15	start	2014	08	24	16:17	UTC	50	44.27	N	136	36.85	W	53.95	64.761
	stop	2014	08	26	22:52	UTC	53	19.22	N	151	32.91	W		
MR1404-AR16	start	2014	08	27	07:58	UTC	53	40.83	N	154	16.60	W	27.67	27.667
	stop	2014	08	28	20:47	UTC	54	05.65	N	162	07.45	W		

Table 3.15.4 Summary of precipitation sampling for PFASs analysis.

On board ID		Date collected					Latitude			Longitude		
		YYYY	MM	DD	hh:mm		deg	min	N/S	deg	min	E/W
MR1404-R01	start	2014	07	17	06:34	UTC	42	55.18	N	145	55.18	E
	stop	2014	07	18	02:34	UTC	42	22.86	N	145	54.52	E
MR1404-R02	start	2014	07	20	18:09	UTC	41	08.66	N	146	53.63	E
	stop	2014	07	25	04:59	UTC	43	33.93	N	154	10.57	E
MR1404-R03	start	2014	07	25	04:59	UTC	43	33.93	N	154	10.57	E
	stop	2014	07	29	06:05	UTC	46	59.43	N	162	15.26	E
MR1404-R04	start	2014	07	29	06:05	UTC	46	59.43	N	162	15.26	E
	stop	2014	08	02	17:14	UTC	47	00.35	N	173	50.21	E
MR1404-R05	start	2014	08	02	17:14	UTC	47	00.35	N	173	50.21	E
	stop	2014	08	06	20:04	UTC	47	02.18	N	173	44.95	W
MR1404-R06	start	2014	08	06	20:04	UTC	47	02.18	N	173	44.95	W
	stop	2014	08	10	02:58	UTC	46	59.59	N	164	58.58	W
MR1404-R07	start	2014	08	10	02:58	UTC	46	59.59	N	164	58.58	W
	stop	2014	08	13	19:53	UTC	47	00.11	N	151	33.75	W
MR1404-R08	start	2014	08	13	19:53	UTC	47	00.11	N	151	33.75	W
	stop	2014	08	17	17:17	UTC	47	00.80	N	143	29.73	W
MR1404-R09	start	2014	08	17	17:17	UTC	47	00.80	N	143	29.73	W
	stop	2014	08	19	23:21	UTC	47	01.04	N	135	04.12	W
MR1404-R10	start	2014	08	19	23:21	UTC	47	01.04	N	135	04.12	W
	stop	2014	08	22	22:34	UTC	47	02.82	N	125	00.00	W
MR1404-R11	start	2014	08	22	22:34	UTC	47	02.82	N	125	00.00	W
	stop	2014	08	26	23:26	UTC	53	20.76	N	151	00.00	W
MR1306-R12	start	2014	08	26	23:26	UTC	53	20.76	N	151	00.00	W
	stop	2014	08	28	04:35	UTC	54	01.69	N	160	04.97	W

(6) Data archives

These data obtained in this cruise will be submitted to the Data Management Group (DMG) of JAMSTEC, and will be opened to the public via "Data Research for Whole Cruise Information in JAMSTEC" in JAMSTEC web site.

(7) References

1) Yamashita N, Kannan K, Taniyasu S, Horii Y, Petrick G, Gamo T, A global survey of perfluorinated acids in oceans, Marine Pollution Bulletin 51 (2005) 658–668
2) Wei S, Chen LQ, Taniyasu S, So MK, Murphy MB, Yamashita N, Yeung LWY, Lam PKS, Distribution of perfluorinated compounds in surface seawaters between Asia and Antarctica, Marine Pollution Bulletin 54 (2007) 1813–1838
3) Yamashita N, Taniyasu S, Petrick G, Wei S, Gamo T, Lam PKL, Kannan K, Perfluorinated acids as novel chemical tracers of global circulation of ocean waters, Chemosphere 70 (2008) 1247–1255
4) Yamashita N, Kannan K, Taniyasu S, Horii Y, Okazawa T, Petrick G, Gamo T, Analysis of Perfluorinated Acids at Parts-Per-Quadrillion Levels in Seawater Using Liquid Chromatography-Tandem Mass Spectrometry, Environ. Sci. Technol. (2004) 38, 5522-5528
5) Taniyasu S, Kannan K, So MK, Gulkowskad A, Sinclair E, Okazawa T, Yamashita N, Analysis of fluorotelomer alcohols, fluorotelomer acids, and short- and long-chain perfluorinated acids in water and biota, Journal of Chromatography A, 1093 (2005) 89–97
6) ISO 25101 (2009 March 1st) Water quality — Determination of perfluorooctanesulfonate (PFOS) and perfluorooctanoate (PFOA) — Method for unfiltered samples using solid phase extraction and liquid chromatography/mass spectrometry

3.16 Methane (CH_4) and Nitrous oxide (N_2O)

September 19, 2014

(1) Personnel

Osamu Yoshida[1,*]

Kanta Chida[1]

Takuya Takahashi[1]

[1] Department of Environmental and Symbiotic Science,
College of Agriculture, Food and Environment Sciences,
Rakuno Gakuen University

* Principal Investigator

(2) Sampling elements

Sampling elements of Rakuno Gakuen University group at hydrographic stations are listed below.

Table 3.16.1. Parameters and hydrographic station numbers for samples collection.

Parameters	Hydrographic Station Numbers (P01)
1. Dissolved CH_4 and N_2O (concentration)	1, 7, 14, 22, 30, 36, 42, 49, 51, 54, 60, 64, 67, 71, 73, 75, 77, 81, 87, 91, 93, 95, 97, 99, 101, 103, 105, 107, 109, 112, 114, 116, 118, 120, 122, 124, 128, 130, 132, 134, 138, 140, 141, 143, 149,151

(3) Methane

Methane concentration distribution as indicators of biogenic methane dynamics in the Pacific Ocean

i. Dissolved CH_4

i-a Introduction

The atmospheric concentrations of the greenhouse gases methane (CH_4) have increased since 1750 due to human activity. In 2011 the concentrations of CH_4 was 1803 ppb exceeded the pre-industrial levels by about 150% (IPCC, 2013). In order to understand the current global CH_4 cycle, it is necessary to quantify its sources and sinks. At present, there remain large uncertainties in the estimated CH_4 fluxes from sources to sinks. The ocean's source strength for atmospheric CH_4 should be examined in more detail, even though it might be a relatively minor source, previously reported to be 0.005 to 3% of the total input to the atmosphere (Cicerone and Oremland, 1988; Bange et al., 1994; Lelieveld et al., 1998).

To estimate an accurate amount of the CH_4 exchange from the ocean to the atmosphere, it is

necessary to explore widely and vertically. Distribution of dissolved CH_4 in surface waters from diverse locations in the world ocean is often reported as a characteristic subsurface maximum representing a supersaturation of several folds (Yoshida et al., 2004; 2011). Although the origin of the subsurface CH_4 maximum is not clear, some suggestions include advection and/or diffusion from local anoxic environment nearby sources in shelf sediments, and *in situ* production by methanogenic bacteria, presumably in association with suspended particulate materials (Karl and Tilbrook, 1994; Katz et al., 1999). These bacteria are thought to probable live in the anaerobic microenvironments supplied by organic particles or guts of zooplankton (Alldredge and Cohen, 1987).

So, this study investigates in detail profile of CH_4 concentration in the water column in the Pacific Ocean to clarify CH_4 dynamics and estimate the flux of CH_4 to the atmosphere.

i-b Materials and methods

Seawater samples are taken by CTD-CAROUSEL system attached Niskin samplers of 12 L at 28 layers and surface layer taken by plastic bucket at 46 hydrographic stations as shown in Table 3.16.1. Each sample was carefully subsampled into 30 mL glass vials to avoid air contamination for analysis of CH_4 concentration. The seawater samples were poisoned by 20 μL (30 mL vials) of mercuric chloride solution (Tilbrook and Karl, 1995; Watanabe et al., 1995), and were closed with rubber-aluminum and plastic caps. These were stored in a dark and cool place until we got to land, where we conducted gas chromatographic analysis of CH_4 concentration at the laboratory.

The analytical method briefly described here: The system consists of a purge and trap unit, a desiccant unit, rotary valves, a gas chromatograph equipped with a flame ionization detector for concentration of CH_4 and data acquisition units. The entire volume of seawater in each glass vial was processed all at once to avoid contamination and loss of CH_4. Precision obtained from replicate determinations of CH_4 concentration was estimated to be better than 5% for the usual concentration of CH_4 in seawater.

i-c Expected results

Subsurface maximum concentrations of CH_4 (>3 nmol kg^{-1}) were expected to be observed in the Pacific Ocean. A commonly-encountered distribution in the upper ocean with a CH_4 peak within the pycnocline (e.g., Ward et al., 1987; Owens et al., 1991; Watanabe et al., 1995; Yoshida et al., 2011). Karl and Tilbrook (1994) suggested the suboxic conditions would further aid the development of microenvironments within particles in which CH_4 could be produced. The organic particles are accumulated in the pycnocline, and CH_4 is produced in the micro reducing environment by methanogenic bacteria. Moreover, *in situ* microbial CH_4 production in the guts of zooplankton can be expected (e.g., Owens et al., 1991; de Angelis and Lee, 1994; Oudot et al., 2002; Sasakawa et al., 2008). Watanabe et al. (1995) pointed out that the diffusive flux of CH_4 from subsurface maxima to air-sea interface is sufficient

to account for its emission flux to the atmosphere. In the mixed layer above its boundary, the CH_4 is formed and discharged to the atmosphere in part, in the below its boundary, CH_4 diffused to the bottom vertically. By using concentration and isotopic composition of CH_4 and hydrographic parameters for vertical water samples, it is possible to clarify its dynamics such as production and/or consumption in the water column.

ii. References

Alldredge, A. A., Y. Cohen: Can microscale chemical patches persist in the sea? Microelectrode study of marine snow, fecal pellets, Science, 235, 689-691, 1987.

Bange, H. W., U. H. Bartell, S. Rapsomanikis, and M. O. Andreae: methane in the Baltic and the North seas and a reassessment of the marine emissions of methane, Global Biogeochem. Cycles, 8, 465–480, 1994.

Cicerone, R. J., and R. S. Oremland: Biogeochemical aspects of atmospheric methane, Global Biogeochem. Cycles, 2, 299–327, 1988.

de Angelis, M. A., and C. Lee: Methane production during zooplankton grazing on marine phytoplankton, Limnol. Oceanogr., 39, 1298-1308, 1994.

Intergovermental Panel on Climate Change: Couplings Between Change in the Climate System and Biogeochemistry, in Climate Change 2013: The Physical Science Basis: Contribution of Working Group I to the Fifth Assessment Report of the Intergovernment Panel on Climate Change, edited by P. Ciais, et al., pp. 465-570, Cambridge University Press, Cambridge, United Kingdom and New York, NY, USA, 2013.

Karl, D. M., and B. D. Tilbrook: Production and transport of methane in oceanic particulate organic matter, Nature, 368, 732–734, 1994.

Katz, M. E., D. K. Pak, G. R. Dickkens, and K. G. Miller: The source and fate of massive carbon input during the latest Paleocene thermal maximum, Scince, 286, 1531–1533, 1999.

Lelieveld, J., P. J. Crutzen, and F. J. Dentener: Changing concentration, lifetime and climate forcing of atmospheric methane, Tellus Ser. B, 50, 128–150, 1998.

Oudot, C., P. Jean-Baptiste, E. Fourre, C. Mormiche, M. Guevel, J-F. Ternon, and P. L. Corre: Transatlantic equatorial distribution of nitrous oxide and methane, Deep-Sea Res., Part I, 49, 1175–1193, 2002.

Owens, N. J. P., C. S. Law, R. F. C. Mantoura, P. H. Burkill, and C. A. Llewellyn: Methane flux to the atmosphere from the Arabian Sea, Nature, 354, 293–296, 1991.

Sasakawa, M., U. Tsunogai, S. Kameyama, F. Nakagawa, Y. Nojiri, and A. Tsuda: Carbon isotopic characterization for the origin of excess methane in subsurface seawater, J. Geophys. Res., 113, C03012, doi: 10.1029/2007JC004217, 2008.

Tilbrook, B. D., and D. M. Karl: Methane sources, distributions and sinks from California coastal waters

to the oligotrophic North Pacific gyre, Mar. Chem., 49, 51–64, 1995.

Ward, B. B., K. A. Kilpatrick, P. C. Novelli, and M. I. Scranton: Methane oxidation and methane fluxes in the ocean surface layer and deep anoxic waters, Nature, 327, 226–229, 1987.

Watanabe, S., N. Higashitani, N. Tsurushima, and S. Tsunogai: Methane in the western North Pacific, J. Oceanogr., 51, 39–60, 1995.

Yoshida, O., H. Y. Inoue , S. Watanabe, S. Noriki, M. Wakatsuchi: Methane in the western part of the Sea of Okhotsk in 1998-2000, J. Geophys. Res., 109, C09S12, doi:10.1029/2003JC001910, 2004.

Yoshida, O., H. Y. Inoue, S. Watanabe, K. Suzuki, and S. Noriki: Dissolved methane distribution in the South Pacific and the Pacific Ocean in austral summer, J. Geophys. Res., 116, C07008, doi:10.1029/2009JC006089, 2011.

3.17 Geochemistry and Microbiology: Nitrogen and Carbon Cycles in the North Pacific

September 19, 2014

(1) Personnel

Akiko Makabe (Tokyo University of Agriculture and Technology)
Chisato Yoshikawa (JAMSTEC)
Shuichiro Matsushima (Tokyo Institute of Technology)
Sakae Toyoda (Tokyo Institute of Technology)
Miho Hirai (JAMSTEC)
Masanori Kaneko (JAMSTEC)
Taichi Yokokawa (Ehime University)
Takuro Nunoura (JAMSTEC)

(2) Introduction

Knowledge about oceanic nitrogen and carbon cycles has been dramatically changed in this decade. In nitrogen cycle, major ammonia oxidizers were believed to be a few lineages of Proteobacteria, but it has been revealed that archaeal ammonia oxidizers (AOA) shared more than 10% of microbial population in dark ocean, and nitrous oxide production is necessary for the growth of AOA. In addition, significant contribution of heterotrophic nitrogen fixation and anaerobic ammonia oxidizers are also been found in the oceanic nitrogen cycle. On the other hand, in carbon cycle, microbial life in dark ocean below mesopelagic water (corresponding to 200-1000 m depth range) is thought to be primarily supported by sinking organic carbons from surface waters. However, it has been recently revealed that the deep-sea biogeochemical cycles are more complex than previously expected, and the dark carbon fixation coupled with nitrification and sulfur- and hydrogen-oxidations is also recognized as another significant organic carbon source in dark ocean (Francis et al. 2007; Alonso-Sáez 2010; Swan et al. 2011; Anantharaman et al. 2013; Herndl and Reinthalar 2013).

Nitrogen cycle

The marine nitrogen cycle in surface waters is known to control biological activity in the ocean, because inorganic forms of nitrogen such as nitrate are indispensable nutrients for phytoplankton. Following the primary production, organic nitrogen compounds are metabolized into ammonium and low molecular organic nitrogen compounds that are substrates for nitrification and/or nitrogen source of microbes. Among the components of marine nitrogen cycle, Nitrous Oxide (N_2O) is recognized as significant anthropogenic greenhouse gas and a stratospheric ozone destroyer. The estimation of global N_2O flux from ocean to the atmosphere is 3.8 $TgNyr^{-1}$ and the estimation varies greatly, from 1.8 to 5.8

$TgNyr^{-1}$ (IPCC, 2013). This is because previous models had estimated N_2O concentration from oxygen concentration indirectly. In fact, marine N_2O production processes are very complicated; hydroxylamine oxidation during nitrification, nitrite reduction during nitrifier denitrification and nitrite reduction during denitrification produce N_2O and N_2O deduction during denitrification consumes N_2O (Dore et al., 1998; Knowles et al., 1981; Rysgaard et al., 1993; Svensson, 1998; Ueda et al., 1993). In addition, currently, previously unknown systems in nitrification in AOA have been reported. One is the N_2O production with unknown pathway using NO as one of the substrate (Santoro et al. 2011; Stieglmeier et al. 2014), and the other is ammonia oxidation via urea degradation in AOA has also been reported (Alonso-Sáez 2012). Therefore marine N_2O production processes are poorly understood quantitatively. N_2O isotopomers (oxygen isotope ratio ($\delta^{18}O$), difference in abundance of $^{14}N^{15}N^{16}O$ and $^{15}N^{14}N^{16}O$ (SP), and average nitrogen isotope ratio ($\delta^{15}N$)) are useful tracers to distinguish these processes and had revealed N_2O production processes in various ocean environments (e.g., Yoshida and Toyoda, 2000), but we need to improve the model with novel findings in the marine nitrogen cycle.

To reduce the uncertainties in global N_2O budget a marine N_2O model constrained by isotope dataset was developed and applied to two time-series stations (St. 73 & a station 4 degree east of St. 1) in the western North Pacific (Yoshikawa et al., in preparation). In this study we conducted water sampling for isotope analysis of N_2O and related substances (NO_3^-, NO_2^-, NH_4^+, DON and Chlorophyll-a) and some key reaction rates (nitrification and nitrogen fixation rates) at eight MBC shallow stations (above 500 m) including St. 1 & 73. Six of the eight stations are located in the subarctic North pacific that is the major high-nitrate low-chlorophyll (HNLC) region. Moreover, we assessed nitrification rate and isotopic signatures of nitrate of the entire water column at more than 10 stations. By using the results of isotope analysis we will validate and improve the marine N_2O isotopomer model and furthermore extend it from one-dimension to three-dimension. Moreover, we examine both inorganic and organic carbon uptake activity associated with AOA during and after the cruise, and identify genetic markers for each process of nitrogen cycle by molecular biology techniques.

Methane in ocean

Methane is a terminal product during decomposition of organic matter and acts as a potential greenhouse gas. The vast quantity of methane (about 500-600 Tg) is annually emitted to atmosphere, in which contribution of methane from ocean accounts for 3% (Conrad, 2009). In surface seawater, concentration of methane is oversaturated respect to the atmosphere, where dissolved oxygen concentration is maxima (Scranton et al., 1977). However, the mechanism of the methane production is still ambiguous, which has been termed the ocean methane paradox. As a traditional hypothesis, methane is produced in micro-anaerobic environments such as in guts of zooplankton and sinking particles of organic matter (Reeburgh, 2007). A recent study suggested bacterial production as byproduct during decomposition of phosphonate (Karl et al., 2008). In lake water where methane concentration is

oversaturated in the surface water as in the case of seawater, a consortium of methanogens and algae, especially cyanobacteria is suggested for source of methane (Grossart et al., 2011). Similar phenomena may be observed in surface seawater.

Recently, we developed high sensitive analysis of coenzyme F_{430}, which catalyzes methanogenic reaction (Kaneko et al., 2014). Since all methanogens harbor F_{430}, it can be a robust biomarker of methanogens. The objective of this study is to investigate distribution of F_{430} and carbon isotopic composition of methane in the surface seawater to clarify quantitative distribution of methanogens and their methanogenic pathway, which should provide important information about methane origin in the surface seawater.

In cases of deep-sea environments, methane from subseafloor environments is a frequently-used as effective chemical tracer for the subseafloor fluid inputs (Tsunogai et al. 1998; German et al. 2010). In the case of Tohoku Earthquake, Kawagucci et al. (2012) detected the high methane concentration with unusual isotopic signatures on the Japan Trench, and identified the high methane flux from the fractures related with the big earthquake. However, no comparative data before the earthquake was obtained in this case. In this cruise, we will examine concentration and isotopic signature of the deep-sea methane on transect of the Chishima-Kuril trench to identify the activity of thrusts associated with the trench system.

(3) Materials and methods

Samples

Seawater samples are taken by CTD-CAROUSEL system attached Niskin samplers of 12 L at 15 layers above 500 m and surface layer taken by plastic bucket at hydrographic stations as shown in Table 3.17.1.

Table 3.17.1. Parameters and hydrographic station names for this study.

Parameters	Hydrographic stations
1. $\delta^{15}N$ and $\delta^{18}O$ of NO_3^-	1, 7, 14, 22, 30, 40, 43, 45, 47, 50, 54, 58, 67, 73, 79, 85, 91, 97, 101, 105, 116, 122, 128, 136, 141, 147
2. $\delta^{15}N$ of Chlorophyll a	1, 54, 73, 91, 101, 116, 128, 141
3. $\delta^{15}N$, SP and$\delta^{18}O$ of dissolved N_2O	54, 73, 91, 101, 116, 128, 141
4. $\delta^{15}N$ and$\delta^{18}O$ of NO_2^-	54, 73, 91, 101, 116, 128, 141
5. $\delta^{15}N$ of NH_4^+, DON, urea	54, 73, 91, 101, 116, 128, 141
6. Nitrification rate	1, 22, 45, 54, 73, 79, 91, 97, 101, 110, 116, 122, 128, 136, 141
7. F_{430}	1, 54, 73, 91, 101, 116, 128, 141
8. $\delta^{13}C$ of CH_4	1, 38-55, 73, 91, 101, 116, 128, 141

Isotopic analyses for N_2O, NO_2, NH_4^+, DON and urea

Sample for N_2O isotopomer analysis was transferred to two of 220 ml glass vials. After an approximately two-fold volume overflow, 500μL of saturated $HgCl_2$ solution were added. The vials were sealed with butyl rubbers and aluminum caps and stored in dark at 4°C until analysis. The $\delta^{15}N$, $\delta^{18}O$ and SP values and concentrations of N_2O in seawater will be determined by slightly modified version of GC-IRMS (PreCon/HP6890 GC/ MAT 252) at TIT described in detail in Yamagishi et al. (2007).

Sample for nitrite isotope analysis was collected into a 100 ml syringe equipped with a DISMIC® filter (pore size: 0.45 μm) and filtered immediately after sampling. The samples were frozen until analysis. The $\delta^{15}N$ and $\delta^{18}O$ values of NO_2^- will be measured after conversion to N_2O using the azide method of McIlvin and Altabet (2005) by GC-IRMS.

Sample for ammonium isotope analysis was collected into 100 ml syringes equipped with a DISMIC® filter (pore size: 0.45 μm) and filtered immediately after sampling. A PTFE pack, which contained a Whatman GF/D filter with 10 μL of 1M H_2SO_4 solution, and 0.3 g of MgO were added to 100 mL of the filtrate. The bottles were shaken by hands at least once a day for 14 days. After ammonium was trapped to the acid, the pack was removed and rinsed with MilliQ water, then stored in a glass bottle with silica gels until analysis. The $\delta^{15}N$ values of ammonium will be measured after conversion to N_2O using wet oxidation and "denitrifier" method of Koba et al. (2010) by GC-IRMS.

Sample for dissolved organic nitrogen (DON) isotope analysis was collected into a 100 ml syringe equipped with a DISMIC® filter (pore size: 0.45 μm) and filtered immediately after sampling. The samples were frozen until analysis. The $\delta^{15}N$ values of DON will be measured after conversion to N_2O using wet oxidation and "denitrifier" method of Knapp et al. (2005) by GC-IRMS.

Sample for urea analysis was collected into a 100 ml syringe equipped with a DISMIC® filter (pore size: 0.45 μm) and filtered immediately after sampling. The samples were frozen until analysis. Concentrations of urea will be measured by spectrophotometric analysis (Revilla et al. 2005).

Sample for nitrate isotope analysis was collected into a 50 ml syringe equipped with a DISMIC® filter (pore size: 0.45 μm) and filtered immediately after sampling. These samples were removed nitrite with sulfamic acid using the method of Granger and Sigman (2009) and preserved at -23°C until chemical analysis. The $\delta^{15}N$ and $\delta^{18}O$ values of NO_3^- will be measured using the "bacterial" method of Sigman et al., (2001) in which N_2O converted from nitrate is analyzed using GasBench/ PreCon/IRMS.

Sample for chlorophyll isotope analysis was collected into 20L light-blocking polypropylene tanks. The samples were filtered under reduced pressure and collected on two-three pre-combusted Whatman GF/F filfers. The filters were double up and wrapped in aluminum foil and stored at -23ºC until analysis. Chlorophyll pigments will be extracted and split into each pigments by HPLS. The $\delta^{15}N$ values of Chlorophyll pigments will be measured by using EA-IRMS at JAMSTEC.

Nitrification activity measurements

Water samples for nitrification activity analysis were transferred into 100 mL glass vials without headspace. Combination of ^{15}N enriched substrates (ammonium, urea, and glutamine (amide or alpha group)) and inhibitors (carboxy-PTIO, allylthiourea, erythromycin, and GC7) were added to each vial. The final concentration of ^{15}N enriched substrates was 50 nM. The glass vials were incubated in dark for 12 hours, 24 hours, 3 days, or 10 days at in situ temperature. After incubation, the samples for nitrate analysis were filtered with a DISMIC® filter (pore size: 0.45 μm) and frozen until analysis. The samples for N_2O analysis were added by 0.5 mL of saturated $HgCl_2$ solution and stored at 4 ºC until analysis. The ^{15}N enrichment of nitrates will be measured by GC-IRMS after conversion to N_2O using the "bacterial" method of Sigman et al. (2001). The ^{15}N enrichment of N_2O will be measured by GC-IRMS described in detail in Yamagishi et al. (2007).

Nitrogen fixation activity measurement

Seawater for nitrogen fixation analysis was collected into four 250ml polycarbonate bottles with septum caps without headspace for incubation. In addition, approx. 175ml of seawater for preparing the $^{15}N_2$ water was also taken in 250ml polyethylene (PE) bottle. About 75ml of filtered/degassed seawater was prepared into a plastic bag by inline filtration and degassing device. The 1.0ml of $^{15}N_2$ gas (99.9 ^{15}N-atom %) was injected into the bag using a gas-tight syringe, then, the bag was shaken for more than 1 hour. The 25ml of $^{15}N_2$ water was injected into 3 incubation bottles using syringe. The seawater in one of the three bottles was vacuum-filtered (76mm Hg) with a Whatman GF/F filter (47 mm) immediately after the injection of $^{15}N_2$ water. The other two bottles and the one bottle without $^{15}N_2$ water were incubated in seawater baths for 24 hours under appropriate screen to simulate the in situ temperature and light intensity. Each incubated sample was filtered after the incubation. The glass filter with particulate matters wrapped with aluminum foil and the filtrated water collected in PE bottles were stored at -20 ˚C until analysis. The ^{15}N enrichment of samples will be measured after conversion to N_2O using wet oxidation and "denitrifier" method of Knapp et al. (2005) by GC-IRMS.

Isotopic analysis of methane

Water samples for $\delta^{13}C$-CH_4 analysis were transferred to 100 mL glass vials from the Niskin sampler without head space. After the vials were sealed with butyl rubber and aluminum caps, 100 μL of saturated $HgCl_2$ solution was added. The water samples were stored until analysis on land. The $\delta^{13}C$ value of Methane will be measured using isotope ratio mass spectrometry using a method of Tsunogai et al. (1998 and 2000).

Biomarker of methanogens

Water samples for F_{430} analysis (5 or 10 L) were filtered (0.01 MPa) with a Whatman GF/F filter (47

mm in diameter). The filter samples were wrapped with aluminum foil and stored at −20°C prior to analysis on land. Extraction and analysis of F_{430} will be conducted at JAMSTEC using a method of Kaneko et al. (2014).

Prokaryotic uptakes of organic and inorganic carbon measurements

See "Prokaryotic activity measurements" in Section 3.18.

Genetic markers of geochemical processes

Microbial cells in water samples were filtrated on cellulose acetate filter (0.2μm) and stored at -80˚C. Environmental DNA or RNA will be extracted from the filtrated cells and used for molecular analyses (e.g. clone analysis and quantitative PCR) to investigate the microbial components related to nitrification, nitrogen fixation and methanogenesis.

(4) Expected results

Nitrogen cycle and microbial carbon uptake associated with nitrogen cycle

In the surface layer, N_2O concentration of water affects the sea-air flux directly (Dore et al., 1998). However the pathway of N_2O production in surface layer is still unresolved. In the surface layer, N_2O is predominantly produced by nitrification, but also by nitrifer-denitrification and denitrification if oxygen concentration is low in the water mass or particles (Maribeb and Laura, 2004). The observed concentrations and isotopomer ratios of N_2O together with those values of substrates for N_2O (NO_3^-, NO_2^-, NH_4^+, DON and Chlorophyll-a) will reveal the pathway of N_2O production in the surface layer and will improve the marine N_2O isotopomer model. Moreover, the horizontal isotope dataset will help to apply the model to the western and northern North Pacific.

Methane

A depth profile of F_{430} concentration in water column will provide information about quantitative distribution of methanogens. The $\delta^{13}C$ value of methane reflects carbon source and methanogenic pathway (Whiticar, 1999). If the profile correlate with other chemical profiles including concentrations of methane, chlorophyll and dissolved oxygen, it can be a strong evidence of that methanogens are source organisms for methane in the surface seawater. The $\delta^{13}C$ value of methane will support presence of methanogen and provide further constraints on methanogenic pathway, In addition with the vertical distribution, a lateral distribution (east-west) of F_{430} and other chemicals will provide insight into environmental factors controlling distribution of methanogens.

(5) References

Francis, C.A., Beman, J.M., and Kuypers, M.M. 2007. New processes and players in the nitrogen cycle:

the microbial ecology of anaerobic and archaeal ammonia oxidation. ISME J 1: 19–27.

Alonso-Sáez L, Galand PE, Casamayor EO, Pedrós-Alió C, Bertilsson S. 2010. High bicarbonate assimilation in the dark by Arctic bacteria. ISME J. 4, 1581–1590.

Swan, BK, Martinez-Garcia, M, Preston, CM, Sczyrba, A, Woyke, T, Lamy, D, Reinthaler, T, Poulton, NJ, Masland, ED, Gomez, ML, Sieracki, ME, DeLong, EF, Herndl, GJ, Stepanauskas, R. 2011. Potential for chemolithoautotrophy among ubiquitous bacteria lineages in the dark ocean. Science, 333, 1296-1300

Anantharaman K, Breier JA, Sheik CS, Dick GJ. 2013. Evidence for hydrogen oxidation and metabolic plasticity in widespread deep-sea sulfur-oxidizing bacteria. Proceedings of the National Academy of Sciences. 110, 330–335.

Herndl GJ, Reinthaler T. 2013. Microbial control of the dark end of the biological pump. Nat Geosci. 6, 718–724.

Dore, J.E., Popp, B.N., Karl, D.M. and Sansone, F.J. 1998. A large source of atmospheric nitrous oxide from subtropical North Pacific surface water, Nature, 396, 63-66.

Granger, J., and D. M. Sigman 2009. Removal of nitrite with sulfamic acid for nitrate N and O isotope analysis with the denitrifier method, Rapid Communications in Mass Spectrometry, 23, 3753-3762.

IPCC Working group I 2013. Climate change 2013: The physical science basis. IPCC The 5th Assessment report, http://www.ipcc.ch/report/ar5/wg1/.

Knowles, R., Lean, D.R.S. and Chan, Y.K. 1981. Nitrous oxide concentrations in lakes: variations with depth and time, Limnology and Oceanography, 26, 855-866.

Maribeb, C.-G. and Laura, F. 2004. N_2O cycling at the core of the oxygen minimum zone off northern Chile, Marine Ecology Progress Series, 280, 1-11.

Rysgaard, S., Risgaard-Petersen, N., Nielsen, L.P. and Revsbech, N.P. 1993. Nitrification and denitrification in lake and estuarine sediments measured by the ^{15}N dilution technique and isotope pairing, Applied and Environmental Microbiology, 59, 2093-2098.

Sigman, D. M., K. L. Casciotti, M. Andreani, C. Barford, M. Galanter, and J. K. Boehlke 2001. A bacterial method for the nitrogen isotopic analysis of nitrate in seawater and freshwater, Anal. Chem., 73, 4145-4153.

Svensson, J.M. 1998. Emission of N_2O, nitrification and denitrification in a eutrophic lake sediment bioturbated by Chironomus plumosus, Aquatic Microbial Ecology, 14, 289-299.

Ueda, S., Ogura, N. and Yoshinari, T. 1993. Accumulation of nitrous oxide in aerobic ground water, Water Research, 27, 1787-1792.

Santoro, A.E., Buchwald, C., McIlvin,M.R., and Casciotti, K.L. 2011. Isotopic signature of N_2O produced by marine ammonia-oxidizing Archaea. Science 333. 1282-1285.

Stieglmeier M., Mooshammer M., Kitzler, B., Wanek, W., Zechmeister-Boltenstern, S., Richter A., and Schleper C. 2014. Aerobic nitrous oxide production through N-nitrosating hybrid formation in

ammonia-oxidizing archaea. ISME J. 8, 1135-1146.

Yamagishi, H., Westley, M.B., Popp, B.N., Toyoda, S., Yoshida, N., Watanabe, S., Koba, K., Yamanaka, Y., 2007. Role of nitrification and denitrification on the nitrous oxide cycle in the eastern tropical North Pacific and Gulf of California. J. Geophys. Res. Biogeosciences 112, n/a–n/a. doi:10.1029/2006JG000227

Yoshida, N. and Toyoda, S.: Constraining the atmospheric N_2O budget from intramolecular site preference in N_2O isotopomers, Nature, 405, 330-334, 2000.

Yoshikawa, C., H. Abe, M.N. Aita, F. Breider, K. Kuzunuki, N.O. Ogawa, H. Suga, N. Ohkouchi, S. O. Danielache, M. Wakita, M.C. Honda, S. Toyoda, N. Yoshida. Insights into the production processes of nitrous oxide in the western north Pacific by using a marine ecosystem isotopomer model, in preparation.

Conrad, R., 2009. The global methane cycle: recent advances in understanding the microbial processes involved. Environ. Microbiol. Rep. 1, 285-292.

Grossart, P. H., Frindte, K., Dziallas, C., Eckert, W. and Tang, W. K., 2011. Microbial methane production in oxygenated water column of an oligotrophic lake. Proc. Natl. Acad. Sci. USA 108, 19657-19661.

Kaneko, M., Takano, Y., Chikaraishi, Y., Ogawa, O. N., Asakawa, S., Watanabe, T., Shima, S., Krüger, M., Matsushita, M., Kimura, H. and Ohkouchi, N, 2014. Quantitative Analysis of Coenzyme F_{430} in Environmental Samples: A New Diagnostic Tool for Methanogenesis and Anaerobic Methane Oxidation. Anal. Chem. 86, 3633-3638.

Karl, M. D., Beversdorf, L., Björkman, M. K., Church, J. M., Martinez, A. and DeLong, F. E., 2008. Aerobic production of methane in the sea. Nature Geoscience 1, 473-478.

Scranton, I. M. and Brewer, G. P., 1977. Occurrence of Methane in near-Surface Waters of Western Subtropical North-Atlantic. Deep-Sea Research 24, 127-138.

Tsunogai, U., Ishibashi, J., Wakita, H. and Gamo, T., 1998. Methane-rich plumes in the Suruga Trough (Japan) and their carbon isotopic characterization. Earth. Planet. Sci. Lett. 160, 97-105.

Tsunogai, U., Yoshida, N., Ishibashi, J. and Gamo, T., 2000. Carbon isotopic distribution of methane in deep-sea hydrothermal plume, Myojin Knoll Caldera, Izu-Bonin arc: Implications for microbial methane oxidation in the oceans and applications to heat flux estimation. Geochim. Cosmochim. Acta 64, 2439-2452.

Whiticar M.J., 1999. Carbon and hydrogen isotope systematics of bacterial formation and oxidation of methane. Chem. Geol. 161, 291-314.

Kawagucci S, Yoshida YT, Noguchi T, Honda MC, Uchida H, Ishibashi H, Nakagawa F, Tsunogai U, Okamura K, Takaki Y, Nunoura T, Miyazaki J, Lin W, Kitazato H, Takai K 2012. Disturbance of deep-sea environments induced by the M9.0 Tohoku Earthquake. Scientific Reports. 2, 270.

McIlvin, M. R., Altabet, M. A. 2005. Chemical conversion of nitrate and nitrite to nitrous oxide for nitrogen and oxygen isotopic analysis in freshwater and seawater, Anal. Chem., 77, 5589-5595,

Knapp, A. N., Sigman, D. M., Lipschultz, F., N. 2005 isotopic composition of dissolved organic nitrogen and nitrate at the Bermuda Atlantic time-series study site, Global Biogeochemical Cycles, 19, GB1018

Koba, K., Inagaki, K., Sasaki, Y., Takebayashi, Y., Yoh, M. 2010. Nitrogen isotopic analysis of dissolved inorganic and organic nitrogen in soil extracts, Earth, life, and isotopes, Kyoto University Press,

Revilla, M., Alexander, J., Glibert, P. M., Urea analysis in coastal waters: comparision of enzymatic and direct methods, Limnol. Oceanogr.: Methods, 3, 290-299, 2005

Tsunogai, U., Ishibashi, J., Wakita, H. & Gamo, T. 1998. Methane-rich plumes in the Suruga Trough (Japan) and their carbon isotopic characterization. Earth Planet Sc Lett 160, 97–105.

German, C. R. et al. 2010. Diverse styles of submarine venting on the ultraslow spreading Mid-Cayman Rise. Proc Natl Acad Sci USA 107, 14020–14025.

3.18 Microbiology: Vertical Profiles of Microbial Abundance and Diversity in the North Pacific

September 19, 2014

(1) Personnel

Taichi Yokokawa (Ehime University)
Seiya Takahashi (Tsukuba University)
Motoo Utsumi (Tsukuba University)
Miho Hirai (JAMSTEC)
Michinari Sunamura (The University of Tokyo)
Takuro Nunoura (JAMSTEC)

(2) Introduction

Prokaryotes play a major role in marine biogeochemical fluxes. Biogeochemical transformation rates and functional diversity of microbes are representative major topics in marine microbial ecology. However, the link between prokaryotes activity and biogeochemistry in the meso- and bathypelagic layers has not been explained systematically despite of the recent studies that highlight the role of microbes in the cycling of organic matter. (Herndl and Reinthaler 2013; Yokokawa et al. 2013). Moreover, microbial diversity and biogeography in bathypelagic and abyssal ocean and its relationship with upper layers and deep-water circulation have also not been well studied (Nagata et al. 2010).

The objectives of this study, which analyze the water columns from sea surface to just above the bottom of the North Pacific, were 1) to determine the abundance of prokaryotes; 2) to study the heterotrophic production and chemo-autotrophic production of prokaryotes (Bacteria and Archaea); 3) to assess the community composition of prokaryotes; 4) to know microbial diversity along water columns in different oceanic regions of the North Pacific; 5) to find the impacts of deep-water circulation on biogeography of bathya and abyssal microbial communities; 6) to identify the effects of the trench geomorphology on the hadal microbial communities in the Kuril Trench.

(3) Methods

Microbial abundance

Samples for microbial abundances (prokaryotes, eukaryotes and viruses) were collected in every routine cast and depth except for stations 142 and 143. Samples were fixed with glutaraldehyde (final concentration 1%) or mixed with Glycerol-EDTA, and frozen at -80°C. The abundance of microbes and viruses will be measured by a flow cytometry in both Univ Tokyo (Sunamura) and JAMSTEC (Nunoura) after nucleic acid staining with SYBR-Green I.

FISH analysis for prokaryotic community composition

The relative abundance of the major prokaryotic groups will be determined by CARD-FISH analysis in Ehime Univ (Yokokawa), Tsukuba Univ (Takahashi & Utsumi) and Univ Tokyo (Sunamura). The samples were filtered onto 0.2-µm polycarbonate filters and stored at -20ºC. Samples for FISH were taken at stations 1, 7, 22, 36, 40, 45, 50, 54, 58, 67, 79, 97, 105, 110, 122, 136 and 147 in the routine casts, and at all the MBC casts (see Section 3.17).

Prokaryotic activity measurements

^{3}H-leucine incorporation rate was determined as a proxy for heterotrophic or mixotrophic prokaryotic production. Triplicate subsamples (1.5 mL) dispensed into screw-capped centrifuge tubes amended with 10 nmol L^{-1} (final concentration) of [^{3}H]-leucine (NET1166, PerkinElmer) and incubated at in situ temperature (± 3ºC) in the dark. One trichloroacetic acid (TCA) killed blank was prepared for each sample. Incubation periods were 1 hour and 24 hours for the upper (0 – 250 m) and deeper (300 – bottom) water layers, respectively. After the incubation, proteins were TCA (final conc. 5%) extracted twice by centrifugation (15000 rpm, 10 min, Kubota 3615-sigma), followed by the extraction with ice-cold 80% ethanol.

The relative contribution of Archaea and Bacteria to total prokaryotic leucine incorporation was determined using antibiotics and an inhibitor; erythromycin (Sigma-Aldrich, final conc. 10 mg mL^{-1}) for bacteria, diphtheria toxin (Sigma-Aldrich, final conc. 10 mg mL^{-1}) and N1-Guanyl-1,7-Diaminoheptane (GC7, BIOSEARCH TECHNOLOGIES, final conc. 1mM) for archaea, and (2-(4-carboxyphenyl)-4, 4,5,5-tetramethylimidazoline-1-oxyl-3-oxide) (carboxy- PTIO; Dojindo Molecular Technology, INC. final conc. 100 mM) for inhibiting ammonia-oxidizing archaea (AOA).

In the laboratory the samples will be radioassayed with a liquid scintillation counter using Ultima-GOLD (Packard) as scintillation cocktail. Quenching is corrected by external standard channel ratio. The disintegrations per minute (DPM) of the TCA-killed blank is subtracted from the average DPM of the samples, and the resulting DPM is converted into leucine incorporation rates.

DIC fixation was measured via the incorporation of 50 mCi of [^{14}C]-bicarbonate (NEC086H005MC, Amersham, SA: 52.5 mCi $mmol^{-1}$) in 20 ml seawater samples. Triplicate samples and formaldehyde-fixed blanks were incubated in the dark at in situ temperature (± 4ºC) for 72 h. Incubations were terminated by adding formaldehyde (1% final concentration) to the samples.

The relative contribution of Archaea, Bacteria and AOA to total prokaryotic DIC fixation was determined using erythromycin (Sigma-Aldrich, final conc. 10 mg mL^{-1}), GC7 (BIOSEARCH TECHNOLOGIES, final conc. 1mM) and PTIO (Dojindo Molecular Technology, INC. final conc. 100 mM) as bacterial, archaeal and AOA inhibitors of protein synthesis, respectively, and compared with the DIC fixation in the control sample.

In the laboratory, the samples will be filtered onto 0.2-µm polycarbonate filters. Subsequently, the

filters are fumed with concentrated HCl for 12 h. The samples will be radioassayed with a liquid scintillation counter using Filter-count (PerkinElmer) as scintillation cocktail. Quenching is corrected by external standard channel ratio. The disintegrations per minute (DPM) of the formaldehyde-killed blank is subtracted from the average DPM of the samples, and the resulting DPM is converted into bicarbonate incorporation rates.

Samples for leucin incorporation activity measurements were taken at stations 1, 7, 14, 22, 45, 73, 79, 97, 110, 122, 136 and 141 in the routine casts, and at all the MBC casts (see Section 3.17), and those for inorganic carbon fixation rates assessed at stations 1, 22, 97 in the routine casts, and stations 1, 54, 43, 73, 116, 141 in MBC casts.

Microbial diversity

Microbial cells in water samples were filtrated on cellulose acetate filter (0.2μm) and stored at -80˚C. Environmental DNA or RNA will be extracted from the filtrated cells and used for 16S/18S rRNA gene tag sequencing using Ion PGM or MiSeq, clone analysis for functional genes (e.g. amoA and nifH), quantitative PCR for genes for 16S rRNA and *amoA*, metagenomics and/or metatranscriptomics. Moreover, selected water samples were mixed with glycerol-EDTA and stored at -80˚C for single cell genomic analyses in collaboration with Bigelow Laboratory. Samples for microbial diversity were taken at stations 1, 7, 14, 22, 30, 36, 39, 40, 43, 45, 47, 50, 54, 58, 67, 73, 79, 83, 85, 87, 91, 97, 105, 110, 116, 122, 128, 136, 141 and 147 in the routine casts, and at all the MBC casts (see Geochemistry and Microbiology: Nitrogen and carbon cyclesin the North Pacific).

Viral diversity

Viral particles were obtained by a chemical flocculation method (John et al. 2012) and filtrated on polycarbonate filter (0.45μm). The filters were stored at 5˚C. Viral particles will be resuspended in ascorbate buffer and then used to following molecular analyses such as metagenomic library construction. Samples for viral diversity were taken at stations 50, 73, 79, 97, 122, 136 and 147.

(4) References

Herndl GJ, Reinthaler T (2013) Microbial control of the dark end of the biological pump. Nature geoscience, 6:718-724

Yokokawa T, Yang Y, Motegi C, Nagata T (2013) Large-scale geographical variation in prokaryotic abundance and production in meso- and bathypelagic zones of the central Pacific and Southern Ocean. Limnology and Oceanography, 58:61-73

Nagata T, Tamburini C, Aristegui J, Baltar F, Bochdansky AB, Fonda-Umani S, Fukuda H, Gogou A, Hansell DA, Hansman RL, Herndl GJ, Panagiotopulos C, Reinthaler T, Sohrin R, Verdugo P,

Yamada N, Yamashita Y, Yokokawa T, Bartlett DH (2010) Emerging concepts on microbial processes in the bathypelagic ocean – ecology, biogeochemistry, and genomics. Deep-Sea Research II 57:1519-1536

John SG, Mendez CB, Deng L, Poulos B, Kauffman AKM, Kern S, Brum J, Polz MF, Boyle EA, Sullivan MB (2011) A simple and efficient method for concentration of ocean viruses by chemical flocculation. Environmental Microbiology Reports 3: 195-202

3.19 Lowered Acoustic Doppler Current Profiler (LADCP)

September 16, 2014

(1) Personnel

Shinya Kouketsu (JAMSTEC) (Principal Investigator, Leg 2)

Hiroshi Uchida (JAMSTEC) (Legs 1 and 2)

(2) Overview of the equipment

An acoustic Doppler current profiler (ADCP) was integrated with the CTD/RMS package. The lowered ADCP (LADCP), Workhorse Monitor WHM300 (Teledyne RD Instruments, San Diego, California, USA), which has 4 downward facing transducers with 20-degree beam angles, rated to 6000 m. The LADCP makes direct current measurements at the depth of the CTD, thus providing a full profile of velocity. The LADCP was powered during the CTD casts by a 48 volts battery pack. The LADCP unit was set for recording internally prior to each cast. After each cast the internally stored observed data was uploaded to the computer on-board. By combining the measured velocity of the sea water and bottom with respect to the instrument, and shipboard navigation data during the CTD cast, the absolute velocity profile can be obtained (e.g. Visbeck, 2002).

The instrument used in this cruise was as follows.

Teledyne RD Instruments, WHM300

S/N 20754(CPU firmware ver. 50.40)

(3) Data collection

In this cruise, data were collected with the following configuration.

Bin size: 4.0 m

Number of bins: 25

Pings per ensemble: 1

Ping interval: 1.0 sec

At the following stations, the CTD cast was carried out without the LADCP, because the maximum pressure was beyond the pressure-proof of the LADCP (6000 m).

Stations from P01_44 to P01_46

Reference

Visbeck, M. (2002): Deep velocity profiling using Lowered Acoustic Doppler Current Profilers: Bottom track and inverse solutions. *J. Atmos. Oceanic Technol.*, **19**, 794-807.

3.20 Micro Rider

September 24, 2014

(1) Personnel

Ichiro Yasuda	(AORI)	: Principal Investigator
Yasutaka Goto	(AORI)	
Maki Nagasawa	(AORI)	
Kosei Komatsu	(AORI)	
Shinya Kouketsu	(JAMSTEC)	
Hiroshi Uchida	(JAMSTEC)	
Katsurou Katsumata	(JAMSTEC)	
Takeshi Kawano	(JAMSTEC)	

(2) Objective

Microstructure observations to evaluate vertical mixing.

(3) Instruments and method

Micro structure observations were carried out by micro-Rider 6000 (MR6000; Rockland Scientific International Inc.), which is mounted CTD rosette and is powered from SBE 9plus. MR6000 has 6 probe slots. We mounted two FP07 thermistors, one micro-Conductivity sensor, and one shear probe to obtain the high-frequency changes in temperature, salinity, and velocity shear. The one dummy probe and LED probe, which is for checking the power on/off are mounted on the residual two slots. We sometimes replaced the probes during this cruise, as the probes didn't work well. The high-frequency pressure and acceleration profiles are also obtained by the sensors in MR6000. The low-frequency profiles of temperature and salinity are archived in the MR6000 from the cables connected with SBE-3 and SBE-4 sensors on the CTD system. We download the data in the MR6000 and make preliminary process to check quality of the measurements with the software provided Rockland Scientific International Inc. After the cruise, we plan to examine the methods of the correction and measurement quality evaluation with the comparison among the micro temperature with CTD rosette, those with free fall instruments, and free fall micro shear structure observations.

(4) Preliminary results

Fig.3.20.1 shows logarithm epsilon value during the cruise.

(5) Micro-Temperature measurement history

- Station 036: T886 (T1 slot) and T883 (T2 slot)

- Station 044-055: MR6000 was detached from the CTD due to over 6000 m observations
- Station 050: T886 was replaced by T416 at T1 slot
- Station 051: T883 was replaced by T887 at T2 slot
- Station 055: T887 was replaced by T494 at T2 slot
- Station 067: T416 was replaced by T496 at T1 slot
- Station 080: T496 was replaced by T886 at T1 slot
- Station 125: The data was lost due to wrong operation

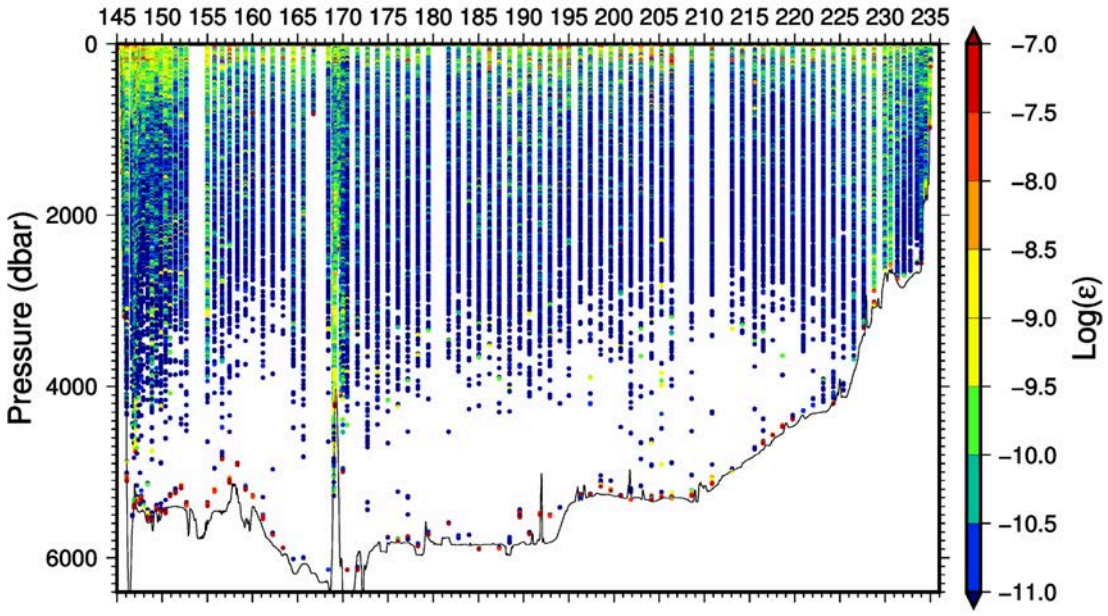

Fig 3.20.1. Vertical section of logarithm of epsilon value.

4 Floats, Drifters and Moorings

4.1 Argo Floats

September 18, 2014

(1) Personnel

Toshio Suga	(JAMSTEC/RCGC): Principal Investigator (not on board)
Shigeki Hosoda	(JAMSTEC/ RCGC): not on board
Kanako Sato	(JAMSTEC/ RCGC): not on board
Mizue Hirano	(JAMSTEC/ RCGC): not on board
Shuhei Masuda	(JAMSTEC/ RCGC): not on board
Hiroshi Matsunaga	(MWJ): Technical Staff (Operation Leader)

(2) Objectives

The objective of deployment is to clarify the structure and temporal/spatial variability in the North Pacific Ocean, especially water masses such as the North Pacific Central Mode Water (CMW). The deployment to this area where Argo float density tends to be sparse also contribute to the international Argo program to construct the global Argo array.

The profiling floats launched in this cruise measure vertical profiles of temperature and salinity automatically every five or ten days. As the vertical resolution of the profiles is very fine, the structure and variability of the water mass can be displayed well. Therefore, the profile data from the floats will enable us to understand the variability and the formation mechanism of the water mass.

(3) Parameters

・water temperature, salinity, pressure, and dissolved oxygen

(4) Methods

i. Profiling float deployment

We launched Navis floats manufactured by Sea Bird Electronics Inc. These floats equip SBE41cp CTD sensor manufactured by Sea-Bird Electronics Inc. as Argo floats.

The floats usually drift at a depth of 1000 dbar (called the parking depth), diving to a depth of 2000 dbar and rising up to the sea surface by decreasing and increasing their volume and thus changing the buoyancy in ten-day cycles. During the ascent, they measure temperature, salinity, and pressure. They stay at the sea surface for approximately thirty minutes, transmitting the CTD data to the land via the Iridium Rudics system, and then return to the parking depth by decreasing volume. The status of floats and their launches are shown in Tables 4.1.1 and 4.1.2.

Table 4.1.1. Status of Navis floats (2000 dbar).

Float Type	Navis float manufactured by Sea-Bird Electronics Inc.
CTD sensor	SBE41cp manufactured by Sea-Bird Electronics Inc.
Cycle	10 days (approximately 30minutes hours at the sea surface)
Iridium transmit type	Router-Based Unrestricted Digital Internetworking Connectivity Solutions (RUDICS)
Target Parking Pressure	1000 dbar
Sampling layers	2dbar interval from 2000 dbar to surface (approximately 1000 layers)

Table 4.1.2. Navis floats launches

Float S/N	WMO ID	Date and Time of Launch(UTC)	Location of Launch	CTD St. No.
F0349	4902144	2014/08/05 12:01	46° 57.564' [N] 177° 11.658'[W]	P01-099
F0350	4902145	2014/08/08 19:27	46°59.1572'[N] 169°20.5832'[W]	P01-106
F0362	4902146	2014/08/09 18:17	47°00.8506'[N] 165°58.8322'[W]	P01-109
F0363	4902147	2014/08/11 01:27	46°59.1870'[N] 161°28.7638'[W]	P01-113

ii. Deployment of S3A with RINKO sensor

We also launched two S3A floats manufactured by MRV Systems (U.S.A), equipped with RINKO dissolved oxygen sensor by JFE Advantec Co.,Ltd (JAC). The CTD sensor of S3A uses SBE41cp manufactured by Sea-Bird Electronics Inc.. The RINKO sensor measures dissolved oxygen concentration in the sea, and their expected accuracy and response time are higher and faster than of Optode4330/3830 by Aanderaa Data Instruments. As the JAC had developed the RINKO sensor for Argo in collaboration with JAMSTEC and recently produces as the commercial product, this launching opportunity was first time to get oxygen data of the RINKO floats in the World. Therefore, another purpose of the launch is to evaluate the accuracy and temporal stability of RINKO sensor comparing with ship board CTD observations. To evaluate more strictly, we had already checked the accuracy and stability of the sensor at air pressure in laboratory.

The two S3A set to drifting level at a depth of 1000 dbar and diving to a depth of 2000 dbar for

measurements every 5 days. The launching position of the S3As was in the warm core ring (WCR) off Hokkaido. As some floats with Optode4330 are observing and there are some cruise tracks of research vessels around the WCR, the area is appropriate to evaluate the RINKO sensor getting nearby CTD and dissolved oxygen data. The status of floats and their launches are shown in Tables 4.1.3 and 4.1.4.

Table 4.1.3. Status of S3A floats (2000 dbar).

Float Type	S3A float manufactured by MRV Systems
CTD sensor	SBE41cp manufactured by Sea-Bird Electronics Inc.
Cycle	5 days (approximately 30minutes hours at the sea surface)
Oxygen sensor	RINKO manufactured by JFE Advantech Co., Ltd
Iridium transmit type	Short Burst Data Service (SBD)
Target Parking Pressure	1000 dbar
Sampling layers	2dbar interval from 2000 dbar to surface (approximately 1000 layers)

Table 4.1.4. S3A floats launches.

Float S/N	Date and Time of Launch(UTC)	Location of Launch	CTD St. No.
7251	2014/07/21 00:32	46°53'4820"[N] 147°03'9921"[E]	P01-050
7252	2014/07/21 00:34	46°53'3933" [N] 147°04'0847" [E]	P01-050

Note: WMOID for S3A is not obtained yet.

(5) Data archive

The real-time data of the launched profiling floats are provided to meteorological organizations, research institutes, and universities via Global Data Assembly Center (GDAC: http://www.usgodae.org/argo/argo.html, http://www.coriolis.eu.org/) and Global Telecommunication System (GTS), and utilized for analysis and forecasts of sea conditions. The real time data of S3A floats will also be provided and opened to the public as Argo equivalent floats following Argo data management procedure, although it is some delay due to some data management issues.

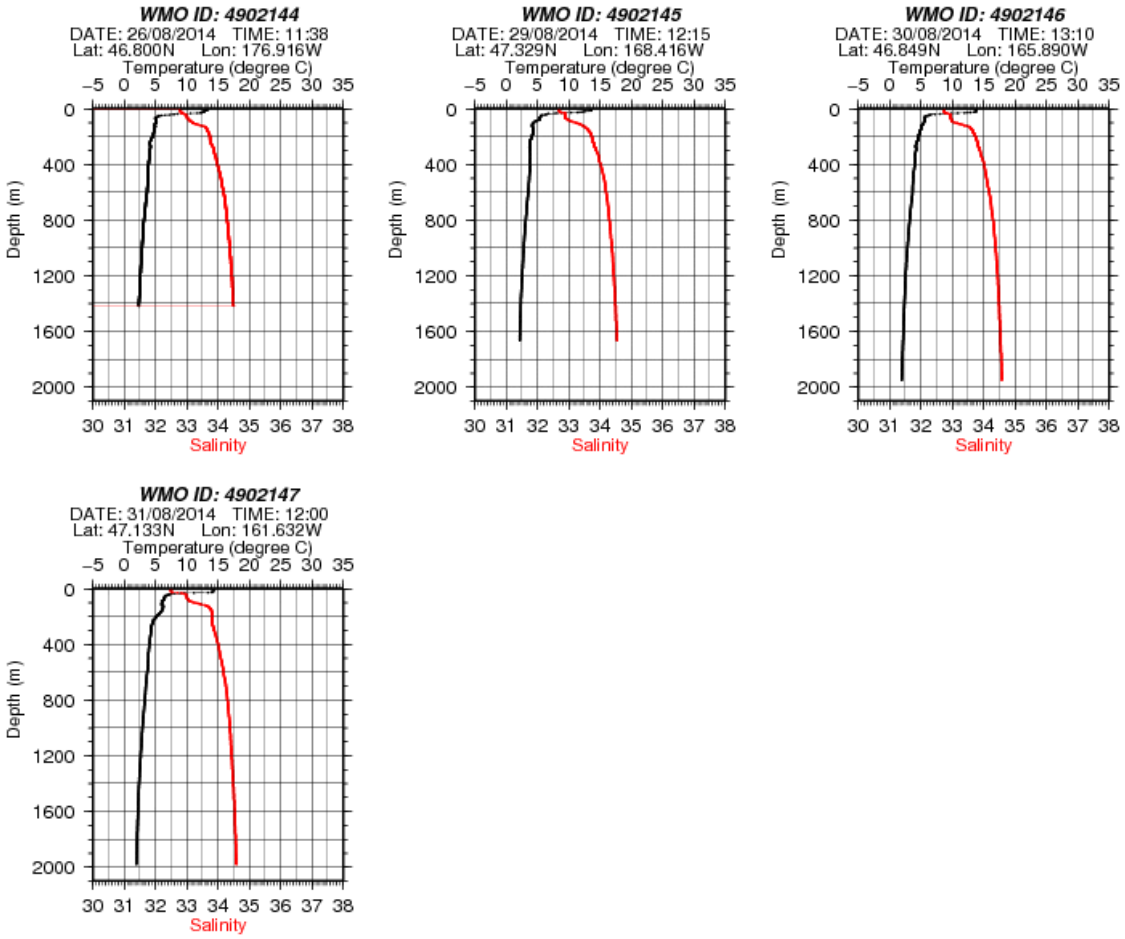

Fig. 4.1.1. First profiles of temperature and salinity from the launched Navis floats.

5 Biological Measurements

5.1 ORI-Net Sampling

September 18, 2014

(1) Personnel

Minoru Kitamura (JAMSTEC)

(2) Objectives

On 11 March 2011, a great earthquake occurred off Tohoku, Japan. This earthquake and the ensuing tsunami inflicted heavy damage on the Fukushima Daiichi nuclear power plant. The fuel rods were exposed and a meltdown occurred in the power plant. By venting, hydrogen explosions and water, contaminated with radionuclides, leaking into the ocean, large amounts of anthropogenic radioactive materials were emitted and circulated around the Northern Hemisphere. These emitted radioactive materials may have an effect on the environment, resources and consequently human health. And they were actually detected from not only terrestrial but also marine biota. The influences of the Fukushima accident to marine biota have been mostly researched in the coastal area off Fukushima, however, studies in oceanic stations have been scarce. Because concentrations of cesium in seawater, sediments and marine biota were previously well documented among the radioactive materials, it is useful to compare the concentrations between before and after the Fukushima accident.

In this cruise, we quantified concentrations of radioactive cesium (^{137}Cs and ^{134}Cs) in oceanic zooplankton communities, three years after the Fukushima accident. We had observed the radiocesium concentration in zooplankton collected from the two oceanic time-series station, K2 (47°N, 160°E) and S1 (30°N, 145°E) from April 2011. Main aim of the present study is to understand temporal change of radioactive concentration of ^{137}Cs and ^{134}Cs in zooplankton community from comparison between the presently and previously observed data. On the other hand, cesium concentrations in seawater will be also observed in this cruise (see chapter 3.13 Radiocesium and Iodine-129).

(3) Methods

Zooplankton was collected from the surface layer at two stations, Stn.1 and 22, during the day and night, respectively (Table 5.1.1). The ORI net (1.6 m in diameter, 8 m long, and 0.33 mm in mesh) was obliquely towed at an average ship speed of 2 knots. Filtering volume of water was estimated using a flow meter mounted in the net mouth. Maximum sampling depth of each trawl was recorded using a depth sensor (DEFI-D50, JFE-Advantec Co. Ltd) attached in the net frame, and the maximum depth was 250 m in both the two sampling stations. Collected zooplankton sample was divided onboard using a sample splitter. 1/32 or 1/64 subsample was fixed and preserved in 5% buffered formalin seawater to analyze

community structure. Micronektonic fish and fish larvae were sorted out from the remained subsamples, and they were fixed and preserved in 10% buffered formalin seawater. Finally, the remaining zooplankton samples was filtered using four to eight pre-weighed 0.1 mm meshes, and was frozen in −20°C to estimate bulk biomass of zooplankton communities and quantify activity concentrations of ^{134}Cs and ^{137}Cs. All formalin fixed or frozen subsamples are stored under Kitamura until analyzing.

Table 5.1.1 Zooplankton samplings for RI analysis

Stn.	Date & Time				Position		Sampling layer (m)	Filtering vol. (m^3)	Subsamples	Remarks
	LST	net in out	UTC	net in out	Lat. (N)	Long. (E)				
1	2014.7.11	14:15 16:13	2014.7.11	5:15 7:13	29°58.78' 29°55.78'	149°16.45' 149°14.13'	0~250	10,871	1/32: Formalin fix. 31/32: Frozen	daytime sampling
22	2014.7.14	0:39 1:29	2014.7.13	15:39 16:29	38°44.16' 38°44.85'	146°16.79' 146°18.03'	0~250	5,257	1/64: Formalin fix. 63/64: Frozen	

(4) Preliminary results and future analysis

After the cruise, frozen zooplankton samples were dried, pulverized, and combusted at up to 450°C to obtain ash. Water content, dry/ wet and ash/dry weights ratios of the zooplankton samples are summarized in the Table 5.1.2. ^{134}Cs and ^{137}Cs radioactivities in the ash samples will be determined by gamma-spectrometry at the Ogoya Underground Laboratory of the Low Level Radioactivity, ultra-low background Ge detecters. Community structure of zooplankton in each sampling station will be also analyzed.

Table. 5.1.2. Biomass, water content and weights ratios of zooplankton samples collected in the western North Pacific, three years after the Fukushima accident.

Stn.	Biomass (mg-dw/m^3)	Water content (%)	Weight ratio	
			Dry/Wet	Ash/Dry
1	3.1	87.1	0.13	0.29
22	22.0	84.0	0.16	0.23

5.2. NORPAC Net Sampling

September 17, 2014

(1) Personnel

Katsunori Kimoto (JAMSTEC) Principal investigator -not on board

Shinya Iwasaki (AORI) -on board (Leg. 2)

Koji Sugie (JAMSTEC) -on board (Leg. 2)

(2) Objective

1. Understanding of microzooplankton assemblages. Shell bearing plankton such as planktic foraminifera is the main research target.

2. Observing the dissolution process of settling planktic foraminiferal shell in the water column.

(3) Method

Microzooplankton samples were taken by vertical tow of single NORPAC plankton net (frame diameter: 45 cm). Applied mesh size is 63 μm. Target depth was 0-50, 50-100, 100-150, 150-200, 200-300, 300-500 m except for St. 54. The towing was carried out from starboard side with vinyl-coated wire winch. The towing speed was 0.5 ms^{-1}. The obtained planktons were sieved by 45 μm nylon mesh. The residue on 45 μm sieve was washed down to the sample cup by ethanol and was preserved in 100 ml ethanol. Planktic foraminifers in these samples will be picked up after the MR14-04 cruise by Dr. Shinya Iwasaki and further research will be continued after the sample arrival to laboratory.

Table5.2.1. Station, date, time, position (latitude and longitude) and target depth in the NORPAC net sampling during MR14-04_leg2.

Station	Start		End		Latitude	Longitude	Target Depth (m)
	Date	Time (UTC)	Date	Time (UTC)			
54	2014/7/22	19:24	2014/7/22	21:10	39 83.31 N	147 42.60 E	0-50, 50-150, 150-300, 500-1000
67	2014/7/25	12:25	2014/7/25	14:25	44 05.09 N	154 59.58 E	0-50, 50-100, 100-150, 150-200, 200-300, 300-500
73	2014/7/27	14:21	2014/7/27	16:15	47 01.04 N	160 01.13 E	0-50, 50-100, 100-150, 150-200, 200-300, 300-500
79	2014/7/30	13:51	2014/7/30	16:15	46 59.70 N	166 44.33 E	0-50, 50-100, 100-150, 150-200, 200-300, 300-500
91	2014/8/2	15:23	2014/8/2	17:17	47 00.31 N	173 49.71 E	0-50, 50-100, 100-150, 150-200, 200-300, 300-500
101	2014/8/5	0:25	2014/8/5	2:12	47 00.19 N	174 57.19 E	0-50, 50-100, 100-150, 150-200, 200-300, 300-500
116	2014/8/11	23:23	2014/8/12	2:30	46 59.73 N	158 08.08 W	0-50, 50-100, 100-150, 150-200, 200-300, 300-500
128	2014/8/15	23:35	2014/8/16	2:30	46 54.11 N	144 26.00 W	0-50, 50-100, 100-150, 150-200, 200-300, 300-500
151	2014/8/16	22:17	2014/8/17	0:12	49 59.41 N	144 58.90 W	0-50, 50-100, 100-150, 150-200, 200-300, 300-500
141	2014/8/21	4:50	2014/8/21	5:40	46 58.58 N	130 01.58 W	0-50, 50-100, 100-150, 150-200, 200-300, 300-500

5.3 Phytoplankton Incubation

September 2, 2014

(1) Personnel

Koji Sugie (JAMSTEC): Principal Investigator (PI)

Shinya Iwasaki (JSPS and AORI)

(2) Objective

On-deck incubation experiment was conducted to assess the synergistic impacts of ocean acidification and global warming on phytoplankton community and biogeochemical cycling of bio-elements.

(3) Parameters

Chlorophyll-*a*, nutrients (NO_3, NO_2, NH_4, PO_4, $Si(OH)_4$), particulate organic carbon, particulate nitrogen, particulate phosphorus, particulate biogenic silica, microscopic observation, flow cytometry, temperature, photosynthetic active radiation, dissolved inorganic carbon, total alkalinity, particulate and dissolved ^{15}N abundance, domoic acid

(4) Instruments and methods

Teflon® coated, Niskin-X sampling bottle attached to a CTD-CMS to collect seawater samples from a depth of 10 m for incubation. Seawater for the incubations were collected at 47°N 160°E (first experiment) and 47°N 148°W (second experiment). Nine treatments were prepared as follows:

LFe:	unamended control
LFeHT:	temperature increased at 4°C relative to the control
LFeHC600:	high CO_2 condition was achieved by adding CO_2 saturated filtered seawaters to the controls to make the seawater pCO_2 ca. 600 μatm.
LFeHC1000:	similar to LFeHC600 but the seawater pCO_2 to be ca. 1000 μatm
HFe:	Fe added to the control to make final conc. to be 5 nmol L^{-1}
HFeHT:	Fe added and temperature increased at 4°C relative to the HFe
HFeHC600:	high CO_2 condition was achieved by adding CO_2 saturated filtered seawaters to make the seawater pCO_2 ca. 600 μatm.
HFeHC1000:	similar to HFeHC600 but the seawater pCO_2 to be ca. 1000 μatm
G.H.:	CO_2 was adjusted ca. 1000 μatm and temperature was increased at 4°C relative to the controls.

Seawater for the experiment was sieved by ca. 200 μm acid-cleaned Teflon-mesh to eliminate mesozooplankton, and the prescreened seawater was poured into six acid washed 50 L polypropylene

tanks to homogenize seawater samples. After Fe and/or CO_2 saturated filtered seawater were added and homogenized, seawater samples were dispensed into acid-washed polyethylene bags. To adjust pCO_2 in the high temperature series, alkalinity was manipulated by the addition of strong alkali (0.1 N NaOH, suprapur Merk). Bags were prepared in duplicate per treatment. Temperature of the incubation tanks were set at 11 and 15°C in the first experiment, and at 14 and 18°C in the second experiment. Incubations were run for 11 and 10 days in the first and second experiment, respectively. Chlorophyll-*a* and nutrients were collected every day, and other parameters were collected periodically (1 to 3 day interval).

(5) Observation log

1st experiment

July 27, 2014 47°00.58 N, 160°01.42 E

2nd experiment

August 15, 2014 47°00.29 N, 148°02.01 W

(6) Preliminary results

1st experiment.

Time course of photosynthetic active radiation (PAR) and temperature, and chlorophyll-*a* concentrations were shown in Figs. 5.3.1 and 5.3.2, respectively.

2nd experiment

Time course of photosynthetic active radiation (PAR) and temperature, and chlorophyll-*a* concentrations were shown in Figs. 5.3.3 and 5.3.4, respectively.

(7) Data archives

All data obtained during MR14-04 cruise will be submitted to Data Management Group (DMG) of JAMSTEC after the sample analysis and validation.

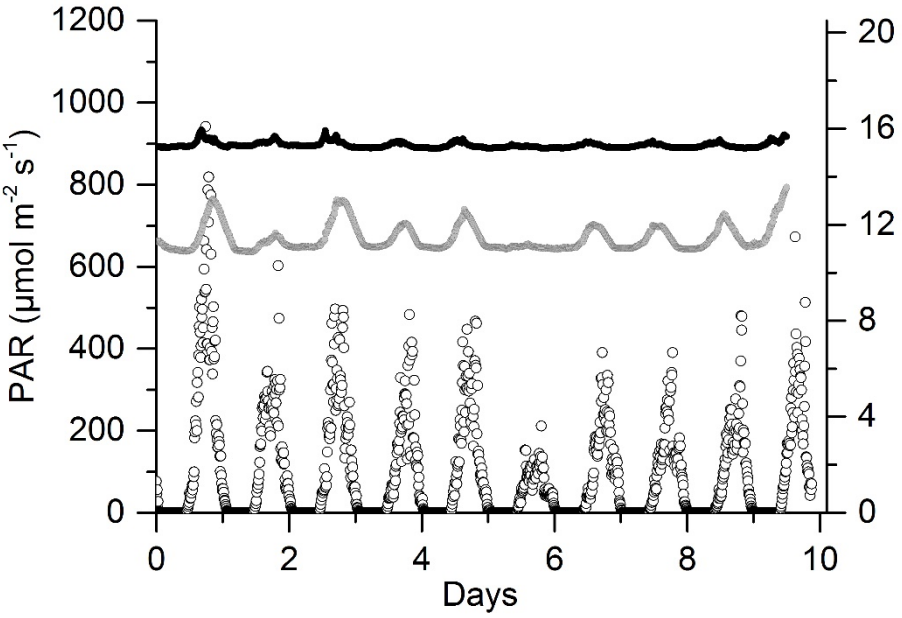

Fig. 5.3.1. Time course of photosynthetic active radiation (PAR, open circle) and temperature (black and gray dots) during the first experiment.

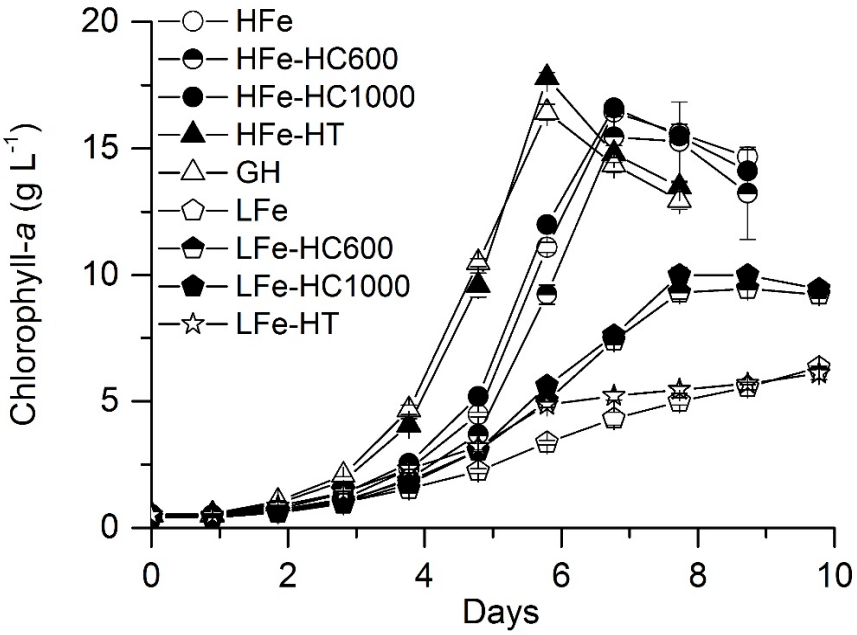

Fig. 5.3.2. Time course of chlorphyll-*a* concentrations during the first experiment. Data represent mean ± range of duplicate incubation bags.

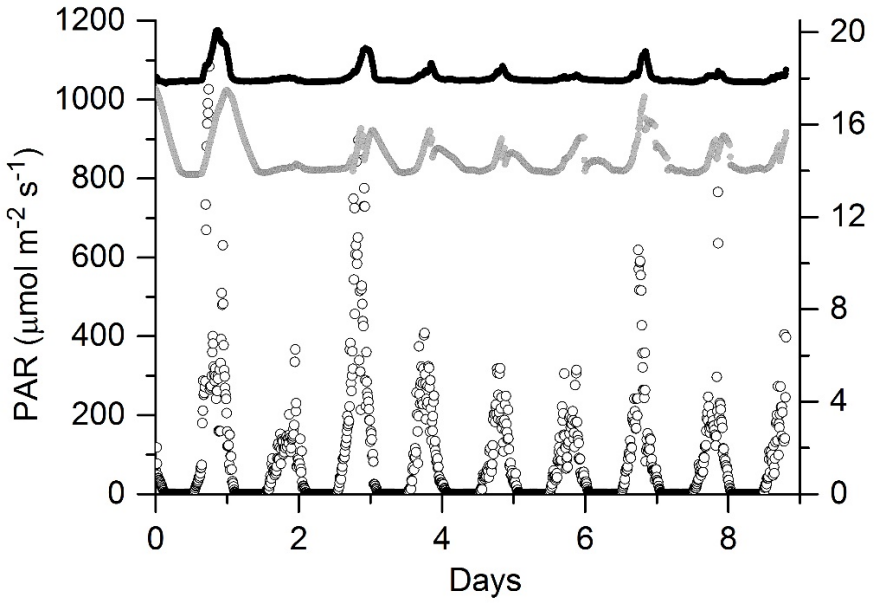

Fig. 5.3.3. Time course of photosynthetic active radiation (PAR, open circle) and temperature (black and gray dots) during the second experiment.

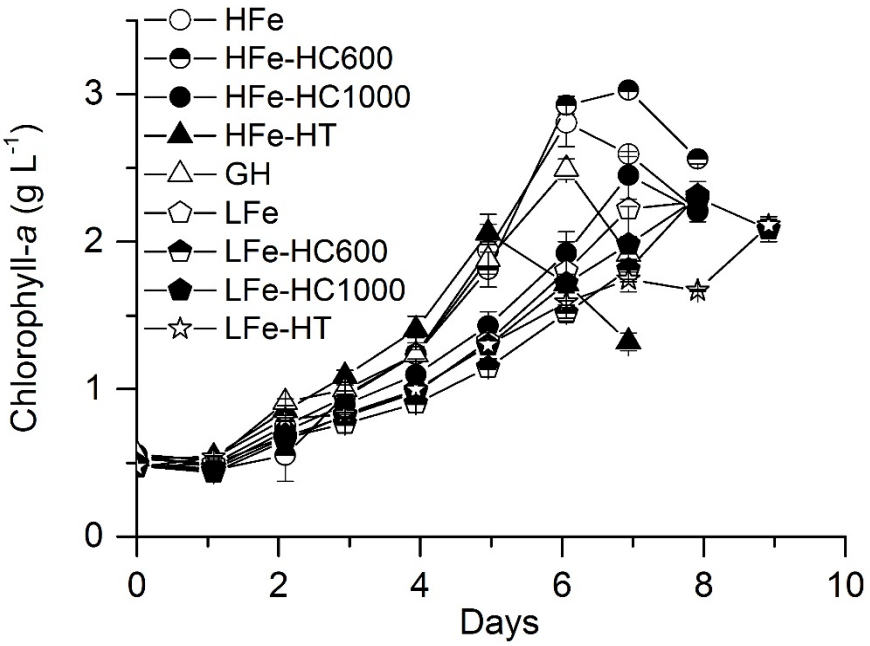

Fig. 5.3.4. Time course of chlorphyll-*a* concentrations during the second experiment. Data represent mean ± range of duplicate incubation bags.

6 Notice on Using

This cruise report is a preliminary documentation as of the end of the cruise. This report may not be corrected even if changes on contents (i.e. taxonomic classifications) may be found after its publication. This report may also be changed without notice. Data on this cruise report may be raw or unprocessed. If you are going to use or refer to the data written on this report, please ask the chief scientist for latest information. Users of data or results on this cruise report are requested to submit their results to the Data Management Group of JAMSTEC.